

Structural elucidation and quantification of novel toxins in marine microalgae by NMR- and molecular modelling-based techniques

Dissertation

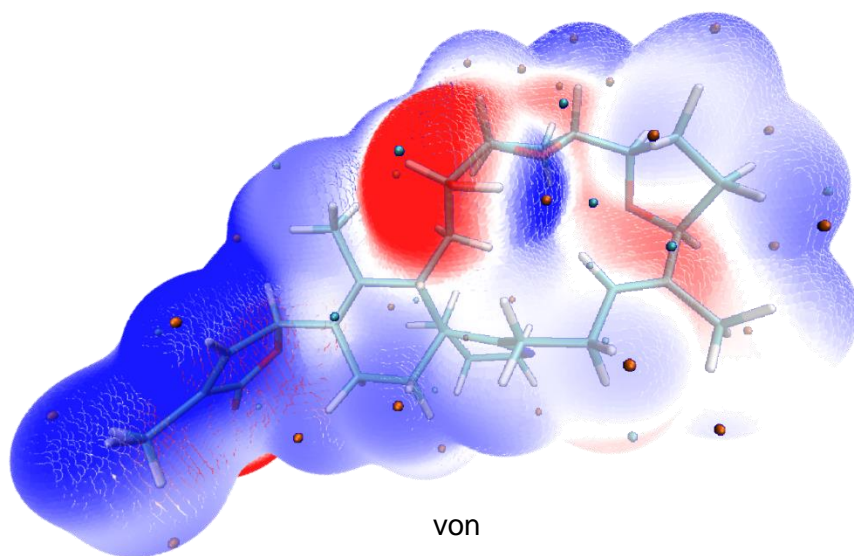
zur Erlangung des Grades

Doktor der Naturwissenschaften (Dr. rer. nat.)

dem Fachbereiches II – Biologie/Chemie

der Universität Bremen

am 14.08.2019 vorgelegt



von

Christian Zurhelle

aus Oldenburg (Oldb)

**Structural elucidation and quantification of novel toxins in marine
microalgae by NMR- and molecular modelling-based techniques**

Dissertation

zur Erlangung des Grades

Doktor der Naturwissenschaften (Dr. rer. nat.)

dem Fachbereiches II – Biologie/Chemie

der Universität Bremen

am 14.08.2019 vorgelegt

von

Christian Zurhelle

aus Oldenburg (Oldb)

- | | |
|---------------|---------------------------|
| 1. Gutachter: | Prof. Dr. Tilmann Harder |
| 2. Gutachter: | Prof. Dr. Peter Spiteller |

Eigenständigkeitserklärung

Die vorliegende Dissertation entstand in der Zeit vom November 2015 bis August 2019 unter Betreuung von Herrn Prof. Dr. Tilmann Harder und Dr. Jan Tebben an der Universität Bremen im Fachbereich 2 Biologie/Chemie und der Sektion Ökologische Chemie am Alfred-Wegener-Institut in Bremerhaven.

Ich, Christian Zurhelle, (Vielstedter Straße 30, 27798 Hude, Matr.-Nr.: 2486113) versichere an Eides Statt durch meine Unterschrift, dass ich die vorstehende Arbeit selbständig und ohne fremde Hilfe angefertigt und alle Stellen, die ich wörtlich dem Sinne nach aus Veröffentlichungen entnommen habe, als solche kenntlich gemacht habe, mich auch keiner anderen als der angegebenen Literatur oder sonstiger Hilfsmittel bedient habe.

Ich versichere an Eides Statt, dass ich die vorgenannten Angaben nach bestem Wissen und Gewissen gemacht habe und dass die Angaben der Wahrheit entsprechen und ich nichts verschwiegen habe.

Die Strafbarkeit einer falschen eidesstattlichen Versicherung ist mir bekannt, namentlich die Strafandrohung gemäß § 156 StGB bis zu drei Jahren Freiheitsstrafe oder Geldstrafe bei vorsätzlicher Begehung der Tat bzw. gemäß § 161 Abs. 1 StGB bis zu einem Jahr Freiheitsstrafe oder Geldstrafe bei fahrlässiger Begehung.

Bremen, den 14. August 2019

Christian Zurhelle

Beginn der Doktorarbeit:	01.11.2015
Dissertation beim Prüfungsausschuss eingereicht am:	14.08.2019
Datum des Kolloquiums:	10.10.2019
1. Gutachter:	Prof. Dr. Tilmann Harder
2. Gutachter:	Prof. Dr. Peter Spiteller

List of publications

Identification of novel neurotoxic gymnodimines and spirolides from the marine dinoflagellate *Alexandrium ostenfeldii*

C. Zurhelle¹, J. Nieva², U. Tillmann², T. Harder^{1,2}, B. Krock², J. Tebben² (2018)

¹ University of Bremen, Department of Biology and Chemistry, Marine Chemistry, Leobener Straße 6, 28359 Bremen, Germany

² Alfred Wegener Institute, Helmholtz Centre for Polar and Marine Research, Section Ecological Chemistry, Am Handelshafen 12, 27570 Bremerhaven, Germany

Marine Drugs **2018**, 16(11), 446

DOI: 10.3390/md16110446

The structure elucidation and *in vitro* toxicity of two novel azaspiracids from cultures of the South China Sea

Ulf Bickmeyer¹, B. I. Escher^{2,3}, H. Gu⁴, T. Harder⁵, B. Krock¹, J. Nieva¹, J. Tebben¹, U. Tillmann¹, S. Wietkamp¹, C. Zurhelle⁵ (alphabetical order)

¹ Alfred Wegener Institute, Helmholtz Centre for Polar and Marine Research, Section Ecological Chemistry, Am Handelshafen 12, 27570 Bremerhaven, Germany

² Department of Cell Toxicology, UFZ – Helmholtz Centre for Environmental Research, Leipzig, Germany

³ Department of Environmental Toxicology, Center for Applied Geosciences, Eberhard Karls University, Tübingen, Germany

⁴ Third Institute of Oceanography, SOA, Xiamen 361005, PR China

⁵ University of Bremen, Department of Biology and Chemistry, Marine Chemistry, Leobener Straße 6, 28359 Bremen, Germany

To be submitted

Structural elucidation, acute oral toxicity of the novel azaspiracid AZA-59 from Puget Sound, USA

J. Deeds¹, T. Harder², J. Kilcoyne³, B. Krock⁴, I. A. Samdal⁵, S. Sosa⁶, J. Tebben⁴, U. Tillmann⁴, V. L. Trainer⁷, A. Tubaro⁸, C. Zurhelle² (alphabetical order)

¹ US Food and Drug Administration Center for Food Safety and Applied Nutrition, 5100 Paint Branch Parkway, College Park, Maryland, 20723, USA

² University of Bremen, Department of Biology and Chemistry, Marine Chemistry, Leobener Straße 6, 28359 Bremen, Germany

³ Marine Institute, Renville, Oranmore, County Galway, Ireland

⁴ Alfred Wegener Institute, Helmholtz Centre for Polar and Marine Research, Section Ecological Chemistry, Am Handelshafen 12, 27570 Bremerhaven, Germany

⁵ Veterinary Institute, PB 8156 Dep., 0033 Oslo, Norway

⁶ IFREMER, Laboratoire Phycotoxines, Rue de l'Île d'Yeu, 44311 Nantes, France

⁷ Northwest Fisheries Science Center, National Marine Fisheries Service, National Oceanic and Atmospheric Administration, 2725 Montlake Blvd. E., Seattle, WA 98112, USA

⁸ Department of Life Sciences, University of Trieste, Via A. Valerio 6, 34127 Trieste, Italy

To be submitted

Danksagung

Ganz herzlich möchte Prof. Dr. Tilmann Harder für die freundliche Aufnahme in seine Arbeitsgruppe, den Zugang zu diesem interessanten Forschungsgebiet danken, den vielen thematischen Diskussionen und den zahlreichen Ratschlägen.

Bei Prof. Dr. Peter Spiteller bedanke ich mich für sein Interesse an meiner Arbeit und dafür, dass er mir als Gutachter zur Verfügung steht.

Den ehemaligen und aktuellen Mitgliedern der Arbeitsgruppe Meereschemie für die freundliche Aufnahme und das angenehme Arbeitsklima. Insbesondere möchte ich mich bei Jenny, Julian, und unseren ehemaligen Studenten Sabrina, Jenny, Sarah und Eike bedanken für die unzähligen gemeinsamen Stunden im Labor. Bei Dr. Jan Tebben möchte ich mich ebenfalls bedanken, der mich durch seine beständige Hilfsbereitschaft und die zahlreichen inhaltlichen und strukturellen Diskussionen und Nachfragen immer wieder motiviert hat.

Ich danke den Mitgliedern der Sektion ökologische Chemie am AWI für die nette Atmosphäre. Mein besonderer Dank geht an Prof. Dr. Boris Koch, Dr. Urban Tilmann, und Dr. Bernd Krock für die Unterstützung durch kritische Nachfragen und die vielen thematischen Diskussionen. Mit Freude denke ich an die vielen gemeinsamen Stunden im Labor mit Joyce und Stephan zurück. Thomas und Anne danke ich für unzählige Kleinigkeiten, die von der Hilfe bei LC-MS Quantifizierungen bis zum spontanen Zapfen von Seewasser reichen.

Dr. Natalja Rakowsky und Dr. Malte Thoma danke ich für das Implementieren von GAMESS und ORCA auf dem HPC-System „Ollie“ und die schnelle und kompetente Hilfe bei Problemen mit „Ollie“. Für ihre Ratschläge bei den *in silico* Methoden möchte ich mich herzlich bei Dr. Tobias Bormann und Florian Kleemiß bedanken.

Für die Hilfe bei der Aufnahme von CD Spektren möchte ich mich bei Dr. Jana Backenköhler, Prof. Dr. Peter Spiteller und Prof. Dr. Lucio Colombi Ciacchi bedanken.

Nicht vergessen möchte meine Familie und Freunde, die mich durchgängig während des Studiums und dem Anfertigen der Arbeit unterstützt haben.

Table of contents

1. General Introduction.....	1
1.1 Harmful algal blooms (HABs) – definition, environmental and societal context.....	1
1.2 Chemical Ecology of dinoflagellates	5
1.3 Biological and chemical diversity of microalgal toxins.....	7
1.4 Legislative regulation of microalgal toxins	21
1.5 Risk assessments of novel toxin derivatives.....	26
1.6 Aims and objectives of this thesis.....	29
2. Identification of novel neurotoxic gymnodimines and spirolides from the marine dinoflagellate <i>Alexandrium ostenfeldii</i>	31
3. Identification of novel Azaspiracids from <i>Azadinium poporum</i>	47
3.1 Introduction	48
3.2 Results and discussion.....	49
3.3 Conclusion	56
3.4 Material and Methods.....	56
4. Full relative assignment of stereochemistry and conformational analysis of GYMs and SPXs by NMR- and molecular modeling-based techniques.....	59
4.1 Introduction	59
4.2 Results and discussion.....	61
4.3 Conclusion	76
4.4 Material and Methods.....	77
5. Summary.....	79
6. Zusammenfassung.....	81
7. Index of abbreviations	83
8. References.....	86

9. Supporting Information's.....	100
9.1 Identification of novel neurotoxic gymnodimines and spirolides from the marine dinoflagellate <i>Alexandrium ostenfeldii</i>	100
9.2 Identification of novel Azaspiracids from <i>Azadinium poporum</i>	163
9.3 Full relative assignment of stereochemistry and conformational analysis of GYMs and SPXs by NMR- and molecular modeling-based techniques	185

1. General Introduction

1.1 Harmful algal blooms (HABs) – definition, environmental and societal context

The marine environment accounts for 70% of the world's surface area (Raymont, 2014). Microbial eukaryotes are an important component of this biome, contribute substantially to global primary production (roughly 50%) and form an important part of the marine food chain (Hallegraeff, 2010; Reynolds, 2007). In most cases, a massive proliferation of the marine phytoplankton, which represents a bloom event, has a positive influence on marine ecosystems (Raymont, 2014). However, in certain cases microbial eukaryotes produce secondary metabolites that are toxic to other organisms in the food chain (such as fish, marine mammals and humans) and pose a negative impact on the ecosystem. Hence, these events are called Harmful Algal Blooms (HABs) (Hallegraeff, 1993).

Commencing with the book Exodus in the Bible (*New International Version*, Exod. 10) (Biblica, 2011), events which could be recognized as HABs are reported throughout history. The transformation of the river Nile into a bloodlike appearance was the first of the ten plagues of Egypt. These phenomena are known as “red tides”, a special type of HABs characterized by discoloration of the water, often with algae of the class *Dinophyceae* as causative organisms (Schoental, 1984). The massive proliferation of dinoflagellates may lead to a discoloration of the water and a mass mortality of aquatic organisms either through production of toxic compounds or through generation of anoxic conditions (Hallegraeff, 1993). It is likely that even the name Red Sea derives from blooms of dinoflagellates and the resulting discoloration of the water (Culotta, 1992).

On his expedition to the coast of British Columbia, Captain George Vancouver had to mourn the death of one man among his crew after consumption of shellfish. The chronic of this disease highly resembled a classical description of a fatal episode of paralytic shellfish poisoning (PSP) (Acres and Gray, 1978). The mussels were harvested in June 1793 in a small cove near Baranof Island (Alaska, USA) (Acres and Gray, 1978). Vancouver subsequently named the bay Poison Cove (Acres and Gray, 1978). Only three years earlier the Russian expedition of Alexander Baranow suffered the loss of some 100 men due to a disease they called “mussel poisoning” on Baranof Island (Anderson, 1960). Further, Vancouver reported about a taboo of local Indian tribes, where it is off-limits to eat shellfish when the seawater became phosphorescent due to dinoflagellate blooms (Hallegraeff, 1993).

In recent history, during the middle of the past century, the frequency and intensity of HABs with noxious and/or toxic dinoflagellates as causative organism has increased (Figure 1.1) (Anderson, 1989; Imai *et al.*, 2006). A recent example was a massive bloom of *Karenia brevis*,

which led to a state of emergency in Florida (USA) in summer 2018. The bloom began in November 2017 and lasted until after October 2018. The bloom affected the coast at a length of 240 km and killed many marine animals due to the neurotoxic brevetoxin. Besides a dead whale shark at the shore, the death of at least a hundred manatees, a dozen dolphins, thousands of fish and 300 sea turtles was reported (Resnick, 2018). The tourism industry suffered due to the smell of rotting marine animals and the risk of skin and eye irritation from swimming in red tide waters. The neurotoxin can be even part of aerosol particles that are formed directly from the ocean, the so called sea spray, and affected people with asthma or other respiratory issues onshore. Lifeguards had to wear gas masks at the hardest-hit stretches of shoreline. Possible long-term effects of breathing air with the toxin are completely unknown (Resnick, 2018).

This example illustrates the broad impact of HABs on human health and economy. The main economic sectors impacted by HABs are:

1. Tourism: smell, deterrent effect of dead animals, health concern for swimmer
2. Fishery: massive loss of fish stocks and resulting lower fishing quotas
3. Shellfish production: ban of shellfish harvest, risk of loss of shellfish stocks

Despite the ban of shellfish harvest during the presence of toxin producing microalgae, over 60,000 cases of food poisoning with toxins produced by microalgae are reported annually (van Dolah, 2000). This number could be an underestimation because some symptoms associated with microalgal toxins, particularly those involving gastrointestinal symptoms, are often incorrectly diagnosed for example as food poisoning from spoiled seafood (Zingone and Enevoldsen, 2000). Estimates of fatal episodes of this kind of poisoning exceed several hundred cases annually (Zingone and Enevoldsen, 2000). A mortality rate of 15% was estimated for paralytic shellfish poisoning, a type of intoxication with contaminated shellfish (Hallegraeff, 1993).

Various factors, primarily of anthropogenic nature, are linked to the frequency and intensity of HAB events (van Dolah, 2000). Toxic dinoflagellates were observed in previously unaffected regions (Dickman and Zhang, 1999; Hallegraeff, 1998; Zhang and Dickman, 1999). Ballast water, which is used to enhance stability of ships without full loading, is a possible vector for introduction of nonindigenous and invasive species to new ecosystems (Cariton and Geller, 1993; Dickman and Zhang, 1999; Hallegraeff, 1998; Zhang and Dickman, 1999). Atmospheric deposition from agricultural, urban, and industrial sources, which bypasses estuarine processes that filter terrestrial sources of nitrogen, caused an long term increase in concentrations of dissolved inorganic nitrogen, which is a limiting nutrient in oceanic, estuarine, and coastal waters (Nixon, 2012; Paerl and Whitall, 1999; van Dolah, 2000). In coastal waters

of developing countries, nitrogen as well as phosphorus concentrations increased by more than four-fold in comparison to several decades ago (Nixon, 2012). Evidence showed a connection between enhanced nutrient load and increased incidence of certain harmful algal blooms (Hallegraeff, 1993; Paerl and Whitall, 1999; van Dolah, 2000). In addition to the eutrophication, the increased total nutrient load, nutrient ratios were altered by anthropogenic sources (Hallegraeff, 1993; Paerl and Whitall, 1999; van Dolah, 2000). Especially low ratios of silica to nitrogen (Si:N) and phosphorous (Si:P) favored growth of dinoflagellates over silica-dependent diatoms (Smayda, 1990).

After a maximum number of red tide incidents in 1976, a decreasing trend of HAB events was observed in the Seto Inland Sea (Figure 1.1) (Imai *et al.*, 2006). This development was a result of the legislative in 1973 to decrease the anthropogenic loading, which had a positively influence the progression of red tide species in this area (Imai *et al.*, 2006). Here, the red tide induced economical damage called for the intervention of the legislative authority. This example demonstrates the long term influence human activities can exert on HAB events.

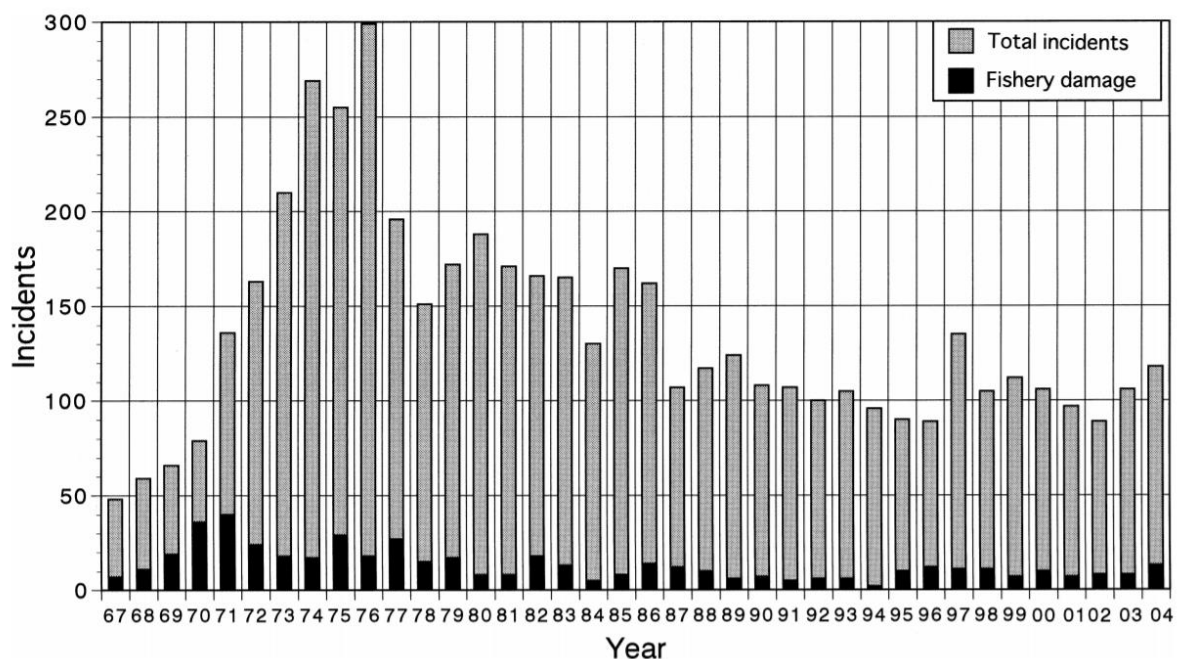


Figure 1.1: Occurrence of red tides in the Seto Inland Sea from 1967 to 2004. Black filled columns indicate incidents with fishery damage such as fish-kills (Imai *et al.*, 2006).

Climatic factors are also linked to the appearance of HABs (van Dolah, 2000). Unusual climatic conditions, such as drought, storm events that produce heavy rainfall, and El Niño Southern Oscillation (ENSO), alter the local conditions and could thereby trigger blooms of dinoflagellates in areas previously unknown for such incidents (Hallegraeff, 2010). For example, conditions caused by the phenomenon of ENSO seem to favor the growth of dinoflagellates in some regions, while in other regions they had a negative correlation between appearance of dinoflagellate blooms and ENSO conditions (Ochoa, 2003).

In addition to short-term climatic events, such as ENSO, long term (global) changes also seem to influence HAB occurrences and intensities (van Dolah, 2000). Increased global average temperature due to climate change, also enhance surface stratification, alter ocean currents, intensify or weaken local nutrient upwelling, stimulate photosynthesis due to elevated CO₂ levels and reduce calcification due to decreased seawater pH (“the other CO₂ problem”) (Hallegraeff, 2010). However, a direct relationship between global climate change and increase of HAB incidences can be confounded by factors such as increased population and industrialization during the same time-span, complicating a direct assignment of HAB increases to climate change (van Dolah, 2000).

HABs will likely further increase in the future as the human population is assumed to rise by over 30% until 2050 (Wilmoth, 2017). To sustain the increased human population, an expansion of production of food resources by agriculture and aquaculture is inevitable, including advance of technologies (van Dolah, 2000). This would further enhance the eutrophication of coastal waters, favoring HABs.

1.2 Chemical Ecology of dinoflagellates

In total, the class *Dinophyceae* covers approximately 2377 species (Gómez, 2012). About 200 species of this phylum are attributed with the ability to form red tides (Smayda and Reynolds, 2003). The red tides, induced by these species, include benign red tides as well as harmful blooms. Only roughly 90 species of the class *Dinophyceae* are attributed with the ability to form toxic HABs (Moestrup *et al.*, 2009 onwards). The *Dinophyceae* are an ancient group of unicellular microbial eukaryotes, named due to a characteristic whirling movement by two flagella. Besides insertion of flagellar, golden-brown plastids, assimilative cell with indented waist, and relatively large nucleus that contains visible chromosomes are also typical characteristics of this genus (Carty and Parrow, 2015). Some members are armored with cellulose plates, which are colloquially called “thecate”, while other species exist unarmored (“athcate”). Even though the members of this group of microalgae are comparatively inefficient at nutrient uptake and show slower growth than other planktic members, they can dominate the plankton (John *et al.*, 2015; Smayda and Reynolds, 2003). Their ecological success is supposed to be the result of their extraordinary physiological diversity and adaptation to specific ecological niches (Dyhrman, 2008). Many dinoflagellates exhibit a mixotrophic life style, that is they employ phototrophic autotrophy (usage of solar energy and inorganic nutrients) and phagotrophic heterotrophy (ingestion of particulate organic matter) as modes to acquire of energy, micro- and macronutrients (Glibert *et al.*, 2008; Stoecker, 1999). Many dinoflagellates act as symbionts or parasites (Hoppenrath *et al.*, 2014). Notably, they produce complex chemical compounds which impact on interactions with competitors and predators (Selander *et al.*, 2006; Tillmann *et al.*, 2008).

Further, different individuals of a single species can differentially express traits, such as cell size, cell shape and the production of secondary metabolites (Wohlrab *et al.*, 2016). This variability reaches even the genetic level of populations on a global level as well as within spatially restricted populations (Wohlrab *et al.*, 2016). Each genetic variant represents a single genotype and these genotypes possess the ability to express traits differently than the other genotypes (Alpermann *et al.*, 2010). Through the differently expressed traits, the single genotypes have an advantage under specific environmental conditions. However, periods with advantageous environmental conditions for one genotype do not suffice to outcompete the other genotypes (Alpermann *et al.*, 2010; Wohlrab *et al.*, 2016). The resulting presence of various genotypes on global scale and within spatially restricted populations, is considered as one of the paradoxes of the plankton (Fox *et al.*, 2010; Hebert and Crease, 1980).

A diverse suite of toxic compounds are known to be produced by dinoflagellates. “Different genotypes within one population can differentially express traits, such as cell size, cell shape and the production of secondary metabolites.” (Wohlrab *et al.*, 2016) In addition to a

quantitative dimension, the production of secondary metabolites differs at the qualitative level. For toxic compounds of dinoflagellates, a broad range of chemical compounds is known (see 1.3). Even though the possible effect of most known compounds on humans is well studied, their ecological purpose remains enigmatic (Sheng *et al.*, 2010). Studies of paralytic shellfish poisoning inducing toxins (PST) exemplify here a possible ecological function of dinoflagellate toxins.

Paralytic shellfish toxins (PST) have been hypothesized to act as a chemical defense against grazing zooplankton (Selander *et al.*, 2006). The predator-prey interactions between dinoflagellates and grazers, such as copepods, are complex (Turner and Tester, 1997). Some copepods ingested PST producing dinoflagellates with no apparent adverse effect, they even seemed to store the toxins several days in their bodies past the time of gut clearance (White, 1981). These toxin containing copepods can be a vector of the toxins to higher trophic levels (White, 1981). In other experiments, however, showed adverse effects of PST-producing dinoflagellates on copepods (Turner and Tester, 1997).

In grazing experiments, copepods showed lower feeding rates on PST producing dinoflagellates than on non-toxic diatoms (Huntley, 1982). Even the bioluminescence of dinoflagellates had a detrimental effect on the feeding behavior of copepods in lab experiments (White, 1979). In coastal waters, areas with high densities of toxic dinoflagellates have been reported to be actively avoided by some copepods (Fiedler, 1982). Further, the interaction between dinoflagellates and copepods seem to also have an influence on the physiology of some dinoflagellates. These dinoflagellates react to the presence of copepods with an increased production of toxic compounds (Selander *et al.*, 2015).

In addition to antigrazing defense, some dinoflagellates use their toxins to hunt for prey themselves (Place *et al.*, 2012). Predation of *Storeatula major*, an unicellular algae, by the dinoflagellate *Karlodinium micrum*, for example, is significant higher in presence of Karlotoxin (KmTX) (Adolf *et al.*, 2006) which immobilizes prey cells (Sheng *et al.*, 2010).

In the studies mentioned above, various genotypes have been tested and the observed effects varied significantly for the different genotypes (*e. g.* Sheng *et al.*, 2010; Turner and Tester, 1997; White, 1979). The interspecies interactions of dinoflagellates could differ for various genotypes, as the genotypes show qualitatively and quantitatively different toxin profiles.

1.3 Biological and chemical diversity of microalgal toxins

Microalgal toxins, primarily of the polyketide group, exhibit a remarkable range of potent biological activities, including ion channel modulation, phosphatase inhibition, hemolysis, mycotoxicity and cytotoxicity (van Wagoner *et al.*, 2014). The marine biotoxins responsible for food poisoning have been historically divided into six groups based on symptoms, origin, and chemical structure (Table 1.1) (Stivala *et al.*, 2015). However, the range of dinoflagellates that produced secondary metabolites exceeds the selection of compounds with oral toxicity (Figure 1.2). Spiroimine toxins, for example, are characterized by a macrocycle and an imine group embedded in a ring system, are potent neurotoxins but nonpoisonous to humans after oral ingestion (and therefore not represented in Table 1.1).

Each group of dinoflagellate secondary metabolites comprise several derivatives. Both groups of azaspiracids and derivatives of saxitoxins (responsible for paralytic shellfish poisoning (PSP)) comprise more than 20 known derivatives (Alpermann *et al.*, 2010; Hess *et al.*, 2014). Even though dinoflagellates may produce the whole range of structural derivatives, the toxin profile of single genotypes is dominated by only a few derivatives (Alpermann *et al.*, 2010). This poses a challenge for food safety monitoring: Each HAB is characterized by its own toxin profile. Therefore, in the case of AZAs for example, over 40 derivatives would have to be consistently monitored to ensure food safety (Hess *et al.*, 2014; Kilcoyne *et al.*, 2018; Rehmann *et al.*, 2008). Toxins often differ only in a small parts of the molecule, but these modifications alter the bioactivity of the compounds (Hess *et al.*, 2014; Kilcoyne *et al.*, 2018). This thesis mainly covers structural derivatives of spirolides, gymnodimines (both chapter 1.3.1), and azaspiracids (chapter 1.3.2) which are introduced in more details in the following sections.

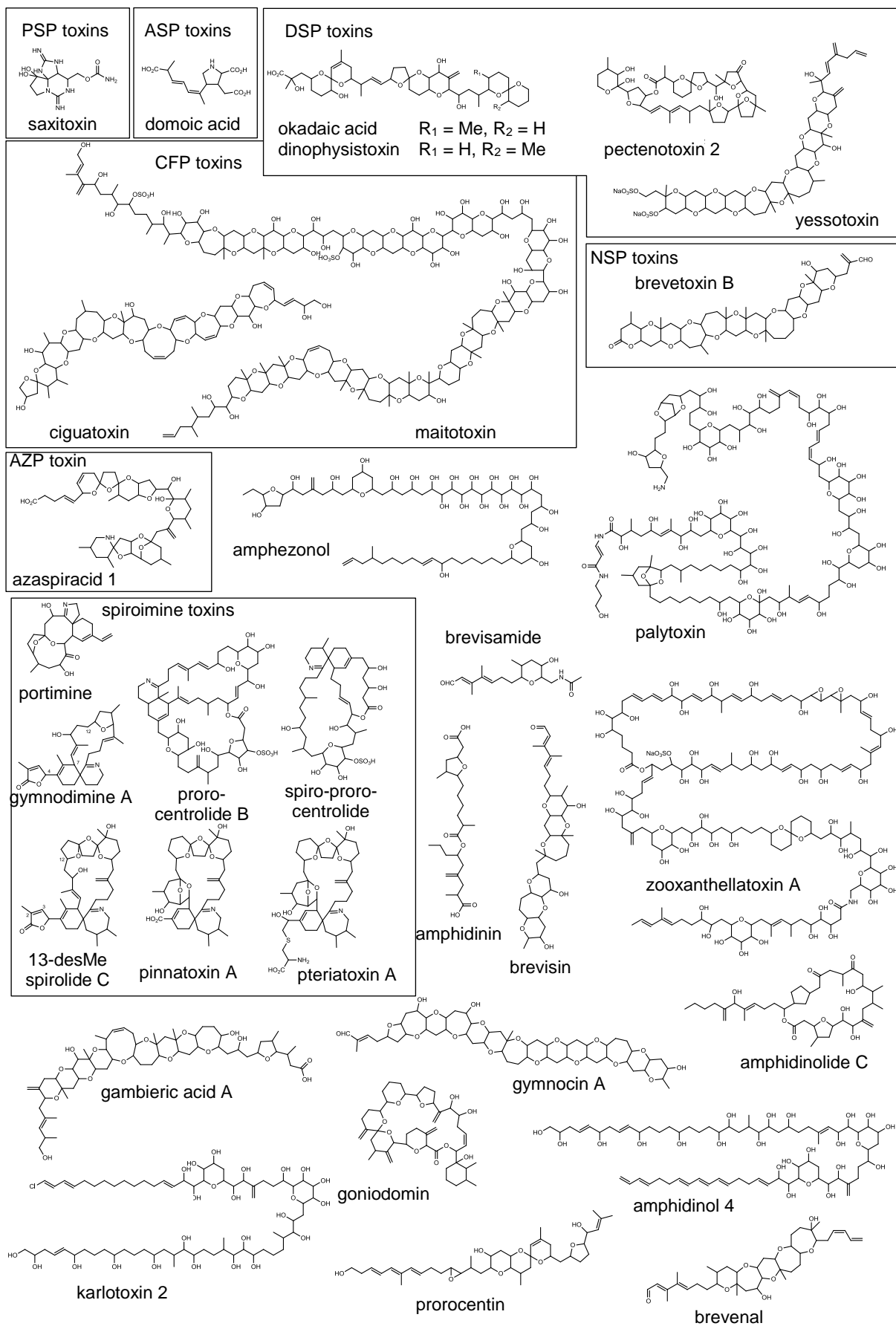


Figure 1.2: Overview of prominent members of dinoflagellate secondary metabolites toxin classes.

Table 1.1: Categories of important biotoxin poisonings: paralytic shellfish poisoning (PSP), amnesic shellfish poisoning (ASP), diarrhetic shellfish poisoning (DSP), azaspiracid poisoning (AZP), neurotoxic shellfish poisoning (NSP), ciguatera fish poisoning (CFP); modified after Bürk *et al.* and Yasumoto (Bürk *et al.*, 1998; Chevallier *et al.*, 2015; Yasumoto, 2000).

	PSP	ASP	DSP	AZP	NSP	CFP
Biological origin	<i>Alexandrium</i> <i>Gymnodinium</i> <i>Pyrodinium</i>	<i>Pseudonitzschia</i>	<i>Dinophysis</i> <i>Prorocentrum</i> <i>Protoceratium</i>	<i>Azadinium</i>	<i>Gymnodinium breve</i>	<i>Gambierdiscus toxicus</i>
Toxin groups	saxitoxin and derivatives	domoic acid (DA)	okadaic acid (OA) pectenotoxin (PTX) dinophysistoxin (DTX) yessotoxin (YTX)	azaspiracid (AZA)	brevetoxin (BTX)	ciguatoxin maitotoxin
Symptoms	paraesthesia; paralyses	memory loss; gastrointestinal disorders	gastrointestinal disorders	gastrointestinal disorders	paraesthesia; ichthyotoxin	paraesthesia; gastrointestinal disorders
Mode of action	blockage of sodium channels	excitatory neurotransmitter	inhibition of protein phosphatases	inhibition of sodium channels	activation of sodium channels	activation of sodium channels
Contaminated food	shellfish	shellfish	shellfish	shellfish	shellfish	fish
Concentration limit (EU)	800 µg/kg shellfish	20 mg/kg shellfish	160 µg/kg shellfish for OA, PTX 1 mg/kg shellfish for YTX	160 µg/kg shellfish	none	none
Regulated toxins (EU)	undefined	DA	OA; PTX 1, 2; DTX 1, 2, 3 (inclusive Esters); YTX, Homo YTX, 45-OH YTX and 45-OH Homo YTX	AZA-1, -2, -3	none	none

1.3.1 Diversity of spirolides and gymnolimines

In 1993 during a routine monitoring of shellfish in New Zealand, oysters were found to be contaminated with a potent mouse neurotoxin (MacKenzie *et al.*, 1995). Shortly after this incidence gymnolimine (GYM) A (**1**) was first described in the marine dinoflagellate *Gymnodinium* sp. (later renamed to *Karenia selliformis*) and identified as the causative compound (Seki *et al.*, 1995). The exact stereochemistry of (**1**) was elucidated by X-ray crystal structure analysis (Stewart *et al.*, 1997). In 2000, GYM B (**2**) was described in *K. selliformis* as a derivative of GYM A (**1**), but with an exocyclic methylene at C-17 and an allylic hydroxyl group at C-18 (Miles *et al.*, 2000). Only three years later, the same authors reported the presence of GYM C (**3**) in *K. selliformis*, which is an isomer of GYM B at C-18 (Miles *et al.*, 2003). Currently, six gymnolimines are fully structurally elucidated (*cf.* Figure 1.3).

Concurrently with the discovery of GYM B and GYM C in Atlantic Canada, *Alexandrium ostenfeldii* was identified as the source of spirolides (Cembella, 2001). These toxins have a similar toxicological effect on mice than gymnolimines and were structurally related to this toxin group (Cembella, 2001). In 2011, van Wagoner *et al.* (van Wagoner *et al.*, 2011) reported the production of 12-methyl GYM A in an isolate of *Alexandrium peruvianum* from New River, NC, USA. *A. peruvianum* is now regarded as conspecific with *Alexandrium ostenfeldii* (Kremp *et al.*, 2014). The occurrence of GYMs in *A. ostenfeldii* was notable as for the first time another genus than *Karenia* was associated with the biosynthesis of gymnolimines. Due to the occurrence in the same dinoflagellate and the high structural similarity to gymnolimines and spirolides, a common biosynthetic pathway for these cyclic imines was proposed (*cf.* chapter 1.3.4) (van Wagoner *et al.*, 2014).

GYMs and SPXs belong to the group of cyclic imine toxins, characterized by a macrocycle and an imine group embedded in a ring system (Molgó *et al.*, 2017). In addition to GYMs and SPXs, the group of cyclic imine toxins comprises pinnatoxins (*Vulcanodinium rugosum*)/pteriatoxins (unknown), portimines (*Vulcanodinium rugosum*), prorocentrolides (*Prorocentrum lima*), and spiro-prorocentrimines (*Prorocentrum* sp.) (Molgó *et al.*, 2017; Selwood *et al.*, 2013; Stivala *et al.*, 2015).

The structural comparison of SPXs and GYMs reveals some conserved features for all known GYMs and SPXs. For example all GYMs and SPXs share the moiety of a five membered ester ring (Figure 1.3, ring A) attached to a cyclohexene ring (Figure 1.3, ring B). The two compound classes are distinguished by ring C (Figure 1.3). While ring C of GYMs consists of a six-membered cyclic imine moiety without attached methyl groups, ring C of SPXs is a seven-membered cyclic imine moiety with one or two attached methyl groups. The side chain of SPXs (C-8 to C-27) exhibits a spiro fused ether ring system. Three different variations are observed

of the side chain for known SPXs. Therefore, SPXs are differentiated by the degree of methylation of ring C and the chemical composition of the side chain. For discrimination of different GYMs, only the structure of the side chain matters (Figure 1.3) (Stivala *et al.*, 2015), which is divided in two parts. For each part of the gymnodimine side chain, two possible moieties are observed (Figure 1.3 left side: blue and green).

This structural diversity is not reflected in the mouse bioassay, as both GYMs or SPXs result in an “all or nothing”-effect after intraperitoneal injection only at different amounts of toxin (Otero *et al.*, 2011). Either the mice died within 20 min after intoxication or a complete recovery without observed consequential damages was observed (Otero *et al.*, 2011). Initially, gymnodimines were described as neurotoxic (Seki *et al.*, 1995), but later it became evident that they bind specifically to muscular and neuronal nicotinic acetylcholine receptors (Bourne *et al.*, 2010; Gill *et al.*, 2003; Kharrat *et al.*, 2008). For the human nicotinic acetylcholine receptors 13-desmethyl SPX C (SPX 1, 4), the best-studied representative of the group of SPXs, is a competitive irreversible antagonism, while GYM A is a competitive reversible antagonism (Richard *et al.*, 2001; Wandscheer *et al.*, 2010). Further 13-desmethyl SPX C is identified as weak activator of L type calcium channels (Hu *et al.*, 1995).

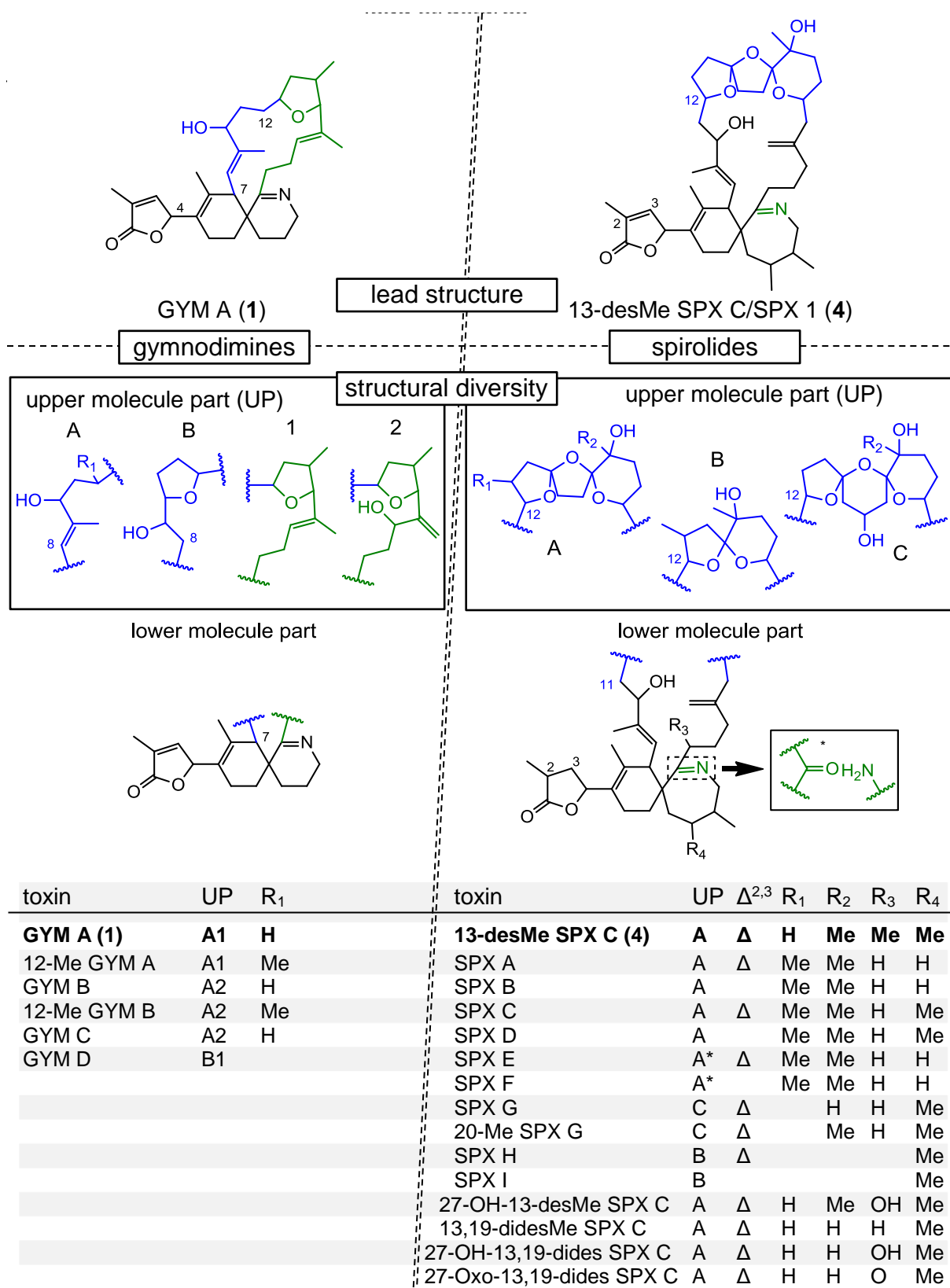


Figure 1.3: Most prominent member and structural derivatives of spiroptides and gymnodimines. In case of SPX E and SPX F, the imine group is replaced by the structure fragment marked with an asterisk (according to Stivala *et al.*, 2015).

1.3.2 Diversity of azaspiracids

An intoxication event in 1995 in the Netherlands led to discovery of the first azaspiracid (AZA, 5) (Satake *et al.*, 1998). At least eight people experienced symptoms known for DSP such as nausea, vomiting, severe diarrhea and stomach cramps after consumption of blue mussels (*Mytilus edulis*) cultivated in West Ireland. Mussels revealed a positive result in the mouse bioassay (MBA) even though the major DSP toxins okadaic acid (OA) and dinophysistoxins (DTXs) were not detected at elevated levels. The causative marine biotoxin was named azaspiracid and described as a nitrogen-containing polyether with a unique spiral ring assembly, a cyclic amine and a carboxylic acid (Satake *et al.*, 1998). The initially proposed structure of AZA-1 (5a, Figure 1.4) had to be revised by comparison of NMR data of the natural toxin (5, Figure 1.4) with that of the synthetic molecule (Nicolaou *et al.*, 2004). The identification of *Azadinium spinosum*, a small (< 20 μm) photosynthetic dinoflagellate with a thin theca, as a source of AZA was achieved a decade later (Tillmann *et al.*, 2009). Today AZAs are also found in other dinoflagellates of the family *Amphidomataceae*, e. g. *Azadinium poporum*, *Azadinium dexteroporum*, and *Amphidoma languida* (Krock *et al.*, 2012; Rossi *et al.*, 2017).

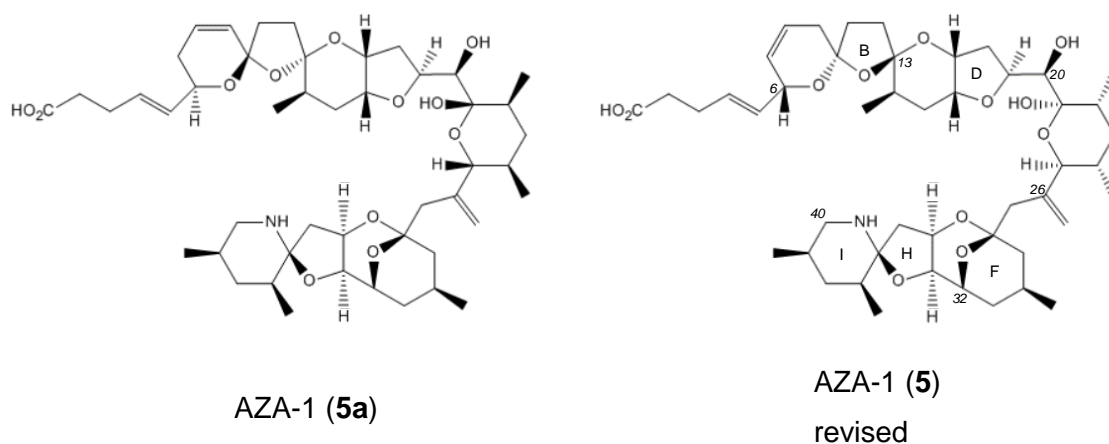
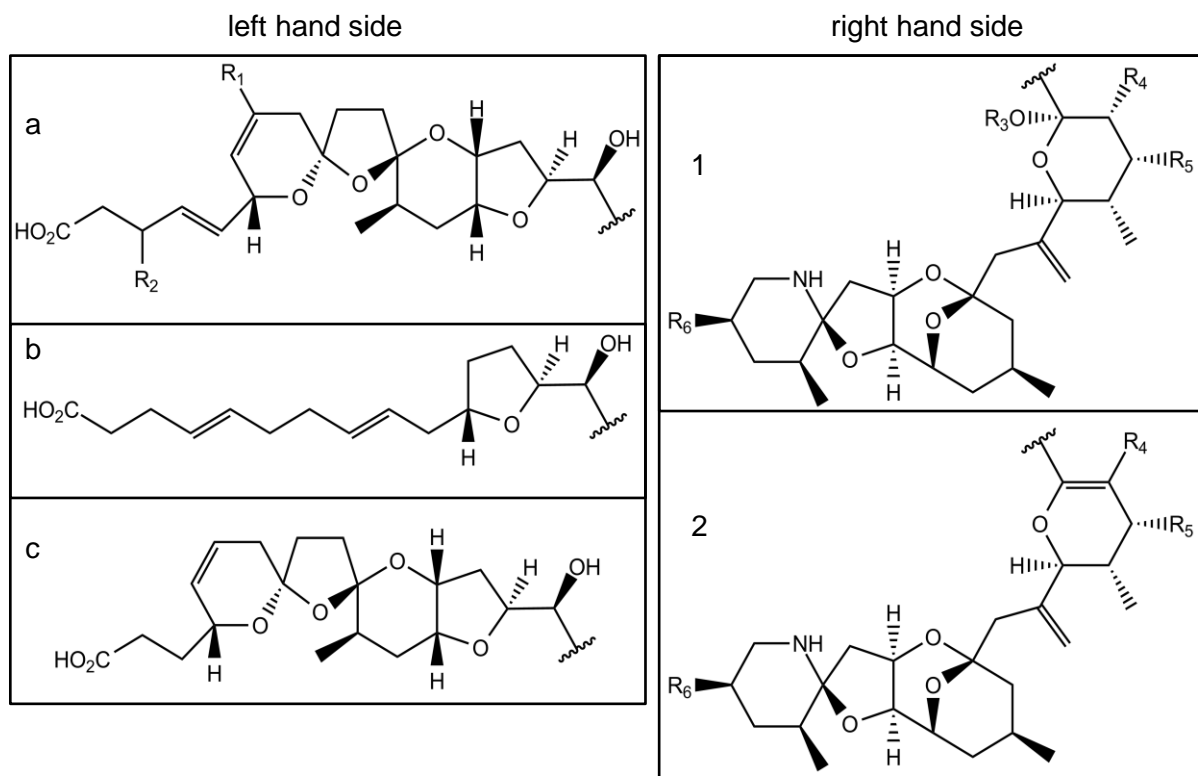


Figure 1.4: Initial incorrect structure (left) and revised structure (right) of AZA-1. Shown are fragmentation patterns of CID fragmentation (characteristic fragments in bold).

Since the discovery of AZA-1, the number of structure derivatives discovered by mass spectrometry has increased greatly (Krock *et al.*, 2019). The new derivatives are by general convention chronologically enumerated based on the time of their discovery, a practice resulting in a mixture of AZAs produced by dinoflagellate and metabolites of shellfish (Krock *et al.*, 2019). Still, most of the derivatives had their structures proposed solely by mass spectrometric investigations without confirmation e.g. by NMR spectroscopy (*cf.* section 1.5). The proposed structures are shown in Figure 1.5 and structures elucidated by NMR are highlighted in grey (Hess *et al.*, 2014). Further, only for three derivatives, concentration

thresholds in shellfish are established, namely for AZA-1, AZA-2 and AZA-3 (European Union, 2004).



	Type	R ₁	7,8	R ₂	R ₃	R ₄	R ₅	R ₆	[M+H] ⁺	Origin
AZA-1	a1	H	Δ	H	H	CH ₃	H	CH ₃	842.5	<i>A. spinosum</i>
37-epi AZA-1	a1	H	Δ	H	H	CH ₃	H	CH ₃	842.5	Abiotic
AZA-2	a1	H	Δ	CH ₃	H	CH ₃	H	CH ₃	856.5	<i>A. spinosum</i>
AZA-3	a1	H	Δ	H	H	H	H	CH ₃	828.5	Shellfish/Abiotic*
AZA-4	a1	OH	Δ	H	H	H	H	CH ₃	844.5	Shellfish/Abiotic*
AZA-5	a1	H	Δ	H	H	H	OH	CH ₃	844.5	Shellfish/Abiotic*
AZA-6	a1	H	Δ	CH ₃	H	H	H	CH ₃	842.5	Shellfish/Abiotic*
AZA-7	a1	OH	Δ	H	H	CH ₃	H	CH ₃	858.5	Shellfish
AZA-8	a1	H	Δ	H	H	CH ₃	OH	CH ₃	858.5	Shellfish
AZA-9	a1	OH	Δ	CH ₃	H	H	H	CH ₃	858.5	Shellfish/Abiotic*
AZA-10	a1	H	Δ	CH ₃	H	H	OH	CH ₃	858.5	Shellfish/Abiotic*
AZA-11	a1	OH	Δ	CH ₃	H	CH ₃	H	CH ₃	872.5	Shellfish
AZA-12	a1	H	Δ	CH ₃	H	CH ₃	OH	CH ₃	872.5	Shellfish
AZA-13	a1	OH	Δ	H	H	H	OH	CH ₃	860.5	Shellfish/Abiotic*
AZA-14	a1	OH	Δ	H	H	CH ₃	OH	CH ₃	874.5	Shellfish

	Type	R ₁	7,8	R ₂	R ₃	R ₄	R ₅	R ₆	[M+H] ⁺	Origin
AZA-15	a1	OH	Δ	CH ₃	H	H	OH	CH ₃	874.5	Shellfish/Abiotic*
AZA-16	a1	OH	Δ	CH ₃	H	CH ₃	OH	CH ₃	888.5	Shellfish
AZA-17	a1	H	Δ	H	H	CO ₂ H	H	CH ₃	872.5	Shellfish
AZA-19	a1	H	Δ	CH ₃	H	CO ₂ H	H	CH ₃	886.5	Shellfish
AZA-21	a1	OH	Δ	H	H	CO ₂ H	H	CH ₃	888.5	Shellfish
AZA-23	a1	OH	Δ	CH ₃	H	CO ₂ H	H	CH ₃	902.5	Shellfish
AZA-25	a2	H	Δ	H	-	H	H	CH ₃	810.5	Shellfish/Abiotic*
AZA-26	a2	H	Δ	H	-	H	=O	CH ₃	824.5	Shellfish/Abiotic*
AZA-27	a2	CH ₃	Δ	H	-	H	H	CH ₃	824.5	Shellfish/Abiotic*
AZA-28	a2	CH ₃	Δ	H	-	H	=O	CH ₃	838.5	Shellfish/Abiotic*
AZA-29	a1	H	Δ	H	CH ₃	H	H	CH ₃	842.5	Shellfish
AZA-30	a1	H	Δ	H	CH ₃	CH ₃	H	CH ₃	856.5	<i>A. spinosum</i>
AZA-32	a1	H	Δ	CH ₃	CH ₃	CH ₃	H	CH ₃	870.5	<i>A. spinosum</i>
AZA-33	b1	-	Δ	-	H	CH ₃	H	CH ₃	716.5	<i>A. spinosum</i>
AZA-34	c1	-	Δ	-	H	CH ₃	H	CH ₃	816.5	<i>A. spinosum</i>
AZA-35	a1	H	Δ	#	H	CH ₃	H	CH ₃	830.5	<i>A. dexteroporum</i>
AZA-36	a1	OH	Δ	CH ₃	H	CH ₃	H	H	858.5	<i>A. poporum</i>
AZA-37	a1	OH	-	H	H	CH ₃	H	H	846.5	<i>A. poporum</i>
AZA-38 ¹	a1	H	-	CH ₃	H	CH ₃	H	H	830.5	<i>Am. languida</i>
AZA-39 ¹	a1	H	-	#	H	CH ₃	H	H	816.5	<i>Am. Languida</i>
AZA-40	a1	CH ₃	Δ	H	H	CH ₃	H	H	842.5	<i>A. poporum</i>
AZA-41	a1	H	Δ	H	H	CH ₃	H	#	854.5	<i>A. poporum</i>
AZA-42		no proposed structure							870.5	<i>A. poporum</i>
AZA-43		no proposed structure							828.5	<i>Am. languida</i>
AZA-44	a1	H	Δ	H	H	CO ₂ H	OH	CH ₃	888.5	Shellfish
AZA-45	a1	CH ₃	Δ	H	H	CO ₂ H	OH	CH ₃	902.5	Shellfish
AZA-46	a1	H	Δ	OH	H	CO ₂ H	OH	CH ₃	904.5	Shellfish
AZA-47	a1	CH ₃	Δ	OH	H	CO ₂ H	OH	CH ₃	918.5	Shellfish
AZA-48	a2	H	Δ	OH	-	H	H	CH ₃	826.5	Shellfish/Abiotic*
AZA-49	a2	CH ₃	Δ	OH	-	H	H	CH ₃	840.5	Shellfish/Abiotic*
AZA-50 ²	a1	H	Δ	CH ₃	H	CH ₃	H	CH ₃	842.5	<i>A. spinosum</i>
AZA-51 ²	a1	OH	Δ	CH ₃	H	CH ₃	H	CH ₃	858.5	<i>A. spinosum</i>
AZA-52		no proposed structure							830.5	<i>Am. Languida</i>
AZA-53		no proposed structure							830.5	<i>Am. languida</i>
AZA-54	a1	H	Δ	#	H	CH ₃	H	CH ₃	870.5	<i>A. dexteroporum</i>

	Type	R ₁	7,8	R ₂	R ₃	R ₄	R ₅	R ₆	[M+H] ⁺	Origin
AZA-55	a1	H	Δ	#	H	CH ₃	H	#	868.5	<i>A. dexteroporum</i>
AZA-56	a1	H	Δ	#	H	CH ₃	H	CH ₃	884.5	<i>A. dexteroporum</i>
AZA-57	a1	H	Δ	#	H	CH ₃	H	CH ₃	844.5	<i>A. dexteroporum</i>
AZA-58	a1	H	Δ	#	H	CH ₃	H	CH ₃	828.5	<i>A. dexteroporum</i>
AZA-59	a1	H	-	OH	H	CH ₃	H	CH ₃	860.5	<i>A. poporum</i>
AZA-60	a2	H	Δ	H	-	H	OH	CH ₃	826.5	Shellfish/Abiotic*
AZA-61	a2	CH ₃	Δ	H	-	H	OH	CH ₃	840.5	Shellfish/Abiotic*
AZA-62	no proposed structure								870.5	<i>A. poporum</i>

Figure 1.5: Proposed derivatives of AZAs with respective mass of the protonated ion ([M+H]⁺) and origin reviewed by Hess *et al.* (Hess *et al.*, 2014) and Kilcoyne *et al.* (Kilcoyne *et al.*, 2018), updated with (Kim *et al.*, 2017; Krock *et al.*, 2019; Krock *et al.*, 2014; Krock *et al.*, 2012; Rossi *et al.*, 2017; Tillmann *et al.*, 2018; Tillmann *et al.*, 2017). Compounds confirmed by NMR are highlighted in grey; compounds highlighted in blue have confirmed structures following decarboxylation to known products; compounds highlighted in yellow have confirmed structures following heat/acid-catalysis to known compounds; compounds highlighted in white have structures inferred by mass spectrometry only; the Type refers to variations of the left hand side and right hand side parts of the molecule. AZA-18, -20, -22, -24, and -27 proposed by Rehmann *et al.* (Rehmann *et al.*, 2008) have been confirmed not to exist naturally; * potential degradation product of natural precursor toxin; # for R₂:proposed with modification of the side chain and/or at ring A (C-1 to C-10); # for R₆: with modification at ring H or ring I; ¹: proposed with demethylation at C-14; ²: proposed with demethylation at C-23.

1.3.3 Biosynthesis of dinoflagellate polyketides

The majority of the toxic compounds produced by dinoflagellates are lipophilic polyketides (van Wagoner *et al.*, 2014). Only few small organic precursors, namely glycolate and glycine, are used beside acetate units by dinoflagellates in the production of polyketides (MacKinnon *et al.*, 2006; van Wagoner *et al.*, 2014; Yamazaki *et al.*, 2011). In comparison to the variety of building blocks utilized by bacteria and fungi, the group of precursors in dinoflagellate polyketide synthesis is limited, whereby the remarkable complexity and variety of dinoflagellate polyketides is even more extraordinary (van Wagoner *et al.*, 2014).

Marine biotoxins occur in a remarkable structural variety with unique features, such as five-, six-, seven-, eight-, and nine-membered ether rings (van Wagoner *et al.*, 2014). In dinoflagellate polyketides, ether rings occur isolated, in spiroketal formations or fused together (van Wagoner *et al.*, 2014). Fused ether rings can contain only two rings (*e. g.* Azaspiracid 1 (5) (Satake *et al.*, 1998)) or as many as eleven as in brevetoxin (Lee *et al.*, 1986; Lin *et al.*, 1981). Often dinoflagellate biotoxins contain series of *trans* fused ether rings, with *syn* stereochemistry across the top and bottom of the molecules, such as in brevetoxin (Rein and Borrone, 1999). The ether oxygen atoms, which acts as one-atom bridge, alternate between the top and bottom side of the molecule (Rein and Borrone, 1999).

These common features can be explained by a biosynthetic pathway for fused ether ring systems in dinoflagellates (Rein and Borrone, 1999). In general polyketides are built, similar to fatty acids, as series of CLAISEN ester condensations with “activated acetate” units in form of malonyl coenzyme A to a start of an acetyl coenzyme A unit until a polyketide chain of the required length and functionality is obtained (Figure 1.6A) (van Wagoner *et al.*, 2014). In contrast to fatty acid biosynthesis, where a saturated acyl chain with little functionality is obtained through ketoreduction, dehydration, and enoyl reduction for each acetate unit, polyketide secondary metabolites show a broad structural variety (van Wagoner *et al.*, 2014). The functional variety of these compounds arises when some or all of the polyketide processing steps are omitted or skipped, resulting in nascent polyketide chains (NPC) containing carbonyl groups (lack of ketoreduction function), hydroxyl groups (lack of dehydration function) and double bonds (lack of an enoyl reduction function) (van Wagoner *et al.*, 2014). In some cases, other small carboxylic acids are used during for NPCs (van Wagoner *et al.*, 2014), carbons of the NPC can be removed (carbon deletion) and methyl group can be added in various ways (β -alkylation, pseudo α -alkylation or methionine derived methyl) (review by van Wagoner *et al.*, 2014). Fused ether ring systems are supposed to form via epoxidation of polyene in the NPC followed by polyepoxide cyclisation (see Figure 1.6B) (Rein and Borrone, 1999). Observations of the incorporation of molecular oxygen in ring systems of a

dinoflagellate polyketide by labeling experiments supports the hypothesized epoxide intermediate (Murata *et al.*, 1998).

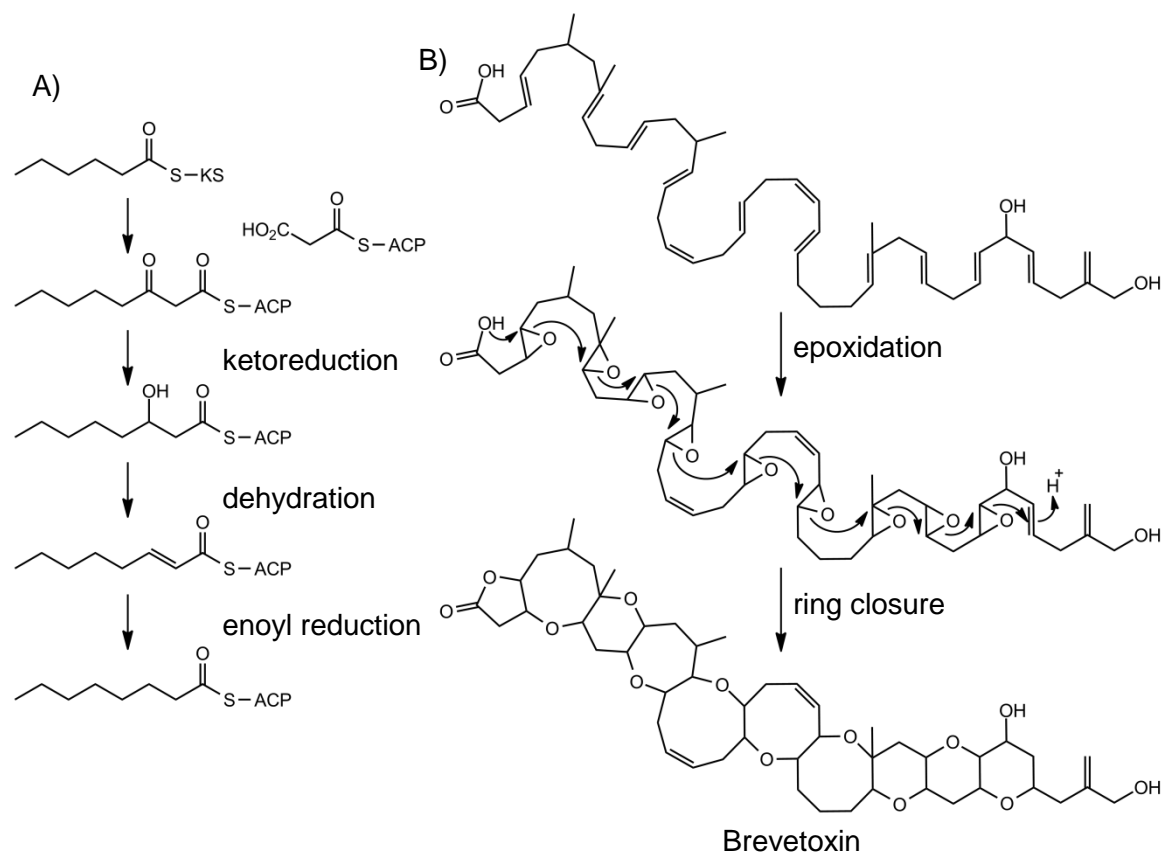


Figure 1.6: Prolongation of polyketide chains (A) and proposed ring closure reaction at the example of brevetoxin (B).

1.3.4 Biosynthesis of spirolides and gymnodimines

The high structural similarity and production through the same organism indicates a common biosynthetic pathway for SPXs and GYMs (van Wagoner *et al.*, 2011). For both groups of polyketides, NPCs have been proposed (Harju *et al.*, 2016; van Wagoner *et al.*, 2014). In case of SPX 1, the polyketide nature has been verified by incorporation experiments with isotope labeled precursors (MacKinnon *et al.*, 2006). These experiments gave insight into the origin of carbon atoms in SPX 1 (see Figure 1.7). Originating from the unfolded nascent polyketide chain (4a) the formation of ring A by ester formation and ring C by nucleophilic attack was suggested (van Wagoner *et al.*, 2014). These reactions were followed by the formation of the spiro fused ether ring system by usage of carbonyls and DIELS ALDER reaction leading to 13-desmethyl SPX C (cf. Figure 1.7) (van Wagoner *et al.*, 2014). The formation of GYM D side chain was proposed by an ether formation via epoxidation establishing ring D and E, as shown in Figure 1.6 for brevetoxin (Harju *et al.*, 2016). Similarly, NPCs as 4a have been proposed for

GYM A, 12-methylGYM A, and GYM D (Harju *et al.*, 2016; van Wagoner *et al.*, 2011; Zurhelle *et al.*, 2018).

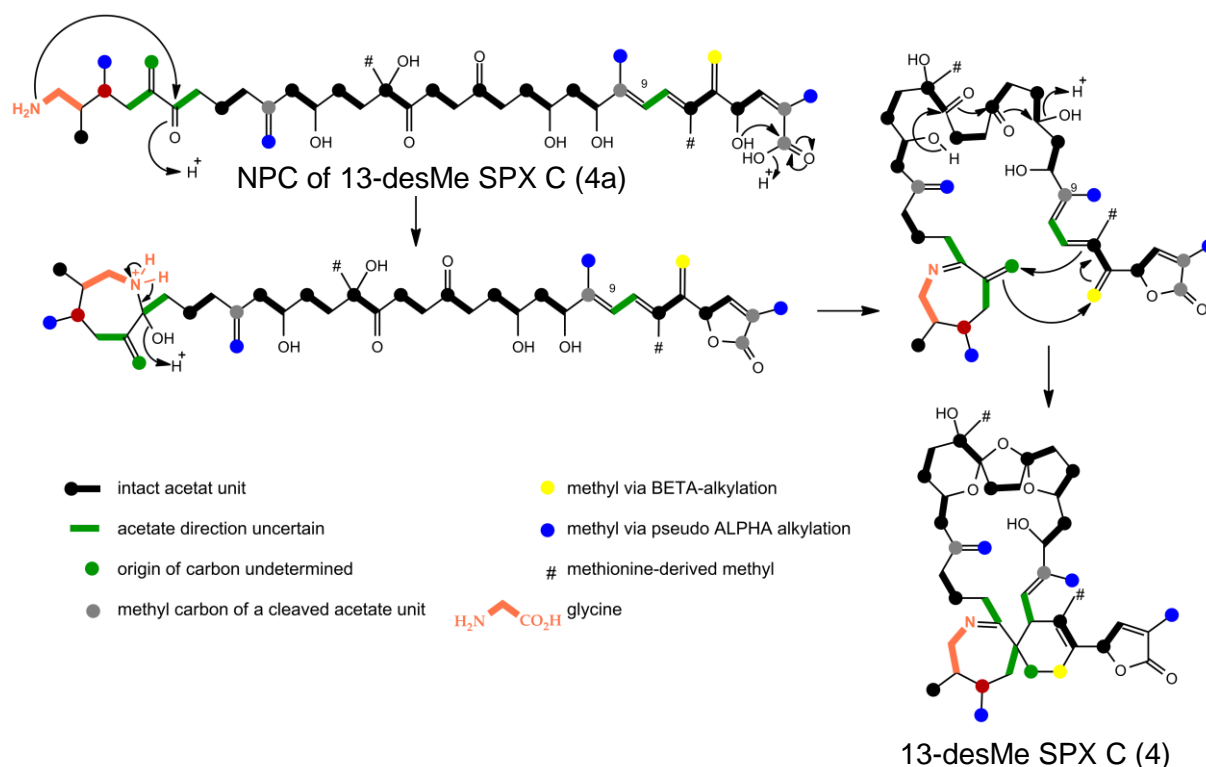


Figure 1.7: Biosynthesis of SPX1 (4) based on the proposed NPC (4a) and origin of carbons according to MacKinnon *et al.* and van Wagoner *et al.* (MacKinnon *et al.*, 2006; van Wagoner *et al.*, 2014).

1.3.5 Biosynthesis of azaspiracids

The biosynthesis pathway of AZAs is yet to be established. Current work suggests biosynthesis *via* a polyketide pathway analogue to other dinoflagellate secondary metabolites (Kalaitzis *et al.*, 2010). The application of biosynthetic principles, observed for other dinoflagellate polyketides, on AZAs suggests a ring formation as shown in Figure 1.8. The nitrogen atom could derive from a glycine unit as in spirolides (cf. chapter 1.3.4). However, in order to confirm the hypothetical biosynthesis of AZAs, feeding studies are required (Kalaitzis *et al.*, 2010).

For the synthesis of AZAs, a convergent strategy was applied. The key steps are a dithiane coupling between a molecule fragment with ABCD ring system and a molecule fragment with ring E, and a Stille coupling between the product of the preceding reaction and molecule fragment with FGHI ring system (Nicolaou *et al.*, 2006; Nicolaou *et al.*, 2004).

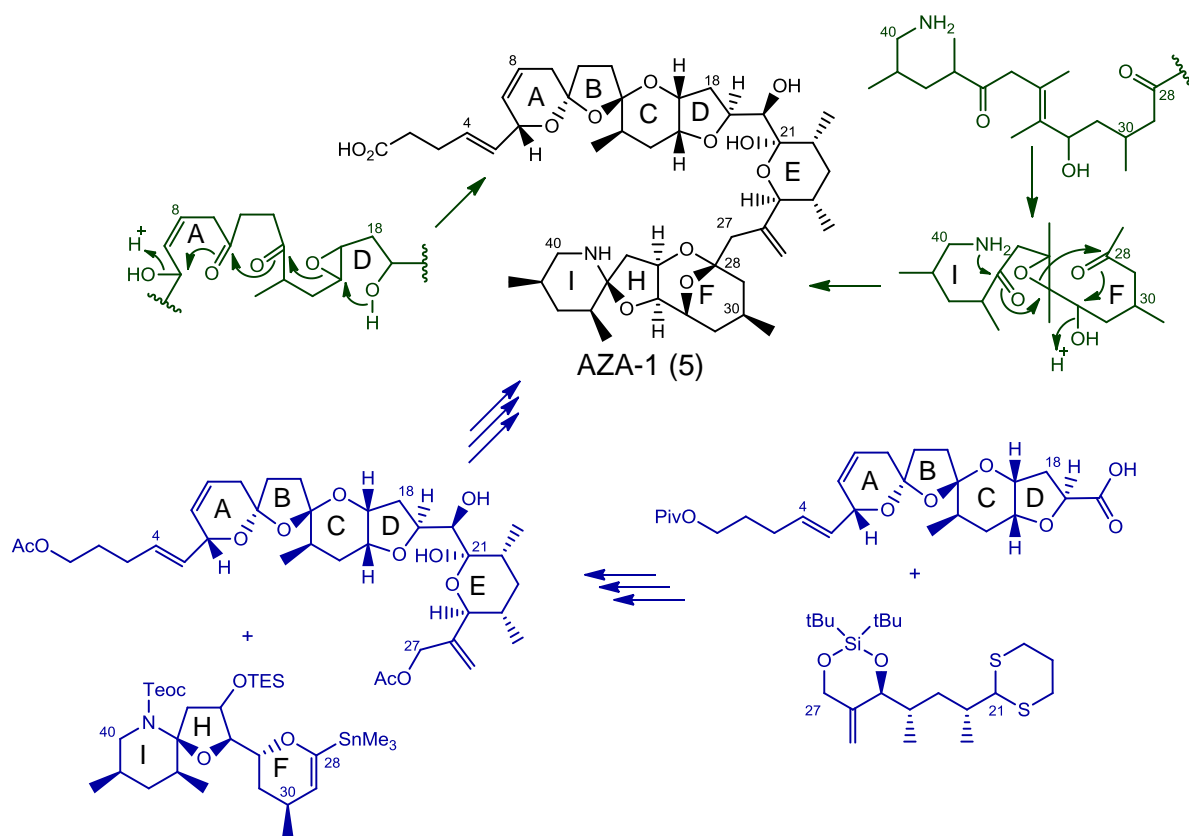


Figure 1.8: Proposed biosynthetic pathway for the formation of the ring systems in AZA-1 based on ring formation reactions of other dinoflagellate polyketides in green and concept of the synthesis pathway of AZA-1 by Nicolaou *et al.* in blue (Nicolaou *et al.*, 2006; Nicolaou *et al.*, 2004).

1.4 Legislative regulation of microalgal toxins

Since the 1930ies, the mouse bioassay (MBA) is used to detect marine biotoxins in shellfish (Christian and Luckas, 2008). The assay has been refined and standardized by the Association of Official Analytical Chemists (AOAC) (Marine biotoxins, 2004). In the MBA a quota of the sample was injected into twenty gram mice and the time till death was recorded. A timeframe of 5 to 15 minutes is preferable, samples with a higher toxicity (lower death time) should be diluted. The toxicity on the basis of the death time is expressed as mouse units. One mouse unit is defined as amount of toxin, which can kill a mouse (20 g) in a certain time. (Marine biotoxins, 2004)

In the EU, liquid chromatography coupled to mass spectroscopy (LC-MS) replaced the MBA as routine method for testing toxic compounds in shellfish (Hess, 2010). The Federal Institute for Risk Assessment (BfR) and the German National Reference Laboratory (NRL) for the Control of Marine Biotoxins expressed concern regarding MBA as definite reference test for marine biotoxins (Bundesinstitut für Risikobewertung, 2005). The MBA has failed to show a good reproducibility between laboratories of member states and even between repeated tests in the same laboratory (Bundesinstitut für Risikobewertung, 2005; Le Doux and Sherwood, 2000; Toti *et al.*, 1991). MBA results may differ due to the variability between animal lineages, sex, age and bodyweight (Nagashima *et al.*, 1991; Prakash *et al.*, 1971; Stabell *et al.*, 1992). In some cases, the MBA has even failed to be sensitive to detect toxins within legal concentration limits (Hess, 2010). In 2005 the EU declared the MBA as unsuitable for routine surveillance of marine biotoxins in shellfish (European Union, 2011). The MBA is still used for verification of presence and assessment of risk for novel toxins (European Union, 2011).

Given its high sensitivity and reproducibility, LC-MS is able to distinguish between individual toxic compounds, while quantifying these compounds simultaneously (Christian and Luckas, 2008). Further, a reliable detection of toxins by LC-MS in comparison to MBA was demonstrated (Suzuki *et al.*, 2005). Even in some samples, which were negative for toxin presence in MBA due to removal of toxins in sample preparation, the presence of toxins was successfully revealed with the LC-MS method (Suzuki *et al.*, 2005).

After LC-MS analysis, the toxicity of a sample is determined for each toxin group by a weighted summation of all toxin concentrations. The weighting factor is the toxic equivalency factor (TEF), which represents the toxicity of a compound in comparison to the main toxin, *e. g.* 1.8 for AZA-2 in comparison to AZA-1 with a toxicity equivalency factor of 1.0 (*cf.* Table 1.2 for AZAs) (Marine biotoxins in shellfish – Azaspiracid group - Scientific Opinion of the Panel on Contaminants in the Food chain, 2008). The determination of toxic equivalency factor can base on acute toxicity to human or animals as in the MBA or other means of assessing toxicity such

as *in vitro* experiments (Louzao *et al.*, 2017). However, results of living animals are still preferred over *in vitro* experiments, because this simplified system (in comparison to the living animal) has to reflect the mode of action of the toxin as in the living animal. In some recent studies, an oral application instead of the intraperitoneal injection is used in MBA, considering the potential human exposure by oral route. However, in the case of AZAs the toxicity of a number of known derivatives is solely based on the Jurkat T lymphocyte cell assay (Kilcoyne *et al.*, 2018; Kilcoyne *et al.*, 2015; Kilcoyne *et al.*, 2014a; Kilcoyne *et al.*, 2014b; Krock *et al.*, 2015). This cell line test requires less toxin material in comparison to the MBA. Even though the order of potency coincides for Jurkat T lymphocyte cell assay and the regulations of the European Food Safety Authority (EFSA), the toxic equivalency factors (TEFs) determined with the Jurkat T cell assay differs in value from the TEFs established by the EFSA and contradict results of the MBA (see Table 1.2) (Kilcoyne *et al.*, 2014a; Pelin *et al.*, 2018; Twiner *et al.*, 2012; Marine biotoxins in shellfish – Azaspiracid group - Scientific Opinion of the Panel on Contaminants in the Food chain, 2008). Based on the toxicity of the compound in relation to the lead structure of the toxin group, expressed as the toxic equivalency factor, an addition to routine surveillance might be reasonable.

Table 1.2: Toxic equivalency factors (TEFs) for the regulated AZAs based on Jurkat T lymphocyte assay (Twiner *et al.*, 2012), MBA with intraperitoneal (i.p.) injection (Kilcoyne *et al.*, 2014a), and oral application (Pelin *et al.*, 2018) in comparison to TEFs established by the European Food Safety Authority (EFSA) (Marine biotoxins in shellfish – Azaspiracid group - Scientific Opinion of the Panel on Contaminants in the Food chain, 2008).

compound	EFSA	Jurkat T	MBA (i.p.)	MBA (oral)
AZA-1	1.0	1.0	1.0	1.0
AZA-2	1.8	8.3	0.6	0.7
AZA-3	1.4	4.5	0.5	0.5

Beside the group of AZAs only three other of the six toxin groups in Table 1.1 are regulated in the European Union (EU). Depending on the type of toxin, the concentration limits in shellfish range from 0.16 mg/kg (AZAs) to 20 mg/kg (DA) (European Union, 2004). The food safety for products of shellfish production sites located in the German Bight is ensured by a cooperation of the three following authorities:

- *Institut für Fische und Fischereierzeugnisse* (IFF) Cuxhaven of the *Niedersächsisches Landesamt für Verbraucherschutz und Lebensmittelsicherheit* (LAVES)
- *Niedersächsischer Landesbetrieb für Wasserwirtschaft, Küsten- und Naturschutz* (NLWKN)
- municipal veterinary and food surveillance authority

The NLWKN maintains an early warning system for toxin producing microalgae that can potentially reach the harvest sites. During July to October, the presence of toxin producing algae in seawater samples is periodically analyzed by microscopy. At shellfish production sites prior to and during harvesting, samples are assessed by the IFF Cuxhaven of the LAVES. The clearance for shellfish harvest requires the negative results in a mussel sample and a seawater sample. The presence of marine biotoxins is determined in shellfish, while the seawater sample is examined for toxin producing algae by microscopy (e. g. *Dinophysis sp.*, *Pseudonitzschia sp.*, *Alexandrium sp.*, *Prorocentrum sp.*, *Protoperidinium sp.* and *Lingulodinium sp.*). (Niedersächsisches Ministerium für Ernährung und Landwirtschaft und Verbraucherschutz, 2016).

The detection and quantification of biotoxins in shellfish (or in algal biomass) is specifically shown here for AZA-1 at the example of a triple quadrupole MS. This represents a tandem in space mass spectrometer, which is usually used in toxin quantification. The first quadrupole selects the parent ion, which is in case of AZA-1 (shown in Figure 1.9) the proton adduct with a m/z ratio of 842. The second quadrupole induces a fragmentation of the parent ions due to a collision with inert gas atoms. The energy of the collision can be varied. Daughter ions of interest are selected at the third quadrupole. In case of AZA-1 the daughter ion with a loss of one water molecule ($m/z = 824$) is used for quantification, while the daughter ion ($m/z = 672$) with an additional dissociation of a neutral particle with $C_9H_{12}O_2$ due to a RETRO-DIELS-ALDER reaction in ring A (Figure 1.9 red line) serves as verification of the analyte as AZA-1. The sample concentration is determined by comparison of the peak areas of the quantification mass transition (m/z 842 \rightarrow m/z 824) for the sample with a dilution series of an analytical standards.

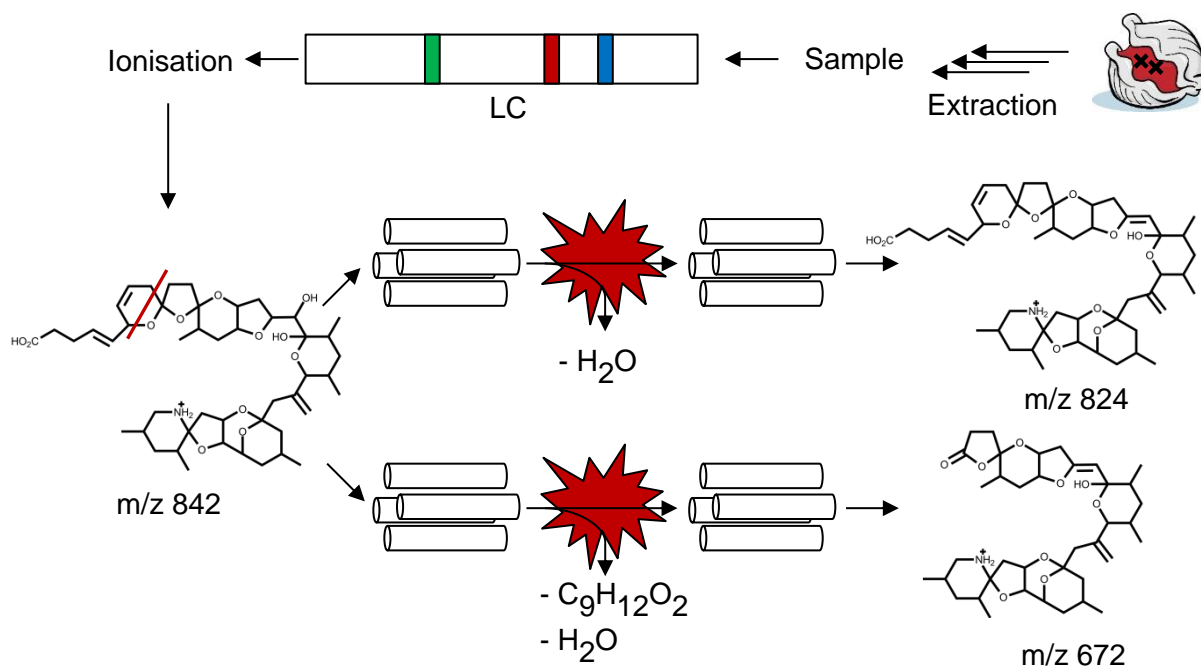


Figure 1.9: Schematic workflow of AZA-1 analysis by LC-MS/MS; Extraction of toxins from biological matrix (represented as mussel; top right); separation of toxins through liquid chromatography (LC; top center); ionization; parent ion of AZA-1 (m/z 842; left side) with fragmentation position due to RETRO-DIELS-ALDER reaction marked with red line and daughter ions for quantification (m/z 824; upper right side) and for validation (m/z 672; lower right side); triple quadrupole in the center with m/z selecting quadrupoles indicated by four cylinders (first on the left, third on the right) and collision quadrupole in the center (red star), with dissociated neutral particles below.

Even though LC-MS has many advantages as routine method for surveillance of toxins in seafood compared to the MBA, the specific disadvantages are:

- Analytical standards of each toxin are necessary for quantification
- Specific detection is possible only for known toxins

In contrast to MBA, where only one representative toxin for a toxin class is used as standard, a reliable LC-MS quantification requires an analytical standard for each derivative of the toxin class, because the signal intensity for given concentrations differs in MS for each one. Structural features determine the degree of ionization as well as the fragmentation pathways of the analytes. Therefore chemical derivatives of the same concentration potentially show different signal intensities in mass spectrometry due to a different behavior (e. g. ionization efficiencies). Further, external factors, such as environmental conditions (e. g. humidity in the laboratory), affect the performance of LC-MS (Sargent, 2013), but this problem is easy to address by the measurement of standards and/or quality control samples routinely over time. The continuous measurement of analytical standards for each toxin requires a supply of standards, which have an accurately and independently determined concentration (e. g. by NMR spectroscopy).

Even though selectivity for specific compounds is an advantage of LC-MS, regarding toxin detection in food items, an excessive selectivity can be considered as disadvantage. Since the mass transitions are selected before the start of the measurement, unregulated or even unknown toxins would be beyond the scope of LC-MS quantification. A limitation to regulated toxins is based on availability of standards and for economic reasons. A lower number of screened toxins helps to provide fast feedback about the condition of the shellfish to the respective production sites, while it reduces expenses for analytical standards of toxins, which were previously not observed in these areas. However, the occurrence of a novel toxin, *e. g.* through introduction of non-indigenous microalgae species via currents or in ballast water of ships, could introduce new toxins in an area, which are not covered through routine surveillance of toxins in shellfish. For example in the group of AZAs, only the three most prominent derivatives in terms of occurrence (AZA-1, AZA-2 and AZA-3) are regulated and monitored, despite more than twenty derivatives have their structure elucidated (Figure 1.5) (European Union, 2011; Marine biotoxins in shellfish – Azaspiracid group - Scientific Opinion of the Panel on Contaminants in the Food chain, 2008).

These non-indigenous species could attract attention in the microscopic analysis of the water samples, even though the focus is set on acquainted species (Niedersächsisches Ministerium für Ernährung und Landwirtschaft und Verbraucherschutz, 2016). The presence of dinoflagellates, which are known for production of toxins, can trigger the same measures (*e. g.* closure of the harvesting areas) as presence of toxins in shellfish (Niedersächsisches Ministerium für Ernährung und Landwirtschaft und Verbraucherschutz, 2016).

1.5 Risk assessments of novel toxin derivatives

In case of a novel derivatives of a marine biotoxin in a shellfish sample, an initial toxicity can be assessed by the MBA, however, this is not suited for routine surveillance because of the reasons stated in chapter 1.4. In order to include new derivatives in a LC-MS based monitoring, the following steps are necessary:

1. Identification of the toxin group
2. Structure elucidation of the toxin
3. Production of analytical standards
4. Assessment of toxicity

Even through some derivatives are observed only in very small cellular concentrations and thus may not substantially contribute to the toxicity for humans, their structure elucidations are of great interest as exemplary shown for the group of AZAs by Krock *et al.* (Krock *et al.*, 2019):

- Increased knowledge of derivatives gives insight to the biosynthetic pathway for production of the toxins.
- Some rare derivatives may serve as geographical marker for the presence of the producing species. In remote areas, where the identification by microscopic and/or genetic tools is not possible, the toxins can serve as chemotaxonomic markers.
- The improved insight in fragmentation patterns of the toxin class, which will be a result of the higher number of derivatives with confirmed structure, will lead to a better prediction of structures of novel derivatives based on the interpretation of their collision induced dissociation (CID) spectra.
- Knowledge of all produced compounds with toxicity to humans will lead to a better risk assessment for the toxins in seafood.

1.5.1 Identification of the toxin group

Each toxin group exhibits a characteristic CID mass fragmentation pattern. The pathways leading to these fragments are similar for the derivatives of the same toxin classes, in some cases even the m/z ratios of the fragments are the same. Therefore a scanning method for the characteristic fragmentation could lead to the discovery of novel derivatives. As an example for such fragmentation, Figure 1.10 shows the characteristic CID fragments of AZA-1. The group 2 fragment (m/z 672), which results of the dissociation of one water molecule and the molecular part containing C-1 to C-9 due to a RETRO-DIELS-ALDER reaction, is used as a qualifier ion for AZA-1 quantification.

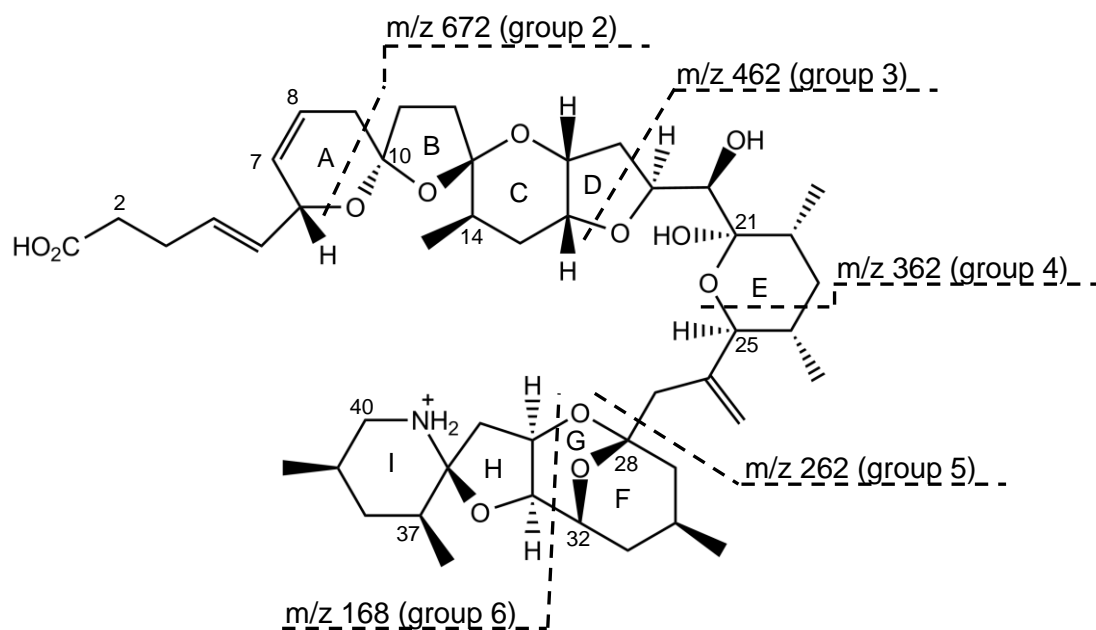


Figure 1.10: Structure of protonated AZA-1 and m/z ratios of characteristic fragmentation groups; dashed lines indicate position of bond cleavages during fragmentation (Adapted after Krock *et al.*, 2012).

After discovery of a novel toxin, commonly the standard toxin of this class (e. g. AZA-1 for all new AZAs) is used as external analytical standard to quantify the novel derivatives. The resulting concentration is expressed as equivalent concentration of the standard toxin. Even though this method is prone to systematic mistakes, due to variations in the response for the different compounds by mass spectrometry, this method enables the comparison of results obtained at different times.

1.5.2 Structure elucidation of the toxin

The measurement of a CID spectra exhibit structural information's, especially the comparison of CID spectra of a novel derivative of a toxin class with the CID spectra of known derivatives allows statements about the structure of the novel compound. By usage of a high resolution CID spectra, the assignment of sum formulas is possible for the fragments. But alone the comparison of CID spectra is not suitable for the structure elucidation. The fragmentation reactions for CID spectra were not systematically investigated, therefore fragments (observed in CID spectra) can often only described as plausible retrospectively (Hesse *et al.*, 2012).

Application of further techniques such as X-ray crystallography (XRD) or nuclear magnetic resonance (NMR) spectroscopy are necessary. Both techniques require purified toxin material, which is obtained through the chromatographic purification of a toxin containing extract either of a mass culture of the toxin producing algae or shellfish biomass. The different experiments in NMR spectroscopy vary in the structural information they contain. However, through

combination of the structural information's obtained in different NMR experiments the structure of the novel derivatives can be elucidated.

Further, *in silico* methods offer the possibility to simulate the NMR properties, the simulated shielding tensors can be correlated with the chemical shift of the compounds. A determination of the stereo centers, in addition to a verification of the determined structure, is possible (Bifulco *et al.*, 2007).

1.5.3 Production of analytical standards

A suitable analytical standard can be produced using the purified toxin for structure elucidation. The pure toxin needs to be quantified. If the available amount of toxin is high enough, gravimetric determination is suitable. Lower amounts are quantified by NMR spectroscopy. The quantification by NMR uses the direct proportionality of the signal intensity and the concentration of the measured compound (Friebolin, 2011). The integrals of the analyte signals are compared with the integrals of tetramethylsilane (TMS), which is quantified by a gravimetric determined amount of an external standard (Cironi *et al.*, 2000).

1.5.4 Assessment of toxicity

In addition to the production of analytical standards, material of the purified novel derivative is used in experiments to assess its toxicity, such as the MBA or cell line tests. With the toxicity of the novel derivative known, the comparison of toxicities could determine the TEF of the novel derivative as required for regular shellfish surveillance (*cf.* section 1.4).

1.6 Aims and objectives of this thesis

Marine biotoxins produced by dinoflagellates exhibit a remarkable structural diversity and mode of action. However, only few toxins are fully characterized and their ecological roles are poorly understood.

I will focus on two classes of toxins: Cyclic imines (specifically gymnodimines and spirolides) and polycyclic ethers (*e. g.* azaspiracids). While the former class is not toxic to humans after oral application, it shows strong neurotoxic effects in other mammalian assays and has been suggested as a potential target for neurodegenerative disease treatment. The latter class possesses an acute oral toxicity in humans and is therefore relevant for food safety surveillance. Additionally, both classes of toxins and their respective producers have received significant attention for their role as ecosystem engineers and marine food chain. Despite this, little is known about the effect of chemical structural diversity on biological activity (*e. g.* toxicity and mode of action) and ecological function.

Experimental strategies that may point to the ecological role of dinoflagellate toxins range from *in vitro* co-cultivation experiments to interaction studies using known receptors and toxin derivatives. For these experiments, purified toxin is either directly required to test its effect on other organisms (*e. g.* potential predators) or indirectly needed as an analytical standard to ensure accurate quantification of the toxin in a biological experiment or for environmental monitoring. Novel or unavailable toxins are often quantified via analytical standards of closely related toxins from the same class. However, this may be inaccurate because structural differences can influence signal intensities in mass spectrometry. Therefore, analytical standards of each respective toxin require an independent verification with absolute detectors (*e. g.* NMR).

My goals are to purify enough of each novel toxin produced by *Alexandrium ostenfeldii* (chapter 2) and *Azadinium poporum* (chapter 3) to allow structural characterization, to produce analytical standards for their accurate quantification and to enable *in vitro* and *in vivo* assessment of toxicity.

In silico stereo-chemical modeling can verify results of the NMR-based structure elucidation (chapter 4). This methodology can also provide further insight in other physical and chemical properties (*e. g.* stereo chemistry, conformation, and electrostatic potential) that are prerequisite for improving our understanding on how these compounds bind to specific proteins or membranes. The goal in the last data chapter of this thesis is to compare measured and simulated spectroscopic properties of cyclic imines to verify their stereo chemistry.

Together, the results from this thesis will facilitate the characterization of structure-activity relationships and will enable the identification of common binding sites. This will ultimately lead to a better understanding of how the large structural diversity of marine dinoflagellate toxins contributes to the success of this protist subgroup.

2. Identification of novel neurotoxic gymnodimines and spirolides from the marine dinoflagellate *Alexandrium ostenfeldii*

Several novel gymnodimines and spirolides were recently discovered by mass spectrometry in a genotype of *Alexandrium ostenfeldii* originally cultured from the North Sea of the coast of the Netherlands (Martens *et al.*, 2017). In this chapter I report the structure elucidation, make theoretical assumptions about likely biosynthetic pathways of their production and discuss the potential ecological impact of these compounds. These results were compiled in a publication describing the structure elucidation of two novel GYMs and two novel SPXs. In this publication, I was responsible for measurement of the NMR spectra, the structure elucidation of the compounds, setting up and the analysis of the quantum chemical calculation, the identification of the biosynthetic implications of the novel compounds, the extraction, the measurement, and the analysis of the novel compounds in natural plankton assemblages, and visualization and writing of the original draft.

Identification of Novel Gymnodimines and Spirolides from the Marine Dinoflagellate
Alexandrium ostenfeldii

C. Zurhelle¹, J. Nieva², U. Tillmann², T. Harder^{1,2}, B. Krock², J. Tebben² (2018)

¹ Marine Chemistry, University of Bremen, Leobener Straße 6, 28359 Bremen, Germany

² Alfred Wegener Institute, Helmholtz Centre for Polar and Marine Research, Section Ecological Chemistry, Am Handelshafen 12, 27570 Bremerhaven, Germany

Marine Drugs **2018**, *16*(11), 446

DOI: 10.3390/md16110446

I contributed in following parts to the paper: data curation, formal analysis, investigation, methodology, validation, visualization, and writing - original draft



Article

Identification of Novel Gymnodimines and Spirolides from the Marine Dinoflagellate *Alexandrium ostenfeldii*

Christian Zurhelle ¹, Joyce Nieva ², Urban Tillmann ² , Tilmann Harder ^{1,2} , Bernd Krock ^{2,*} and Jan Tebben ^{2,*}

¹ Marine Chemistry, University of Bremen, Leobener Straße 6, 28359 Bremen, Germany; zurhelle@uni-bremen.de (C.Z.); tharder@uni-bremen.de (T.H.)

² Alfred Wegener Institute, Helmholtz Centre for Polar and Marine Research, Section Ecological Chemistry, Am Handelshafen 12, 27570 Bremerhaven, Germany; joyce.nieva@awi.de (J.N.); Urban.Tillmann@awi.de (U.T.)

* Correspondence: bernd.krock@awi.de (B.K.); jtebben@awi.de (J.T.); Tel.: +49-471-4831-2055 (B.K.); +49-471-4831-1086 (J.T.)

Received: 13 September 2018; Accepted: 5 November 2018; Published: 14 November 2018



Abstract: Cyclic imine toxins are neurotoxic, macrocyclic compounds produced by marine dinoflagellates. Mass spectrometric screenings of extracts from natural plankton assemblages revealed a high chemical diversity among this toxin class, yet only few toxins are structurally known. Here we report the structural characterization of four novel cyclic-imine toxins (two gymnodimines (GYMs) and two spirolides (SPXs)) from cultures of *Alexandrium ostenfeldii*. A GYM with m/z 510 (**1**) was identified as 16-desmethylGYM D. A GYM with m/z 526 was identified as the hydroxylated degradation product of (**1**) with an exocyclic methylene at C-17 and an allylic hydroxyl group at C-18. This compound was named GYM E (**2**). We further identified a SPX with m/z 694 as 20-hydroxy-13,19-didesmethylSPX C (**10**) and a SPX with m/z 696 as 20-hydroxy-13,19-didesmethylSPX D (**11**). This is the first report of GYMs without a methyl group at ring D and SPXs with hydroxyl groups at position C-20. These compounds can be conceived as derivatives of the same nascent polyketide chain, supporting the hypothesis that GYMs and SPXs are produced through common biosynthetic genes. Both novel GYMs **1** and **2** were detected in significant amounts in extracts from natural plankton assemblages (**1**: 447 pg; **2**: 1250 pg; **11**: 40 pg per mL filtered seawater respectively).

Keywords: gymnodimine; spirolide; structure elucidation; neuro-toxin; *Alexandrium ostenfeldii*; harmful algal boom (HAB)

1. Introduction

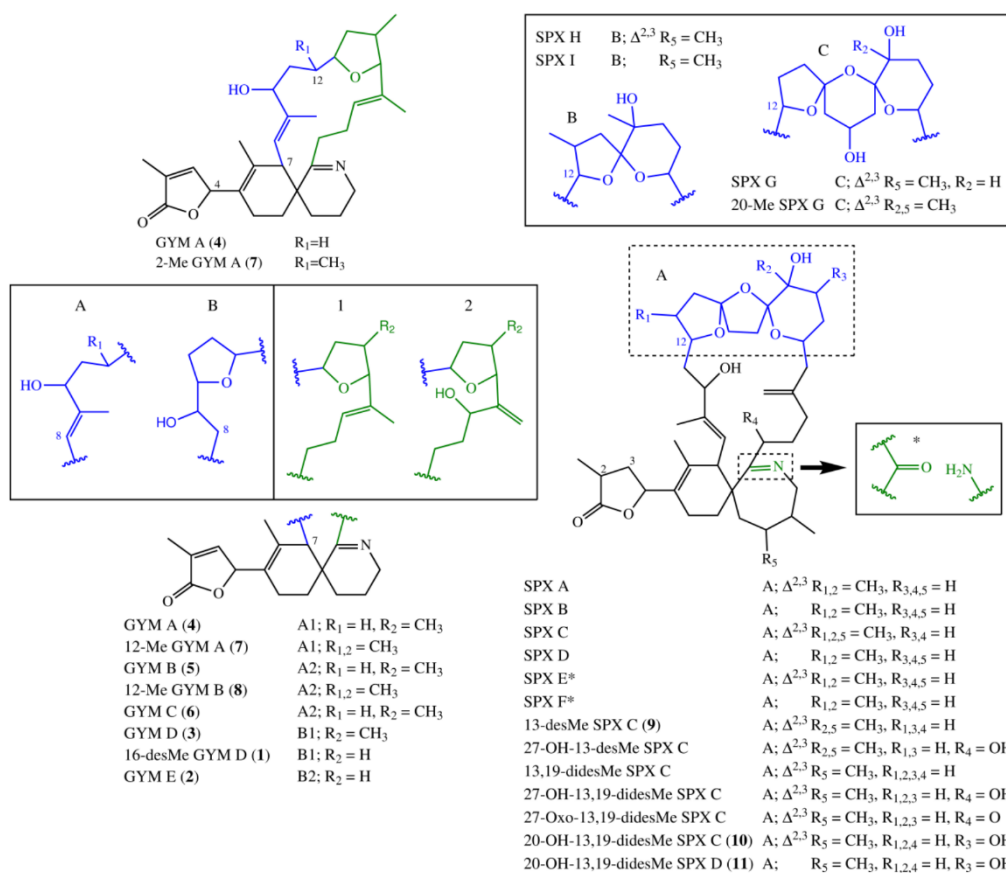
Cyclic imines are fast acting phycotoxins associated with harmful marine algal blooms and shellfish toxicity. Their chemical structures have a macrocycle of 14 to 27 atoms in common and two conserved features that include the cyclic imine group and spiroketal ring system. These toxins have been detected in extracts from plankton net tows, in vitro dinoflagellate cultures, and in shellfish tissue. Cyclic imine toxins are further divided into gymnodimines, pinnatoxins/pteriatoxins, portimine, prorocentrolides, spirolides, and spiro-prorocentrimine; for reviews see [1,2]. Currently, 36 of these toxins have been structurally elucidated; however, a much greater structural diversity has been inferred from mass spectrometric fragmentation data of microalgal and shellfish extracts [3,4].

Fifteen spirolide derivatives (herein referred to as SPXs) and six gymnodimine derivatives (GYMs) are structurally characterized (Figure 1). Structurally, SPXs and GYMs are highly similar.

The dinoflagellate *Karenia selliformis* produces GYMs [1] while some strains of *Alexandrium ostenfeldii* produce both GMYs and SPXs [5,6]. Van Wagoner et al. [7] suggested that this structural similarity is due to common biosynthetic genes. SPXs and GYMs are derived from a linear nascent polyketide chain which is formed by incorporation of small acid units such as acetate and glycine [7]. Originating from an unfolded nascent polyketide chain (NPC), ring B is formed by a Diels Alder reaction, ring A by ester formation, and ring C by nucleophilic attack of a terminal amine group on a carbonyl carbon (C-21 in GYM A), resulting in an imine group [8]. An ether formation via epoxidation is suggested as mechanism to form ring D to F in 13-desmethyl SPX C or ring D and E in GYM D [7,8].

Cyclic imines are classified as “fast-acting”, because they induce rapid onset of neurological symptoms followed by death within minutes in mouse bioassays [9]. Both GYMs and SPXs bind to acetylcholine receptors [10,11]. The effect of 13-desmethyl SPX C was diminished after protection of the primary binding site of muscarinic acetylcholine receptors with high concentrations of atropine, suggesting an interaction of the spirolide with the orthologous binding site of the muscarinic acetylcholine receptor [11]. Competition-binding assays confirmed that GYM A reversibly inhibits broad range of nicotinic acetylcholine receptors [10].

Martens et al. [6] postulated the presence of various unknown SPXs and two unknown GYMs in addition to GYM A (originally characterized by Seki et al. [12]) and SPX 1 [13] from LC-MS analysis of extracts obtained from cultures of *A. ostenfeldii*. The overarching objective of this work was to purify and structurally characterize these novel cyclic imines and to investigate if all structural derivatives of SPXs and GYMs can be linked back to the same nascent polyketide chain.



2. Results and Discussion

2.1. Structure Elucidation of 16-Desmethylgymnodimine D (1)

The empirical formula of compound **1** was determined as $C_{31}H_{43}NO_5$ by high resolution mass spectrometry (HR-ESI-MS) experiments. HR-MS/MS data (Table 1) indicated one less CH_2 group between C16–21 compared to GYM D. The 600 MHz NMR spectroscopic data of **1** in Pyr-d5 are summarized in Table 2. The NMR-data confirmed a high similarity between the new GYM **1** and GYM D [8]. Larger deviation between carbon shifts of **1** and GYM D was only observed for C-6 and both furan rings (D and E, Figure 2). Due to the overlap of chemical shifts of C-6 and the pyridine signal, a direct determination of the ^{13}C -chemical signal was not possible. The carbon shift for C-6 was estimated from HMBC data. The highest deviation in chemical shifts in comparison to GYM-D was observed at C-15 and C-16. No methyl group was observed at C-16. This was confirmed by a DEPT experiment, which showed a negative signal for C-21, characteristic for a CH_2 -group. Initial multiplicity-edited HSQC measurements showed a positive signal for C-21, suggesting a methine or methyl group at that position. We suspect that a partial proton transfer from C-21 to the nitrogen atom caused the positive signal in that experiment.

The relative stereochemistry of **1** was determined by NOESY and ROESY experiments. C-19 and C-20 showed *E* conformation based on the nuclear Overhauser effect (NOE) between H-20_{ab} and H-29. Further NOE signals were observed between H-9 and H-21. Both showed a NOE with H-7 and H-19 suggesting these protons were directed to the center of macro cyclic ring. The NOE between H-7 and H-21 suggested a small dihedral angle between H7, C-7, C-23 and C-22. Therefore, H-10 and H13 (ring E), as well as H-14 and H-17 (ring D), were on the same side of the tetrahydrofuran rings. H-10 showed a spatial proximity to H-27, suggesting an outward direction of H-10, H-13, H-14, and H-17 from the macro cyclic ring. The complete assignment of centers of chirality at ring E was not possible due to the missing methyl-group at C-16 in comparison to GYM D and the accompanying distinction of groups bound to C-16. No coupling was observed between H-9 and H-10, suggesting a dihedral angle between C-9 and H-9, as well as C-10 and H-10 of circa 90° . To determine stereochemistry at C-4, the circular dichroism (CD) spectrum of **1** was compared to the CD spectrum of GYM A and compared with simulated CD spectra for both (B3LYP optimized) stereoisomers. The experimental CD spectra and simulated CD spectra (Figure S23) of **1** suggest an *S* configuration at C-4, the same as for GYM A (4). Based on all available data, the proposed structure of 16-desmethyl GYM D is shown in Figure 2.

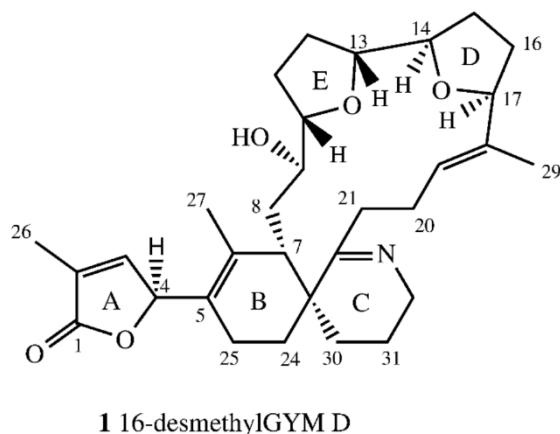


Figure 2. Structure of 16-desmethylgymnodimine D (**1**, numeration as per gymnodimine D).

Table 1. Exact and measured accurate masses (m/z) for $[M + H]^+$ at m/z 510 and m/z 526 and their product ions obtained with LC-HRMS.

16-Desmethylgymnodimine D (1)				Gymnodimine E (2)			
Formula	Measured	Calculated	Δ /ppm	Formula	Measured	Calculated	Δ /ppm
C ₃₁ H ₄₄ O ₅ N	510.3212	510.3214	−0.33	C ₃₁ H ₄₄ O ₆ N	526.3163	526.3163	−0.04
				C ₃₁ H ₄₂ O ₅ N	508.3060	508.3057	0.43
C ₃₁ H ₄₂ O ₄ N	492.3111	492.3108	−0.54	C ₃₁ H ₄₀ O ₄ N	490.2951	490.2952	−0.12
C ₃₀ H ₄₄ O ₄ N	482.3264	482.3265	−0.07	C ₃₀ H ₄₂ O ₄ N	480.3108	480.3108	−0.14
				C ₃₀ H ₄₂ O ₃ N	464.3159	464.3159	−0.12
				C ₂₃ H ₃₂ O ₄ N	386.2324	386.2326	−0.46
C ₂₀ H ₃₀ O ₃ N	332.2218	332.2220	−0.18	C ₂₀ H ₂₈ O ₃ N	330.2063	330.2064	−0.12
C ₁₆ H ₂₄ O ₂ N	262.1800	262.1802	−0.16	C ₁₆ H ₂₂ O ₂ N	260.1645	260.1645	−0.17
C ₁₇ H ₂₆ O ₂ N	260.2007	260.2009	−0.17	C ₁₇ H ₂₄ O ₂ N	258.1852	258.18524	−0.12
C ₁₄ H ₂₀ N	202.1589	202.1590	−0.09	C ₁₄ H ₂₀ N	202.1590	202.1590	0.09
C ₁₄ H ₁₈ N	200.1433	200.1434	−0.05	C ₁₄ H ₁₈ N	200.1434	200.1434	0.14
				C ₁₂ H ₁₆ ON	190.1227	190.1226	0.07
C ₁₃ H ₁₈ N	188.1433	188.1434	−0.05	C ₁₃ H ₁₈ N	188.1434	188.1434	0.16
C ₁₃ H ₁₆ N	186.1277	186.1277	−0.02	C ₁₃ H ₁₆ N	186.1278	186.1277	0.25
				C ₁₃ H ₁₄ N	184.1120	184.1120	0.19
C ₁₂ H ₁₆ N	174.1277	174.1277	−0.02	C ₁₂ H ₁₆ N	174.1277	174.1277	0.21
C ₁₂ H ₁₄ N	172.1120	172.1121	−0.05	C ₁₂ H ₁₄ N	172.1121	172.1121	0.09
C ₁₁ H ₁₆ N	162.1276	162.1277	−0.08	C ₁₁ H ₁₆ N	162.1277	162.1277	0.1
C ₁₁ H ₁₄ N	160.1121	160.1121	−0.02	C ₁₁ H ₁₄ N	160.1121	160.1121	0.2
C ₁₁ H ₁₂ N	158.0965	158.0964	0.03	C ₁₁ H ₁₂ N	158.0965	158.0964	0.36

Table 2. NMR spectroscopic data of 16-desmethylgymnodimine D (1). * Position numbering is analog to gymnodimine D.

Position *	δ (¹³ C)/ppm	δ (¹ H)/ppm	COSY	HSQC-TOCSY H -> C	HMBC H -> C
1	175.5				
2	130.2				
3	148.6	7.05	4, 26	4, 26	1, 2, 4, 26
4	81.6	5.93	3, 26	3, 26	2, 3, 5, 6, 25
5	125.9				
6	136	(by HMBC)			
7	43.6	3.16	8, 24	8, 25, 27	5, 6, 8, 9, 22, 23
8	31.8	1.9	8	7, 11	11, 13
9	71.6	3.66	10, 11	10, 8	7, 8, 10
10	83.4	3.94	9, 15	9, 15, 8	8, 9, 12, 14
11	27	1.79	10	8, 9, 12	9
12	24.9	1.77	13		13, 14, 15
13	78.6	4.36	11, 14	11, 14, 16	14, 12
14	82.5	4.13	16	11, 13, 16	12, 13
15	29.4	1.99	1.76	12	9, 14
16	32.1	1.79		15	14, 15
17	82.9	4.15	15	12, 15, 16	18, 19, 28
18	133.1				
19	124.9	5.99	17, 20, 21, 28	20, 21	18, 28, 17, 20, 21
20	21.9	3	2.1	19, 21, 29	18, 19, 21, 22
21	31.8	2.76	20	20	19, 20, 22
22	173.3				
23	42.7				
24	33.6	1.59	1.37	7, 8/21, 25, 25, 27	7, 22, 23, 25, 30
25	19.7	1.49	1.94	27, 30, 24, 32	
26	11	1.99	3, 4	3, 4	1, 2, 3
27	18.1	1.92		25, 8, 24, 7	5, 6, 7
29	15.3	1.61		20, 21	17, 18, 19
30	26	1.54	1.44	32, 31	23, 32
31	20.5	1.47		32, 30, 24?	23, 32
32	50.3	3.71	3.48	32, 31	22, 30, 31

2.2. Structure Elucidation of Gymnodimine E (2)

The structure of GYM E was determined by HRMS/MS spectra, NMR spectra ($^1\text{H-NMR}$, COSY, HSQC, HSQC-TOCSY) and comparison of NMR data of **2** with GYM B (**5**), GYM D (**3**), and 16-desmethylGYM D (**1**). The empirical formula of **2** was determined as $\text{C}_{31}\text{H}_{43}\text{NO}_6$ by HR-ESIMS. The HRMS/MS spectra of **2** and **1** were almost identical with an up-shift of 15.9950 Da for the fragments larger than m/z 300, suggesting one additional oxygen (Table 1). HR-MS/MS spectra of **2** also showed a downshift of 2 Da of the fragments above m/z 258 in comparison with **1** (Table 1) suggesting an additional double bond associated with ring D, introduced by elimination of an additional hydroxyl group in the parent ion. These data suggested that **2** had a similar structure as **1** with an additional hydroxyl group located either at the sidechain between ring C and ring D, or at ring D.

Proton and carbon chemical shifts of **2** revealed a high similarity to **1**, with the exception for C-19, C-20 and C-29 (Table 3). The signal at C-19 suggested a hydroxyl group in comparison to a double bond for **1** at that position. Additionally, **2** showed a characteristic signal for an exocyclic double bond at C-29. Chemical shifts for sidechain between ring C and ring D (C-19 to C-21 and C-29) exhibited closer similarity of chemical shifts to GYM B and GYM C than to **1** (see Table 3, [14,15]). The spin systems

for **2** were determined from COSY, $^1\text{H-}^1\text{H}$ COSY, and HSQC-TOCSY spectra and are shown in Figure 3. HSQC

Table 3. Proton and carbon chemical shifts of **1** and **2** in comparison to GYM D [8], GYM B [14] and GYM C [15]. The signals for the sidechain between ring C and D are underlined. GYM, gymnodimine derivative.

No.	1		GYM D [8]				2			GYM B [14]		GYM C [15]	
	¹³ C	¹ H	¹³ C	¹ H	¹³ C	¹ H	¹³ C	¹ H	¹³ C	¹ H	¹³ C	¹ H	
1	175.5		175.2								174.7		
2	130.2		130.2								130.3		
3	148.6	7.05	148.5	6.96	149.8	6.93			147.1	6.91		6.91	
4	81.6	5.93	81.1	5.95	81	5.88				5.84		5.85	
5	125.9		125.7								125.2		
6	136.0	by HM BC	137.4								132.8		
7	43.6	3.16	44.2	3.09	44.5	3.11				3.63		3.63	
8	31.8	1.9	1.43	30.9	1.82	1.43	30.3	1.74	1.22	125.9	5.28		5.31
9	71.6	3.66		72.5	3.96		74.9	3.66		140.4			
10	83.4	3.94		84.3	4.02		84.5	3.92		80	3.94		3.94
11	27.0	1.79	1.56	28.4	1.99	1.85	29	1.74			2.08	1.48	1.97
12	24.9	1.77		25.9	1.85		25.2	1.73	1.52		1.4	1.15	1.36
13	78.6	4.36		80.3	4.27		81.1	4.12			4.09		4
14	82.5	4.13		78.7	4.09		81.6	3.89		34.8	1.77–1.82		1.78
15	29.4	1.99	1.76	34.5	1.91	1.22	26.4	1.76	1.56	41.1	2.71		2.65
16	32.1	1.79		36	2.3	2.3	29.7	1.84		90.9	3.85		3.89
17	82.9	4.15		84.5	4.09		82.1	4.21					
18	133.1			129.7							<u>81.7</u>	<u>4.11</u>	
19	<u>125</u>	<u>5.99</u>		<u>127.8</u>	<u>5.98</u>		<u>73.4</u>	<u>4.58</u>			<u>2.4</u>	<u>1.49</u>	<u>2.06</u>
20	<u>21.9</u>	<u>3</u>	<u>2.1</u>	<u>21.8</u>	<u>3</u>	<u>2.14</u>	<u>36.9</u>	<u>2.36</u>			<u>2.64</u>	<u>2.23</u>	<u>2.62</u>
21	31.8	2.76		32.1	2.64	2.38	32.4	2.79					2.21
22	173.3			172.8									
23	42.7			43.5									
24	33.6	1.59	1.37	33.6	1.64	1.33	30.3	1.51	1.3		1.77	1.54	1.77
25	19.7	1.49		19.8	1.93	1.53	19.9	1.88	1.42		2.06	1.54	2.06
26	11.0	1.99		10.7	1.96		10.7	1.85			1.96		1.96
27	18.1	1.92		17.9	2.06		17.3	2.03			1.71		1.71
28				16.7	0.86						1.91		1.78
29	15.3	1.61		15.4	1.56		109.2	5.69	5		0.96		0.98
30	26.0	1.54	1.44	26.9	1.52	1.44	25.2	1.72	1.62		5.32	5.19	5.18
31	20.5	1.47		20.3	1.44		20.2	1.36	1.24		1.95	1.54	1.91
32	50.3	3.71	3.48	50.1	3.73	3.51	50.3	3.75	3.3		1.54	1.54	1.57
											3.57	3.4	3.52–3.45

2.3. Structure Elucidation of 20-Hydroxy-13,19-didesmethyl-SPX C (10)

The empirical formula of compound **10** was determined as C₄₁H₆₀O₈N by HR-ESIMS. Based on CID spectra, Martens et al. (2017) previously proposed a structure similar to 11,23-dihydroxy-19-dehydroxy-13-desmethyl-SPX C for this compound. The CID spectra showed a downshift of 16 Da in the A-type fragment cluster (*m/z* 444 to *m/z* 428), indicating two hydroxyl-groups between C-1 to C-11 and one between C-22 and C-23.

The NMR experiments revealed no methyl group at C-19, but instead an additional hydroxyl-group at C-20 (Table 4, Figure 4). The COSY and HMBC experiments clearly revealed correlations from H-23 to C-21 (HMBC) and from H-20 to H-19 and H-21 (COSY), supporting a six-membered ether diol (ring D) structure element (Figure 5). The signals corresponding to C-27 were not detected in MeOD. This was likely due to imine-enamine tautomerism induced proton exchange at this position and reminiscent of similar observations with GYM A [12]. For this reason, GYMs are generally measured in Pyr-d₅. Upon re-analysis of **10** in Pyr-d₅, the signal for C-27 was clearly detected (Table 4). The signal intensity for C-28 also improved in Pyr-d₅. The NMR data contradicted the earlier structural determination of **10** by CID [6]. Therefore, we reanalyzed **10** by HR-MS/MS (Table 5) and propose a fragmentation pathway as shown in Figure 6. Martens et al. interpreted the fragment at *m/z* 446 as a Group 1-type fragment corresponding to the *m/z* 444 fragment in **9** (Figure 6) [6]. Instead, we suggest, this fragment is formed by dissociation of the bond between C-11 and C-12 leading to the A-type fragment with two hydroxyl groups. This is supported by the observation of the dehydration of the hydroxyl groups resulting in fragments *m/z* 428 (C₂₆H₄₀O₅N⁺) and *m/z* 410 (C₂₆H₃₈O₄N⁺). In conclusion, we interpret the A-type fragment upshift in comparison

to **9** as 2 Da contrary to the previously proposed downshift by 16 Da [6]. The observed fragment of m/z 464 ($C_{26}H_{42}O_5N^+$) as analogous to the m/z 462 fragment observed for **9**. Therefore, both NMR and HR-MS/MS data supported 20-Hydroxy-13,19-didesMethyl-SPX C as proposed structure of compound **10**. Yields were insufficient to assign the stereochemistry of **10**; therefore, the planar structure of **10** is shown in Figure 4.

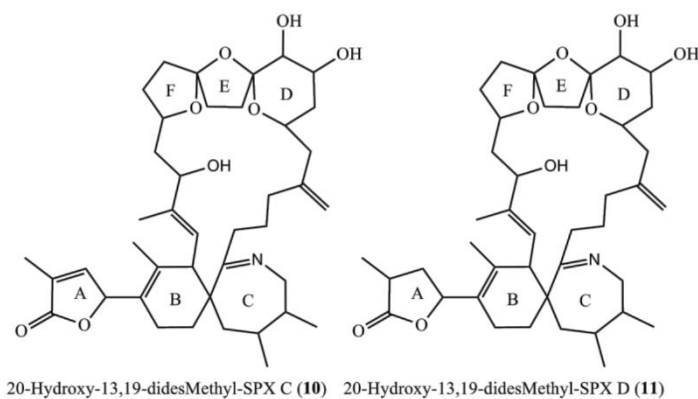


Figure 4. Planar structures of the two novel spirolides 20-Hydroxy-13,19-didesmethyl-SPX C (**10**) and 20-Hydroxy-13,19-didesmethyl-SPX D (**11**).

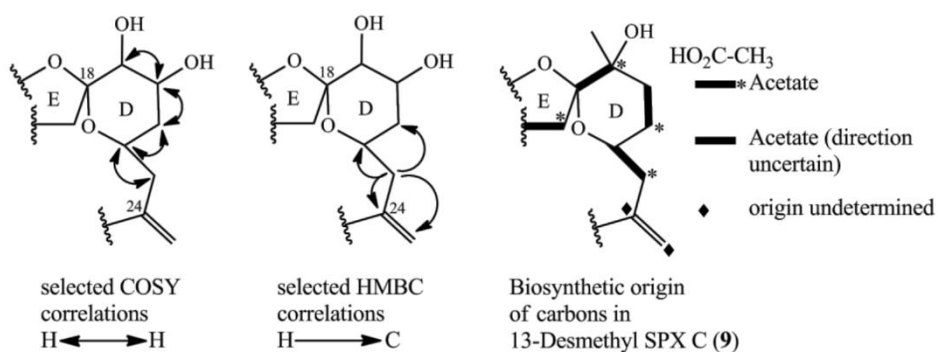


Figure 5. Selected COSY and HMBC correlations in the D-ring system for determining the position of hydroxyl-groups and part of biosynthetic origin of carbons of 13-desmethylSPX C (**9**) [16].

Table 4. Proton and carbon chemical shift of SPX A, SPX C, 13-desmethyl SPX C (all in CD₃OD by Hu et al.), 20-hydroxy-13,19-didesmethyl-SPX D (**11**, CD₃OD), and 20-hydroxy-13,19-didesmethyl-SPX C (**10**, recorded in CD₃OD and C₅D₅N); * was not detected in MeOD.

No.	10 (CD ₃ OD)		10 (C ₅ D ₅ N)		11		SPX A [13]			SPX C [13]		13-DesMe SPX C [13]						
	¹³ C	¹ H	¹³ C	¹ H	¹³ C	¹ H	¹³ C	¹ H		¹³ C	¹ H	¹³ C	¹ H					
1	176.7		175.7		182.3		177.1		177.1		176.8							
2	130.7		130		36.3	2.84	130.8		130.7		131							
3	149.5	7.18	148.3	7	35.7	2.58	1.69	150	7.12	149.9	7.12	149.5	7.13					
4	82	6	80.9	5.82	79	5.43		82.5	5.94	82.5	5.95	82	5.98					
5	126		124.9		129.7			125.9		126		126.4						
6	133.4		133.5		131			134.9		134.7		133.2						
7	48.2	3.76	47.6	3.39	47.6	3.72		48.8	3.57	49.1	3.56	48.1	3.78					
8	123.3	5.22	123.6	5.25	123.4	5.21		124.4	5.34	124.2	5.2	122.5	5.16					
9	145.9		143.5		144.8			144.5		144.6		146						
10	76.5	4.1	76.4	4.38	76.6	4.09		76.7	4.16	76.8	4.15	76.8	4.15					
11	45.4	2.34	1.35	45.4	2.73	1.66	44.8	2.34	1.34	39.7	1.61	2.14	39.6	1.57	2.14	45.2	1.37	2.25
12	79.6	4.37		79.4	4.71		79.6	4.37		81.7	4.33		81.7	4.31		79.8	4.3	
13	32.2	2.33	1.66	31.8	2.16		32	2.32	1.66	35.3	2.42		35.4	2.41		32.8	1.7	2.27
14	37.4	2.31	2.03	37.2	1.96	1.77	37.2	2.31	2.02	45.7	2.13	2.26	45.8	2.14	2.26	38.2	1.95	2.29
15	118.5		117.0		118.8			117.3		117.4		118.1						
16	34.7	2.1		34.8	2.3	2.1	34.6	2.1		36.6	2.04	2.19	36.5	2.04	2.22	35.2	2.07	2.21
17	35.8	2.29	2.03	35.5	2.5	2.19	36.2	2.3	2	31.5	1.76	2.14	31.5	1.74	2.11	32.1	1.79	2.2
18	110.7		110.3		110.9			112.5		112.5		112.2						
19	71.4	3.45		71.3	3.68		71.2	3.46		71.2		71.1						
20	69.7	3.96		69.3	4.18		69.8	3.95		35.8	1.47	1.84	35.8	1.49	1.81	35.7	1.49	1.81
21	38.3	1.95	1.41	38.4	2.06	1.36	37.8	1.96	1.4	30.2	1.23	1.59	30.2	1.24	1.55	29.9	1.28	1.58
22	64.6	4.17		63.7	4.54		64.4	4.16		69.4	4		69.3	3.97		69.1	3.97	
23	46.3	2.42	2.14	46.9	2.69	2.29	46.2	2.42	2.14	47.5	2.02	2.34	47.6	2.01	2.37	46.3	2.06	2.41
24	145.4		147.5		146			147.8		147.8		145.6						
25	36.4	1.99		35.6	2.55	1.75	37.1	2.04		35.9	1.6	2.12	36	1.58	2.1	34.6	1.83	2.05
26	24.3	1.96	1.7	23.0	2.47	1.46	24	1.94	1.7	23.7	1.39	2.02	23.4	1.4	2.02	21.8	1.83	2.01
27	*	*	*	34.9	2.3	2.1	35.8	2.25		35.6	2.34	2.41	35.6	2.32	2.43	36	2.82	3.1
28	*		174.4		181			179.3		178.6		201.3						
29	51.6		52.7		52.1			51.4		50.8		52.4						
30	36.9	1.95	1.75	37.5	1.47		36.4	1.97	1.76	28	1.65	1.9	38.3	1.55	1.73	36.7	1.79	2.01
31	37	1.08		35.8	1.22		36.7	1.09		32.1	1.06	1.78	36.9	1.16		37.5	1.04	
32	39.2	1.58		40.6	1.25		39.2	1.58		33.6	1.88		41.2	1.36		38.8	1.67	
33	52	4.07	3.57	52.8	3.67	3.61	51.9	4.1	3.57	53.1	3.48	3.72	53.3	3.44	3.76	51.8	3.55	4.18
34	31.8	1.96	1.78	31.4	1.64	1.32	33.2	1.82		32.2	1.55	1.8	32.4	1.52	1.8	32.4	1.67	1.98
35	20	2.25	1.67	19.2	2.07	1.47	20.2	2.41	2.09	20.4	1.56	2.11	20.3	1.51	2.14	20.3	1.72	2.27
36	10.2	1.93		10.7	1.85		14.5	1.26		10.4	1.88		10.4	1.86		10.5	1.9	
37	16.6	1.77		16.7	1.53		16.4	1.67		17	1.71		17.1	1.72		16.7	1.74	
38	12.3	1.92		12.6	1.98		12.2	1.92		12.2	1.85		12.3	1.87		12.9	1.91	
39								15.8	1.2		15.6	1.19						
40								22.5	1.19		22.5	1.19				22.7	1.2	
41	113.8	4.92	4.89	110.6	4.83	4.81	113.5	4.93		111.4	4.77	4.75	111.3	4.75	4.78	112.6	4.81	4.92
42	19.1	1.09		20.1	1.29		19.2	1.09		21	0.92		19.4	0.98		18.9	1.05	
43	20	1.09		20.0	0.85		19.2	1.09					21.1	0.95		20.1	1.11	

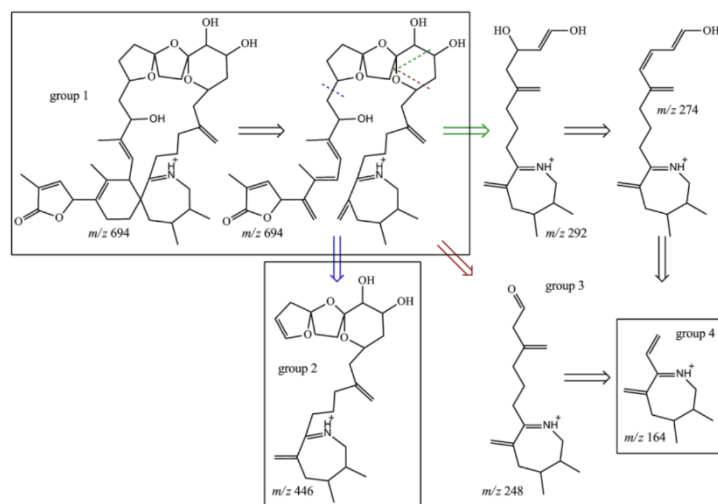


Figure 6. Structures of characteristic fragments in CID-spectra of compound **10**; fragmentation sites marked with dashed line; resulting structure is indicated by arrow in the same color.

Table 5. Exact and measured accurate masses (m/z) for $[M + H]^+$ at m/z 694 and m/z 696 and their product ions obtained with LC-HRMS.

10				11			
Formula	Measured	Calculated	Δ/ppm	Formula	Measured	Calculated	Δ/ppm
C ₄₁ H ₆₂ O ₈ N	696.44727	696.4470	0.4	C ₄₁ H ₆₀ O ₈ N	694.4307	694.4313	-0.98
C ₄₁ H ₆₀ O ₇ N	678.4365	678.4364	0.14	C ₄₁ H ₅₈ O ₇ N	676.4203	676.4208	-0.64
C ₄₁ H ₅₈ O ₆ N	660.4261	660.4259	0.34	C ₄₁ H ₅₆ O ₆ N	658.4100	658.4102	-0.37
C ₄₁ H ₅₆ O ₅ N	642.4155	642.4153	0.35	C ₄₁ H ₅₄ O ₅ N	640.3995	640.3997	-0.27
C ₄₁ H ₅₄ O ₄ N	624.4050	624.4047	0.47	C ₄₁ H ₅₂ O ₄ N	622.3890	622.3891	-0.17
C ₂₆ H ₄₂ O ₆ N	464.3011	464.3007	0.84	C ₂₆ H ₄₂ O ₆ N	464.3007	464.3007	0.12
C ₂₆ H ₄₀ O ₅ N	446.2903	446.2901	0.55	C ₂₆ H ₄₀ O ₅ N	446.2900	446.2901	-0.14
C ₂₆ H ₃₈ O ₄ N	428.2798	428.2795	0.73	C ₂₆ H ₃₈ O ₄ N	428.2794	428.2795	-0.2
C ₂₆ H ₃₆ O ₃ N	410.2692	410.2690	0.47	C ₂₆ H ₃₆ O ₃ N	410.2689	410.269	-0.2
C ₂₆ H ₃₄ O ₂ N	392.2585	392.2584	0.35	C ₂₆ H ₃₄ O ₂ N	392.2584	392.2584	0.04
C ₁₈ H ₃₀ O ₂ N	292.2271	292.2271	0.13	C ₁₈ H ₃₀ O ₂ N	292.2269	292.2271	0.7
C ₁₈ H ₂₈ ON	274.2166	274.2165	0.04	C ₁₈ H ₂₈ ON	274.2164	274.2165	-0.51
C ₁₆ H ₂₆ ON	248.2009	248.2009	0.21	C ₁₆ H ₂₆ ON	248.2008	248.2009	-0.41
C ₁₆ H ₂₄ N	230.1904	230.1903	0.45	C ₁₆ H ₂₄ N	230.1903	230.1903	-0.21
C ₁₄ H ₂₂ N	204.1748	204.1747	0.8	C ₁₄ H ₂₂ N	204.1747	204.1747	-0.04
C ₁₁ H ₁₈ N	164.1435	164.1434	0.876	C ₁₁ H ₁₈ N	164.1434	164.1434	0.16

2.4. Structure Elucidation of 20-Hydroxy-13,19-didesmethyl-SPX D

The empirical formula of compound **11** was determined as C₄₁H₆₀O₈N by HR-ESI-MS. CID-spectra showed the same fragmentation pathway as for **10** except for an upshift of 2 Da, suggesting a reduced double bond between C-1 and C-12. NMR data supported this, showing a reduced double bond in the butenolide ring (C-2/3, Table 4) in comparison to **10** and in accordance with the spectra for SPX D [17]. Therefore, we propose the structure of **11** as 20-Hydroxy-13,19-didesmethyl-SPX D as shown in Figure 4.

2.5. Biosynthesis of GYMs and SPXs

SPXs and GYMs share many structural features (Figure 1) [5,8,12–15,17–24] and are likely biosynthesized by common genes [7]. The compounds elucidated in this study introduce a new

degree of variability to the structural diversity of GYMs and SPXs. This is the first report of a GYM without a methyl group at ring D, and that of a SPX with an additional hydroxyl group at C-20. In future studies aiming at the discovery of novel toxins, this new structural diversity should be taken into consideration.

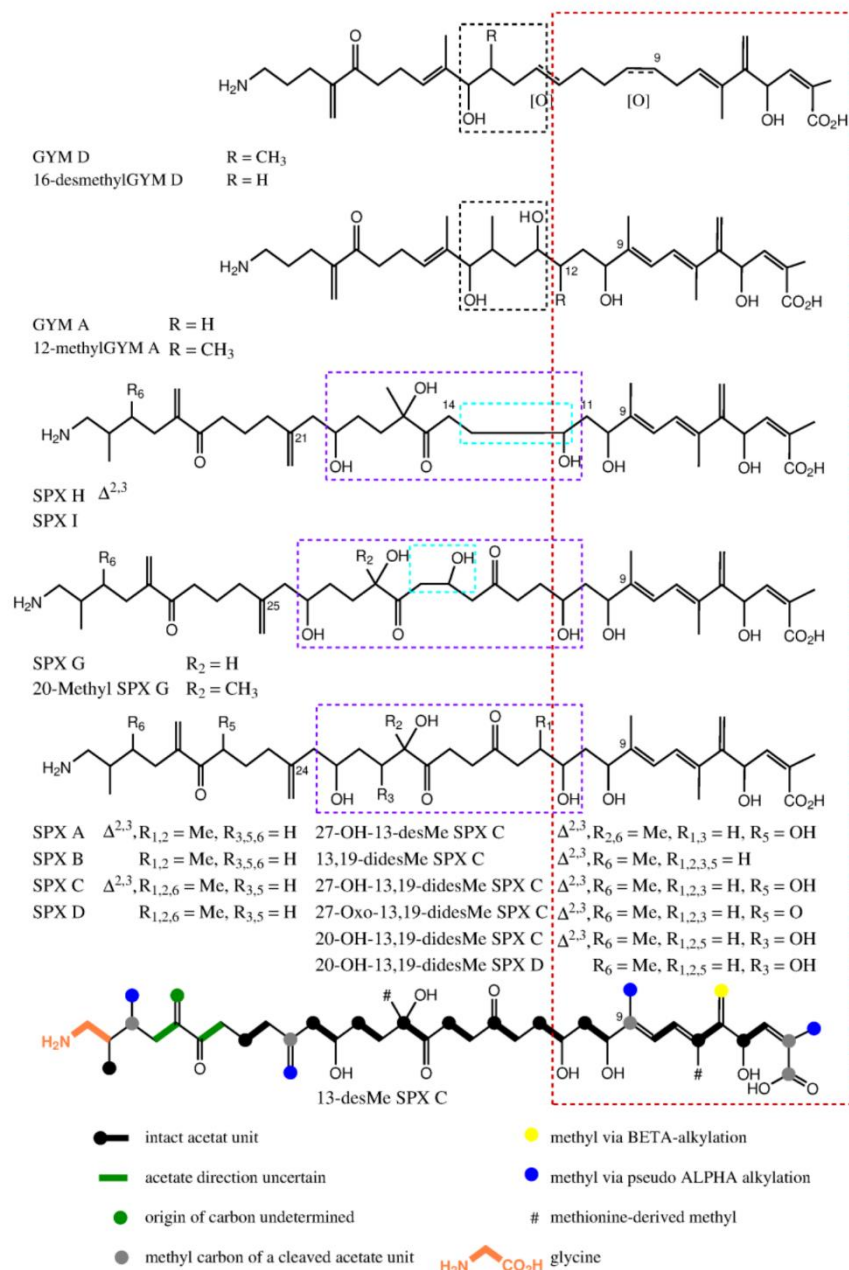


Figure 7. Stacked view of proposed nascent polyketide chains for spirolides and gymnodimines; part with high similarity cornered in red; ring D of GYMs cornered in black; difference between nascent polyketide chains of spirolides are cornered in light blue and origins for rings D, E and F are cornered in violet. The proposed nascent polyketide chain of 13-Desmethyl spirolide C is shown at the bottom with the colored biological origin of nuclei.

Compound **1** and GYM D [8] can be conceived from the same putative nascent polyketide chain (NPC), the only difference being the missing methyl alkylation at C-16. In comparison to GYM A, both of these compounds have one additional carbon between C-7 and C-12 and one less methyl group around C-9 (Figure 7). In the assembled toxin, this difference in NPCs, leads to one additional ring (Figure 1). An additional carbon could indicate a cleaved acetate unit in GYM A, which is a common moiety in dinoflagellate polyketides [7].

The novel spirolides **10** and **11** differ by an unsaturated bond between C-2 and C-3. These SPXs can be conceived from the same NPC with an additional hydroxyl-group at C-20 and one less methyl-group at C-19 in comparison to 13-desmethylSPX C (9). In 9, C-20 and C-21 originate from an intact acetate (Figure 5, C20 from the carboxylic acid, C21 from the methyl group of the acetate) [16]. An incomplete reduction during assembly of NPC would lead to a hydroxylation at C-20 as in **10** and **11** (Figure 7). Therefore, only small changes in the biosynthetic pathway may explain most structural differences between GYMs and SPXs, supporting the hypothesis that these compounds are synthesized by expression of common genes.

2.6. Formation of GYM E

An artificial degradation of GYM A to either GYM B or GYM C is generally considered as unlikely, because this would require both isomerization and oxidation [15]. However, we found evidence for an abiotic reaction of 16-desmethyl GYM D to GYM E. The formation of GYM E in a methanolic extract was observed by sequential mass spectrometric quantification of a 16-desmethyl GYM D containing extract, whereby the relative amount of 16-desmethyl GYM D decreased whereas the concentration of GYM E increased (Data not shown). The proposed mechanism of this reaction (Figure 8) combines isomerization and oxidation in a single reaction step.

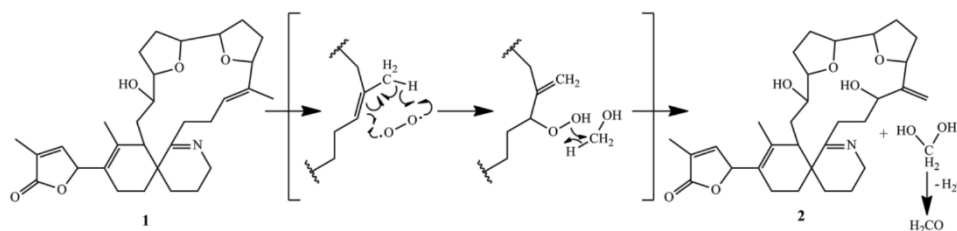


Figure 8. Proposed reaction mechanism of degradation of 16-desmethyl GYM D to GYM E.

2.7. Quantification of the Novel Cyclic Imines in Natural Plankton Assemblages

To confirm the presence of the novel toxins in natural plankton assemblages, extracts of plankton filtered onto glass fiber filters were analyzed by LC-MS/MS with the transitions for **1**, **2**, **10** and **11** (Table 6). The samples were collected in July 2013 during a bloom in Ouwerkerkse Kreek (51°62' N, 3°99' E, The Netherlands) from which the cultured strain *A. ostenfeldii* OKNL48 was also first isolated [25]. GYM **1** (447 pg·mL⁻¹) was detected in concentrations similar to GYM A (561 pg·mL⁻¹) while concentrations of GYM **2** (1250 pg·mL⁻¹) even exceeded concentrations of GYM A.

Table 6. Concentrations of GYM A (4), 16-desmethylgymnodimine D (1), Gymnodimine E (2), SPX 1 (9), 20-Hydroxy-13,19-didesMethyl-SPX C (10), and 20-Hydroxy-13,19-didesMethyl-SPX D (11) in a re-analysis of plankton net samples collected from three stations during previous study by van der Waal et al. [25].

Station	GYM A	1	2	SPX 1	10	11
All in pg per mL Filtered Sea Water						
SL92-1	204	160	619	61	2	15
SL92-2	561	447	1250	211	8	40
SL92-3	2	1	3	0	0	0

3. Materials and Methods

3.1. Cell Culture and Sample Preparation

Alexandrium ostenfeldii was isolated in July 2013 during a bloom in Ouwerkerkse Kreek, The Netherlands and characterized by LC-MS (as strain OKNL48) [6]. Batches of 15 L of OKNL48 were treated with Acetone (7% final concentration) and the toxin content extracted with conditioned HP-20 (25 g per 15 L, 48 h, Diaion Supelco). The resin was collected by filtration and desalted, dried, and stored at $-20\text{ }^{\circ}\text{C}$. The pooled resin (460 g) from a total of 270 L was eluted with methanol, dried under vacuo, and applied to preparative reversed phase chromatography (C18, 25 mm \times 310 mm, 5 mL min^{-1}) and eluted with a stepwise gradient from water-ACN (80:20) to 100% ACN (30 fractions total). The presence of **1** and **2** was confirmed by LC-MS and the toxin-containing fraction dried, taken up in water-ACN (1:1) (2 mL) and applied to HPLC reversed-phase purification on a C8 column (10 \times 150 mm, Machery & Nagel) with solvent A: water and solvent B: acetonitrile (ACN) both containing 0.1% FA. After injection, the samples were eluted isocratically at 15% B for 5 min, followed by a 20 min gradient to 100% B and held for 5 min. The reequilibration phase at 15% B was 5 min. The final purification step was performed under isocratic elution with water-ACN 45:55 over for 30 min on a Phenyl-Hexyl column (4.6 mm \times 150 mm, 1.5 mL \cdot min^{-1} , Machery & Nagel). The yields of these fractions were insufficient for structure elucidation of **10** and **11**, therefore, a total of 60 L additional culture was extracted and purified as described above.

Water samples for the analysis of natural plankton assemblages were taken with a bucket from the surface at three Ouwerkerkse Kreek stations: SL92-1 (51°37'33.7" N 3°59'23.7" E), SL92-2 (51°37'45.5" N 3°59'35.9" E), and SL92-3 (51°37'44.0" N 3°59'25.8" E). The water was filtered onto GFF filters (0.4 μm) and frozen until analysis. Briefly, GFF filters were extracted by reciprocal shaking at maximum speed (6.5 $\text{m} \cdot \text{s}^{-1}$) for 45 s in a FP 120 FastPrep instrument (Bio101, Thermo Savant, Illkirch, France) containing 0.5 g lysing matrix D (Thermo Savant, Illkirch, France), and 750 μL methanol (Merck, Darmstadt, Germany). After homogenization, the samples were centrifuged (16,000 g, 15 min, 4 $^{\circ}\text{C}$, Centrifuge 5415R, Eppendorf, Hamburg, Germany). Each supernatant was transferred to a spin-filter (pore-size 0.45 μm , Millipore Ultrafree, Eschborn, Germany) and centrifuged for 30 s at 3220 g. Filtrates were transferred into HPLC vials (Agilent Technologies, Waldbronn, Germany) for LC-MS/MS analysis.

3.2. Analyses of Cyclic Imines by Chromatography Tandem Mass Spectrometry (LC-MS/MS)

Chromatographic fractions were diluted 1:1000 in 96-well plates and analyzed on a LC-MS/MS system in SRM mode (UPLC: I-Class, MS/MS: Xevo; Waters). The flow-rate was 0.6 mL \cdot min^{-1} isocratic elution with ACN-water (95:5) containing 2.0 mM ammonium formate and 50 mM formic acid resulting in immediate co-elution of all analytes. The runtime was 0.5 min. Cyclic imine containing fractions, filter extracts and the purified toxins were quantified against 13-desMethyl-spirolide C and GYM A (certified reference material; NRC, Halifax, NS, Canada) and expressed as reference standard equivalents (GYM A or SPX1 equivalents) [6] on the same instrumentation as above as follows: A UPLC BEH C18 reverse phase column (Acquity 50 mm \times 2.1 mm, 1.7 μm , Waters, Milford, CT, USA) was used with a flow-rate of 0.6 mL \cdot min^{-1} at 40 $^{\circ}\text{C}$. A gradient elution was performed with two eluants, where eluant A was water and eluent B was acetonitrile/water (95:5 v/v), both containing 2.0 mM ammonium formate and 50 mM formic acid. Initial conditions were 0.5 min column equilibration with 30% B, followed by a linear gradient to 100% B in 3 min, and isocratic elution for 1 min with 100% B. The system was then returned to initial conditions. The fragments used for the detection of the cyclic imines are given in Table S1.

3.3. HR-MS/MS

Accurate mass measurements and fragmentation spectra were acquired with a QExactive Plus mass spectrometer (Thermo Fisher Scientific, Bremen, Germany), using electrospray ionization at a flow-rate of 5 μL per minute. MS measurements were performed in full MS mode with a resolution

of 280,000, a scan range of 150 to 2000 m/z in positive mode using a spray voltage of 3 kV. Capillary temperature was set to 320 °C and the sheath gas was set to 5. Calibration was done against the Calmix standard (Thermo Fisher Scientific).

3.4. NMR Analyses

Purified compounds were dried under vacuo and taken up in 45 μ L deuterated pyridine (Pyr- d_5) containing 0.03% TMS (compounds GYM A, **1**, **2** and **10**) or 45 μ L deuterated methanol (MeOD; SPX STD, **10** and **11**). NMR experiments were performed in 1.7 mm microtubes at 292 K with a AVANCE II 600 MHz NMR spectrometer (BRUKER) and a CPTCI microcryoprobe. Chemical shift referencing was performed against TMS. BRUKER standard pulse programs were used except for heteronuclear multiple bond correlation (IMPACT-HMBC) [26].

3.5. Quantum Chemical Simulation of CD Spectra

Minimal energy geometry was calculated with the GAMESS software package [27,28]. GAMESS was run in parallel on the Linux cluster Cray CS400 “Ollie” at Alfred Wegener Institute’s computing centre, using 36 MPI-tasks on one compute node with two Intel Xeon E5-2697v4 “Broadwell” 18-core CPUs. A semi empirical PM3 level optimization was used prior to density functional theory (DFT) optimization. B3LYP was used in combination with the 6-31G(d) basis set and the “Conductor-like continuum Solvent MOdel” (COSMO) in the “Self-Consistent Reaction Field” method (SCRFF). Geometries with minimal energy were used for calculation of rotatory strengths applying time depended DFT with B3LYP, 6-31G(d), and SCRFF with COSMO in the ORCA software package [29]. The simulated CD spectrum of **1** was obtained by applying Gaussian broadening to each transition as previously described by Li et al. [30] and adjusted manually to the height of experimental data.

4. Conclusions

Here, we report the structural elucidation of two novel gymnodimines (16-desmethyl GYM D and GYM E) and two novel spirolides (20-Hydroxy-13,19-didesMethyl-SPX C and 20-Hydroxy-13,19-didesMethyl-SPX D) originally detected in cultures of *A. ostenfeldii* [6]. The analysis of a plankton sample obtained during an *A. ostenfeldii* bloom revealed high concentrations of the two novel gymnodimines and one of the spirolides in natural plankton assemblages. 16-desmethyl GYM D and GYM E add new structural variability to the class of GYM toxins. The nascent polyketide chain of GYM D, 16-desmethyl GYM D and GYM E has one more carbon between ring B (C-7) and a furan ring D (C-14) in comparison to all other known SPXs and GYMs. We suggest that this difference in chain length is due to a biosynthetic cleavage of the acetate unit at C-9. This applies to all other cyclic imine toxins whereas this acetate unit is preserved in GYM D-type gymnodimines and spirolides. In comparison, 20-Hydroxy-13,19-didesMethyl-SPX C and 20-Hydroxy-13,19-didesMethyl-SPX D are synthesized from an incomplete reduction of the acetate at C-20. Notably, despite a high structural similarity of SPXs and GYMs, only strains of *A. ostenfeldii* have been confirmed to produce both compound classes. A comparison of the genetic or proteomic differences between *Karenia selliformis* (only GYMs reported) and *A. ostenfeldii* (producing either only SPXs or both toxin groups) may be a promising approach to identify the biosynthetic mechanisms underlying these structural differences.

Supplementary Materials: The following are available online at <http://www.mdpi.com/1660-3397/16/11/446/s1>, Figure S1: Structures of known and novel gymnodimines; Figure S2: Structures of known and novel spirolides; Figures S4–S22 NMR-spectra of **1**; Figure S23: CD-spectra of **1** and **4** and simulated CD spectra of **1**, S24–S31 NMR-spectra of **2**; Figures S32–S53 NMR-spectra of **10**; Figures S54–S62 NMR-spectra of **11**; Table S1: Mass transitions of spiroimines included in LC-MS/MS analysis; Figure S63: LC-MS/MS chromatogram of station SL92-2. Raw NMR data (Topspin) and annotated Mestre files are available in the data repository PANGAEA <https://doi.pangaea.de/10.1594/PANGAEA.895116>.

Author Contributions: Conceptualization, U.T., B.K., and J.T.; Data curation, C.Z.; Formal analysis, C.Z.; Investigation, C.Z., U.T., B.K., and J.T.; Methodology, C.Z., J.N., U.T., B.K., and J.T.; Supervision, U.T., T.H., B.K.,

and J.T.; Validation, C.Z.; Visualization, C.Z.; Writing—original draft, C.Z., U.T., B.K., and J.T.; Writing—review and editing, U.T., T.H., B.K., and J.T.

Funding: This work was partially funded by the Helmholtz-Gemeinschaft Deutscher Forschungszentren through the research program “Polar regions And Coasts in the changing Earth System” (PACES) of the Alfred Wegener Institut-Helmholtz Zentrum für Polar- und Meeresforschung.

Acknowledgments: We thank Dedmer van de Waal (NIOO) for providing plankton field samples and associated information from Ouwerkerkse Kreek and Wolfgang Drebing (AWI) for assistance in bulk culturing and toxin extraction. We thank Peter Spiteller (University Bremen) for assistance with the acquisition of the CD spectra. We thank Natalja Rakowsky and Malte Thoma (both AWI) for the HPC implementation of the quantum chemical simulation.

Conflicts of Interest: The authors declare no conflict of interest. The funders had no role in the design of the study; in the collection, analyses, or interpretation of data; in the writing of the manuscript, or in the decision to publish the results.

References

1. Molgó, J.; Marchot, P.; Araújo, R.; Benoit, E.; Iorga, B.I.; Zakarian, A.; Taylor, P.; Bourne, Y.; Servent, D. Cyclic imine toxins from dinoflagellates: A growing family of potent antagonists of the nicotinic acetylcholine receptors. *J. Neurochem.* **2017**, *142*, 41–51. [[CrossRef](#)] [[PubMed](#)]
2. Stivala, C.E.; Benoit, E.; Araújo, R.; Servent, D.; Novikov, A.; Molgó, J.; Zakarian, A. Synthesis and biology of cyclic imine toxins, an emerging class of potent, globally distributed marine toxins. *Nat. Prod. Rep.* **2015**, *32*, 411–435. [[CrossRef](#)] [[PubMed](#)]
3. Rundberget, T.; Aasen, J.A.B.; Selwood, A.I.; Miles, C.O. Pinnatoxins and spirolides in Norwegian blue mussels and seawater. *Toxicon* **2011**, *58*, 700–711. [[CrossRef](#)] [[PubMed](#)]
4. Tillmann, U.; Kremp, A.; Tahvanainen, P.; Krock, B. Characterization of spirolide producing *Alexandrium ostenfeldii* (Dinophyceae) from the western Arctic. *Harmful Algae* **2014**, *39*, 259–270. [[CrossRef](#)]
5. Van Wagoner, R.M.; Misner, I.; Tomas, C.R.; Wright, J.L. Occurrence of 12-methylgymnodimine in a spirolide-producing dinoflagellate *Alexandrium peruvianum* and the biogenetic implications. *Tetrahedron Lett.* **2011**, *52*, 4243–4246. [[CrossRef](#)]
6. Martens, H.; Tillmann, U.; Harju, K.; Dell’Aversano, C.; Tartaglione, L.; Krock, B. Toxin variability estimations of 68 *Alexandrium ostenfeldii* (Dinophyceae) strains from the netherlands reveal a novel abundant gymnodimine. *Microorganisms* **2017**, *5*, 29. [[CrossRef](#)] [[PubMed](#)]
7. Van Wagoner, R.M.; Satake, M.; Wright, J.L.C. Polyketide biosynthesis in dinoflagellates: What makes it different? *Nat. Prod. Rep.* **2014**, *31*, 1101–1137. [[CrossRef](#)] [[PubMed](#)]
8. Harju, K.; Koskela, H.; Kremp, A.; Suikkanen, S.; de La Iglesia, P.; Miles, C.O.; Krock, B.; Vanninen, P. Identification of gymnodimine D and presence of gymnodimine variants in the dinoflagellate *Alexandrium ostenfeldii* from the Baltic Sea. *Toxicon* **2016**, *112*, 68–76. [[CrossRef](#)] [[PubMed](#)]
9. Munday, R.; Towers, N.R.; MacKenzie, L.; Beuzenberg, V.; Holland, P.T.; Miles, C.O. Acute toxicity of gymnodimine to mice. *Toxicon* **2004**, *44*, 173–178. [[CrossRef](#)] [[PubMed](#)]
10. Kharrat, R.; Servent, D.; Girard, E.; Ouanounou, G.; Amar, M.; Marrouchi, R.; Benoit, E.; Molgó, J. The marine phycotoxin gymnodimine targets muscular and neuronal nicotinic acetylcholine receptor subtypes with high affinity. *J. Neurochem.* **2008**, *107*, 952–963. [[CrossRef](#)] [[PubMed](#)]
11. Wandscheer, C.B.; Vilariño, N.; Espiña, B.; Louzao, M.C.; Botana, L.M. Human muscarinic acetylcholine receptors are a target of the marine toxin 13-desmethyl C spirolide. *Chem. Res. Toxicol.* **2010**, *23*, 1753–1761. [[CrossRef](#)] [[PubMed](#)]
12. Seki, T.; Satake, M.; MacKenzie, L.; Kaspar, H.F.; Yasumoto, T. Gymnodimine, a new marine toxin of unprecedented structure isolated from New Zealand oysters and the dinoflagellate, *Gymnodinium* sp. *Tetrahedron Lett.* **1995**, *36*, 7093–7096. [[CrossRef](#)]
13. Hu, T.; Burton, I.W.; Cembella, A.D.; Curtis, J.M.; Quilliam, M.A.; Walter, J.A.; Wright, J.L.C. Characterization of Spirolides A, C, and 13-Desmethyl C, new marine toxins isolated from toxic plankton and contaminated shellfish. *J. Nat. Prod.* **2001**, *64*, 308–312. [[CrossRef](#)] [[PubMed](#)]
14. Miles, C.O.; Wilkins, A.L.; Stirling, D.J.; MacKenzie, A.L. New analogue of gymnodimine from a *Gymnodinium* species. *J. Agric. Food Chem.* **2000**, *48*, 1373–1376. [[CrossRef](#)] [[PubMed](#)]

15. Miles, C.O.; Wilkins, A.L.; Stirling, D.J.; MacKenzie, A.L. Gymnodimine C, an isomer of gymnodimine B, from *Karenia selliformis*. *J. Agric. Food Chem.* **2003**, *51*, 4838–4840. [[CrossRef](#)] [[PubMed](#)]
16. MacKinnon, S.L.; Cembella, A.D.; Burton, I.W.; Lewis, N.; LeBlanc, P.; Walter, J.A. Biosynthesis of 13-desmethyl spirolide C by the dinoflagellate *Alexandrium ostenfeldii*. *J. Org. Chem.* **2006**, *71*, 8724–8731. [[CrossRef](#)] [[PubMed](#)]
17. Hu, T.; Curtis, J.M.; Oshima, Y.; Quilliam, M.A.; Walter, J.A.; Watson-Wright, W.M.; Wright, J.L.C. Spirolides B and D, two novel macrocycles isolated from the digestive glands of shellfish. *J. Chem. Soc. Chem. Commun.* **1995**, *20*, 2159–2161. [[CrossRef](#)]
18. Roach, J.S.; LeBlanc, P.; Lewis, N.I.; Munday, R.; Quilliam, M.A.; MacKinnon, S.L. Characterization of a dispiroketal spirolide subclass from *Alexandrium ostenfeldii*. *J. Nat. Prod.* **2009**, *72*, 1237–1240. [[CrossRef](#)] [[PubMed](#)]
19. Ciminiello, P.; Dell'Aversano, C.; Fattorusso, E.; Forino, M.; Grauso, L.; Tartaglione, L.; Guerrini, F.; Pistocchi, R. Spirolide toxin profile of Adriatic *Alexandrium ostenfeldii* cultures and structure elucidation of 27-hydroxy-13,19-didesmethyl spirolide C. *J. Nat. Prod.* **2007**, *70*, 1878–1883. [[CrossRef](#)] [[PubMed](#)]
20. MacKinnon, S.L.; Walter, J.A.; Quilliam, M.A.; Cembella, A.D.; LeBlanc, P.; Burton, I.W.; Hardstaff, W.R.; Lewis, N.I. Spirolides isolated from Danish strains of the toxigenic dinoflagellate *Alexandrium ostenfeldii*. *J. Nat. Prod.* **2006**, *69*, 983–987. [[CrossRef](#)] [[PubMed](#)]
21. Aasen, J.; MacKinnon, S.L.; LeBlanc, P.; Walter, J.A.; Hovgaard, P.; Aune, T.; Quilliam, M.A. Detection and identification of spirolides in norwegian shellfish and plankton. *Chem. Res. Toxicol.* **2005**, *18*, 509–515. [[CrossRef](#)] [[PubMed](#)]
22. Hu, T.; Curtis, J.M.; Walter, J.A.; Wright, J.L. Characterization of biologically inactive spirolides E and F: Identification of the spirolide pharmacophore. *Tetrahedron Lett.* **1996**, *37*, 7671–7674. [[CrossRef](#)]
23. Sleno, L.; Chalmers, M.J.; Volmer, D.A. Structural study of spirolide marine toxins by mass spectrometry. Part II. Mass spectrometric characterization of unknown spirolides and related compounds in a cultured phytoplankton extract. *Anal. Bioanal. Chem.* **2004**, *378*, 977–986. [[CrossRef](#)] [[PubMed](#)]
24. Aasen, J.A.B.; Hardstaff, W.; Aune, T.; Quilliam, M.A. Discovery of fatty acid ester metabolites of spirolide toxins in mussels from Norway using liquid chromatography/tandem mass spectrometry. *Rapid Commun. Mass Spectrom.* **2006**, *20*, 1531–1537. [[CrossRef](#)] [[PubMed](#)]
25. Van de Waal, D.B.; Tillmann, U.; Martens, H.; Krock, B.; van Scheppingen, Y.; John, U. Characterization of multiple isolates from an *Alexandrium ostenfeldii* bloom in The Netherlands. *Harmful Algae* **2015**, *49*, 94–104. [[CrossRef](#)]
26. Furrer, J. A robust, sensitive, and versatile HMBC experiment for rapid structure elucidation by NMR: IMPACT-HMBC. *Chem. Commun.* **2010**, *46*, 3396–3398. [[CrossRef](#)] [[PubMed](#)]
27. Schmidt, M.W.; Baldrige, K.K.; Boatz, J.A.; Elbert, S.T.; Gordon, M.S.; Jensen, J.H.; Koseki, S.; Matsunaga, N.; Nguyen, K.A.; Su, S.; et al. General atomic and molecular electronic structure system. *J. Comput. Chem.* **1993**, *14*, 1347–1363. [[CrossRef](#)]
28. Gordon, M.S.; Schmidt, M.W. Advances in electronic structure theory: GAMESS a decade later. In *Theory and Applications of Computational Chemistry*; Dykstra, C.E., Frenking, G., Kim, K.S., Scuseria, G.E., Eds.; Elsevier: Amsterdam, The Netherlands, 2005; Chapter 41; pp. 1167–1189.
29. Neese, F. Software update: The ORCA program system, version 4.0. *WIREs Comput. Mol. Sci.* **2018**, *8*, e1327. [[CrossRef](#)]
30. Li, X.-C.; Ferreira, D.; Ding, Y. Determination of Absolute Configuration of Natural Products: Theoretical Calculation of Electronic Circular Dichroism as a Tool. *Curr. Org. Chem.* **2010**, *14*, 1678–1697. [[CrossRef](#)] [[PubMed](#)]



3. Identification of novel Azaspiracids from *Azadinium poporum*

This chapter describes the structure elucidation of two novel Azaspiracids (AZAs), namely AZA-40, and AZA-59, produced by two genotypes of the dinoflagellate *Azadinium poporum* originally isolated from Fangchenggang, South China Sea and Puget Sound, Washington State, USA respectively. The data presented in this chapter will be published as part of two collaborative publications focusing on the toxicity of these novel compounds and implications for human health and food safety. My contribution was prerequisite for these studies and provided pure toxin sufficient for mouse bioassays by intraperitoneal injection ((Kilcoyne *et al.*, 2014a), performed by Silvio Sosa), ELISA method development ((Samdal *et al.*, 2015), performed by Ingunn Anita Samdal) and *in vitro* cell line toxicity ((Escher *et al.*, 2012; Miller *et al.*, 2010; Wang *et al.*, 2006), performed by Beate Escher). In both papers, I was responsible for the mass-culturing of the dinoflagellates, purification of the toxins, structure elucidation and the calibration/quantification.

The structure elucidation and *in vitro* toxicity of two novel azaspiracids from cultures of the South China Sea

Ulf Bickmeyer¹, B. I. Escher^{2,3}, H. Gu⁴, T. Harder⁵, B. Krock¹, J. Nieva¹, J. Tebben¹, U. Tillmann¹, S. Wietkamp¹, C. Zurhelle⁵ (alphabetical order)

¹ Alfred Wegener Institute, Helmholtz Centre for Polar and Marine Research, Section Ecological Chemistry, Am Handelshafen 12, 27570 Bremerhaven, Germany

² Department of Cell Toxicology, UFZ – Helmholtz Centre for Environmental Research, Leipzig, Germany

³ Department of Environmental Toxicology, Center for Applied Geosciences, Eberhard Karls University, Tübingen, Germany

⁴ Third Institute of Oceanography, SOA, Xiamen 361005, PR China

⁵ University of Bremen, Department of Biology and Chemistry, Marine Chemistry, Leobener Straße 6, 28359 Bremen, Germany

To be submitted (the journal depends on the results of the bioassays e. g. Harmful Algae)

I contributed in following parts to the paper: data curation, formal analysis, investigation, methodology, validation, and visualization

Structural elucidation, acute oral toxicity of the novel azaspiracid AZA-59 from Puget Sound, USA

J. Deeds¹, T. Harder², J. Kilcoyne³, B. Krock⁴, I. A. Samdal⁵, S. Sosa⁶, J. Tebben⁴, U. Tillmann⁴, V. L. Trainer⁷, A. Tubaro⁸, C. Zurhelle² (alphabetical order)

¹ US Food and Drug Administration Center for Food Safety and Applied Nutrition, 5100 Paint Branch Parkway, College Park, Maryland, 20723, USA

² University of Bremen, Department of Biology and Chemistry, Marine Chemistry, Leobener Straße 6, 28359 Bremen, Germany

³ Marine Institute, Renville, Oranmore, County Galway, Ireland

⁴ Alfred Wegener Institute, Helmholtz Centre for Polar and Marine Research, Section Ecological Chemistry, Am Handelshafen 12, 27570 Bremerhaven, Germany

⁵ Veterinary Institute, PB 8156 Dep., 0033 Oslo, Norway

⁶ IFREMER, Laboratoire Phycotoxines, Rue de l'Île d'Yeu, 44311 Nantes, France

⁷ Northwest Fisheries Science Center, National Marine Fisheries Service, National Oceanic and Atmospheric Administration, 2725 Montlake Blvd. E., Seattle, WA 98112, USA

⁸ Department of Life Sciences, University of Trieste, Via A. Valerio 6, 34127 Trieste, Italy

To be submitted (the journal depends on the results of the bioassays e. g. Harmful Algae)

I contributed in following parts to the paper: data curation, formal analysis, investigation, methodology, validation, and visualization

3.1 Introduction

Since the discovery of azaspiracids (AZAs) in 1998, 40 structure derivatives have been reported, 17 of which have been confirmed by NMR (see Figure 1.5). This study reports the structure elucidation of two unknown AZAs, namely AZA-40, and AZA-59.

The compounds AZA-40 were first detected by mass-spectrometry in cultures of *Azadinium poporum* from the South China Sea (Krock *et al.*, 2014). AZA-40 can be mistaken for AZA-1 in liquid chromatography-mass spectrometric analyses because of similar retention times and fragmentation into the same the quantifier ion (m/z 842 \rightarrow 824).

AZA-59 was first discovered in cultures of a genotypes of *A. poporum* isolated from Puget Sound, , USA, WA (Kim *et al.*, 2017). Anecdotal evidence by consumers of gastrointestinal disorders after consumption of Puget Sound shellfish supported the presence of a potentially new toxin since no regulated toxins were detected by food-safety monitoring and no aquaculture closures were issued (Kim *et al.*, 2017). These incidents triggered this study to chemically characterize the putative novel toxin and provide analytical reference material for bioassays and chemical analyses to include this toxin in food-safety monitoring.

3.2 Results and discussion

3.2.1 Structure elucidation of AZA-40

Previously, AZA-40 (**6**) a novel Azaspiracid (AZA) with identical m/z of 842 as AZA-1 and similar chromatographic characteristics was identified in cultures of *Azadinium poporum* obtained from the South China Sea (Krock *et al.*, 2014). The absence of the characteristic qualifier transition observed in AZA-1 (m/z 842 \rightarrow 672) suggested the presence of an unknown AZA. The MS²-spectra of the novel molecule revealed a similar MS fragmentation pattern as compared to AZA-1 but with a mass difference of minus 14 Da (CH₂), indicating an additional methyl-group between C-1 and C-9 and a missing methyl-group in part of the molecule consisting C-33 to C-39 (rings H, I). A more precise localization was not possible by MS characterization (Krock *et al.*, 2014).

Apart from the lower mass, high similarity between the CID-spectra of AZA-1 and AZA-40 suggested a high structure similarity of these molecules (cf. Table 3.1). The NMR spectra of both molecules confirmed the structural similarities.

Table 3.1: Calculated and measured accurate masses (m/z) for [M + H]⁺ of AZA-40 and its product ions obtained with HRMS in comparison to the parent ion and corresponding fragments of AZA-1.

AZA-40				AZA-1	
Formula	Measured	Calculated	Δ/ppm	Formula	m/z
C ₄₇ H ₇₂ NO ₁₂	842.50524	842.50490	0.41	C ₄₇ H ₇₂ NO ₁₂	842
C ₄₇ H ₇₀ NO ₁₁	824.49479	824.49434	0.55	C ₄₇ H ₇₀ NO ₁₁	824
C ₃₇ H ₅₆ NO ₉	658.39530	658.39496	0.52	C ₃₈ H ₅₆ NO ₉	672
C ₃₇ H ₅₄ NO ₈	640.38476	640.38439	0.57	C ₃₈ H ₅₆ NO ₈	654
C ₂₆ H ₄₂ NO ₅	448.30605	448.30575	0.67	C ₂₇ H ₄₄ NO ₅	462
C ₂₆ H ₄₀ NO ₄	430.29546	430.29519	0.63	C ₂₂ H ₃₆ NO ₃	362
C ₂₁ H ₃₄ NO ₃	348.25347	348.25332	0.43	C ₁₆ H ₂₆ NO ₃	280
C ₁₅ H ₂₂ NO ₂	248.16460	248.16451	0.38	C ₁₆ H ₂₄ NO ₂	262
C ₉ H ₁₆ NO	154.12273	154.12264	0.58	C ₁₀ H ₁₈ NO	168

The spin system of ring I of AZA-40 (Figure 3.1) was identified by TOCSY and HSQC-TOCSY experiments. The chemical shift of C-37 in the 135° DEPT experiment revealed a positive signal, whereas the chemical shift of C-39 showed a negative signal, confirming a single methyl group at C-37 in ring I of AZA-40. Therefore, AZA-40 lacks the methyl group at C-39 in comparison to AZA-1. The additional methyl-group of AZA-40 between C-1 to C-9 identified by CID, was annotated to either C-7 or C-8 by NMR. The COSY correlation between proton at

C-6 and the additional methyl-group suggested C-7 as the most likely position of the methyl group. However, a COSY correlation between proton of C-6 and C-9 revealed a close spatial proximity between C-6 and C-9, suggesting a methylene group (C-9) at position 7 and a double bond between positions 8 and 9. This COSY correlation (C-6/C-9) was also observed during the first structural elucidation of AZA-1 by Satake *et al.* (Satake *et al.*, 1998)(*cf.* Chapter 1.3.2, Figure 1.4). This initial annotation was later corrected (Figure 3.1) by comparison of the natural toxin with a synthesized version and its precursor (Nicolaou *et al.*, 2004). This long-range COSY coupling (C-6 to C-9 in **6**; Figure 3.2) was also observed in a simpler structure, such as lissoketal (**7**: C-1 to C-4) (Hopmann and Faulkner, 1997). Therefore, the COSY coupling between the methyl group and the proton at C-6 did not equivocally assign the position of the methyl group to C-7. Further HMBC correlations of the additional methyl group to C-7, C-8 and C-9 suggested C-8 as the most likely position for this methyl group. Generally, a methyl group at C-8 is a known feature for AZAs. For example, AZA-2 (**8**), AZA-9 and AZA-10 carry methyl groups at C-8 (*cf.* Figure 3.2) and both show a COSY coupling between proton at C-6 and protons of the methyl group attached to C-8 (Kilcoyne *et al.*, 2015).

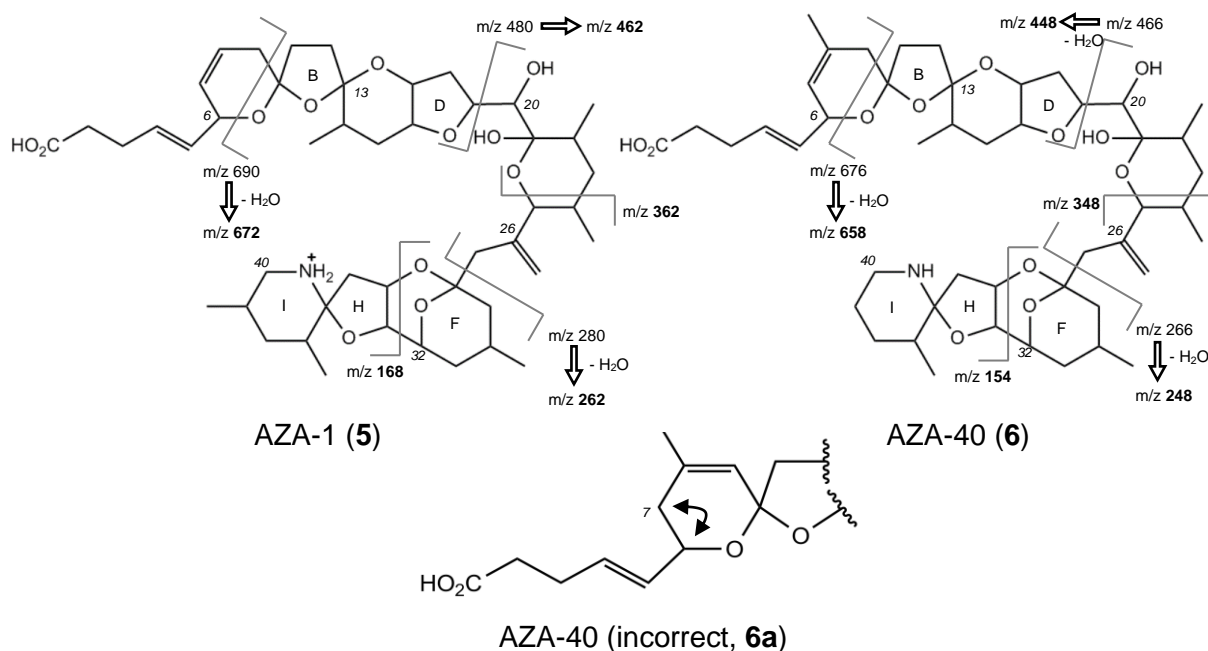


Figure 3.1: Structures of AZA-1 and AZA-40 with characteristic CID fragments (bold m/z values) according to Krock *et al.* (Krock *et al.*, 2014) and the incorrect structure of AZA-40 as indicated by COSY correlation between methylene group and C-6 (**6a**). Numbers and letters indicate the atom position and ring position respectively.

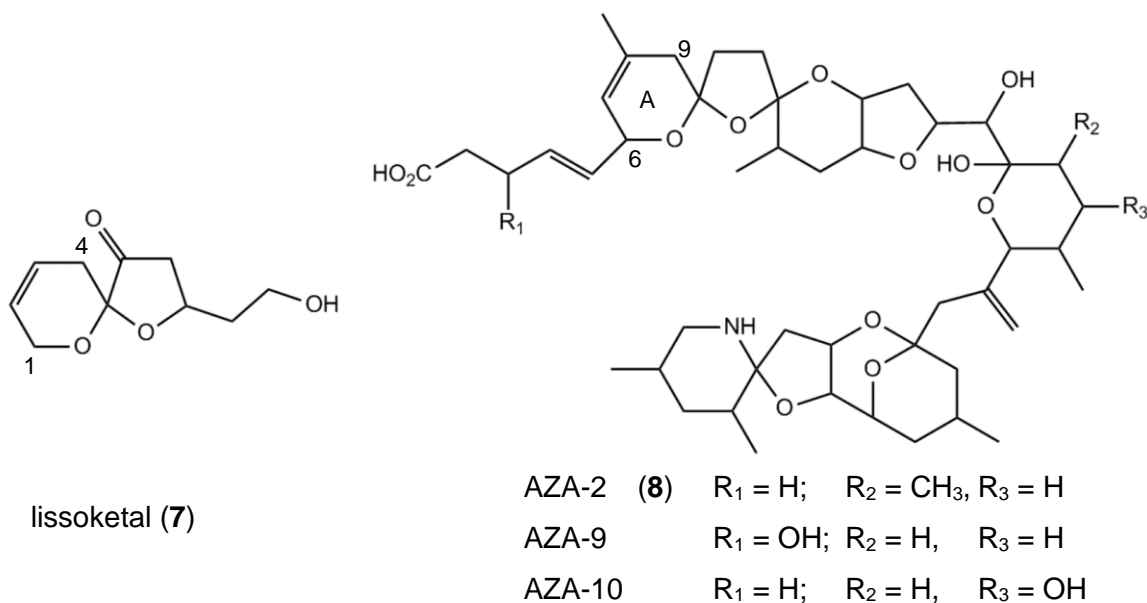


Figure 3.2: Structures of lissoketal (7), AZA-2 (8), AZA-9 and AZA-10. Numbers and letters indicate the atom position and ring position respectively.

Finally, the comparison of the chemical shifts of AZA-40 with literature NMR data of AZA-2 (Table 3.2) revealed high similarity of chemical shifts especially for nuclei of ring A (Nicolaou *et al.*, 2006; Ofuji *et al.*, 1999). Therefore, the position of the methyl group was unequivocally established at C-8, concluding that AZA-40 is structurally similar to AZA-1, but lacking the methyl group at C-39 and with an additional methyl group at C-8.

Table 3.2: The NMR chemical shifts (δ) of the novel AZA-40 (*cf.* section 9.2.1 for spectra) in comparison with the NMR chemical shifts (δ) of AZA-2 (Ofuji *et al.*, 1999).

No.	AZA-2 (8)			AZA-40 (6)			No.	AZA-2 (8)			AZA-40 (6)		
	¹³ C	¹ H		¹³ C	¹ H			¹³ C	¹ H		¹³ C	¹ H	
1	177.8 ^a			181.5			22-Me	17.2	0.89		14.2	0.92	
2	35.6	2.34	2.34	38.4	2.24		23	39	1.43	1.43	38.3	1.42	
3	29.5	2.31	2.31	30.2	2.33		24	43.1	1.33		41.5	1.38	
4	132.8	5.68		133.2	5.74		24-Me	18.9	0.83		17.8	0.83	
5	132.1	5.42		130.7	5.41		25	80.4	3.97		79.5	3.94	
6	73.3	4.72		72.4	4.74		26	149.1			147.4		
7	123.6	5.32		122.7	5.36		=CH2	118.1	5.35	5.17	115.2	5.25	5.11
8	132.8			130.7			27	50.1	2.42	2.24	49.0	2.36	2.17
8-Me	23.8	1.67		22.8	1.71		28	99.5			97.7		
9	41.1	2.42	1.97	40.1	2.44	1.99	29	44.9	2.03	1.36	44.5	1.99	1.32
10	108.3			107.1			30	27.2	2.22		26.4	2.27	
11	34	2.33	1.65	37.1	2.18	1.97	30-Me	24.1	0.93		23.6	0.95	
12	38.3	2.16	1.96	32.9	2.36	1.67	31	36.1	1.82	1.51	35.6	1.8	1.49
13	112.1			111.1			32	73.6	4.35		72.6	4.27	
14	31.7	2.00		30.6	2.04		33	82.4	4.06		79.1	3.76	
14-Me	17.4	0.93		16.5	0.95		34	75.6	5.00		75.3	4.82	
15	33.4	1.83	1.73	32.2	1.83	1.77	35	42.4	2.62	2.49	42.8	2.4	1.95
16	79	3.87		77.5	3.9		36	97.5			96.3		
17	74.2	4.2		72.9	4.19		37	36.5	1.97		37.3	1.74	
18	37.7	1.98	1.98	37.9	2.13	2.04	37-Me	16.2	0.97		15.9	0.9	
19	79.9	4.42		78.7	4.42		38	38.4	1.68	1.29	25.6	1.59	
20	77.6	3.93		76.6	3.53		39	30.2	1.86		30.8	1.57	
21	101			99.5			39-Me	19.3	0.94				
22	37.6	2.07		38.5	2.26		40	46.9	2.91	2.83	40.1	2.95	2.56

^a ¹³C chemical shifts at C-1 were deduced from HMBC.

3.2.2 Structure elucidation of AZA-59 (10)

While AZA-40 were found in cultures of *A. poporum* from the South China Sea, another putative novel AZA was discovered in cultures of *A. poporum* originating from Puget Sound (Seattle) (Kim *et al.*, 2017). It was reported as AZA-59 with a m/z 860 for the protonated form, which revealed CID fragments typical for AZA-1 (5), namely m/z 462, m/z 362, m/z 262 and m/z 158 (Figure 3.3) (Kim *et al.*, 2017). Based on the comparison of the CID-spectra, Kim *et al.* proposed AZA-59 to be similar to AZA-1 with a hydroxyl-group at C-3 and hydration of double bond between C-7 and C-8 as showed in Figure 3.3 (Kim *et al.*, 2017).

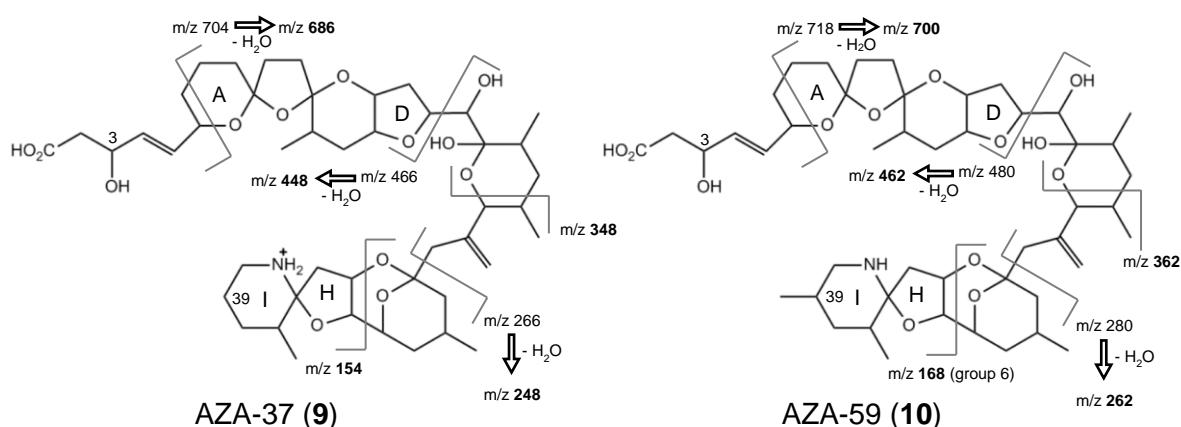


Figure 3.3: Structures and characteristic CID-fragments (bold m/z values) of AZA-37 and AZA-59 (Kim *et al.*, 2017; Krock *et al.*, 2012).

AZA-59 was suggested to be structurally similar to AZA-37 with an additional methyl group at C-39. The sum formulas of all fragment ions for AZA-59 revealed an additional CH_2 in comparison to AZA-37 (Table 3.3), which supports the proposed position of the methyl group.

Table 3.3: Exact and measured accurate masses (m/z) for $[\text{M} + \text{H}]^+$ of AZA-59 and its product ions obtained with HRMS in comparison to parent ion and corresponding fragments of AZA-37 (group 6 fragments (*cf.* Figure 3.3) were not detected).

AZA-59 (10)				AZA-37 (9)	
Formula	Measured	Calculated	Δ/ppm	Formula	m/z
$\text{C}_{47}\text{H}_{74}\text{NO}_{13}$	860.51612	860.51547	0.76	$\text{C}_{46}\text{H}_{72}\text{NO}_{13}$	846
$\text{C}_{47}\text{H}_{72}\text{NO}_{12}$	842.50437	842.5049	-0.64	$\text{C}_{46}\text{H}_{70}\text{NO}_{12}$	828
$\text{C}_{40}\text{H}_{62}\text{NO}_9$	700.44205	700.44191	0.2	$\text{C}_{39}\text{H}_{60}\text{NO}_9$	686
$\text{C}_{40}\text{H}_{60}\text{NO}_8$	682.43152	682.43134	0.26	$\text{C}_{39}\text{H}_{58}\text{NO}_8$	668
$\text{C}_{27}\text{H}_{44}\text{NO}_5$	462.3216	462.3214	0.43	$\text{C}_{26}\text{H}_{42}\text{NO}_5$	448
$\text{C}_{22}\text{H}_{36}\text{NO}_3$	362.26899	362.26897	0.04	$\text{C}_{21}\text{H}_{34}\text{NO}_3$	348
$\text{C}_{16}\text{H}_{24}\text{NO}_2$	262.18019	262.18016	0.13	$\text{C}_{15}\text{H}_{22}\text{NO}_2$	248

The proposed structure of AZA-59 was confirmed by NMR. Chemical shifts of proton and carbon nuclei of compound **10** were highly similar to the corresponding proton and carbon chemical shifts of AZA-37, except for nuclei of ring I (Table 3.4, Figure 3.3). The highest discrepancy of chemical shifts between AZA-59 and AZA-37 was observed at C-38 to C-40. Notably, C-39 in AZA-59 was identified by 135° DEPT as CH-group unlike a CH₂-group in AZA-37. An additional methyl group at C-39 distinguished AZA-59 from AZA-37.

Table 3.4: Comparison of NMR chemical shifts (δ) of novel AZA-59 (cf. section 9.2.2 for spectra) and AZA-37 (Krock et al., 2015).

No.	AZA-37 (9)		AZA-59 (10)		No.	AZA-37 (9)		AZA-59 (10)	
	¹³ C	¹ H	¹³ C	¹ H		¹³ C	¹ H	¹³ C	¹ H
1	180.3		178.5		22-Me	17.2	0.92	16.66	0.94
2	46.1	2.33	44.94	2.39	23	39.1	1.43 1.43	38.39	1.45
3	71.4	4.39	70.55	4.45	24	43	1.35	42.57	1.36
4	134.6	5.70	133.44	5.72	24-Me	18.9	0.84	18.31	0.86
5	133.1	5.65	132.89	5.68	25	80.3	4.00	79.75	4.00
6	73.3	4.35	72.56	4.38	26	149		149.9	
7	38.4	1.87 1.43	32.29	1.68 1.34	=CH ₂	117.8	5.33 5.15	117.21	5.37 5.19
8	22.2	1.77 1.70	21.54	1.93 1.76	27	50.4	2.42 2.25	49.6	2.44 2.27
8-Me					28	99.4		99.5	
9	36.6	1.83 1.70	37.73	1.70	29	45	2.05 1.36	44.29	2.07 1.4
10	109.1		109.3		30	27.2	2.23	26.57	2.25
11	33.9	2.33 1.69	37.8	2.08 1.90	30-Me	24.3	0.96	23.73	0.97
12	32.8	2.03 1.83	33.2	2.31 1.64	31	36.1	1.84 1.52	35.45	1.86 1.54
13	111.8		112		32	73.7	4.37	72.94	4.38
14	31.8	2.01	31.17	2.01	33	82.1	4.05	81.76	4.09
14-Me	17.5	0.9	16.87	0.91	34	75.7	5	74.99	5.03
15	33.5	1.87 1.76	32.93	1.88 1.82	35	42.7	2.60 2.49	41.9	2.66 2.51
16	78.9	3.94	78.42	3.95	36	98		97.5	
17	74.3	4.29	73.61	4.29	37	36.7	1.98	36.07	2.03
18	37.6	2.07 2.00	36.95	2.11 2.03	37-Me	16.4	0.97	15.68	1.01
19	79.9	4.44	79.34	4.45	38	29.7	1.67 1.63	37.76	1.73 1.32
20	77.4	3.93	76.95	3.96	39	23.8	1.70	29.5	1.93
21	101		101.1		39-Me			18.69	0.98
22	37.6	2.07	36.8	2.05	40	41.2	3.17 2.99	46.34	2.92 2.85

3.2.3 Quantitative comparison of AZA-1 by LC-MS and NMR

AZA-1 is commonly used as analytical LC-MS standard for other AZA derivatives. While NMR-based quantification only relies on the concentration and the number of nuclei responsible for the NMR signal, LC-MS quantification varies due to the ionization efficiency and fragmentation resulting in highly variable signal intensities even for molecules with similar structural features.

The correlation between both quantifications is shown in Figure 3.4. The slope of nearly 1 for AZA-40 and AZA-59 highlighted the equivalence of both methods, suggesting that AZA-1 serves as a reliable analytical standard for the quantification of AZA-40 and AZA-59.

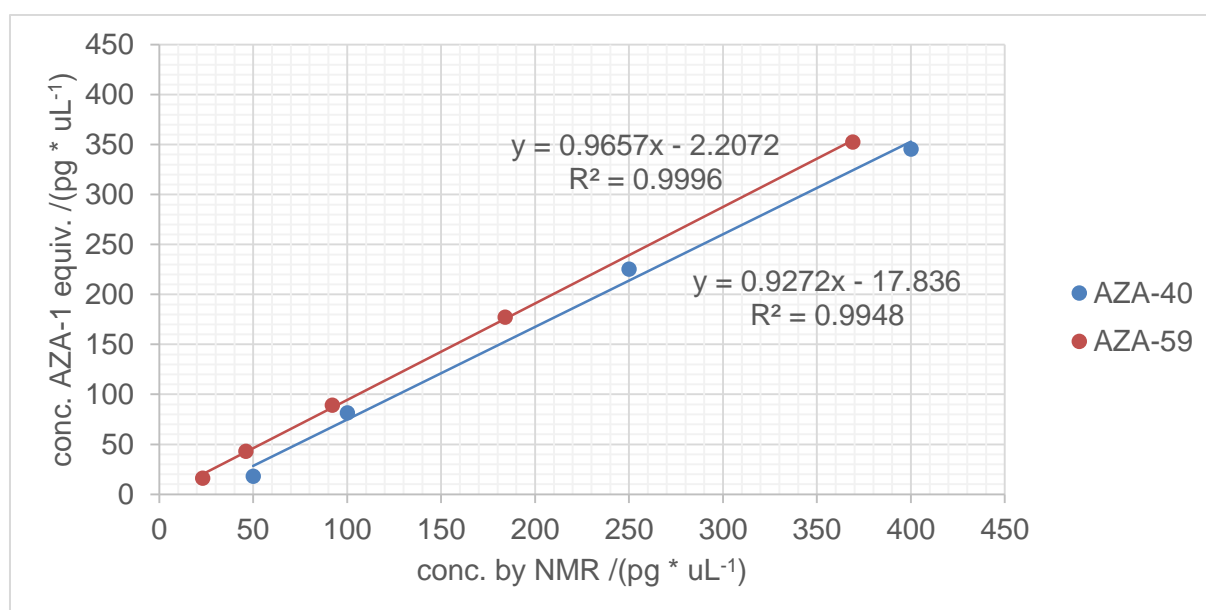


Figure 3.4: Quantitative comparison of AZA-40 and -59 by LC-MS analysis with AZA-1 as external analytical standard (y-axis) and NMR (x-axis).

The quantifier ion in LC-MS based quantification of AZAs corresponds in structure to the parent ion after a dehydration. A dehydration reaction in CID-fragmentation is usually induced by a hydroxyl group or a carboxylic acid. The comparison between the chemical environments of the AZA hydroxyl groups show a high degree of similarity for these three AZA derivatives, only AZA-59 differs with an additional hydroxyl group at C-3. However, the structural alteration was not reflected in the LC-MS analysis (Figure 3.4). In conclusion, the quantification of AZA-40 and AZA-59 as AZA-1 equivalent by LC-MS differs in median only 33 pg/uL and 7 pg/uL from quantification by NMR.

3.3 Conclusion

We elucidated the structure of two novel AZAs, namely AZA-40 and AZA-59. AZA-40 is structurally closely related to AZA-1, with an additional methyl group at C-8 but no methyl group at C-39. AZA-59 most closely resembled AZA-37 but with an additional methyl group at C-39.

The purified toxin was used to compare the accurate concentration (by NMR) and LC-MS analysis with AZA-1 as external, analytical standard. This comparison revealed a very good correlation of both means of quantification. The structural differences between these three AZA derivatives seem to have no influence on the quantification.

Both, the purification and the structure elucidation are prerequisites for toxicity studies.

3.4 Material and Methods

3.4.1 Cell culture and sample preparation of AZA-40

Azadinium poporum strain AZBH 03, was isolated May 2010 in the South China Sea (21°23' N, 109°07' E), China and shown to produce novel AZA-40 (Krock *et al.*, 2014). Mass cultures of 800 L were grown in half-strength K-medium (Keller *et al.*, 1987), without ammonia and full strength concentration of vitamins and salts. Cells were separated by a flow-through centrifugation and the flow through was directly run through a pre-conditioned HP-20 column (ca. 300 g, Diaion Supelco). The retentate was desalted and eluted with methanol. The concentrated algal cell pellet was freeze dried and extracted with acetone. The acetone extract was diluted with MilliQ to a final concentration of 7% acetone, loaded onto a HP-20 column (dimensions 40 mm x 150 mm), desalted and eluted with methanol.

3.4.2 Cell culture and sample preparation of AZA-59

A. poporum cultures producing AZA-59 were obtained from sediment samples of Puget Sound, Washington State (USA) and characterized by LC-MS/MS (as strain 121E10) (Kim *et al.*, 2017). A mass culture of strain 121E10 was grown in half-strength K-medium with modifications as in 3.4.1 (Keller *et al.*, 1987) and harvested accordingly. The supernatant and the extracted cell pellet were applied to pre-conditioned HP-20 (ca. 300 g, Diaion Supelco). The supernatant was chromatographed at original concentration, the acetone extracted cell pellet was dissolved in 7% acetone and chromatographed accordingly on HP-20. The retentate was desalted and eluted with methanol.

3.4.3 Sample preparation and separation

The toxin-containing fractions were dried under vacuo with a small amount of silica gel prior applying to silica chromatography. Compounds were eluted by stepwise elution (20% increments) from 100% hexane to 100% ethyl acetate to 100% methanol. All azaspiracid containing fractions were pooled and subjected to LC reversed-phase purification on a C18 column (15 × 310 mm, MERCK LOBAR) with solvent A: water with ammonium formate (AF)/formic acid (FA) buffer, solvent B: Methanol with AF/FA buffer and solvent C: acetonitrile (AcN). After injection, the samples were eluted isocratically at 50% A and 50% B for 10 min, followed by a 30 min gradient to 100% B and held for 10 min, and a 20 min elution at 100% C. A final purification step was performed at HPLC with solvent A: water and solvent B: AcN both with AF/FA buffer on an ISIS C18 column (10 mm × 150 mm, 4 mL min⁻¹, Machery & Nagel). After an initial phase of 55% solvent B for 9 min, a gradient to 60% B in 1 min was applied and another gradient in 1 min to 100% B. These conditions were held for 4 min. Salt and buffer were removed by small SPE cartridge. Purity of toxins was determined by NMR spectroscopy (cf. chapter 3.4.5).

3.4.4 LC-HRMS

Accurate mass measurements of AZA-40 and AZA-59 were acquired in a direct measurement with a QExactive Plus mass spectrometer (Thermo Fisher Scientific, Bremen, Germany), using a heated electrospray ionization (HESI-II) source at a flow-rate of 5 µL per minute. MS measurement were performed in full MS mode with a resolution of 280,000, a scan range of 150 to 2000 m/z in positive mode using a spray voltage of 3.5 kV.

3.4.5 NMR Analyses

Purified compounds **6** and **10** were dried under vacuo and dissolved in 40 µL deuterated methanol (3.33 ppm of residual CHD₂OD for ¹H-NMR and 49.0 ppm for ¹³C). BRUKER standard pulse programs as well as IMPACT-HMBC as described by Furrer (Furrer, 2010) were used. NMR experiments were measured at 292 K with a BRUKER AVANCE II 600 MHz NMR spectrometer equipped with a 1.7 mm CPTCI cryoprobe. The spectra were referenced to the solvent residual peak.

For NMR quantification of AZA-59, the dried sample was dissolved in 60 µL deuterated methanol containing 5.78 mmol/L 1,4-dioxane, confirmed by external calibration, and transferred to a 1.7 mm NMR tube. Proton spectra were acquired with ns = 32, aq = 3 s and d1 = 17 s. For bioactivity assays, 250 µg were stored away in a combusted Wheaton ampule under argon atmosphere.

For NMR quantification of AZA-40, the dried sample was dissolved in 40 μL deuterated methanol containing 1.90 mmol/L tetramethylsilane, confirmed by prompt external calibration, and transferred to a 1.7 mm NMR tube. Proton spectra were acquired with $n_s = 32$, $aq = 3$ s and $d1 = 27$ s.

Further dilution series of AZA-40 and AZA-59, respectively, were prepared for the comparison of accurate quantification by NMR with LC-MS based quantification.

3.4.6 Quantification of Azaspiracids by liquid chromatography tandem mass spectrometry (LC-MS/MS)

The LC-MS analysis was performed on a LC-MS/MS system in selected reaction monitoring mode (HPLC: model 1100, Agilent, Waldbronn, Germany), equipped with a reverse-phase analytical C8 column (Hypersil BDS 120 Å, 50 x 2 mm, 3 μm , Phenomenex, Aschaffenburg, Germany) at 20°C with a flow-rate of 0.2 mL·min⁻¹ as previously described by Kim *et al.* (Kim *et al.*, 2017). A gradient elution was performed with two eluents, where eluent A was water and eluent B was acetonitrile/water (95:5 v/v), both containing 2.0 mM ammonium formate and 50 mM formic acid. Initial conditions were 8 min column equilibration with 30% B, followed by a linear gradient to 100% B in 8 min, and isocratic elution for 10 min with 100% B. The system was then returned to initial conditions. The detection parameters of the AZAs were shown in Table 3.5.

Table 3.5: Selected reaction monitoring parameters for the quantification (Krock *et al.*, 2019).

mass transition (m/z)	common name	retention time /min	time /msec	collision energy /V
842 > 824	AZA-1	2.25	20.0	40
842 > 824	AZA-40	1.97	20.0	40
860 > 842	AZA-59	1.65	20.0	40

4. Full relative assignment of stereochemistry and conformational analysis of GYMs and SPXs by NMR- and molecular modeling-based techniques

Based on the structural elucidation of GYMs and SPXs in Chapter 2, this chapter deals with a combination of *in silico* methods and NMR spectroscopy to determine the stereochemistry of these biotoxins. The established method will eventually be applied to AZA-40 and AZA-59 (chapter 3), but is beyond the scope of this thesis due to the significantly higher computational time requirements for AZAs in comparison to GYMs and SPXs.

4.1 Introduction

The stereochemistry of bioactive compounds can significantly influence the biological effect, a prominent example is the compound thalidomide (Contergan ©). A compound with only one stereogenic center, whereas both isomers show a completely different effect in the human body. While the *R*-isomer of thalidomide has a sedative effect, a teratogenic effect is associated with the *S*-isomer (Maio, 2001). Further, the knowledge of the stereochemistry enables the usage of *in silico* tools to determine the molecular properties. The simulations of biological and chemical experiments on a computer are often labeled with the term *in silico*. To a certain degree, the toxicity of a compound can be explained with a single known primary target protein as previously reported for saxitoxin and its analogues. The comparison between the interactions between the toxin and the target protein (the change in Gibbs free energy) of various compounds of the toxin class can reveal the toxicity prior *in vitro* and *in vivo* studies. However, additional *in vitro* and *in vivo* studies are still necessary to validate the simulated data, because between the binding interactions and the toxicity is no linear correlation. (Durán-Riveroll *et al.*, 2016)

Another usage of the *in silico* simulated molecular properties is the determination of the stereochemistry by comparison of the experimental data with simulated properties of all possible stereoisomers. The molecular properties observed in circular dichroism (CD) as well as NMR spectra are reported to depend on the stereochemistry and were already applied in the field of microalgal toxins (Ciminiello *et al.*, 2009; Zurhelle *et al.*, 2018). The simulation of CD spectra was used to determine the stereochemistry of 16-desmethyl GYM D (**11**), which is in addition to GYM A (determined by X-ray crystal structure analysis) the only GYM with fully elucidated stereochemistry. The comparison between the strength of nuclear overhauser

effects (NOEs) and spatial closeness derived from simulations led to the stereochemistry at 13,19-didesmethyl SPX C (Ciminiello *et al.*, 2009).

The accurate simulation of the molecular parameters requires careful selection of input geometries (procedure according to Ciminiello *et al.*, 2009). Therefore, a preoptimized 3D structure is subjected to a simulated annealing procedure, whereby the compound is repeatedly simulated at high temperature to surpass rotary boundaries, followed by a cooling period to almost room temperature (300 K) in order to find geometries with minimized potential energy. The structures obtained by the simulated annealing procedure are subsequently subjected to geometry optimizations in force field and semi-empirical *ab-initio* calculations (AM1 level of theory). The geometries with highest abundance, determined by the potential energy obtained in semi-empirical structure optimization, are compared. The representative structures are selected and subjected to determination of shielding tensors on the B3LYP level of theory. The obtained shielding tensors are equivalent to chemical shift observed in NMR spectroscopy.

In this chapter, I evaluate *in silico* simulated NMR data of GYM E and 20-hydroxy-13,19-didesmethylSPX C to determine the stereochemistry after establishment of the method with 16-desmethylGYM D (**11**) and 13-desmethyl SPX C (**4**). To establish the simulation of shielding constants compound **11** was chosen. This compound requires lower computing time for similar levels of theory due to fewer atoms in comparison to SPXs, while possessing the same structure motif at C-4 as SPXs, whose stereochemistry is not possible to elucidate solely with NMR spectroscopy. Since the stereochemistry at C-4 of 13-desmethyl SPX C, the lead structure of SPXs, is yet to be elucidated, the application of validated methods such as CD spectrometry is necessary.

4.2 Results and discussion

4.2.1 Method development with 16-desmethy GYM D (11)

A decisive factor for the accurate simulation of shielding constants is the careful selection of the input structure. In order to cover a sufficiently wide range of possible input structures, a simulated annealing procedure was applied. The heating and cooling rates were optimized to achieve a broad variety of geometries ($n = 200$) for further optimization (data not shown). Starting with these 200 possible input structures, two strategies were pursued to select the most important ones to limit computing time (*cf.* Figure 4.1). One strategy comprised the optimization on the semi-empiric AM1 level for all geometries obtained by simulated annealing (*cf.* Figure 4.1 a). The second strategy (*cf.* Figure 4.1 b) was the selection of 50 geometries with highest difference based on dihedral angles. The comparison of geometries based on dihedral angles offers a deep insight in the geometry, while being independent of rotation and translation of the whole molecule. After division of the whole set of geometries into 50 groups by hierarchical clustering (HCA) of each group, one geometry was selected by application of a principal component analysis (PCA). The selected geometries were subjected to geometry optimization on semi-empiric AM1 level and all 200 structures derived from the simulated annealing procedure were subjected to single point calculation (AM1 level).

The geometries obtained by each strategy were screened for the geometry with the lowest AM1 energy. Dominant geometries with AM1 energies 10 kJ/mol above the lowest AM1 were selected for further structure optimizations and determination of shielding parameters on various levels of theory. This resulted in five and three selected geometries for each strategy respectively (Figure 4.1 a, b). Both, the restricted Hartree-Fock (RHF) method as well as density functional theory (DFT) with B3LYP or TPSSH approximation were then used as levels of theory.

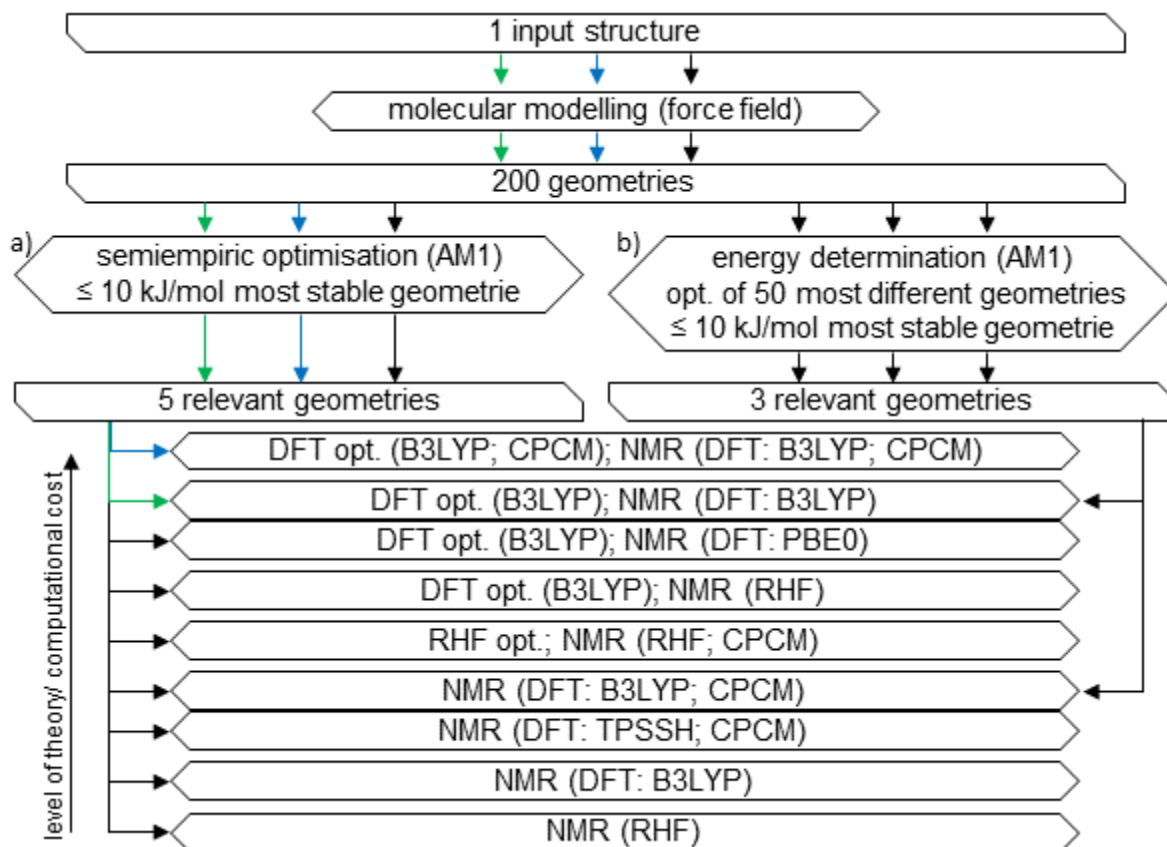


Figure 4.1: Workflow of NMR simulations by different methods using shielding constants of 16-desmethyl GYM D; RHF calculations were performed with the 6-31+G(d) basis set; DFT calculations were performed with the def2-TZVPP basis set and def2/JK auxiliary basis set.

The shielding tensors, obtained for each level of theory, were averaged according to the BOLTZMANN distribution and correlated with the corresponding chemical shift. Theoretical chemical shifts were then derived from the resulting linear regression of the averaged shielding tensors. These were compared with measured chemical shifts (*cf.* Table 9.1; Zurhelle *et al.*, 2018) resulting in a $\Delta\delta$ value. The proton chemical shifts showed deviations of up to $\Delta\delta = 0.96$ ppm between simulated and measured data at RHF level of theory and of up to $\Delta\delta = 0.54$ ppm at the highest level of theory. The standard deviations of the $\Delta\delta$ varied only slightly for the used levels of theory. However, for carbon chemical shifts the differences between simulated and measured data varied significantly for the used levels of theory.

The lowest $\Delta\delta$ values were observed for simulation of shielding constants by application of density functional theory (DFT, B3LYP functional) after an additional optimization at the same level of theory for the selected geometries of strategy “a” (*cf.* Figure 4.1 and Table 4.1 in green). The usage of “conductor like polarizable continuum model” (CPCM, Figure 4.1 and Table 4.1 in blue) to simulate the effect of a solvent was better suited to reduce the discrepancies between measured and simulated data (max. $\Delta\delta$), but the increased computational time requirements did not justify the slight improvement in accuracy.

Table 4.1: Comparison of measured NMR data with simulated shielding constants for different levels of theory (St. Indicates the used strategy of pre-optimization; Std. div: standard deviation; max.: maximum).

St.	theoretical level		¹³ C		¹ H	
	opt. Type	NMR	Std. div $\Delta\delta$	max. $\Delta\delta$	Std. div $\Delta\delta$	max. $\Delta\delta$
a	B3LYP, CPCM	B3LYP, CPCM	2.02	4.75	0.24	0.56
a	B3LYP	B3LYP	2.00	5.00	0.24	0.58
b	B3LYP	B3LYP	3.27	8.80	0.24	0.68
a	B3LYP	PBE0	2.40	5.64	0.26	0.67
a	B3LYP	RHF	3.89	8.39	0.28	0.76
a	RHF	RHF	4.10	8.85	0.29	0.96
a		B3LYP, CPCM	3.09	7.00	0.28	0.68
b		B3LYP, CPCM	2.52	4.94	0.21	0.54
a		TPSSh, CPCM	3.20	7.35	0.27	0.61
a		B3LYP	2.86	7.94	0.31	0.77
a		RHF	4.88	9.44	0.33	0.86

After the selection of relevant geometries using strategy “a”, the geometry optimization and simulation of shielding tensors was performed on DFT level of theory with B3LYP as approximations to the exchange–correlation energy (*cf.* Figure 4.1 green path). This simulation showed a comparatively good agreement between simulated and real data.

In order to test the usefulness of this method, two theoretical stereoisomers of compound **11** were used. The inversion of stereo centers of the side chain (*cf.* Figure 4.2 top right) should greatly influence the chemical environment, and consequently the chemical shift for both tetrahydrofuran moieties resulting in a clear difference to the chemical shift of the natural isomer. A better agreement between simulated and measured NMR data was also expected from the change of the configuration of C-4 (*cf.* Figure 4.2 top center). Notably, the stereochemistry at C-4 is not assessable by NMR spectroscopy alone.

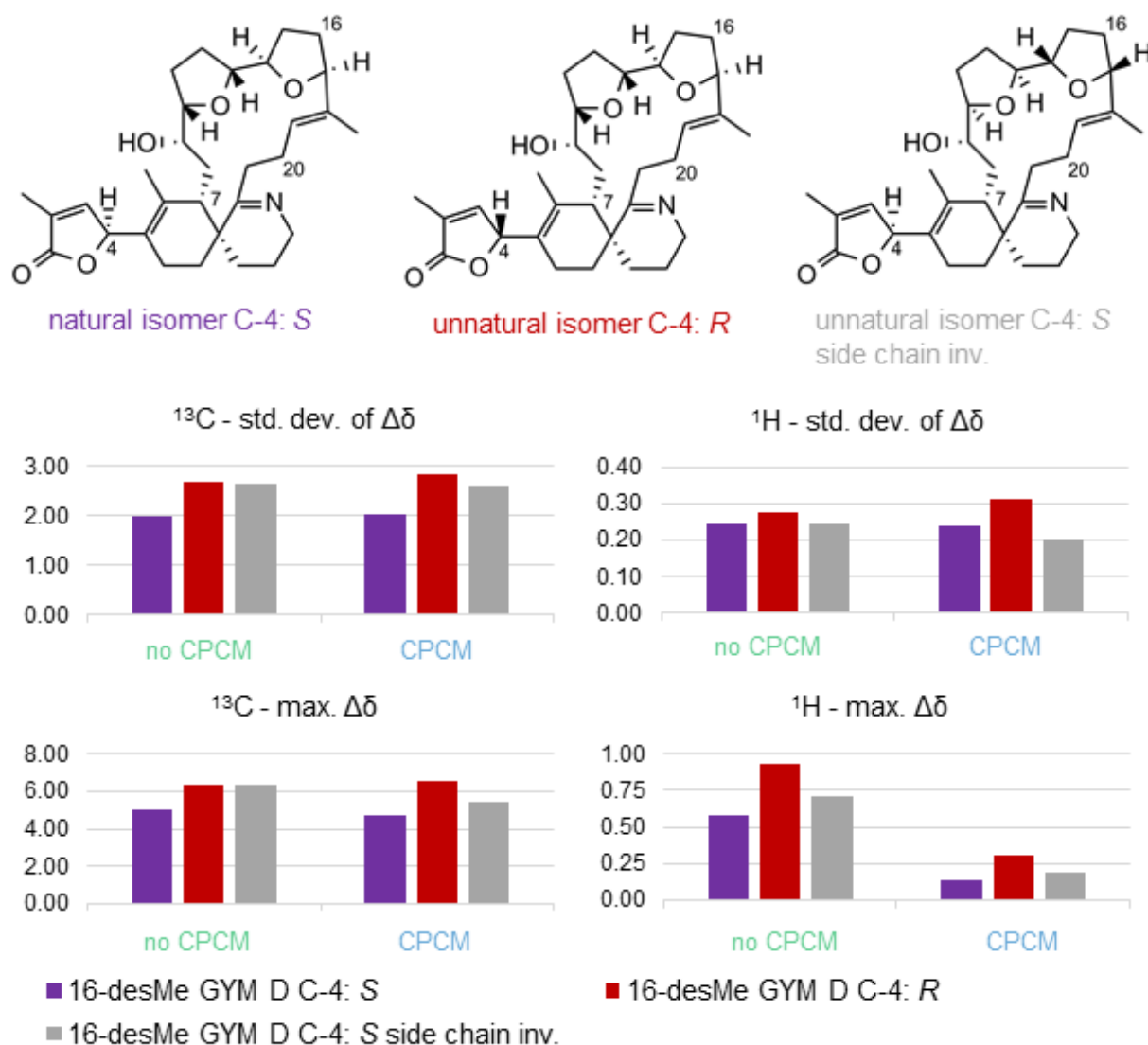


Figure 4.2: Structures and comparison of standard deviation (std. dev.) overall and around C-4 and highest (max.) $\Delta\delta$ value for three stereoisomers of 16-desmethyl GYM D; left side without CPCM; right side with CPCM (cf. section 9.3.1 for chemical shifts).

The standard deviations and maximal differences between simulated and NMR data is shown in Figure 4.2 for all three isomers of 16-desmethyl GYM D. The values for both theoretical isomers are close, while the $\Delta\delta$ values of the natural isomer is lower. Therefore, this method shows the potential to elucidate the configuration of stereo centers, which are not assessable by NMR spectroscopy.

4.2.2 Evaluation with 13-desmethyl SPX C (4)

Despite being the best studied spiroside, the stereochemistry of 13-desmethyl SPX C at C-4 is still unknown. *In silico* methods with Gauge Including Atomic Orbitals (GIAO) approach in combination with NMR spectroscopy were successfully applied to the elucidation of C-4 in 16-desmethyl GYM D (*cf.* chapter 4.2.1). Further, CD spectroscopy can also be simulated *in silico*, allowing a comparison with measured spectroscopic data and assignment of stereo centers close to chromophores as C-4 (Maksimenka, 2010). In case of 13-desmethyl SPX C, the comparison between measured and simulated CD spectra (*cf.* Figure 4.3) indicated S-configuration at C-4.

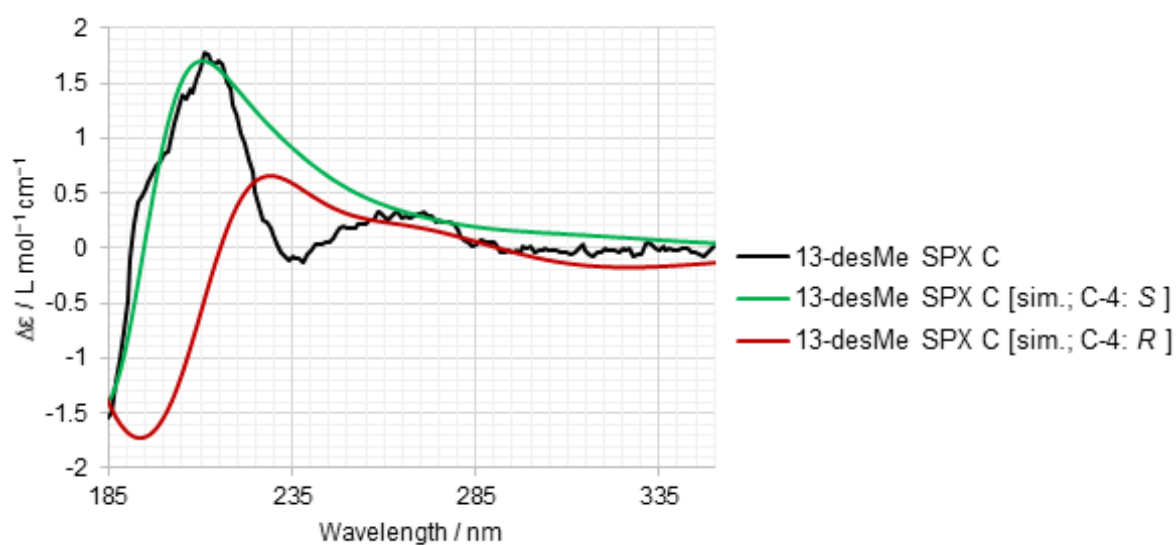


Figure 4.3: Measured CD-spectrum of 13-desmethyl SPX C with simulated spectra for both configurations at C-4.

In contrast to GYM 11, the NMR spectra of compound 4 were recorded in deuterated methanol. To estimate the effect of this solvent, the simulations of the isomer with S configuration were performed with and without the CPCM solvation model. The best agreement between measured and simulated data was obtained with the CPCM solvation model during both optimization and determination of shielding parameters (Figure 4.4). In contrast to pyridine, the significant improvement through application of CPCM solvation model justified its usage.

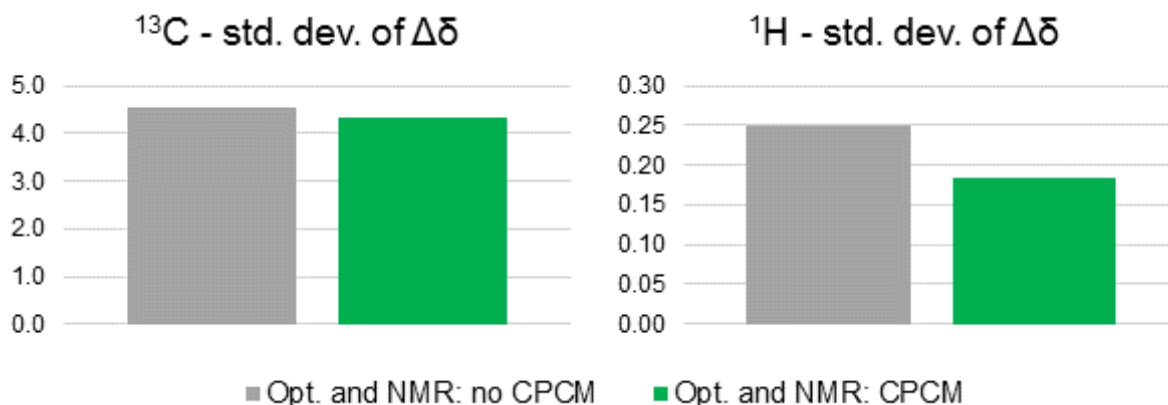


Figure 4.4: Comparison of standard deviation (std. dev.) of $\Delta\delta$ values for different applications of CPCM.

The imine carbon (C-28) showed the highest discrepancy between measured ($\delta = 201.3$ ppm (Hu *et al.*, 2001)) and simulated ($\delta = 179.7$ ppm) data. This discrepancy may result from partial or complete protonation of the imine group, consequently both protonation states were included in the investigation.

Especially for carbon chemical shifts, a better agreement between measured and simulated shifts was observed for the protonated form (Figure 4.5). However, the standard deviation and maximal $\Delta\delta$ for both protonation states were either lower or very similar to the C-4 *S* isomer. This was in agreement with the results obtained by CD spectroscopy. In conclusion, the combination of *in silico* techniques and NMR spectroscopy unequivocally identified the stereochemistry of the cyclic imine toxins under investigation.

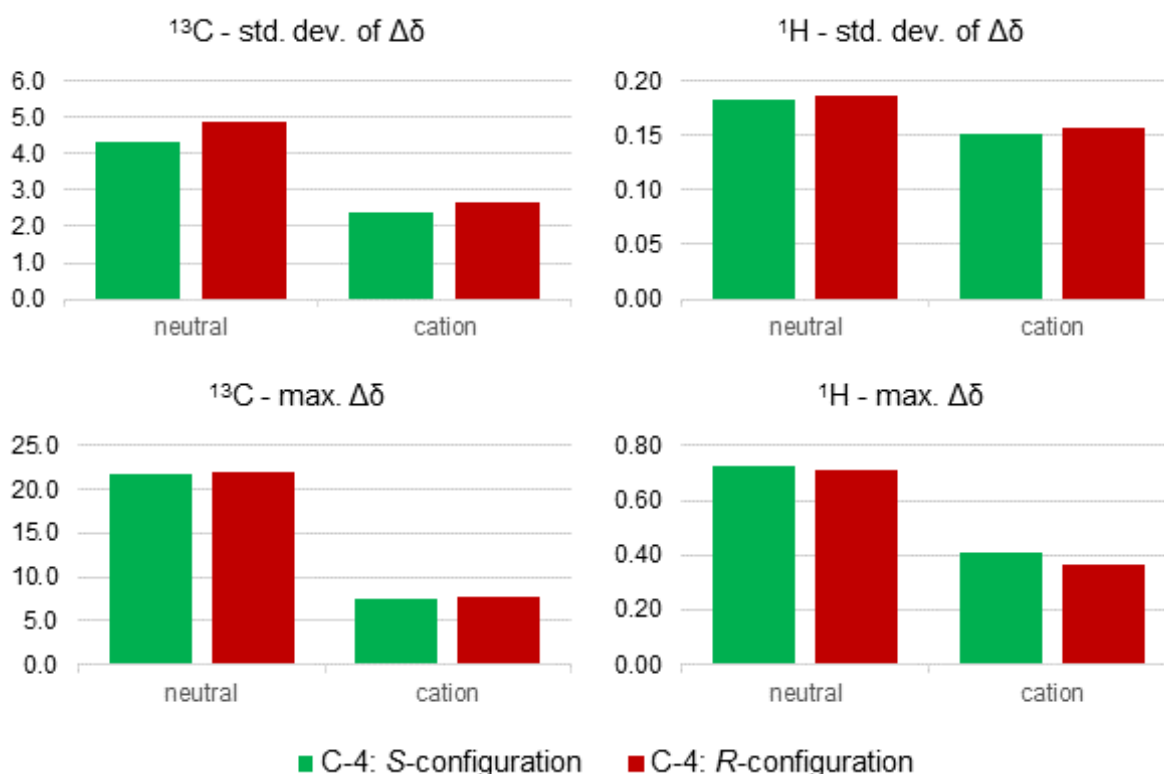


Figure 4.5: Comparison of standard deviation (std. dev.) and highest (max.) $\Delta\delta$ value for both C-4 isomers and protonation states of 13-desmethyl SPX C (4) (cf. section 9.3.3 for chemical shifts).

4.2.3 Verification of proposed structure of GYM E (12)

The structure elucidation of GYM E was performed with a low amount of toxin, therefore only chemical shifts of protons and respective carbons were reported (Zurhelle *et al.*, 2018). Proton and carbon chemical shifts of **12** revealed a high similarity to 16-desmethyl GYM D (**11**), with the exception for C-19, C-20 and C-29 (Zurhelle *et al.*, 2018). These nuclei belong to the exocyclic methylene group and the allylic hydroxyl group which are absent in **11**. Based on the evidence, that **12** is a potential degradation product of **11**, the same stereochemistry was assumed. This hypothesis is supported by the high similarity of NMR chemical shifts between **12** and **11**. Only the stereochemistry for C-19 could not be assigned by comparison of measured NMR spectra.

The application of *in silico* methods offers the verification of the proposed structure, while providing additional insight to the stereochemistry of GYM E. Both configurations at C-19 are plausible, therefore both were subjected to the *in silico* simulation of NMR shielding constants. The simulated NMR spectra with S configuration at C-19 showed a higher similarity to measured NMR data (cf. Figure 4.6). GYM **12** shared the configuration at C-19 with the corresponding stereo center in GYM B (Miles *et al.*, 2000). The expected chemical shift for

R-configuration at the allylic hydroxyl group (C-19 in GYM E) would be lower than the observed chemical shift of GYM E, based on the comparison with GYM B and GYM C and the simulated data.

The comparison of the potential energy for the most stable geometry of the natural and unnatural C-19 conformer showed that the unnatural isomer had a lower potential energy. A non-stereo selective degeneration mechanism would favor the formation of the product with lower potential energy, which is represented by the unnatural C-19 isomer. Consequently, the putative degradation of **11** into GYM E seems to be stereo selective and favors the product with the higher potential energy.

Since only little knowledge about the configuration at C-4 for GYMs and SPXs is available, GYM E with *R*-configuration at C-4 and *S*-configuration at C-19 was additionally simulated (Figure 4.6). While the overall standard deviation of $\Delta\delta$ values of protons and carbons were very similar for both configurations of C-4, the standard deviation for the nuclei around C-4 unequivocally revealed *S*-configuration at C-4.

For GYM E, the effect of stereochemistry at C-4 on $\Delta\delta$ values is not as strong as for 16-desmethyl GYM D. This is a result of the higher number of quaternary carbons without measured chemical shift in the environment of the stereogenic center C-4 than in the environment of the stereogenic center at C-19. But still, the influence of C-4 on the measured surrounding nuclei seems to be strong enough to assign the stereochemistry at this position.

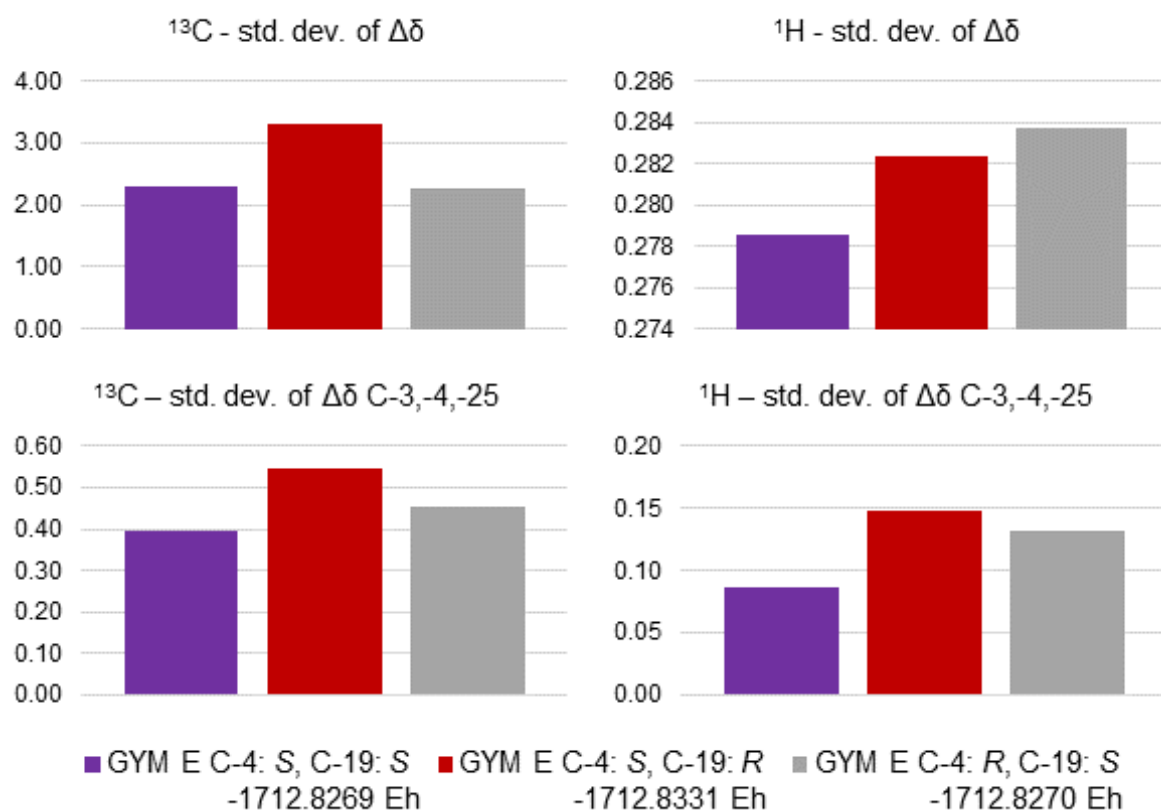


Figure 4.6: Comparison of standard deviation (std. dev.) and highest (max.) $\Delta\delta$ value for three stereoisomers of GYM E (12), each with the lowest potential energy (cf. section 9.3.2 for chemical shifts).

4.2.4 Stereochemistry of 20-Hydroxy-13,19-didesmethyl-SPX C (13)

The preliminary assignment of the stereochemistry of 20-Hydroxy-13,19-didesmethyl-SPX C (13) with NOEs reduced the number of possible stereoisomers. The NOE between H-7 and H-38 indicated *E*-configuration at the double bond between C-8 and C-9. A linkage between the stereo centers C-7 and C-29 was indicated by a NOE between H-7 and H27, implying either *S*-configuration at C-7 together with *R*-configuration at C-29, or both configurations inverted. However, the mentioned configuration (C-7: *S* and C-29: *R*) was indicated by the NOEs of H-34b to H-7 and H-34a to H-33. The strong NOE between H-42 and H-43 indicated an equatorial position of both methyl groups. These methyl groups of the modeled geometries of 13-desmethyl SPX C have an equatorial orientation. Therefore, both C-31 and C-32 were assigned with *S*-configuration in analogy to 13-desmethyl SPX C.

Proton H-22 showed NOEs to other protons in the macrocycle (e. g. H-25, H-11), whereas H-17 and H-12 did not reveal such NOEs. Therefore, H-22 is directed towards the macrocycle and H-12 and methylene groups of the ether ring in the middle (C-16 and C-17) are directed away from the macrocycle. H-19 faces away from the macrocycle as indicated by the NOE

between H-17 and H-19. Further, the proton H-19 showed a NOE to H-21 and H-20 in addition to a small coupling constant ($^3J_{\text{HH}}$ near 0 Hz). In conclusion, the proton H-19 has axial orientation, while an equatorial orientation is assigned to H-20. The NOE between H-22 and both protons of at C-25 indicated equatorial orientation for H-22. In conclusion, *S*-configuration was assigned at C-12 and *R*-configuration at C-15, C-18, C-19, C-20, and C-22. The configuration at C-4 and C-10 are to be elucidated by the integration of in silico methods.

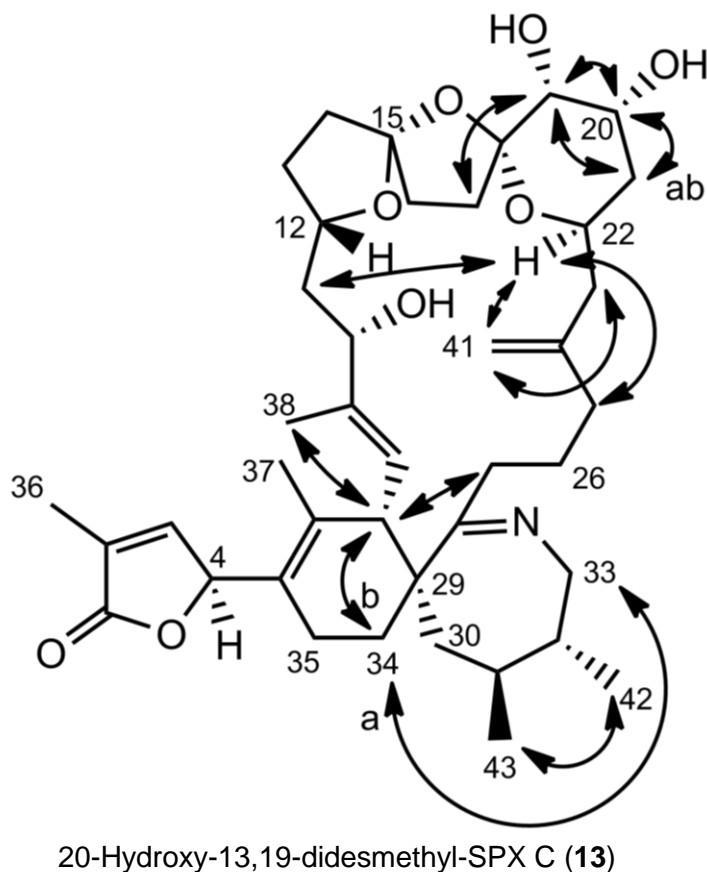


Figure 4.7: Stereochemistry of 20-Hydroxy-13, 19-didesmethyl-SPX C with selected NOEs (C-4: *S*; C-10: *S* configuration).

The best agreement between measured and simulated data was observed for the molecule with *S* configuration at both positions C-4 and C-10 (*cf.* Figure 4.8). The isomer with *R* configuration at both positions revealed the best fit in terms of the highest discrepancy between measured and simulated chemical shifts of carbon nuclei. However, for all three modelled isomers this $\Delta\delta$ value exhibited by the carbon at position C-41, suggested a systematic influence due to the lack of a solvation model. Given the long distance between carbon C-41 and the stereo centers of interest, the observation of high $\Delta\delta$ values at C-41 is not related to the stereochemistry of neither C-4 nor C-10. Therefore, the stereochemistry of 20-Hydroxy-13, 19-didesmethyl-SPX C is suggested to resemble the stereochemistry of 13-desmethyl SPX C. This conclusion supports the concept of a common biosynthetic for SPXs, whereas the nascent

polyketide chain differs slightly for the different derivatives (Anttila *et al.*, 2016; van Wagoner *et al.*, 2014).

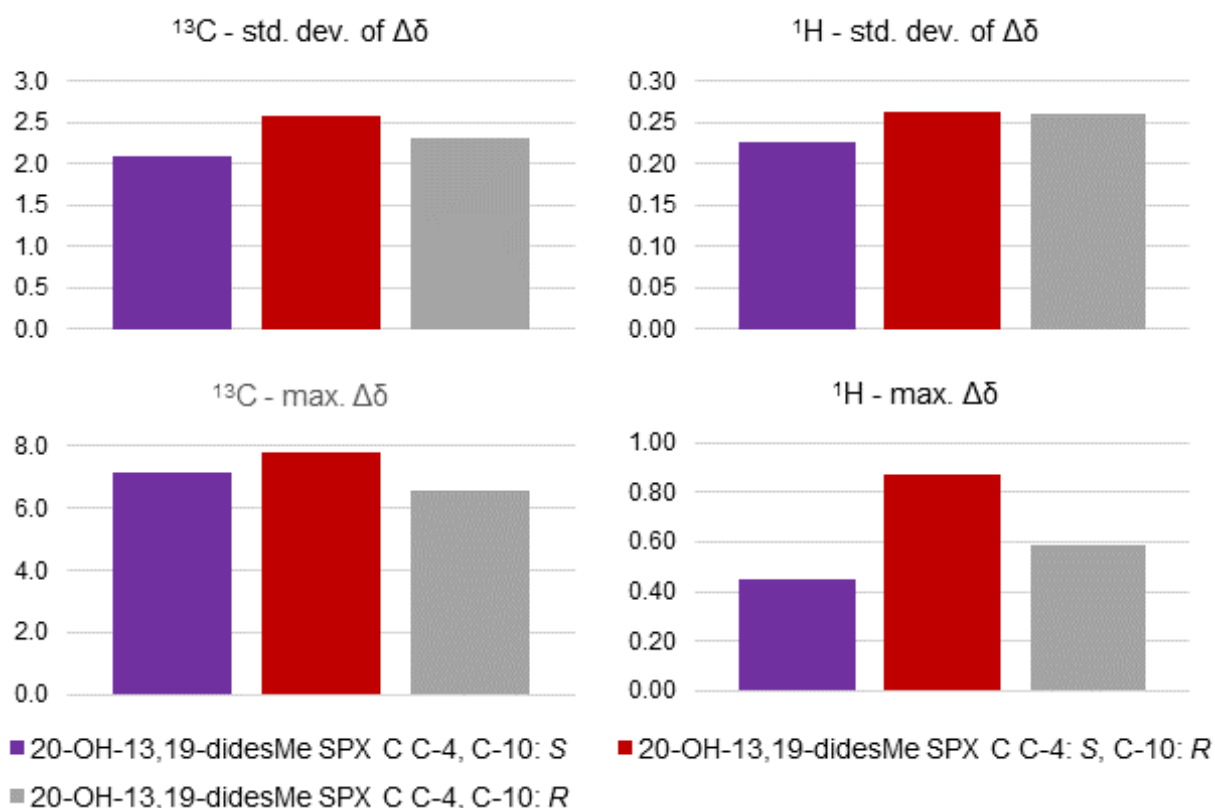


Figure 4.8: Comparison of standard deviation (std. dev.) and highest (max.) $\Delta\delta$ value for three stereoisomers of 20-Hydroxy-13, 19-didesmethyl-SPX C (13) (*cf.* section 9.3.4 for chemical shifts).

4.2.5 Stereochemistry of C-4 of cyclic imine toxins

The simulated compounds cumulatively suggest for the *S*-configuration at C-4 for all considered compounds. Out of all six gymnodimines and spiroldes with elucidated conformation at C-4, only one spirolide namely 13,19-didesmethyl SPX C (Ciminiello *et al.*, 2009) shows *R*-configuration at this position.

The simulated NMR chemical shifts were examined for systematic changes of the chemical shift induced by the configuration at C-4 (*cf.* Figure 4.9). Even though members of the lactone ring (C-1 to C-4) did not show different chemical shifts for the configurations at C-4, a systematic effect was observed for C-6, and the methylene group C-35 (corresponds to C-25 in GYMs). The simulated carbon chemical shifts of C-6 and methylene group C-35 of SPXs and C-25 of GYMs, respectively, were shifted towards lower field (higher frequencies) for *S* configuration at C-4 in comparison to *R* configuration at C-4. The chemical shifts of the *S* configuration showed better agreement with measured chemical shifts. The simulated

chemical shifts of H-35a for *S* configuration were shifted towards lower field in comparison to *R* configuration. This effect was more pronounced for SPXs in comparison to GYMs. For the other proton of this methylene group (H-35b), the influence of *S* configuration at C-4 led to a shift towards higher field in comparison to *R* configuration at C-4.

The effect of stereochemistry at C-4 on chemical shifts of methylene group C-35 in SPXs is based on the combined influence of the lactone oxygen (between C-1 and C-4) and methylene group C-30 (*cf.* Figure 4.9). For the C-4 *S* isomer, both groups were in spatial proximity to H-35a, which caused a downfield shift in comparison to the isomer with *R* configuration at C-4, where only the methylene group interacted with H-35a. The proton H-35b of the C-4 *S* isomer was neither influenced by lactone oxygen nor methylene group, while the spatial proximity between lactone oxygen and the proton H-35b in the C-4 *R* isomer led to a downfield shift. This effect on the methylene group at C-25 was weaker for GYMs, because of a greater distance between both methylene groups given the smaller ring size of imine ring. The difference in chemical shift at C-6 was caused by the interaction between stereo center at C-7 and the orientation of ester ring.

The influence of chirality at C-4 on chemical shift of nuclei at ring B was an indication for the influence of stereochemistry at this position on biological activity. As the stereochemistry of C-4 influences the chemical shift, it also influences the electron density of ring B. Therefore, it should affect the binding strength between compound and a target protein.

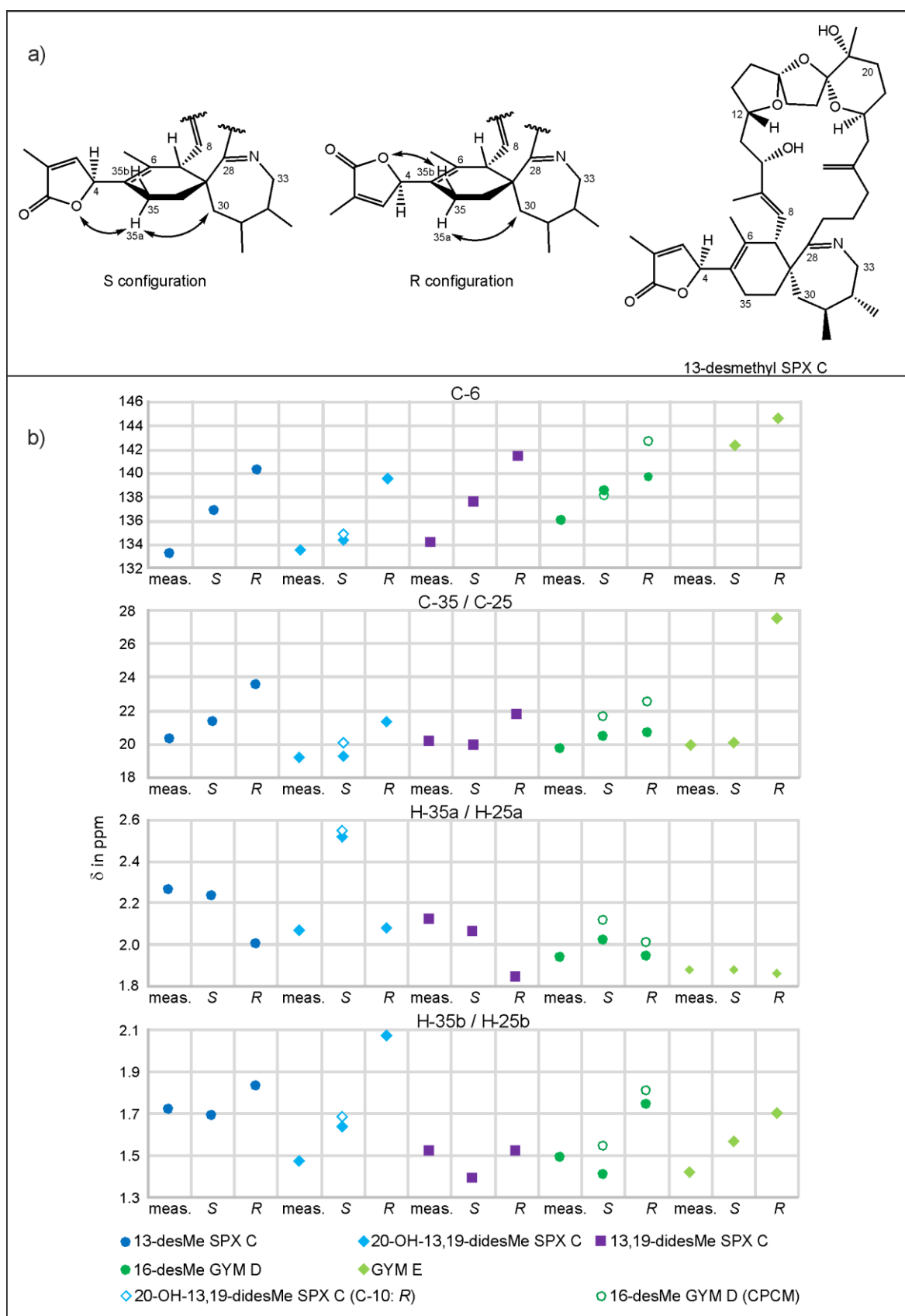


Figure 4.9: Systematic effects of the stereochemistry at C-4 on selected chemical shifts of neighboring nuclei and the causative structural motive at the example of 13-desmethyl SPX C. The position C-35 in SPXs corresponds to position C-25 in GYMs. Measured chemical shifts of 13-desmethyl SPX C and 13,19-didesmethyl SPX C were taken from Hu *et al.* and Ciminiello *et al.* (Ciminiello *et al.*, 2009; Hu *et al.*, 2001).

In addition to the chemical shifts of the modelled cyclic imine toxins, the measured and simulated chemical shifts of 13,19-didesmethyl SPX C (Ciminiello *et al.*, 2009), the only cyclic imine toxin with proposed *R* configuration at C-4, were added to Figure 4.9. Even though the chemical shift of H-35b was inconclusive, the measured chemical shifts of C-6, C-35 and H-35a showed a high similarity to the simulated chemical shifts of the *S* isomer. This outcome refutes the proposed stereochemistry at C-4 of 13,19-didesmethyl SPX C (Ciminiello *et al.*, 2009).

The Ciminiello group proposed the configuration of C-4 for 13,19-didesmethyl SPX C by comparison of modelled intramolecular distances and strength of NOE-signal strength in addition to carbon–proton vicinal coupling constants. The latter was used to determine the preferred orientation of the lactone ring in relation to ring B which contains C-6 and C-35. In the preferred rotation of the bond C-4 and C-5, proton H-4 was characterized by a *gauche* conformation to C-6 and C-35. The observed NOEs revealed a spatial proximity between H-3 and methyl protons at C-37 as well as of H-4 to methyl protons at C-37 and H-35b (1.52 ppm), with the methyl protons closer to H-4 than H-35b. Among the modelled conformers (Ciminiello *et al.*, 2009), only the *gauche* conformer with *R* configuration at C-4 ($\alpha = -53^\circ$; Table 4.2) was plausible. The *S* conformer was ruled out, because it was not compatible with the spatial proximity between H-4 and H-35b. (Ciminiello *et al.*, 2009)

The rationale of Ciminiello *et al.* (Ciminiello *et al.*, 2009) to assign *R* configuration only considered single conformers. However, for systems without one dominant, highly populated conformer (>85%), the averaging of multiple conformers is necessary (Bifulco *et al.*, 2007). Besides the modelled distances of single conformers of 13,19-didesmethyl SPX C from Ciminiello *et al.* (Ciminiello *et al.*, 2009), Table 4.2 reveals the averaged distances of 13,19-didesmethyl SPX C, 13-desmethyl SPX C (neutral and protonated) and 20-Hydroxy-13,19-didesmethyl SPX C. Evidently, the modelled, averaged distances between H-4 and H-35b were either equal or shorter for the C-4 *S* isomer. Consequently, the argument to rule out the *S* isomer of 13,19-didesmethyl SPX C, is to be refuted for averaged distances. Moreover, the averaged distances of the *S* isomer matched the observed NOEs of Ciminiello *et al.* (Ciminiello *et al.*, 2009) even better than the averaged distances of the *R* isomer (Table 4.2), especially regarding the required spatial proximity between H-3 and H-37. As consequence, C-4 of 13,19-didesmethyl SPX C was revised and unambiguous assigned with *S* configuration.

Table 4.2: Dihedral angle α values and related intramolecular distances measured on AM1 conformers of C-4 *R* and *S* isomers of 13,19-didesmethyl SPX C taken from Ciminiello *et al.* (Ciminiello *et al.*, 2009). Averaged intramolecular distances of 13-desmethyl SPX C (neutral and protonated) and 20-Hydroxy-13,19-didesmethyl SPX C from AM1 conformers.

Family/Compound	Dihedral angle α	H-3–H-37 /Å	H-4–H-37 /Å	H-4–H-35b /Å
C-4: <i>R</i>				
13,19-didesmethyl SPX C: <i>anti</i>	168°	3.3	3.8	2.5
13,19-didesmethyl SPX C: <i>gauche</i> ⁻	-53°	2.5	2.1	3.3
13,19-didesmethyl SPX C: <i>gauche</i> ⁺	43°	4.7	2.3	3.7
13,19-didesmethyl SPX C: averaged		3.7 ± 0.5	1.9 ± 0.4	3.5 ± 0.4
13-desMe SPX C [neutral]		3.7 ± 0.4	1.8 ± 0.2	3.5 ± 0.4
13-desMe SPX C [protonated]		2.3 ± 0.2	2.1 ± 0.1	3.7 ± 0.1
20-Hydroxy-13,19-didesmethyl SPX C		3.5 ± 0.4	1.9 ± 0.2	3.2 ± 0.6
C-4: <i>S</i>				
13,19-didesmethyl SPX C: <i>anti</i>	-176°	3.4	3.7	2.2
13,19-didesmethyl SPX C: <i>gauche</i> ⁺	39°	2.3	2.3	3.7
13,19-didesmethyl SPX C: <i>gauche</i> ⁻	-41°	4.2	2.4	3.7
13,19-didesmethyl SPX C: averaged		2.6 ± 0.7	2.2 ± 0.3	3.3 ± 0.2
13-desMe SPX C [neutral]		2.2 ± 0.2	2.1 ± 0.2	3.3 ± 0.3
13-desMe SPX C [protonated]		2.3 ± 0.1	2.2 ± 0.1	3.4 ± 0.1
20-Hydroxy-13,19-didesmethyl SPX C		2.2 ± 0.2	2.1 ± 0.2	3.2 ± 0.3

4.3 Conclusion

The combination of NMR spectroscopy and *in silico* simulations of NMR spectra is a necessary strategy for the assignment of stereochemistry in complex molecules. With regard to the chosen level of theory, the higher the level of theory, the higher the quality of the simulated data. Therefore, simulations were performed on the B3LYP/def2-TZVPP/def2/JK level of theory. The CPCM solvation model increased the accuracy for the solvent methanol, while the application of this solvent model was not necessary for compounds measured in pyridine. This method was successfully applied to elucidate the stereochemistry of GYM E, 20-hydroxy-13,19-didesmethyl SPX C and 13,19-didesmethyl SPX C, and its application to other marine biotoxins is currently done.

By application of CD spectroscopy, 13-desmethyl SPX C was identified to have *S* configuration at C-4. The stereochemistry of 20-Hydroxy-13,19-didesmethyl SPX C was elucidated similar to 13-desmethyl SPX C with *R* configuration at C-20. GYM E shares similar stereochemistry of 16-desmethyl GYM D, with the exception of *S* configuration at C-19.

All the simulated compounds had *S*-configuration at C-4. Out of the six gymnodimines and spiroptides with elucidated conformation at C-4, only one spiroptide, namely 13,19-didesmethyl SPX C (Ciminiello *et al.*, 2009), was assigned with *R*-configuration at this position. Due to the simulation of chemical shifts, the configuration at C-4 of 13,19-didesmethyl SPX C was revised and assigned with *S* configuration. In conclusion, the majority of SPXs and GYMs exhibit common stereochemistry, as expected for a common biosynthetic pathway of these two compound classes.

As stated above, the effect of C-4 on the molecule, especially ring B, is strong enough to influence the chemical shift of the B ring. Therefore, the configuration at C-4 influences the electron density and is suggested to influence the binding strength to a target protein.

4.4 Material and Methods

4.4.1 Parameter setup

The planar structures with limited information's about stereoisomerism were obtained in previous NMR studies (*cf.* Chapter 2 and 3). These form the foundation for the simulations, where the simulated NMR properties of all possible stereoisomers were compared with the experimental chemical shifts. The initial three dimensional coordinates for all stereoisomers of the compounds were obtained through AVOGADRO software package (Hanwell *et al.*, 2012). The structure files, created by AVOGADRO software package (Hanwell *et al.*, 2012), were used in the software VISUAL MOLECULAR DYNAMICS (VMD) (Humphrey *et al.*, 1996) and SWISSPARAM (Zoete *et al.*, 2011) to obtain input structures for the molecular dynamics simulation using the NANOSCALE MOLECULAR DYNAMICS program (NAMD) (Phillips *et al.*, 2005). All simulations were either performed on a Lenovo ThinkPad workstation or on the Linux cluster Cray CS400 "Ollie" at Alfred Wegener Institute's computing center.

4.4.2 Conformational search

A simulated annealing procedure (Kirkpatrick *et al.*, 1983) in the NANOSCALE MOLECULAR DYNAMICS (NAMD) software (Phillips *et al.*, 2005) package was applied for the conformal search according to the parameter described by Ciminiello *et al.* (Ciminiello *et al.*, 2009). The simulation was performed with a time steps length of 1 fs. The distance-dependent dielectric constant was set to the value of methanol ($\epsilon = 33^*r$). A total of 200 simulated annealing cycles were performed and each compromised following steps:

- Equilibration (10 ps) at 300 K
- Stepwise temperature increase ($\Delta T = 10$ K) with 4ps equilibration at each step
- Equilibration (20 ps) at 1000 K
- Stepwise temperature decrease ($\Delta T = 20$ K) with 4ps equilibration at each step
- Equilibration (2 ps) at 300 K

The geometries obtained in each cycle of the simulated annealing were subjected to geometry optimization, subsequently with force field and with ab initio calculations on AM1 level of theory. The semi-empirical AM1 structure optimization as well as a following frequency analysis were performed with the GENERAL ATOMIC MOLECULAR AND ELECTRONIC STRUCTURE SYSTEM (GAMESS) software package (Gordon and Schmidt, 2005).

The AM1 conformers were ranked on the basis of their conformational energy values and grouped into families according to the values of dihedral angles. For each group within a

tolerance of 10 kJ mol⁻¹ above the lowest conformational energy, a representative geometry was chosen. The chosen geometries were subjected to geometry optimization on the B3LYP/def2-TZVPP/RIJCOSX/def2/J level of theory. For 13-desmethyl SPX C, the NMR solvent (MeOD) was simulated with the conductor-like polarizable continuum model (CPCM) and parameters of methanol.

4.4.3 Determination of shielding tensors

The representative geometries were subjected to shielding tensor simulation in the ORCA software package (Neese, 2018). The simulation utilized GIAO and def2-TZVPP basis sets with def2/JK auxiliary basis sets, with the RIJK approximation, on the B3LYP level of theory. For 13-desmethyl SPX C, the NMR solvent (MeOD) was simulated with the CPCM and parameters of methanol.

The shielding tensors of the conformers were averaged based on a BOLTZMANN distribution of their potential energy.

4.4.4 Evaluation of simulated shielding constants

The averaged shielding tensors of each nuclei was correlated with the respective NMR shift and based on a linear regression translated into a simulated chemical shift. Based on the comparison of simulated and measured NMR shifts, the standard deviation was determined according following formula:

$$std. dev. \Delta\delta = \sqrt{\frac{1}{N} \sum_{i=1}^N (\delta_{i,simulated} - \delta_{i,measured})^2}$$

Further, the highest difference between measured and simulated data was used for interpretation.

4.4.5 Circular dichroism spectroscopy

The representative geometries of both C-4 isomers of 13-desMe SPX C (**4**) were subjected to simulation of rotatory strengths applying time depended DFT on B3LYP level of theory with def2-TZVPP/def2/J, RIJCOSX approximation and CPCM solvation model. The simulated CD spectrum of **4** was obtained by applying Gaussian broadening to each transition as previously described by Li *et al.* (Li *et al.*, 2010) and adjusted manually to the height of experimental data

5. Summary

Marine biotoxins produced by dinoflagellates exhibit a remarkable structural diversity. During the course of this thesis, I have elucidated six novel compounds in total, two for each of the toxin groups of AZAs, GYMs, and SPXs.

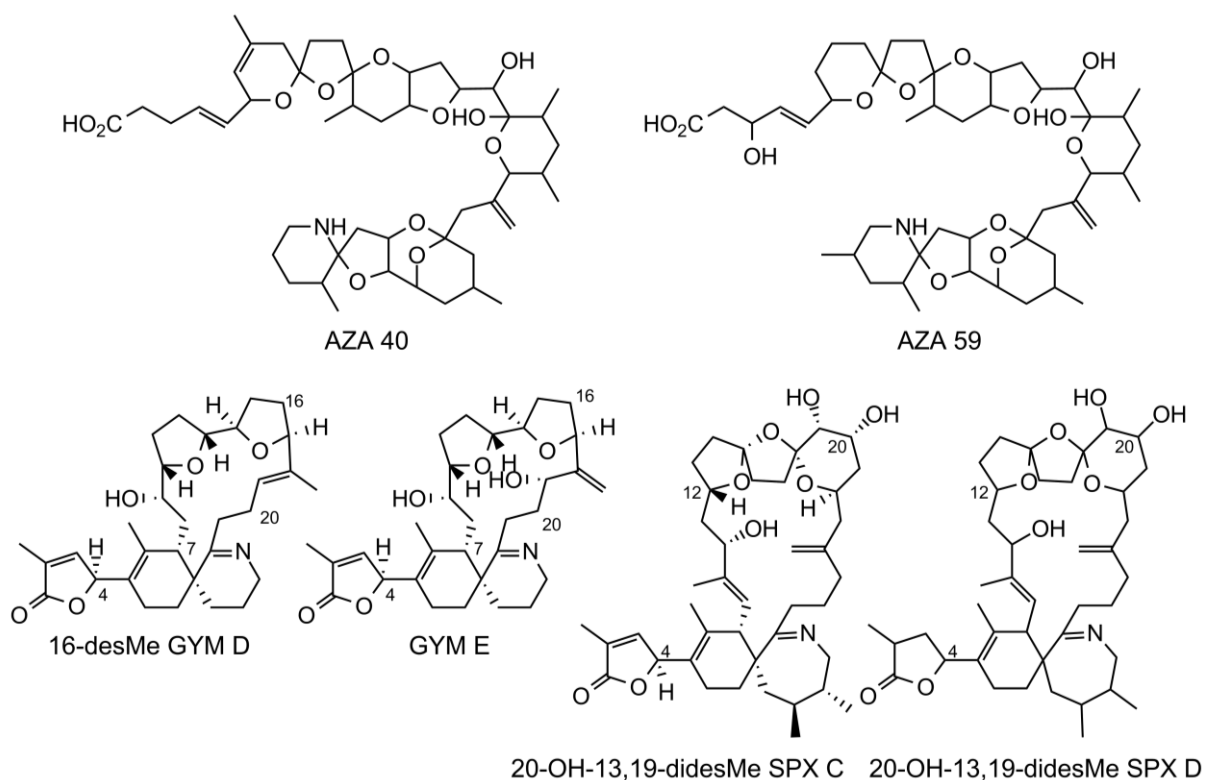


Figure 5.1: Compounds elucidated in this thesis.

The purified toxin material of AZA-40 and -59 will now be tested for toxicity in comparison to the reference standard, AZA-1. Pending the confirmation of toxicity (as determined by S. Sosa, permit application pending) AZA-40 and -59 should then be included in the mandatory list of toxins in the shellfish monitoring program.

In GYMs and SPXs novel structural features were discovered, namely the missing methyl group at C-16 for GYMs and an additional hydroxyl group at C-20 for SPXs respectively. As the example of the AZAs showed, other derivatives with these structural features are likely. Further, four cyclic imine toxins had their full relative stereochemistry elucidated. The simulated chemical shifts revealed a systematic effect between the chirality at C-4 and neighboring nuclei. Based on this systematic effect, reasonable doubts arise towards determination of *R* configuration at C-4 in 13,19-didesmethyl SPX C. The configuration of C-4 was assigned with simulated and measured NMR spectra, suggesting that all tested GYMs and SPXs have the *S*

configuration at that position. This assignment supports the hypothesis of a common biosynthetic pathway for both compound groups.

Given the knowledge of full relative conformation of GYM and SPXs, the next step is to link common structural features to bioactivity (e. g. toxicity). Figure 5.2 shows the similarities in electrostatic potential simulated *in silico* for the GYM and SPXs discussed in this thesis (DFT, B3LYP/def2-TZVPP/def2/JK, calculated with ORCA (Neese, 2018) and Multiwfn (Lu and Chen, 2012)). These results foreshadow the ultimate goal to simulate theoretical binding properties for these toxins *in silico* with their reported receptor proteins (Bourne *et al.*, 2010). One of the underlying ecological questions for these studies is, why microalgal genotypes produce a high structural diversity of similar toxins and how these differ in their binding targets and binding potentials.

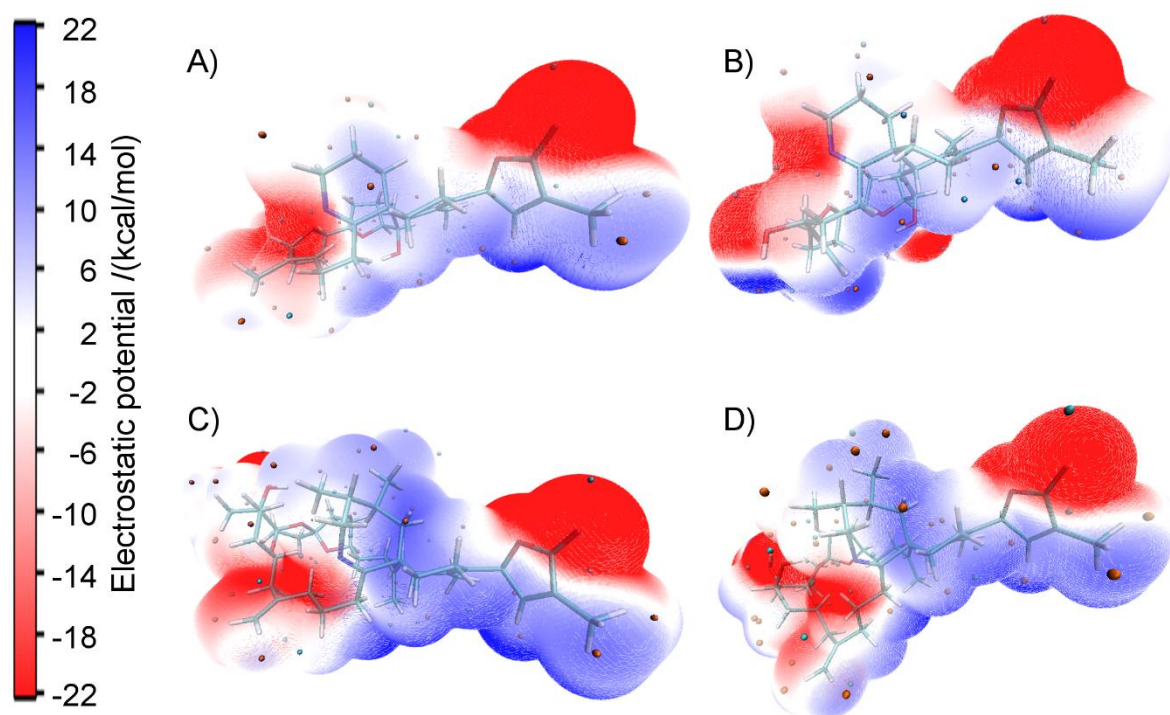


Figure 5.2: Electrostatic potential of 16-desmethyl GYM D (A), GYM E (B), 13-desmethyl SPX C (C), and 20-hydroxy-13,19-didesmethyl SPX C (D).

6. Zusammenfassung

Marine Biotoxine von Dinoflagellaten eine beeindruckende strukturelle Vielfalt. Im Rahmen dieser Arbeit konnte ich die Struktur von sechs dieser Verbindungen aufklären, jeweils zwei stammen aus den Toxinklassen der Azaspirazide, Gymnodimine, und Spirolide.

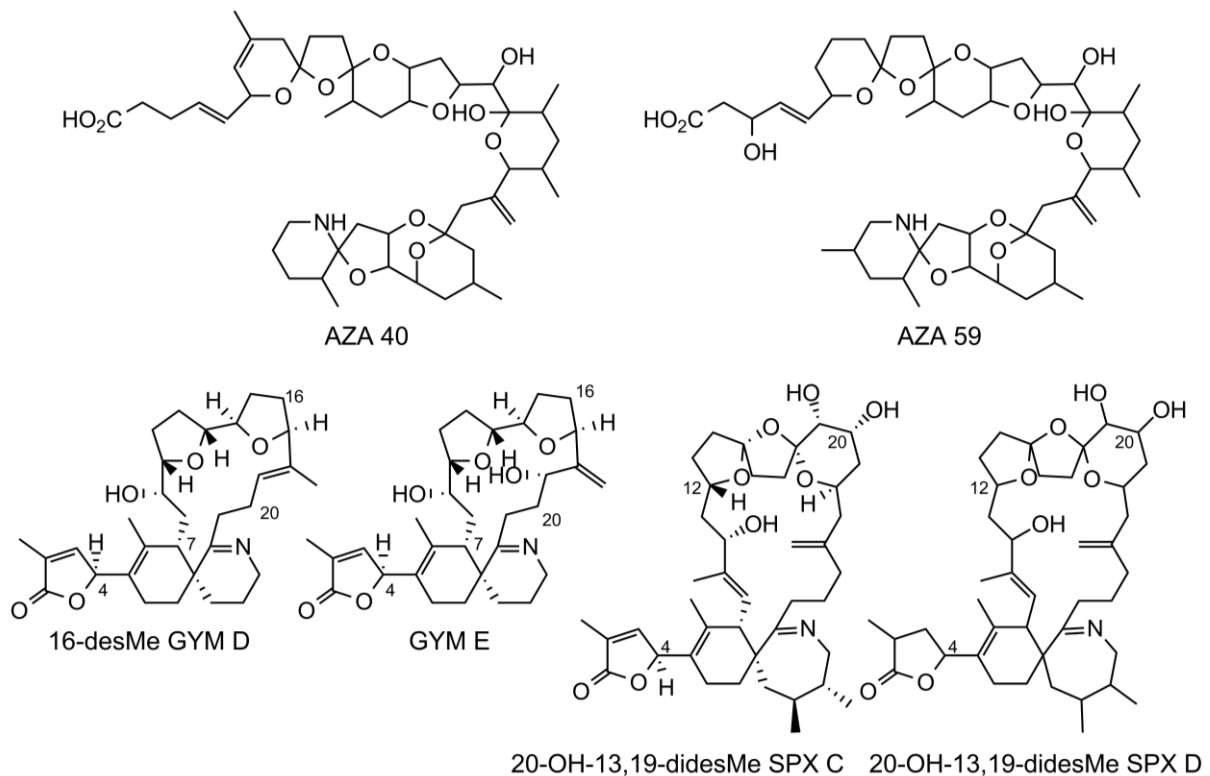


Abbildung 6.1: Im Rahmen dieser Arbeit aufgeklärte Verbindungen.

Das aufgereinigte Toxinmaterial von AZA-40 und -59 wird nun im Vergleich zum Referenzstandard AZA-1 auf Toxizität getestet. In Abhängigkeit von der Toxizität der neuen Verbindungen (wie von S. Sosa ermittelt, Genehmigung ausstehend) empfiehlt sich die Aufnahme in die regulierte Überwachung von Muscheln.

Die Gymnodimine und Spirolide in Abbildung 6.1 zeigen für diese Substanzklassen neue Strukturmerkmale. Bei den Gymnodiminen ist die fehlende Methylgruppe an C-16 ein neues Strukturmotiv. Während dies bei den Spiroliden der erste Bericht von einer Alkoholgruppe an C-20 ist. Wie das Beispiel der Azaspirazide zeigte, sind weitere Derivate mit diesen Merkmalen wahrscheinlich. Weiterhin wurde die Stereochemie von vier Cycloimin Toxinen aufgeklärt. Die Konfiguration an C-4 zeigte einen systematischen Einfluss auf die simulierten chemischen Verschiebungen benachbarter Atome. Dieser Effekt ließ an der von Ciminiello *et al.* bestimmten *R* Konfiguration bei 13,19-didesmethylspirolid C (Ciminiello *et al.*, 2009) zweifeln. Die *S* Konfiguration wurde durch den Vergleich zwischen gemessenen und simulierten chemischen Verschiebungen bei 13,19-didesmethylspirolid C nachgewiesen, was auf eine *S*

Konfiguration bei allen getesteten Spiroliden und Gymnodiminen schließen lässt. Diese Zuordnung stützt die Hypothese eines gemeinsamen Biosynthesewegs für beide Verbindungsgruppen

In Anbetracht der Kenntnis der vollständigen relativen Konformation bei Gymnodiminen und Spiroliden besteht der nächste Schritt darin, gemeinsame Strukturmerkmale mit der Bioaktivität (z. B. Toxizität) zu verknüpfen. Die Abbildung 6.2 zeigt, wie ähnlich sich die simulierten elektrostatischen Potentiale für die in dieser Arbeit diskutierten Gymnodimine und Spirolide sind (DFT, B3LYP/def2-TZVPP/def2/JK, berechnet mit ORCA (Neese, 2018) und Multiwfn (Lu and Chen, 2012)). Diese Ergebnisse deuten das ultimative Ziel an, die theoretischen Bindungseigenschaften dieser Toxine *in silico* mit dem entsprechenden Rezeptorprotein (Bourne *et al.*, 2010) zu simulieren. Eine der zugrunde liegenden ökologischen Fragen für diese Studien ist, warum bei Mikroalgen die verschiedenen Genotypen eine hohe strukturelle Vielfalt ähnlicher Toxine produzieren und wie sich diese in ihren Bindungszielen und Bindungsstärke unterscheiden.

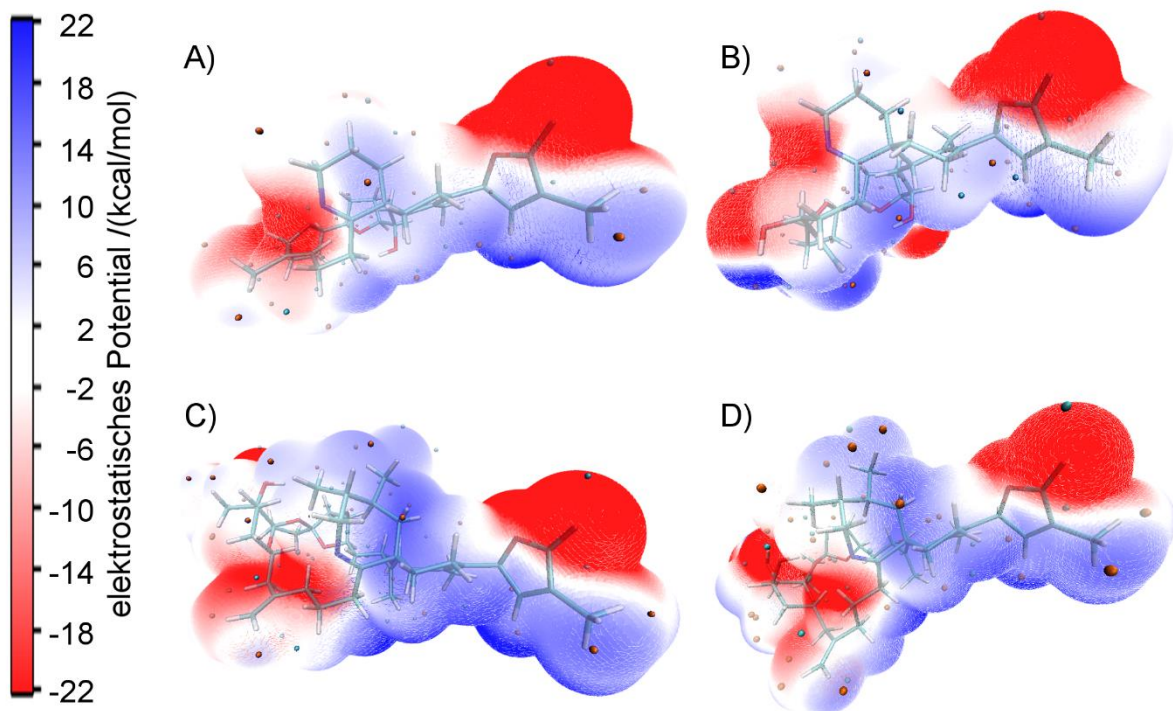


Abbildung 6.2: Das elektrostatische Potential von 16-Desmethylgymnodimin D (A), Gymnodimin E (B), 13-Desmethylspiroliid C (C), und 20-Hydroxy-13,19-didesmethylspiroliid C (D).

7. Index of abbreviations

AF	ammonium formiate
AM1	Austin Model 1 (a semi empiric method)
amu	atomic mass unit
AOAC	Association of Official Analytical Chemists
ASP	amnesic shellfish poisoning
AZAs	azaspiracids
AZP	azaspiracid poisoning
B3LYP	a DFT exchange-correlation functional (Becke, 3-parameter, Lee-Yang-Parr)
BfR	<i>Bundesinstitut für Risikobewertung</i>
BTX	brevetoxin
°C	degree Celsius
CD	circular dichroism
<i>cf.</i>	compare with (<i>cōnfer</i>)
CFP	ciguatera fish poisoning
CID	collision induced dissociation
COSY	correlated spectroscopy
CPCM	conductor-like polarizable continuum model
δ	chemical shift
DA	domoic acid
DMSO	dimethyl sulfoxide
DSP	diarrheic shellfish poisoning
DTX	dinophysistoxin
ec	endcapped
EFSA	European Food Safety Authority
<i>e. g.</i>	for example (<i>exempli gratia</i>)
ELISA	enzyme-linked immunosorbent assay
ENSO	El Niño Southern Oscillation
ESI	electrospray ionization
<i>et al.</i>	<i>et alia</i>
EU	European Union
eV	electron volt
Exod.	Exodus (Book II of Mose)
FA	formic acid
g	gram
GYM	gymnodimine
HAB	harmful algae blooms

HMBC	heteronuclear multiple bond correlation
HPLC	high-performance liquid chromatography
HRMS	high resolution mass spectrometry
HSQC	heteronuclear single quantum correlation
Hz	Hertz
IFF	<i>Institut für Fische und Fischereierzeugnisse</i>
i.p.	<i>intraperitoneal</i>
<i>in silico</i>	experiments performed on a computer (Pseudo-Latin for “in silicon”)
<i>in vitro</i>	experiment at microorganisms outside their normal biological context (Latin for “in the glass”)
<i>in vivo</i>	experiment at the living animal (Latin for “within the living”)
<i>J</i>	coupling constant
K	Kelvin
KmTX	karlotoxin
LAVES	<i>Niedersächsisches Landesamt für Verbraucherschutz und Lebensmittelsicherheit</i>
LC-MS	liquid chromatography coupled to mass spectroscopy
M	molar
m	multipllett
MBA	mouse bioassay
Me	methyl
MeCN	acetonitrile
MeOD	deuterated methanol
MeOH	methanol
mg	milligrams
MHz	megahertz
mL	milliliter
μL	microliter
mmol	millimol
MS	mass spectrometry
<i>m/z</i>	mass to charge ratio
neg	negative
NLWKN	<i>Niedersächsischer Landesbetrieb für Wasserwirtschaft, Küsten- und Naturschutz</i>
nm	nanometer
NMR	nuclear magnetic resonance
NPC	nascent polyketide chain
NRL	National Reference Labor

NSP	neurotoxic shellfish poisoning
OA	okadaic acid
<i>p. a.</i>	<i>pro analysi</i>
pos	positive
ppm	parts per million
PSP	paralytic shellfish poisoning
PTX	pectenotoxin
R	organic Rest
rpm	rounds per minute
R_t	retention time
RT	room temperature
sp.	species
SPE	solid phase extraction
SPX	spirolide
STX	saxitoxin
TEF	toxic equivalency factor
TMS	tetramethylsilane
TPSSh	a DFT exchange-correlation functional
USA	United States of America
XRD	X-ray crystallography
YTX	yessotoxin

8. References

- Acres, J., Gray, J., 1978. Paralytic shellfish poisoning. *Canadian Medical Association journal* 119, 1195–1197.
- Adolf, J.E., Bachvaroff, T.R., Krupatkina, D.N., Nonogaki, H., Brown, P.J., Lewitus, A.J., Harvey, H.R., Place, A.R., 2006. Species specificity and potential roles of *Karlodinium micrum* toxin. *African Journal of Marine Science* 28, 415–419. 10.2989/18142320609504189.
- Alpermann, T.J., Tillmann, U., Beszteri, B., Cembella, A.D., John, U., 2010. Phenotypic Variation and Genotypic Diversity in a Planktonic Population of the Toxigenic Marine Dinoflagellate *Alexandrium tamarese* (*Dinophyceae*). *Journal of Phycology* 46, 18–32. 10.1111/j.1529-8817.2009.00767.x.
- Anderson, D.M., 1989. Toxic algal blooms and red tides: A global Perspective. *Red tides: Biology, environmental science, and toxicology*.
- Anderson, L.S., 1960. Toxic shellfish in British Columbia. *American journal of public health and the nation's health* 50, 71–83.
- Anttila, M., Strangman, W., York, R., Tomas, C., Wright, J.L.C., 2016. Biosynthetic Studies of 13-Desmethylspirolide C Produced by *Alexandrium ostenfeldii* (= *A. peruvianum*): Rationalization of the Biosynthetic Pathway Following Incorporation of ¹³C-Labeled Methionine and Application of the Odd-Even Rule of Methylation. *J. Nat. Prod.* 79, 484–489. 10.1021/acs.jnatprod.5b00869.
- Biblica, 2011. Holy Bible: New International Version. <https://www.biblegateway.com>. Accessed 9 December 2018.
- Bifulco, G., Dambruoso, P., Gomez-Paloma, L., Riccio, R., 2007. Determination of relative configuration in organic compounds by NMR spectroscopy and computational methods. *Chemical reviews* 107, 3744–3779. 10.1021/cr030733c.
- Bourne, Y., Radic, Z., Aráoz, R., Talley, T.T., Benoit, E., Servent, D., Taylor, P., Molgó, J., Marchot, P., 2010. Structural determinants in phycotoxins and AChBP conferring high affinity binding and nicotinic AChR antagonism. *Proceedings of the National Academy of Sciences of the United States of America* 107, 6076–6081. 10.1073/pnas.0912372107.
- Bundesinstitut für Risikobewertung, 2005. Mouse bioassay not suitable as a reference method for the regular analysis of algae toxins in mussels: BfR Expert Opinion No. 032/2005, Germany.

- Bürk, C., Usleber, E., Martlbauer, E., 1998. Intoxications through marine algae toxins - A review. *Archiv für Lebensmittelhygiene* 49, 16–20.
- Cariton, J.T., Geller, J.B., 1993. Ecological roulette: The global transport of nonindigenous marine organisms. *Science (New York, N.Y.)* 261, 78–82. 10.1126/science.261.5117.78.
- Carty, S., Parrow, M.W., 2015. Dinoflagellates, in: *Freshwater Algae of North America*. Elsevier, pp. 773–807.
- Cembella, A.D., 2001. Association of the gonyaulacoid dinoflagellate *Alexandrium ostenfeldii* with spirolide toxins in size-fractionated plankton. *Journal of Plankton Research* 23, 1413–1419. 10.1093/plankt/23.12.1413.
- Chevallier, O.P., Graham, S.F., Alonso, E., Duffy, C., Silke, J., Campbell, K., Botana, L.M., Elliott, C.T., 2015. New insights into the causes of human illness due to consumption of azaspiracid contaminated shellfish. *Scientific reports* 5, 9818. 10.1038/srep09818.
- Christian, B., Luckas, B., 2008. Determination of marine biotoxins relevant for regulations: From the mouse bioassay to coupled LC-MS methods. *Analytical and bioanalytical chemistry* 391, 117–134. 10.1007/s00216-007-1778-x.
- Ciminiello, P., Catalanotti, B., Dell'Aversano, C., Fattorusso, C., Fattorusso, E., Forino, M., Grauso, L., Leo, A., Tartaglione, L., 2009. Full relative stereochemistry assignment and conformational analysis of 13,19-didesmethyl spirolide C via NMR- and molecular modeling-based techniques. A step towards understanding spirolide's mechanism of action. *Organic & biomolecular chemistry* 7, 3674–3681. 10.1039/b907649b.
- Cironi, P., Álvarez, M., Albericio, F., 2000. ¹H NMR spectroscopy with internal and external standards for the quantification of libraries. *Mol Divers* 6, 165–168. 10.1023/B:MODI.0000006842.76275.a0.
- Culotta, E., 1992. Red menace in the world's oceans. *Science (New York, N.Y.)* 257, 1476+.
- Dickman, M., Zhang, F., 1999. Mid-ocean exchange of container vessel ballast water. 2: Effects of vessel type in the transport of diatoms and dinoflagellates from Manzanillo, Mexico, to Hong Kong, China. *Mar. Ecol. Prog. Ser.* 176, 253–262. 10.3354/meps176253.
- Durán-Riveroll, L.M., Cembella, A.D., Band-Schmidt, C.J., Bustillos-Guzmán, J.J., Correa-Basurto, J., 2016. Docking Simulation of the Binding Interactions of Saxitoxin Analogs Produced by the Marine Dinoflagellate *Gymnodinium catenatum* to the Voltage-Gated Sodium Channel Nav1.4. *Toxins* 8. 10.3390/toxins8050129.

- Dyhrman, S.T., 2008. Molecular approaches to diagnosing nutritional physiology in harmful algae: Implications for studying the effects of eutrophication. *Harmful Algae* 8, 167–174. 10.1016/j.hal.2008.08.016.
- Escher, B.I., Dutt, M., Maylin, E., Tang, J.Y.M., Toze, S., Wolf, C.R., Lang, M., 2012. Water quality assessment using the AREc32 reporter gene assay indicative of the oxidative stress response pathway. *Journal of environmental monitoring : JEM* 14, 2877–2885. 10.1039/c2em30506b.
- European Union, 2004. Verordnung (EG) NR. 853/2004 des Europäischen Parlaments und des Rates: (EG) NR. 853/2004.
- European Union, 2011. Verordnung (EU) Nr. 15/2011 der Kommission vom 10. Januar 2011 zur Änderung der Verordnung (EG) Nr. 2074/2005 hinsichtlich anerkannter Testmethoden zum Nachweis mariner Biotoxine in lebenden Muscheln: EU Nr.15/2011.
- Fiedler, P.C., 1982. Zooplankton avoidance and reduced grazing responses to *Gymnodinium splendens* (*Dinophyceae*). *Limnol. Oceanogr.* 27, 961–965. 10.4319/lo.1982.27.5.0961.
- Fox, J.W., Nelson, W.A., McCauley, E., 2010. Coexistence mechanisms and the paradox of the plankton: Quantifying selection from noisy data. *Ecology* 91, 1774–1786.
- Friebolin, H., 2011. Basic one- and two-dimensional NMR spectroscopy, 5th ed. Wiley-VCH, Weinheim, 418 pp.
- Furrer, J., 2010. A robust, sensitive, and versatile HMBC experiment for rapid structure elucidation by NMR: IMPACT-HMBC. *Chemical communications* 46, 3396–3398. 10.1039/C000964D.
- Gill, S., Murphy, M., Clausen, J., Richard, D., Quilliam, M., MacKinnon, S.L., LaBlanc, P., Mueller, R., Pulido, O., 2003. Neural Injury Biomarkers of Novel Shellfish Toxins, Spirolides: A Pilot Study Using Immunochemical and Transcriptional Analysis. *NeuroToxicology* 24, 593–604. 10.1016/S0161-813X(03)00014-7.
- Glibert, P.M., Mayorga, E., Seitzinger, S., 2008. *Prorocentrum minimum* tracks anthropogenic nitrogen and phosphorus inputs on a global basis: Application of spatially explicit nutrient export models. *Harmful Algae* 8, 33–38. 10.1016/j.hal.2008.08.023.
- Gómez, F., 2012. A quantitative review of the lifestyle, habitat and trophic diversity of dinoflagellates (*Dinoflagellata*, *Alveolata*). *Systematics and Biodiversity* 10, 267–275. 10.1080/14772000.2012.721021.

- Gordon, M.S., Schmidt, M.W., 2005. Advances in electronic structure theory, in: Theory and Applications of Computational Chemistry. Elsevier, pp. 1167–1189.
- Hallegraeff, G.M., 1993. A review of harmful algal blooms and their apparent global increase*. *Phycologia* 32, 79–99. 10.2216/i0031-8884-32-2-79.1.
- Hallegraeff, G.M., 1998. Transport of toxic dinoflagellates via ships' ballast water: Bioeconomic risk assessment and efficacy of possible ballast water management strategies. *Mar. Ecol. Prog. Ser.* 168, 297–309. 10.3354/meps168297.
- Hallegraeff, G.M., 2010. Ocean Climate Change, Phytoplankton Community Responses, and Harmful Algal Blooms: A formidable predictive Challenge. *Journal of Phycology* 46, 220–235. 10.1111/j.1529-8817.2010.00815.x.
- Hanwell, M.D., Curtis, D.E., Lonie, D.C., Vandermeersch, T., Zurek, E., Hutchison, G.R., 2012. Avogadro: An advanced semantic chemical editor, visualization, and analysis platform. *Journal of cheminformatics* 4, 17. 10.1186/1758-2946-4-17.
- Harju, K., Koskela, H., Kremp, A., Suikkanen, S., La Iglesia, P. de, Miles, C.O., Krock, B., Vanninen, P., 2016. Identification of gymnodimine D and presence of gymnodimine variants in the dinoflagellate *Alexandrium ostenfeldii* from the Baltic Sea. *Toxicon* 112, 68–76. 10.1016/j.toxicon.2016.01.064.
- Hebert, P.D.N., Crease, T.J., 1980. Clonal Coexistence in *Daphnia pulex* (Leydig): Another Planktonic Paradox. *Science (New York, N.Y.)* 207, 1363–1365.
- Hess, P., 2010. Requirements for screening and confirmatory methods for the detection and quantification of marine biotoxins in end-product and official control. *Analytical and bioanalytical chemistry* 397, 1683–1694. 10.1007/s00216-009-3444-y.
- Hess, P., McCarron, P., Krock, B., Kilcoyne, J., Miles, C.O., Botana, L., 2014. Azaspiracids: Chemistry, biosynthesis, metabolism, and detection, 799–822.
- Hesse, M., Meier, H., Zeeh, B., 2012. *Spektroskopische Methoden in der organischen Chemie: 114 Tabellen*, 8th ed. Thieme, Stuttgart, 499 pp.
- Hopmann, C., Faulkner, D., 1997. Lissoketal, a spiroketal from the Palauan ascidian *Lissoclinum voeltzkowi*. *Tetrahedron Letters* 38, 169–170. 10.1016/S0040-4039(96)02265-4.
- Hoppenrath, M., Murray, S.A., Chomérat, N., Horiguchi, T., 2014. Marine benthic dinoflagellates: Unveiling their worldwide biodiversity. E. Schweizerbart'sche Verlagsbuchhandlung (Nägele u. Obermiller), Stuttgart, 276 pp.

- Hu, T., Burton, I.W., Cembella, A.D., Curtis, J.M., Quilliam, M.A., Walter, J.A., Wright, J.L.C., 2001. Characterization of Spirolides A, C, and 13-Desmethyl C, New Marine Toxins Isolated from Toxic Plankton and Contaminated Shellfish. *J. Nat. Prod.* 64, 308–312. 10.1021/np000416q.
- Hu, T., Curtis, J.M., Oshima, Y., Quilliam, M.A., Walter, J.A., Watson-Wright, W.M., Wright, J.L.C., 1995. Spirolides B and D, two novel macrocycles isolated from the digestive glands of shellfish. *J. Chem. Soc., Chem. Commun.*, 2159. 10.1039/C39950002159.
- Humphrey, W., Dalke, A., Schulten, K., 1996. VMD: Visual molecular dynamics. *Journal of Molecular Graphics* 14, 33–38. 10.1016/0263-7855(96)00018-5.
- Huntley, M.E., 1982. Yellow water in La Jolla Bay, California, July 1980. II. suppression of zooplankton grazing. *Journal of Experimental Marine Biology and Ecology* 63, 81–91. 10.1016/0022-0981(82)90052-1.
- Imai, I., Yamaguchi, M., Hori, Y., 2006. Eutrophication and occurrences of harmful algal blooms in the Seto Inland Sea, Japan. *Plankton Benthos Res* 1, 71–84. 10.3800/pbr.1.71.
- John, U., Tillmann, U., Hülskötter, J., Alpermann, T.J., Wohlrab, S., van de Waal, D.B., 2015. Intraspecific facilitation by allelochemical mediated grazing protection within a toxigenic dinoflagellate population. *Proceedings. Biological sciences* 282, 20141268. 10.1098/rspb.2014.1268.
- Kalaitzis, J.A., Chau, R., Kohli, G.S., Murray, S.A., Neilan, B.A., 2010. Biosynthesis of toxic naturally-occurring seafood contaminants. *Toxicon : official journal of the International Society on Toxinology* 56, 244–258. 10.1016/j.toxicon.2009.09.001.
- Keller, M.D., Selvin, R.C., Claus, W., Guillard, R.R.L., 1987. Media for the Culture of Oceanic Ultraphytoplankton. *Journal of Phycology* 23, 633–638. 10.1111/j.1529-8817.1987.tb04217.x.
- Kharrat, R., Servent, D., Girard, E., Ouanounou, G., Amar, M., Marrouchi, R., Benoit, E., Molgó, J., 2008. The marine phycotoxin gymnodimine targets muscular and neuronal nicotinic acetylcholine receptor subtypes with high affinity. *Journal of neurochemistry* 107, 952–963. 10.1111/j.1471-4159.2008.05677.x.
- Kilcoyne, J., Jauffrais, T., Twiner, M.J., Doucette, G.J., Aasen Bunes, J.A., Sosa, S., Krock, B., Séhet, V., Nulty, C., Salas, R., Clarke, D., Geraghty, J., Duffy, C., Foley, B., John, U., Quilliam, M.A., McCarron, P., Miles, C.O., Silke, J., Cembella, A., Tillmann, U., Hess, P., 2014a. Azaspiracids – Toxicological Evaluation, Test Methods and Identification of the

- Source Organisms (ASTOX II). Marine Institute. Marine Research Sub-Programme (NDP 2007-2013) Series. <http://hdl.handle.net/10793/970>.
- Kilcoyne, J., McCarron, P., Twiner, M.J., Rise, F., Hess, P., Wilkins, A.L., Miles, C.O., 2018. Identification of 21,22-Dehydroazaspiracids in Mussels (*Mytilus edulis*) and *in Vitro* Toxicity of Azaspiracid-26. *J. Nat. Prod.* 81, 885–893. 10.1021/acs.jnatprod.7b00973.
- Kilcoyne, J., Nulty, C., Jauffrais, T., McCarron, P., Herve, F., Foley, B., Rise, F., Crain, S., Wilkins, A.L., Twiner, M.J., Hess, P., Miles, C.O., 2014b. Isolation, structure elucidation, relative LC-MS response, and *in vitro* toxicity of azaspiracids from the dinoflagellate *Azadinium spinosum*. *J. Nat. Prod.* 77, 2465–2474. 10.1021/np500555k.
- Kilcoyne, J., Twiner, M.J., McCarron, P., Crain, S., Giddings, S.D., Foley, B., Rise, F., Hess, P., Wilkins, A.L., Miles, C.O., 2015. Structure Elucidation, Relative LC-MS Response and *In Vitro* Toxicity of Azaspiracids 7-10 Isolated from Mussels (*Mytilus edulis*). *Journal of agricultural and food chemistry* 63, 5083–5091. 10.1021/acs.jafc.5b01320.
- Kim, J.-H., Tillmann, U., Adams, N.G., Krock, B., Stutts, W.L., Deeds, J.R., Han, M.-S., Trainer, V.L., 2017. Identification of Azadinium species and a new azaspiracid from *Azadinium poporum* in Puget Sound, Washington State, USA. *Harmful Algae* 68, 152–167. 10.1016/j.hal.2017.08.004.
- Kirkpatrick, S., Gelatt, C.D., Vecchi, M.P., 1983. Optimization by simulated annealing. *Science (New York, N.Y.)* 220, 671–680. 10.1126/science.220.4598.671.
- Kremp, A., Tahvanainen, P., Litaker, W., Krock, B., Suikkanen, S., Leaw, C.P., Tomas, C.R., 2014. Phylogenetic relationships, morphological variation, and toxin patterns in the *Alexandrium ostenfeldii* (*Dinophyceae*) complex: Implications for species boundaries and identities. *Journal of Phycology* 50, 81–100. 10.1111/jpy.12134.
- Krock, B., Tillmann, U., Potvin, É., Jeong, H.J., Drebing, W., Kilcoyne, J., Al-Jorani, A., Twiner, M.J., Göthel, Q., Köck, M., 2015. Structure Elucidation and *in Vitro* Toxicity of New Azaspiracids Isolated from the Marine Dinoflagellate *Azadinium poporum*. *Marine drugs* 13, 6687–6702. 10.3390/md13116687.
- Krock, B., Tillmann, U., Tebben, J., Trefault, N., Gu, H., 2019. Two novel azaspiracids from *Azadinium poporum*, and a comprehensive compilation of azaspiracids produced by *Amphidomataceae*, (*Dinophyceae*). *Harmful Algae* 82, 1–8. 10.1016/j.hal.2018.12.005.
- Krock, B., Tillmann, U., Voß, D., Koch, B.P., Salas, R., Witt, M., Potvin, E., Jeong, H.J., 2012. New azaspiracids in *Amphidomataceae* (*Dinophyceae*). *Toxicon : official journal of the International Society on Toxinology* 60, 830–839. 10.1016/j.toxicon.2012.05.007.

- Krock, B., Tillmann, U., Witt, M., Gu, H., 2014. Azaspiracid variability of *Azadinium poporum* (*Dinophyceae*) from the China Sea. *Harmful Algae* 36, 22–28. 10.1016/j.hal.2014.04.012.
- Le Doux, M., Sherwood, H., 2000. Proficiency Testing of Eight French Laboratories in Using the AOAC Mouse Bioassay for Paralytic Shellfish Poisoning: Interlaboratory Collaborative Study. *Journal of AOAC International* 83, 305–310.
- Lee, M.S., Repeta, D.J., Nakanishi, K., Zagorski, M.G., 1986. Biosynthetic origins and assignments of ^{13}C NMR peaks of brevetoxin B. *Journal of the American Chemical Society* 108, 7855–7856. 10.1021/ja00284a072.
- Li, X.-C., Ferreira, D., Ding, Y., 2010. Determination of Absolute Configuration of Natural Products: Theoretical Calculation of Electronic Circular Dichroism as a Tool. *Current organic chemistry* 14, 1678–1697. 10.2174/138527210792927717.
- Lin, Y.-Y., Risk, M., Ray, S.M., van Engen, D., Clardy, J., Golik, J., James, J.C., Nakanishi, K., 1981. Isolation and structure of brevetoxin B from the “red tide” dinoflagellate *Ptychodiscus brevis* (*Gymnodinium breve*). *Journal of the American Chemical Society* 103, 6773–6775. 10.1021/ja00412a053.
- Louzao, M.C., Abal, P., Vilariño, N., 2017. Toxicity equivalence factors for regulated and non-regulated marine toxins. *Current Opinion in Food Science* 18, 64–70. 10.1016/j.cofs.2017.11.008.
- Lu, T., Chen, F., 2012. Multiwfn: A multifunctional wavefunction analyzer. *J. Comput. Chem.* 33, 580–592. 10.1002/jcc.22885.
- MacKenzie, L., Rhodes, L.L., Till, D., Chang, F.H., Kaspar, H.F., Haywood, A., Kapa, J., Walker, B., 1995. A *Gymnodinium* sp. bloom and the contamination of shellfish with lipid soluble toxins in New Zealand, Jan-April 1993. *Harmful Marine Algal Blooms*, 795–800.
- MacKinnon, S.L., Cembella, A.D., Burton, I.W., Lewis, N.I., LeBlanc, P., Walter, J.A., 2006. Biosynthesis of 13-desmethyl spirolide C by the dinoflagellate *Alexandrium ostenfeldii*. *The Journal of organic chemistry* 71, 8724–8731. 10.1021/jo0608873.
- Maio, G., 2001. Zur Geschichte der Contergan-Katastrophe im Lichte der Arzneimittelgesetzgebung. *Deutsche medizinische Wochenschrift* (1946) 126, 1183–1186. 10.1055/s-2001-17888.
- Maksimenka, K., 2010. Absolute Configuration by Circular Dichroism: Quantum Chemical CD Calculations. Dissertation, Würzburg.

2004. Marine biotoxins. Food and Agriculture Organization of the United Nations, Rome, 278 pp.
2008. Marine biotoxins in shellfish – Azaspiracid group - Scientific Opinion of the Panel on Contaminants in the Food chain. EFS2 6, 133. 10.2903/j.efsa.2008.723.
- Martens, H., Tillmann, U., Harju, K., Dell'Aversano, C., Tartaglione, L., Krock, B., 2017. Toxin Variability Estimations of 68 *Alexandrium ostenfeldii* (*Dinophyceae*) Strains from The Netherlands Reveal a Novel Abundant Gymnodimine. *Microorganisms* 5, 29. 10.3390/microorganisms5020029.
- Miles, C.O., Wilkins, A.L., Stirling, D.J., MacKenzie, A.L., 2000. New Analogue of Gymnodimine from a *Gymnodinium* Species. *Journal of agricultural and food chemistry* 48, 1373–1376. 10.1021/jf991031k.
- Miles, C.O., Wilkins, A.L., Stirling, D.J., MacKenzie, A.L., 2003. Gymnodimine C, an isomer of gymnodimine B, from *Karenia selliformis*. *Journal of agricultural and food chemistry* 51, 4838–4840. 10.1021/jf030101r.
- Miller, S.C., Huang, R., Sakamuru, S., Shukla, S.J., Attene-Ramos, M.S., Shinn, P., van Leer, D., Leister, W., Austin, C.P., Xia, M., 2010. Identification of known drugs that act as inhibitors of NF-kappaB signaling and their mechanism of action. *Biochemical pharmacology* 79, 1272–1280. 10.1016/j.bcp.2009.12.021.
- Moestrup, Ø., Akselman-Cardella, R., Fraga, S., Hoppenrath, M., Iwataki, M., Komárek, J., Larsen, J., Lundholm, N., Zingone, A., 2009 onwards. IOC-UNESCO Taxonomic Reference List of Harmful Micro Algae. <http://www.marinespecies.org/hab>. Accessed 18 May 2019.
- Molgó, J., Marchot, P., Aráoz, R., Benoit, E., Iorga, B.I., Zakarian, A., Taylor, P., Bourne, Y., Servent, D., 2017. Cyclic imine toxins from dinoflagellates: A growing family of potent antagonists of the nicotinic acetylcholine receptors. *Journal of neurochemistry*, 41–51. 10.1111/jnc.13995.
- Murata, M., Izumikawa, M., Tachibana, K., Fujita, T., Naoki, H., 1998. Labeling Pattern of Okadaic Acid from $^{18}\text{O}_2$ and $[^{18}\text{O}_2]$ Acetate Elucidated by Collision-Induced Dissociation Tandem Mass Spectrometry. *Journal of the American Chemical Society* 120, 147–151. 10.1021/ja971547p.
- Nagashima, Y., Noguchi, T., Kawabata, T., Hashimoto, K., 1991. Dose-death time curves of paralytic shellfish poisons in ddY strain mice. *Nippon Suisan Gakkaishi* 57, 699–704. 10.2331/suisan.57.699.

- Neese, F., 2018. Software update: The ORCA program system, version 4.0. WIREs Comput Mol Sci 8, e1327. 10.1002/wcms.1327.
- Nicolaou, K.C., Frederick, M.O., Petrovic, G., Cole, K.P., Loizidou, E.Z., 2006. Total synthesis and confirmation of the revised structures of azaspiracid-2 and azaspiracid-3. *Angewandte Chemie (International ed. in English)* 45, 2609–2615. 10.1002/anie.200600295.
- Nicolaou, K.C., Vyskocil, S., Koftis, T.V., Yamada, Y.M.A., Ling, T., Chen, D.Y.-K., Tang, W., Petrovic, G., Frederick, M.O., Li, Y., Satake, M., 2004. Structural revision and total synthesis of azaspiracid-1, part 1: Intelligence gathering and tentative proposal. *Angewandte Chemie (International ed. in English)* 43, 4312–4318. 10.1002/anie.200460695.
- Niedersächsisches Ministerium für Ernährung und Landwirtschaft und Verbraucherschutz, 2016. Niedersächsische Ausführungshinweise für die Überwachungsbehörden zur Durchführung der Muschelhygieneüberwachung.
- Nixon, S.W., 2012. Coastal marine eutrophication: A definition, social causes, and future concerns. *Ophelia* 41, 199–219. 10.1080/00785236.1995.10422044.
- Ochoa, J.L., 2003. ENSO phenomenon and toxic red tides in Mexico. *Geofísica Internacional* 42, 505–515.
- Ofuji, K., Satake, M., McMahon, T., Silke, J., James, K.J., Naoki, H., Oshima, Y., Yasumoto, T., 1999. Two analogs of azaspiracid isolated from mussels, *Mytilus edulis*, involved in human intoxication in Ireland. *Nat. Toxins* 7, 99–102. 10.1002/(SICI)1522-7189(199905/06)7:3<99:AID-NT46>3.0.CO;2-L.
- Otero, A., Chapela, M.-J., Atanassova, M., Vieites, J.M., Cabado, A.G., 2011. Cyclic imines: Chemistry and mechanism of action: a review. *Chemical research in toxicology* 24, 1817–1829. 10.1021/tx200182m.
- Paerl, H.W., Whitall, D.R., 1999. Anthropogenically-derived atmospheric nitrogen deposition, marine eutrophication and harmful algal bloom expansion: Is there a link? *Ambio* 28, 307–311.
- Pelin, M., Kilcoyne, J., Nulty, C., Crain, S., Hess, P., Tubaro, A., Sosa, S., 2018. Toxic equivalency factors (TEFs) after acute oral exposure of azaspiracid 1, -2 and -3 in mice. *Toxicology letters* 282, 136–146. 10.1016/j.toxlet.2017.10.016.

- Phillips, J.C., Braun, R., Wang, W., Gumbart, J., Tajkhorshid, E., Villa, E., Chipot, C., Skeel, R.D., Kalé, L., Schulten, K., 2005. Scalable molecular dynamics with NAMD. *J. Comput. Chem.* 26, 1781–1802. 10.1002/jcc.20289.
- Place, A.R., Bowers, H.A., Bachvaroff, T.R., Adolf, J.E., Deeds, J.R., Sheng, J., 2012. *Karlodinium veneficum*—The little dinoflagellate with a big bite. *Harmful Algae* 14, 179–195. 10.1016/j.hal.2011.10.021.
- Prakash, A., Medcof, J.C., Tennant, A.D., 1971. paralytic shellfish poisoning in eastern Canada. Fisheries Research Board of Canada, Ottawa, Canada.
- Raymont, J.E.G., 2014. *Plankton & Productivity in the Oceans: Volume 1: Phytoplankton*, 2nd ed. Elsevier Science, Burlington, 504 pp.
- Rehmann, N., Hess, P., Quilliam, M.A., 2008. Discovery of new analogs of the marine biotoxin azaspiracid in blue mussels (*Mytilus edulis*) by ultra-performance liquid chromatography/tandem mass spectrometry. *Rapid communications in mass spectrometry* : RCM 22, 549–558. 10.1002/rcm.3385.
- Rein, K.S., Borrone, J., 1999. Polyketides from dinoflagellates: Origins, pharmacology and biosynthesis. *Comparative Biochemistry and Physiology Part B: Biochemistry and Molecular Biology* 124, 117–131. 10.1016/S0305-0491(99)00107-8.
- Resnick, B., 2018. Why Florida's red tide is killing fish, manatees, and turtles: Where the red tide is, and why it's so dangerous for marine life. *Vox*. <https://www.vox.com/energy-and-environment/2018/8/30/17795892/red-tide-2018-florida-gulf-sarasota-sanibel-okeechobee>. Accessed 24 November 2018.
- Reynolds, C.S., 2007. *The ecology of phytoplankton*. Univ. Press, Cambridge, 535 pp.
- Richard, D., Arsenaulf, E., Cembella, A., Quilliam, M., 2001. Investigations into the Toxicology and Pharmacology of Spirolides, a Novel Group of Shellfish Toxins, in: *Harmful Algal Blooms 2000*: pp 383390. Proceedings of the Ninth International Conference on Harmful Algal Blooms. Intergovernmental Oceanographic Commission of UNESCO, Paris, France, 383-386.
- Rossi, R., Dell'Aversano, C., Krock, B., Ciminiello, P., Percopo, I., Tillmann, U., Soprano, V., Zingone, A., 2017. Mediterranean *Azadinium dexteroporum* (*Dinophyceae*) produces six novel azaspiracids and azaspiracid-35: A structural study by a multi-platform mass spectrometry approach. *Analytical and bioanalytical chemistry* 409, 1121–1134. 10.1007/s00216-016-0037-4.

- Samdal, I.A., Løvberg, K.E., Briggs, L.R., Kilcoyne, J., Xu, J., Forsyth, C.J., Miles, C.O., 2015. Development of an ELISA for the Detection of Azaspiracids. *Journal of agricultural and food chemistry* 63, 7855–7861. 10.1021/acs.jafc.5b02513.
- Sargent, M., 2013. Guide to achieving reliable quantitative LC-MS measurements. LGC Limited.
- Satake, M., Ofuji, K., Naoki, H., James, K.J., Furey, A., McMahon, T., Silke, J., Yasumoto, T., 1998. Azaspiracid, a New Marine Toxin Having Unique Spiro Ring Assemblies, Isolated from Irish Mussels, *Mytilus edulis*. *Journal of the American Chemical Society* 120, 9967–9968. 10.1021/ja981413r.
- Schoental, R., 1984. Mycotoxins and the Bible. *Perspectives in Biology and Medicine* 28, 117–120. 10.1353/pbm.1984.0002.
- Seki, T., Satake, M., MacKenzie, L., Kaspar, H.F., Yasumoto, T., 1995. Gymnodimine, a new marine toxin of unprecedented structure isolated from New Zealand oysters and the dinoflagellate, *Gymnodinium* sp. *Tetrahedron Letters* 36, 7093–7096. 10.1016/0040-4039(95)01434-J.
- Selander, E., Kubanek, J., Hamberg, M., Andersson, M.X., Cervin, G., Pavia, H., 2015. Predator lipids induce paralytic shellfish toxins in bloom-forming algae. *Proceedings of the National Academy of Sciences of the United States of America* 112, 6395–6400. 10.1073/pnas.1420154112.
- Selander, E., Thor, P., Toth, G., Pavia, H., 2006. Copepods induce paralytic shellfish toxin production in marine dinoflagellates. *Proceedings. Biological sciences* 273, 1673–1680. 10.1098/rspb.2006.3502.
- Selwood, A.I., Wilkins, A.L., Munday, R., Shi, F., Rhodes, L.L., Holland, P.T., 2013. Portimine: A bioactive metabolite from the benthic dinoflagellate *Vulcanodinium rugosum*. *Tetrahedron Letters* 54, 4705–4707. 10.1016/j.tetlet.2013.06.098.
- Sheng, J., Malkiel, E., Katz, J., Adolf, J.E., Place, A.R., 2010. A dinoflagellate exploits toxins to immobilize prey prior to ingestion. *Proceedings of the National Academy of Sciences of the United States of America* 107, 2082–2087. 10.1073/pnas.0912254107.
- Smayda, T.J., 1990. Novel and Nuisance Phytoplankton Blooms in the Sea: Evidence for a Global Epidemic, in: Granéli, E., Sundström, B., Edler, L., Anderson, D.M. (Eds.), *Toxic Marine Phytoplankton*, New York, pp. 29–40.

- Smayda, T.J., Reynolds, C.S., 2003. Strategies of marine dinoflagellate survival and some rules of assembly. *Journal of Sea Research* 49, 95–106. 10.1016/S1385-1101(02)00219-8.
- Stabell, O.B., Steffenak, I., Aune, T., 1992. An evaluation of the mouse bioassay applied to extracts of 'diarrhoetic' shellfish toxins. *Food and Chemical Toxicology* 30, 139–144. 10.1016/0278-6915(92)90149-F.
- Stewart, M., Blunt, J.W., Munro, M.H., Robinson, W.T., Hannah, D.J., 1997. The absolute stereochemistry of the New Zealand shellfish toxin gymnodimine. *Tetrahedron Letters* 38, 4889–4890. 10.1016/S0040-4039(97)01050-2.
- Stivala, C.E., Benoit, E., Aráoz, R., Servent, D., Novikov, A., Molgó, J., Zakarian, A., 2015. Synthesis and biology of cyclic imine toxins, an emerging class of potent, globally distributed marine toxins. *Natural product reports* 32, 411–435. 10.1039/C4NP00089G.
- Stoecker, D.K., 1999. Mixotrophy among Dinoflagellates. *J Eukaryotic Microbiology* 46, 397–401. 10.1111/j.1550-7408.1999.tb04619.x.
- Suzuki, T., Jin, T., Shiota, Y., Mitsuya, T., Okumura, Y., Kamiyama, T., 2005. Quantification of lipophilic toxins associated with diarrhetic shellfish poisoning in Japanese bivalves by liquid chromatography-mass spectrometry and comparison with mouse bioassay. *Fisheries Sci* 71, 1370–1378. 10.1111/j.1444-2906.2005.01104.x.
- Tillmann, U., Alpermann, T.J., John, U., Cembella, A., 2008. Allelochemical interactions and short-term effects of the dinoflagellate *Alexandrium* on selected photoautotrophic and heterotrophic protists. *Harmful Algae* 7, 52–64. 10.1016/j.hal.2007.05.009.
- Tillmann, U., Edvardsen, B., Krock, B., Smith, K.F., Paterson, R.F., Voß, D., 2018. Diversity, distribution, and azaspiracids of *Amphidomataceae* (*Dinophyceae*) along the Norwegian coast. *Harmful Algae* 80, 15–34. 10.1016/j.hal.2018.08.011.
- Tillmann, U., Elbrächter, M., Krock, B., John, U., Cembella, A., 2009. *Azadinium spinosum* gen. et sp. nov. (*Dinophyceae*) identified as a primary producer of azaspiracid toxins. *European Journal of Phycology* 44, 63–79. 10.1080/09670260802578534.
- Tillmann, U., Jaén, D., Fernández, L., Gottschling, M., Witt, M., Blanco, J., Krock, B., 2017. *Amphidoma languida* (*Amphidomatacea*, *Dinophyceae*) with a novel azaspiracid toxin profile identified as the cause of molluscan contamination at the Atlantic coast of southern Spain. *Harmful Algae* 62, 113–126. 10.1016/j.hal.2016.12.001.

- Toti, L., Croci, L., De Medici, D., Gizzarelli, S., Di Pasquale, M., Orfice, L., Stazi, A., 1991. Evaluation of Yasumoto test for the determination of DSP toxin in shellfish. Proceedings of Symposium on Marine Biotoxins, 107–110.
- Turner, J.T., Tester, P.A., 1997. Toxic marine phytoplankton, zooplankton grazers, and pelagic food webs. *Limnol. Oceanogr.* 42, 1203–1213. 10.4319/lo.1997.42.5_part_2.1203.
- Twiner, M.J., El-Ladki, R., Kilcoyne, J., Doucette, G.J., 2012. Comparative effects of the marine algal toxins azaspiracid-1, -2, and -3 on Jurkat T lymphocyte cells. *Chemical research in toxicology* 25, 747–754. 10.1021/tx200553p.
- van Dolah, F.M., 2000. Marine algal toxins: Origins, health effects, and their increased occurrence. *Environmental health perspectives* 108 Suppl 1, 133–141. 10.1289/ehp.00108s1133.
- van Wagoner, R.M., Misner, I., Tomas, C.R., Wright, J.L.C., 2011. Occurrence of 12-methylgymnodimine in a spirolide-producing dinoflagellate *Alexandrium peruvianum* and the biogenetic implications. *Tetrahedron Letters* 52, 4243–4246. 10.1016/j.tetlet.2011.05.137.
- van Wagoner, R.M., Satake, M., Wright, J.L.C., 2014. Polyketide biosynthesis in dinoflagellates: What makes it different? *Natural product reports* 31, 1101–1137. 10.1039/C4NP00016A.
- Wandscheer, C.B., Vilariño, N., Espina, B., Louzao, M.C., Botana, L.M., 2010. Human muscarinic acetylcholine receptors are a target of the marine toxin 13-desmethyl C spirolide. *Chemical research in toxicology* 23, 1753–1761. 10.1021/tx100210a.
- Wang, X.J., Hayes, J.D., Wolf, C.R., 2006. Generation of a stable antioxidant response element-driven reporter gene cell line and its use to show redox-dependent activation of nrf2 by cancer chemotherapeutic agents. *Cancer research* 66, 10983–10994. 10.1158/0008-5472.CAN-06-2298.
- White, A.W., 1981. Marine zooplankton can accumulate and retain dinoflagellate toxins and cause fish kills. *Limnol. Oceanogr.* 26, 103–109. 10.4319/lo.1981.26.1.0103.
- White, H.H., 1979. Effects of dinoflagellate bioluminescence on the ingestion rates of herbivorous zooplankton. *Journal of Experimental Marine Biology and Ecology* 36, 217–224. 10.1016/0022-0981(79)90117-5.

- Wilmoth, J., 2017. Press briefing for the launch of the World Population Prospects: The 2017 revision, UN Headquarters, New York.
- Wohlrab, S., Tillmann, U., Cembella, A., John, U., 2016. Trait changes induced by species interactions in two phenotypically distinct strains of a marine dinoflagellate. *The ISME journal* 10, 2658–2668. 10.1038/ismej.2016.57.
- Yamazaki, M., Tachibana, K., Satake, M., 2011. Complete ¹³C-labeling pattern of yessotoxin a marine ladder-frame polyether. *Tetrahedron* 67, 877–880. 10.1016/j.tet.2010.12.015.
- Yasumoto, T., 2000. Historic considerations regarding seafood safety, in: *Seafood and Freshwater toxins: Pharmacology, Physiology and Detection*, New York, pp. 1–17.
- Zhang, F., Dickman, M., 1999. Mid-ocean exchange of container vessel ballast water. 1: Seasonal factors affecting the transport of harmful diatoms and dinoflagellates. *Mar. Ecol. Prog. Ser.* 176, 243–251. 10.3354/meps176243.
- Zingone, A., Enevoldsen, H.O., 2000. The diversity of harmful algal blooms: A challenge for science and management. *Ocean & Coastal Management* 43, 725–748. 10.1016/S0964-5691(00)00056-9.
- Zoete, V., Cuendet, M.A., Grosdidier, A., Michielin, O., 2011. SwissParam: A fast force field generation tool for small organic molecules. *J. Comput. Chem.* 32, 2359–2368. 10.1002/jcc.21816.
- Zurhelle, C., Nieva, J., Tillmann, U., Harder, T., Krock, B., Tebben, J., 2018. Identification of Novel Gymnodimines and Spirolides from the Marine Dinoflagellate *Alexandrium ostenfeldii*. *Marine drugs* 16. 10.3390/md16110446.

9. Supporting Information's

9.1 Identification of novel neurotoxic gymnodimines and spirolides from the marine dinoflagellate *Alexandrium ostenfeldii*

All raw NMR data (Topspin) and annotated Mestre files of this section are available in the data repository PANGAEA <https://doi.pangaea.de/10.1594/PANGAEA.895116>.

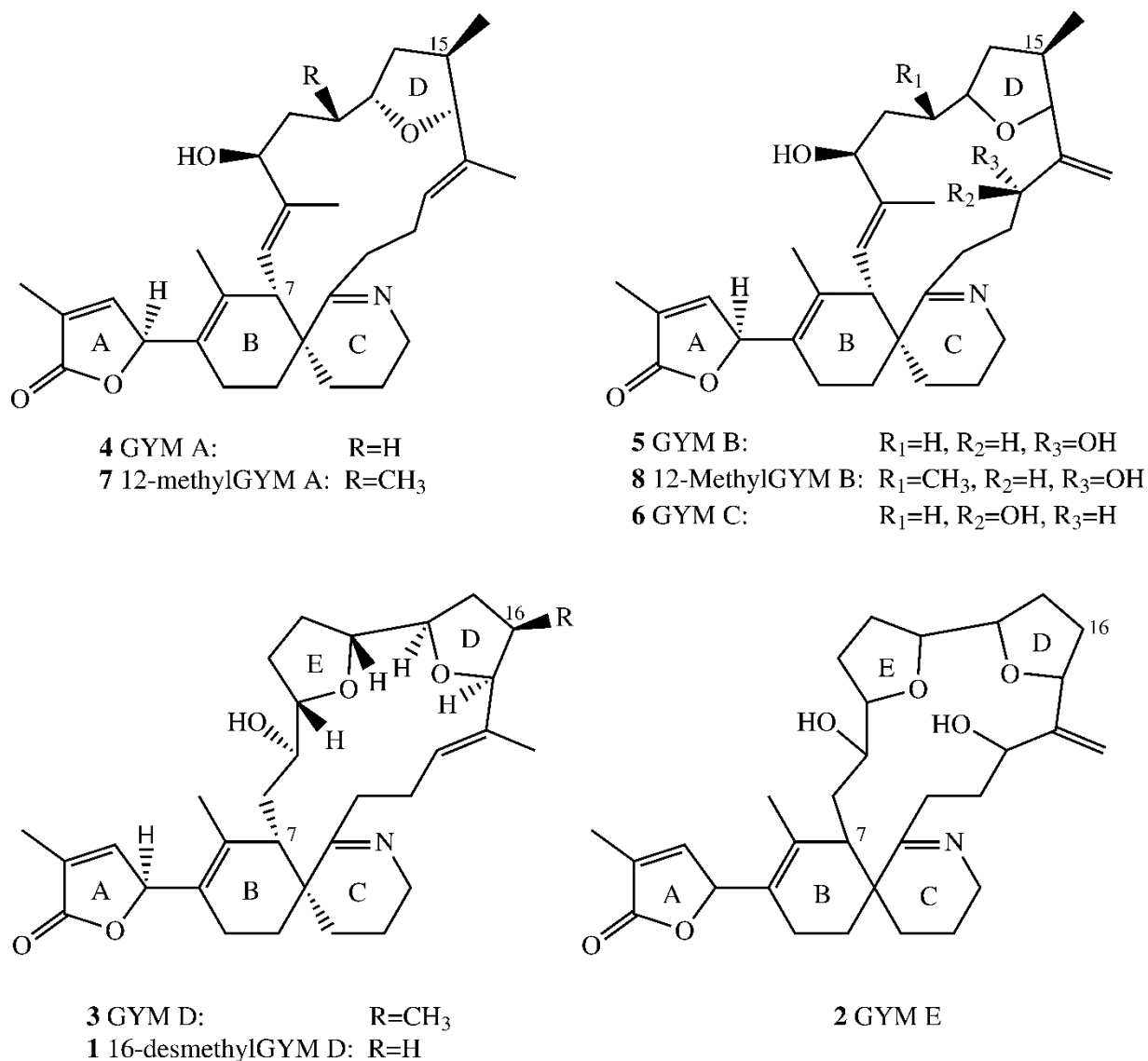
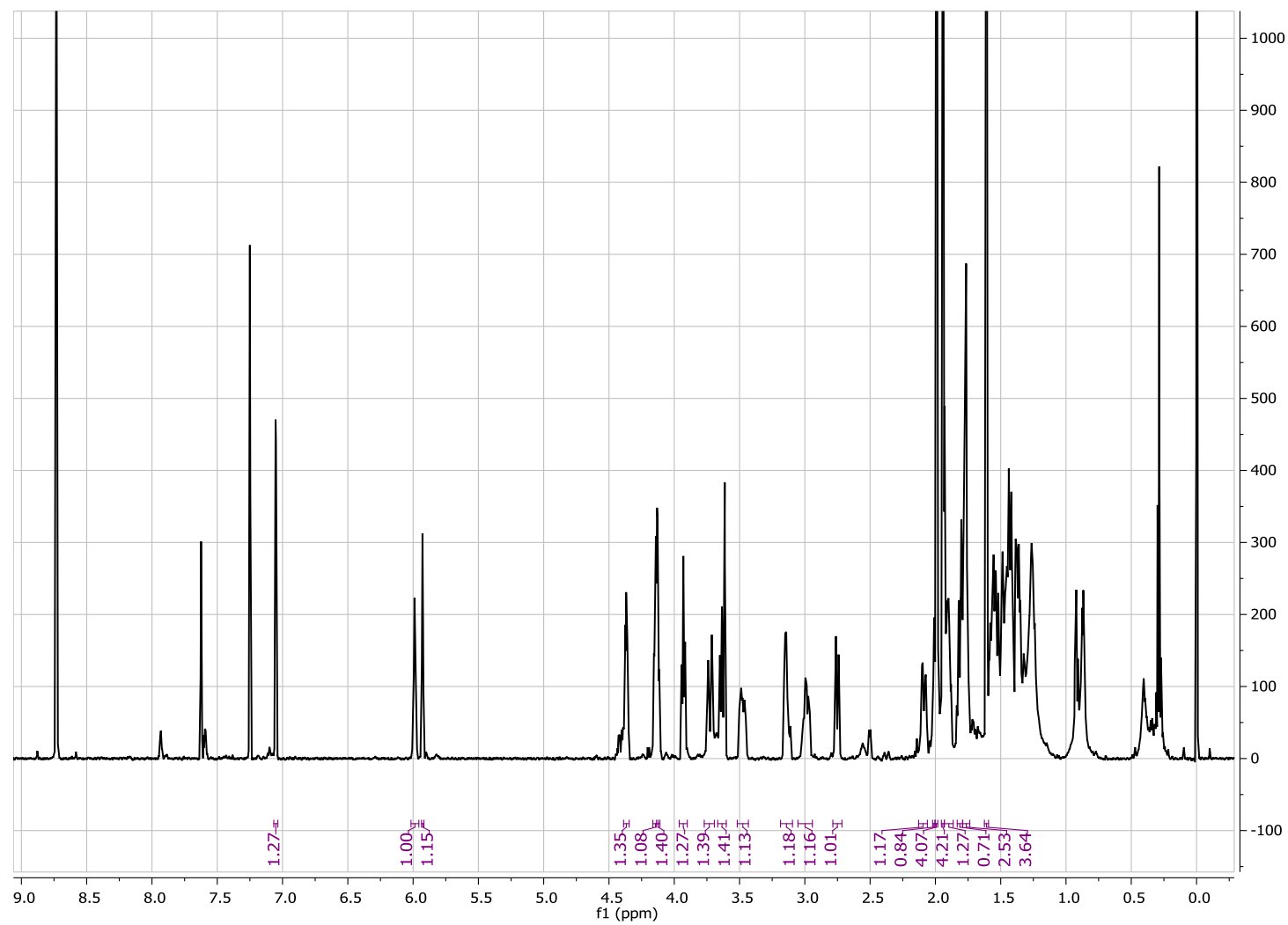


Figure 9.1: Structures of known and novel gymnodimines.

Figure 9.2: Structures of known and novel spirolides.

9.1.1 NMR-spectra of 16-desmethyl GYM D

Figure 9.3: 1D Proton spectra of 16-desmethyl GYM D (600 MHz, pyridine-d₅).

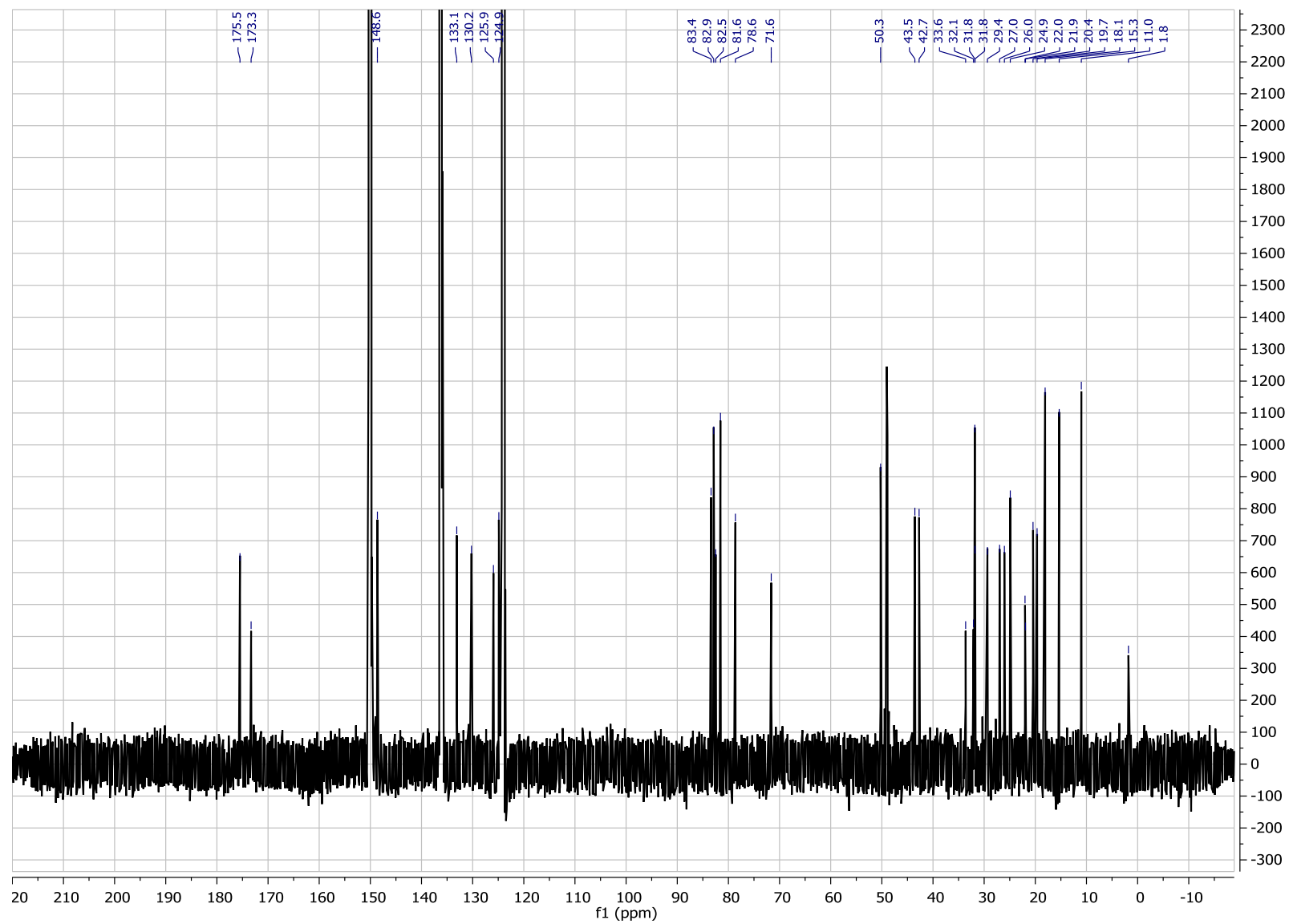


Figure 9.4: 1D ^{13}C -spectra of 16-desmethyl GYM D (150 MHz, pyridine- d_5).

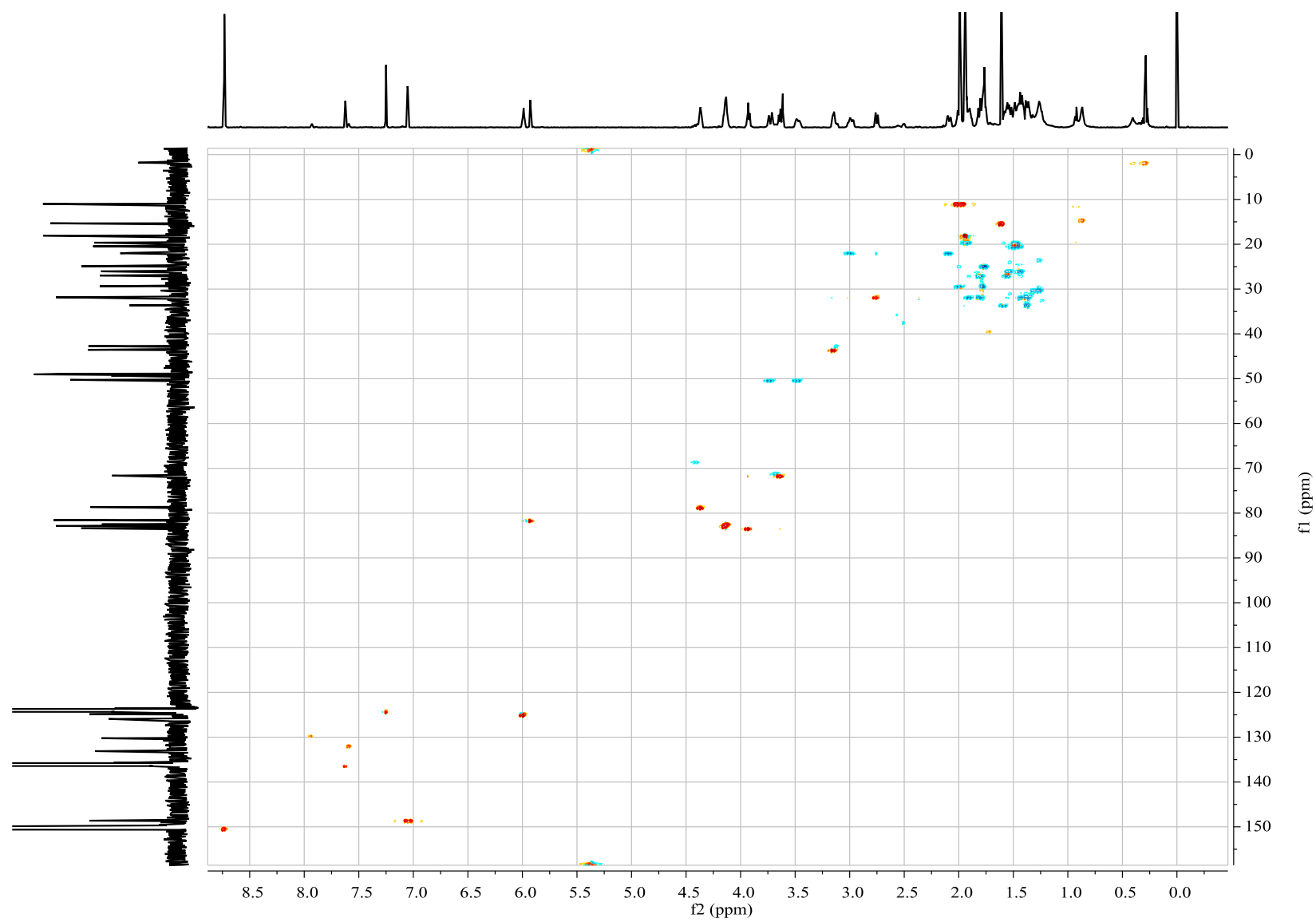


Figure 9.5: Multiplicity-edited 2D HSQC spectra of 16-desmethyl GYM D (600 MHz Proton frequency, pyridine- d_5).

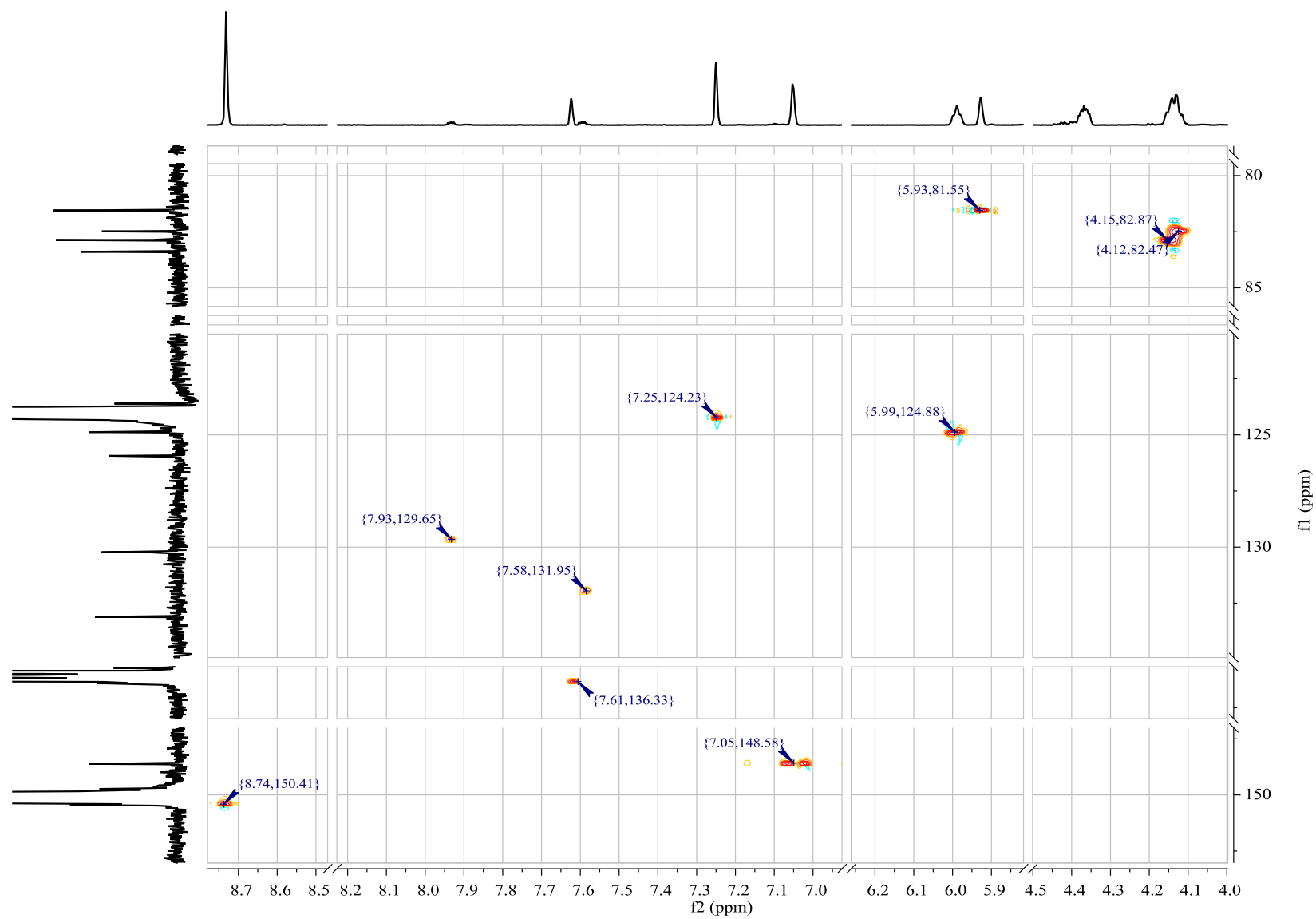


Figure 9.6: Slice 1 of multiplicity-edited 2D HSQC spectra of 16-desmethyl GYM D (600 MHz Proton frequency, pyridine-d₅).

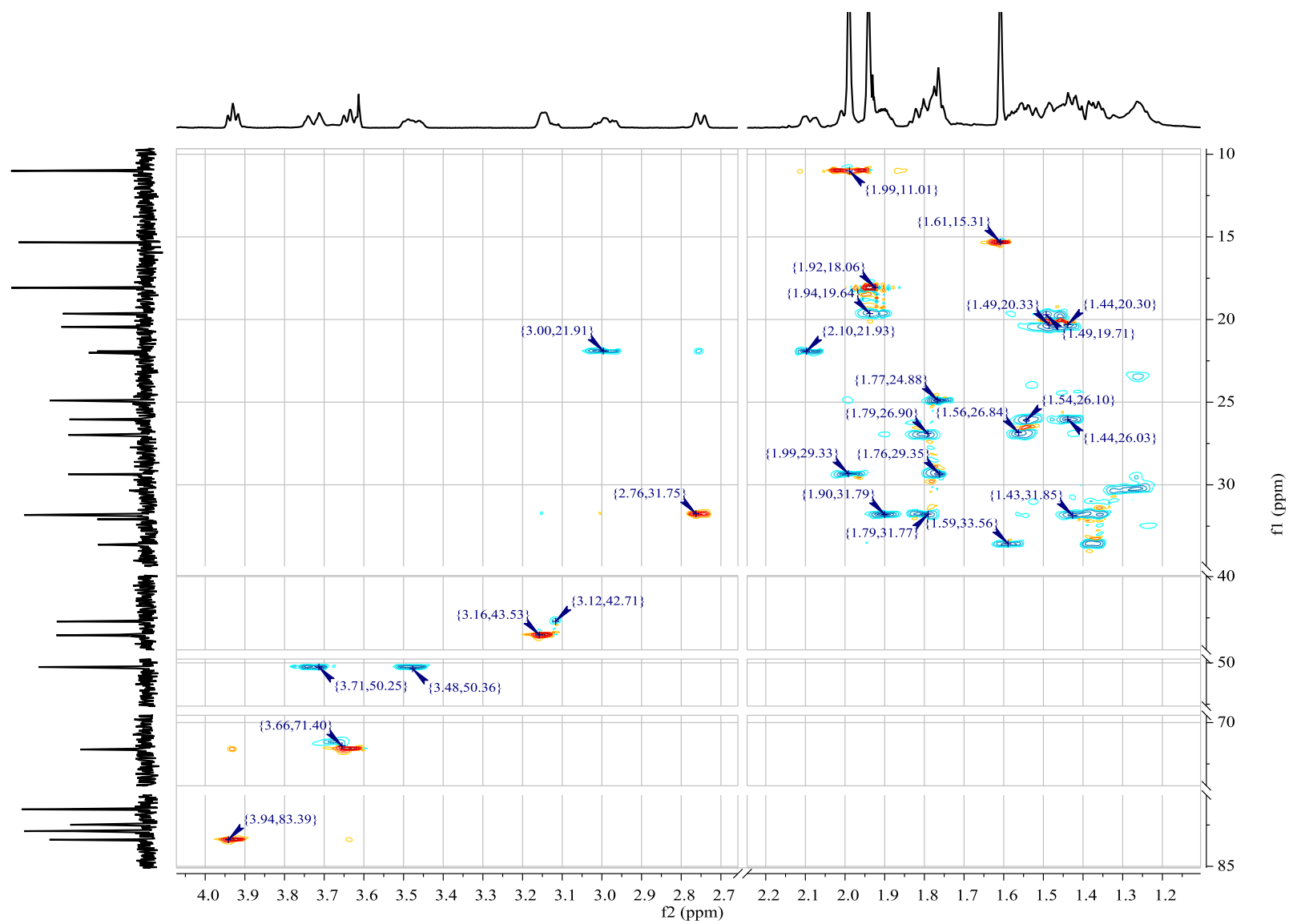


Figure 9.7: Slice 2 of multiplicity-edited 2D HSQC spectra of 16-desmethyl GYM D (600 MHz Proton frequency, pyridine-d₅).

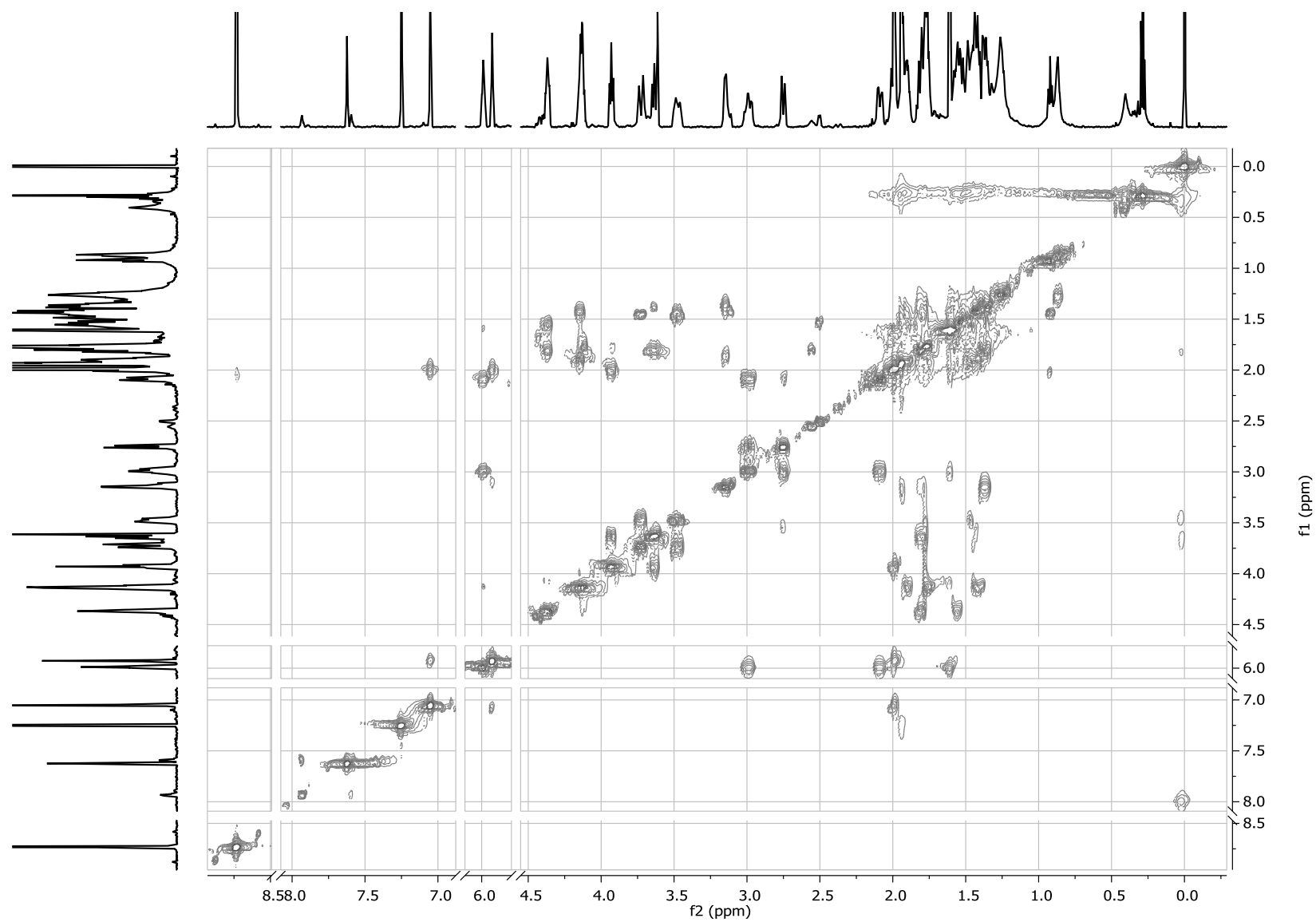


Figure 9.8: 2D COSY spectra of 16-desmethyl GYM D (600 MHz, pyridine-d₅).

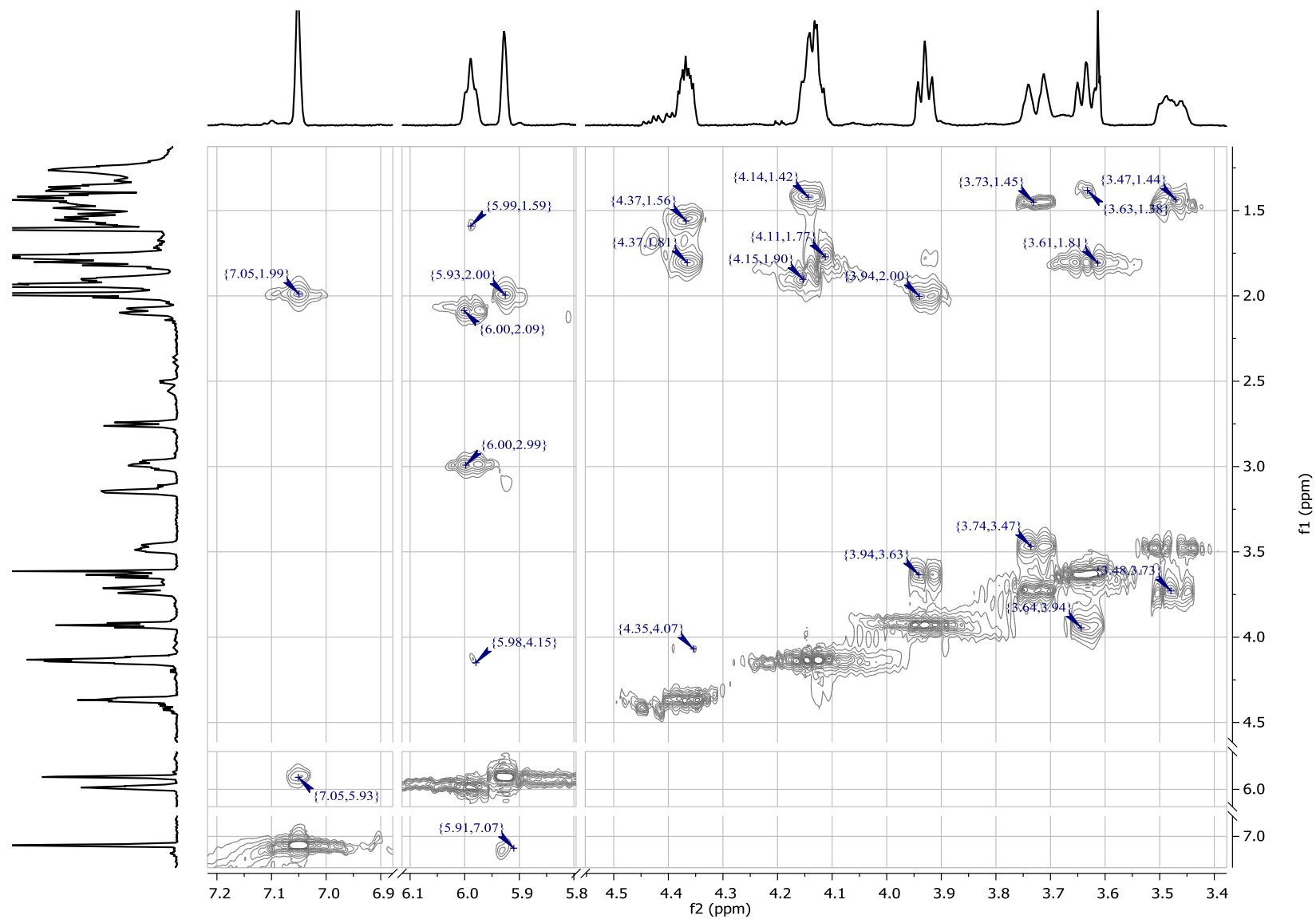


Figure 9.9: Slice 1 of 2D COSY spectra of 16-desmethyl GYM D (600 MHz, pyridine-d₅).

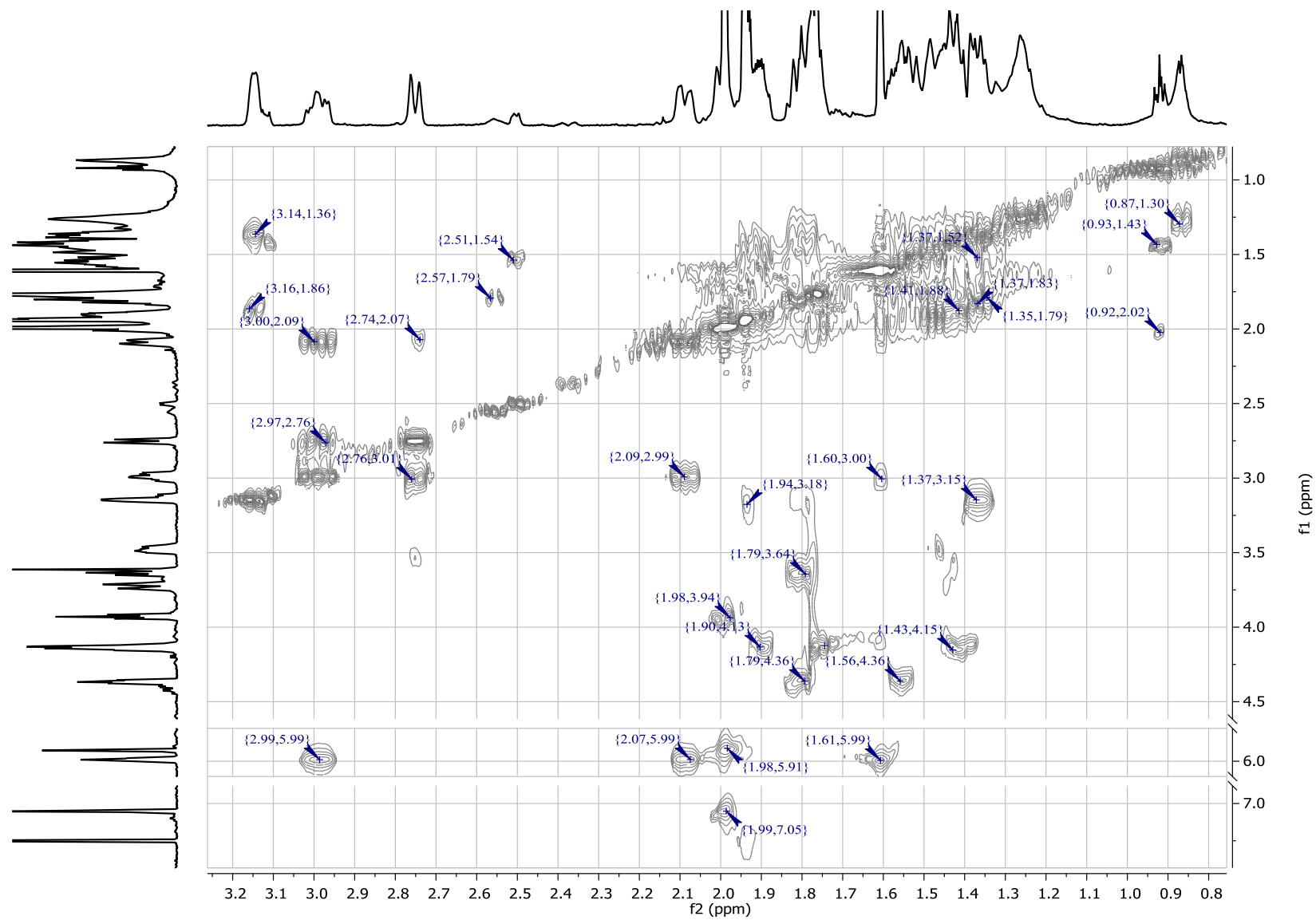


Figure 9.10: Slice 2 of 2D COSY spectra of 16-desmethyl GYM D (600 MHz, pyridine- d_5).

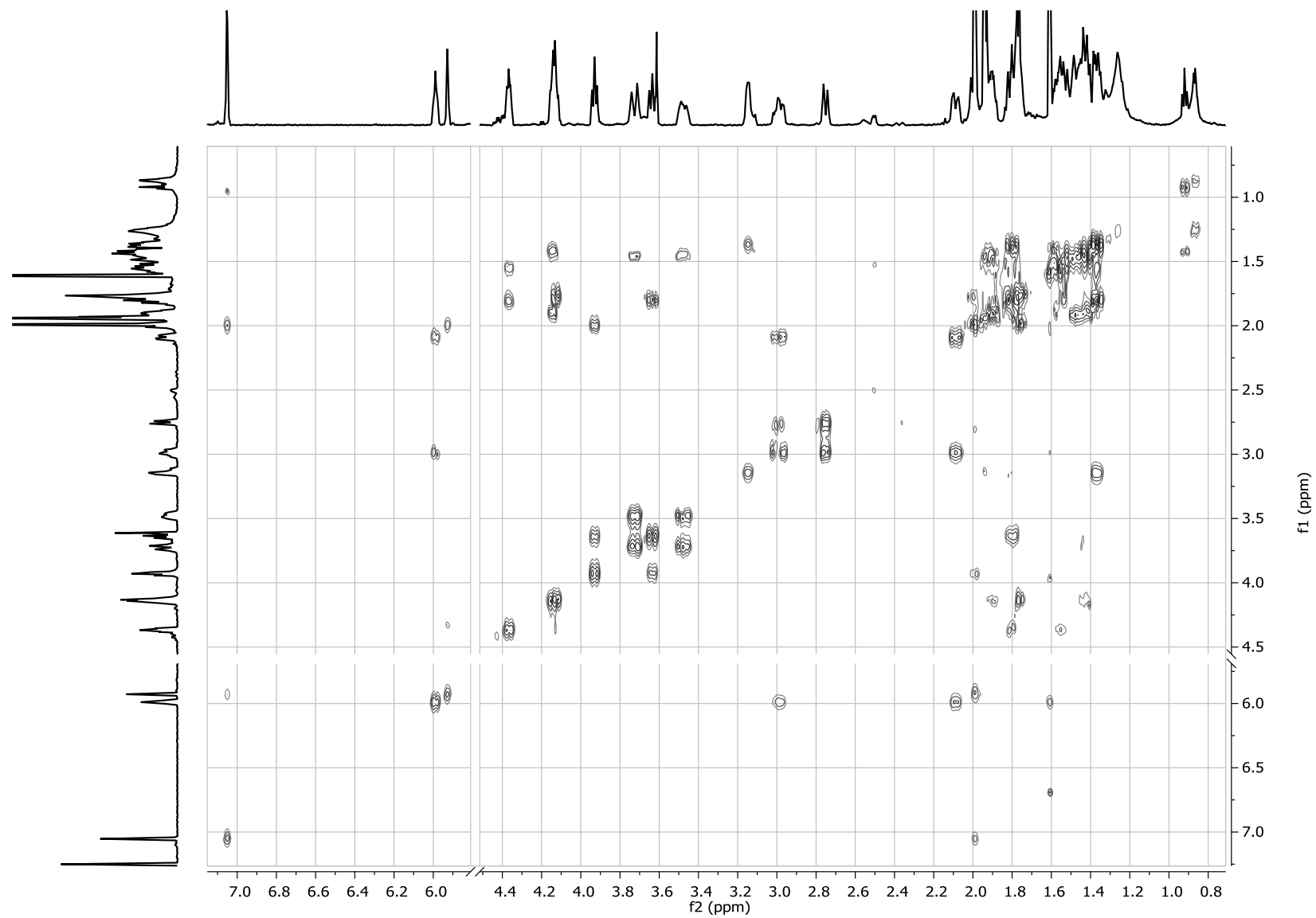


Figure 9.11: 2D double quantum filtered COSY spectra of 16-desmethyl GYM D (600 MHz, pyridine-d₅).

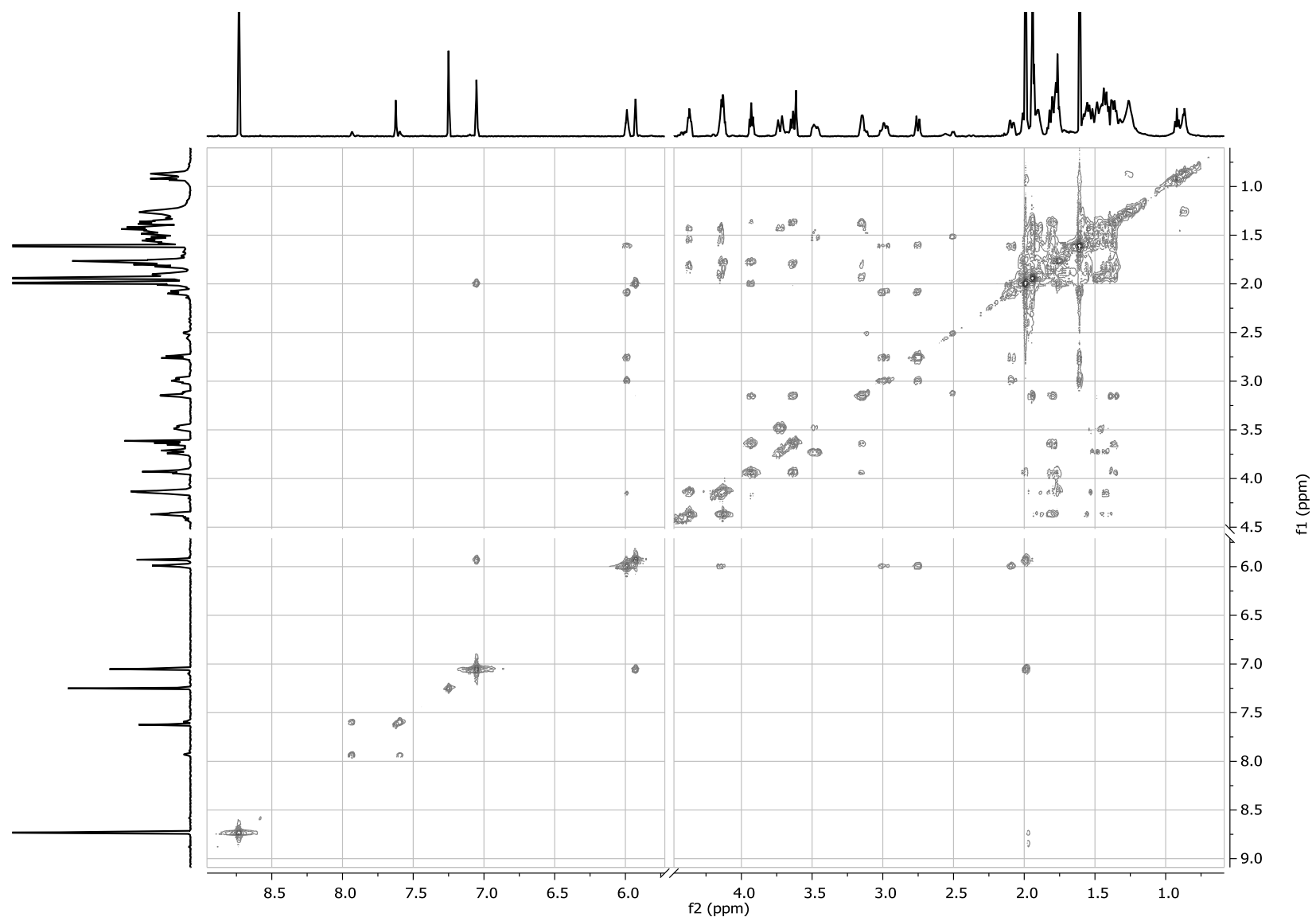


Figure 9.12: 2D TOCSY spectra of 16-desmethyl GYM D (600 MHz, pyridine-d₅).

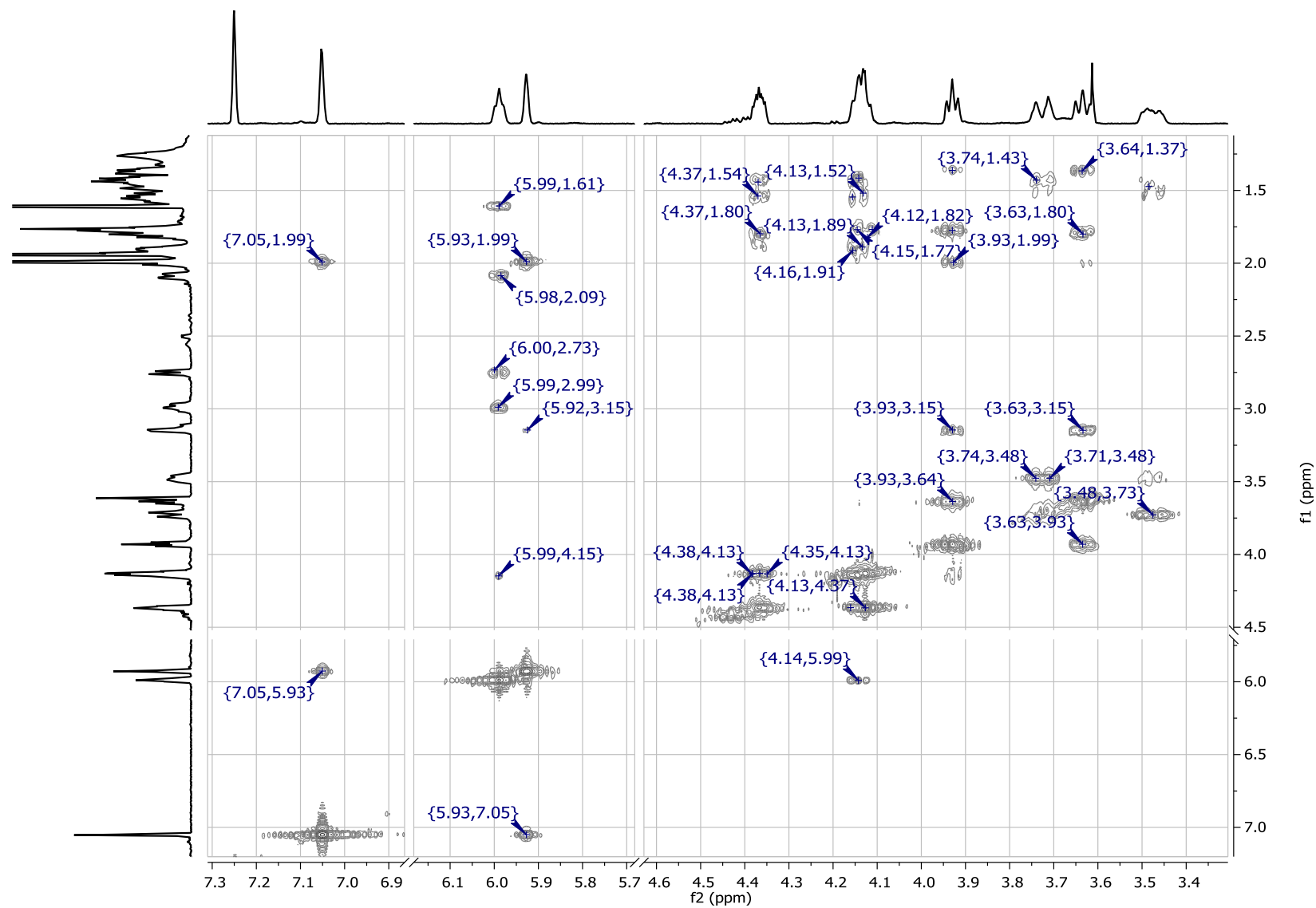


Figure 9.13: Slice 1 of 2D TOCSY spectra of 16-desmethyl GYM D (600 MHz, pyridine-d₅).

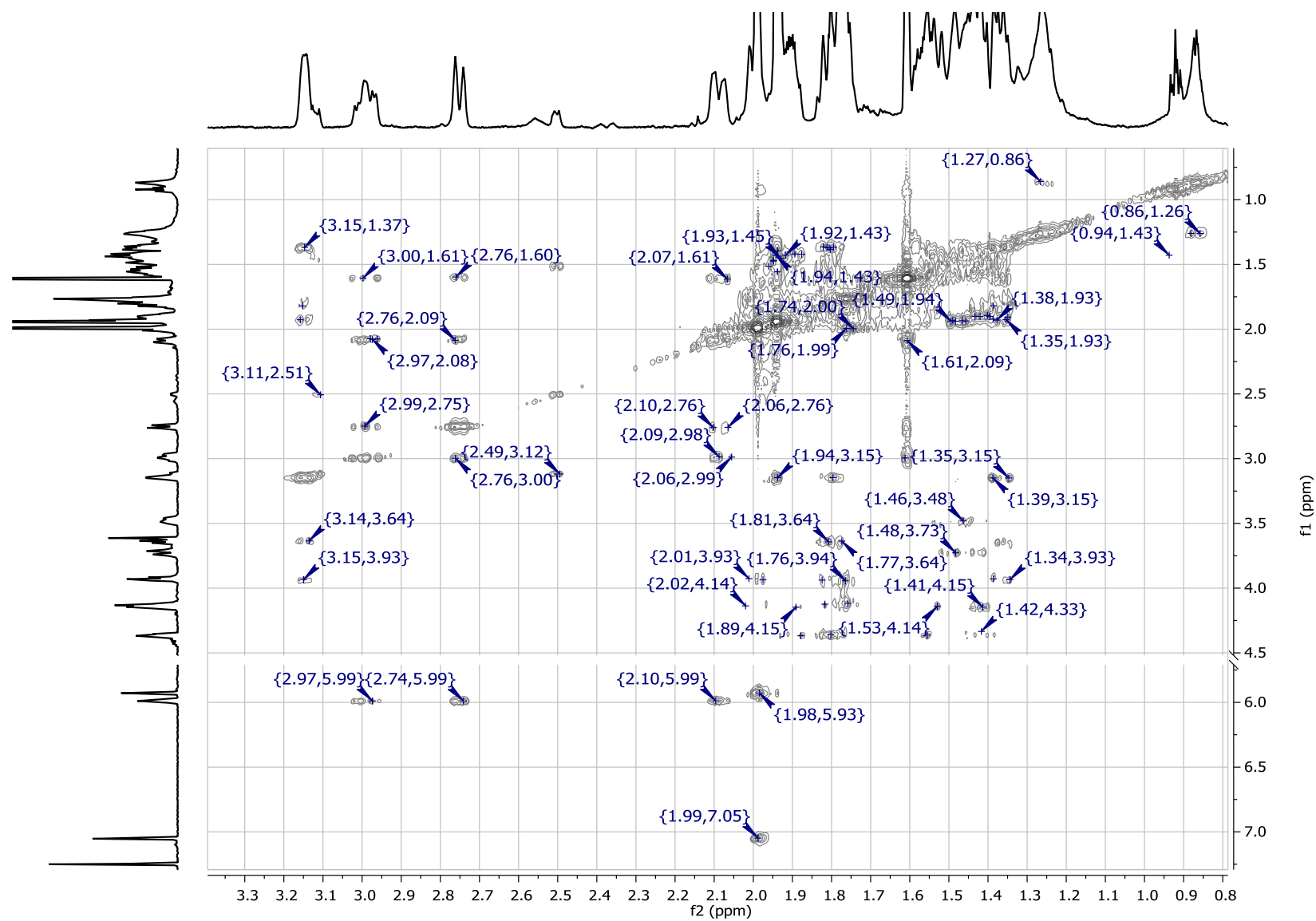


Figure 9.14: Slice 2 of 2D TOCSY spectra of 16-desmethyl GYM D (600 MHz, pyridine-d₅).

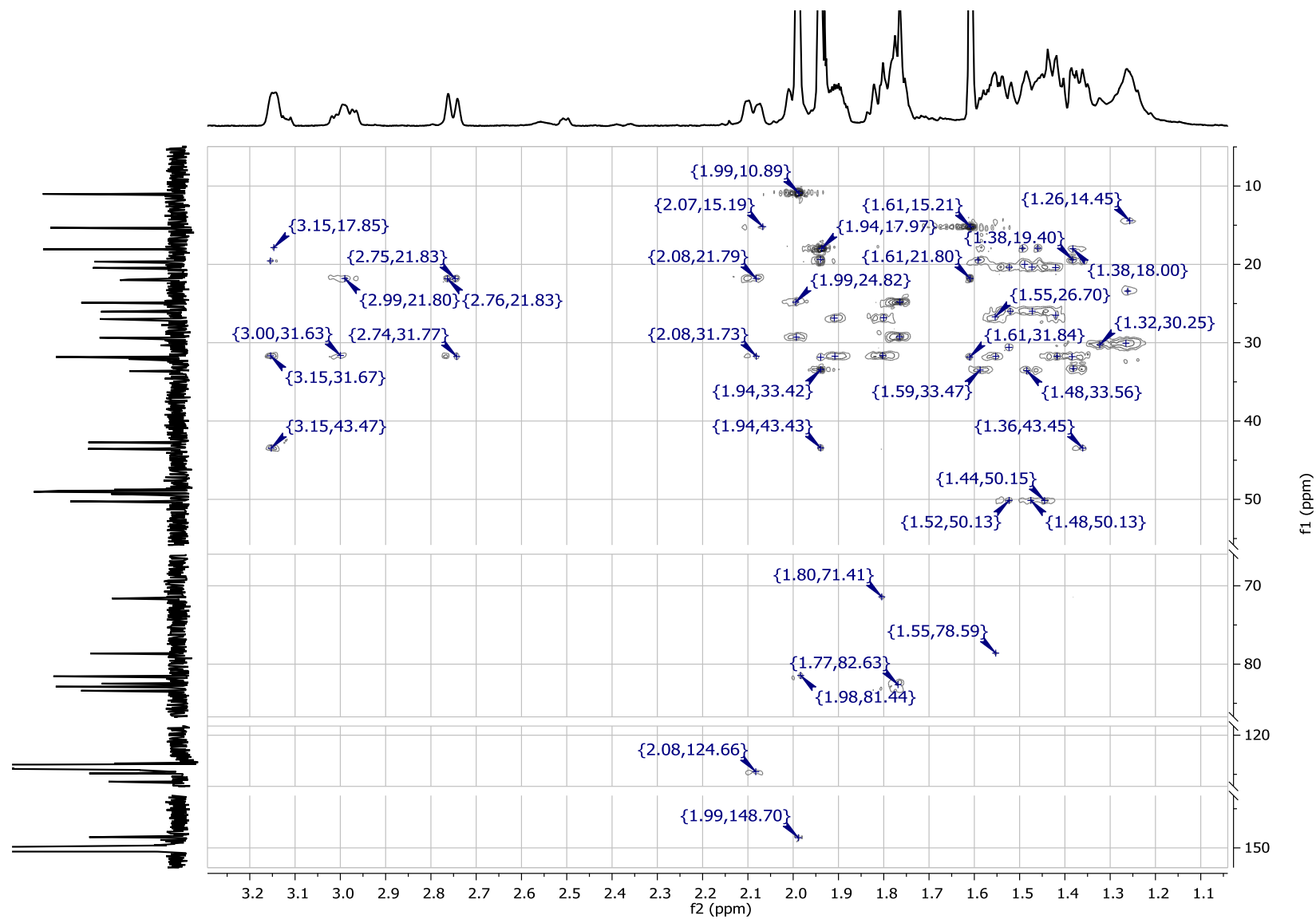


Figure 9.15: HSQC-TOCSY spectra of 16-desmethyl GYM D (600 MHz Proton frequency, pyridine-d₅).

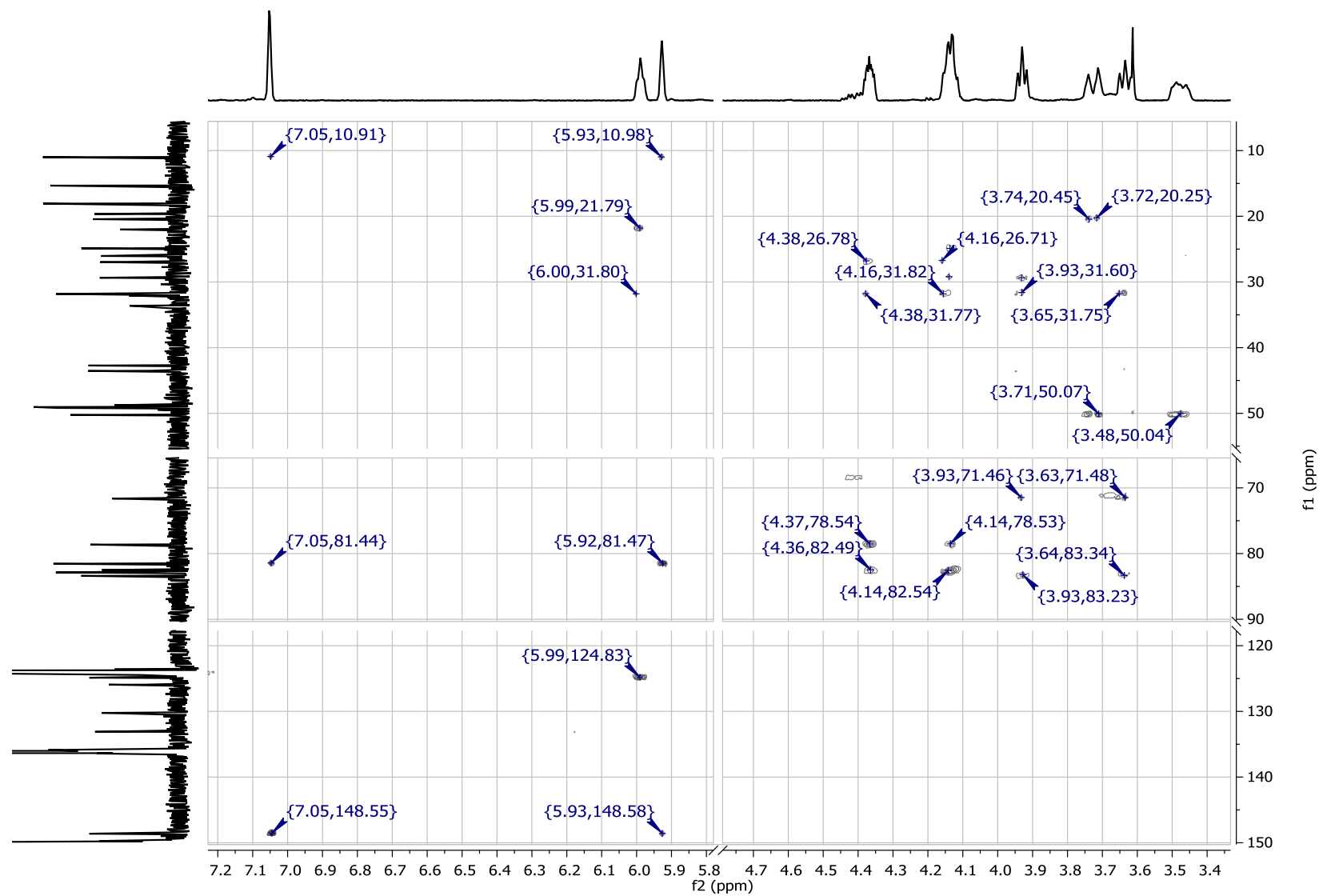


Figure 9.16: Slice 1 of HSQC-TOCSY spectra of 16-desmethyl GYM D (600 MHz Proton frequency, pyridine-d₅).

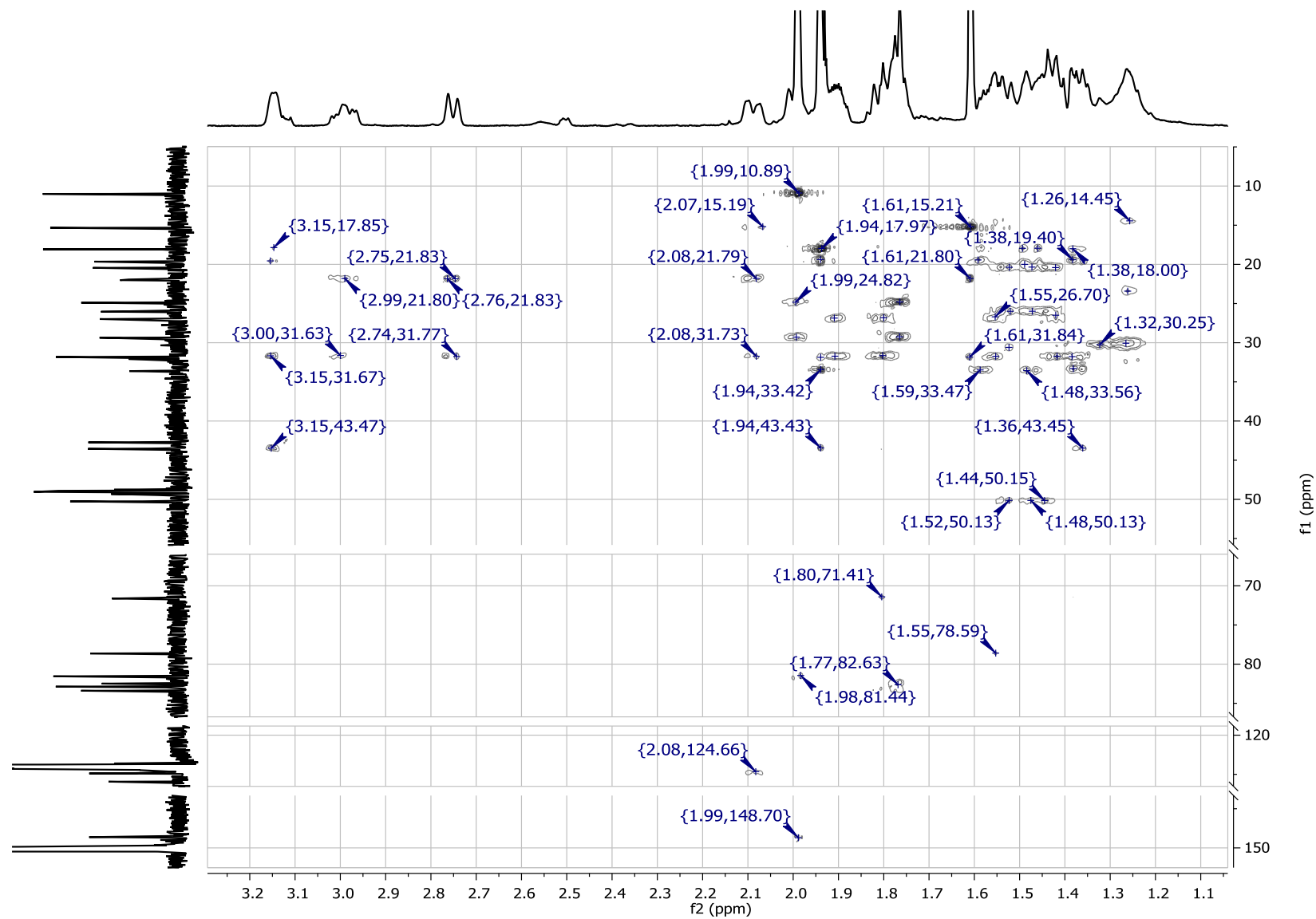


Figure 9.17: Slice 2 of HSQC-TOCSY spectra of 16-desmethyl GYM D (600 MHz Proton frequency, pyridine-d₅).

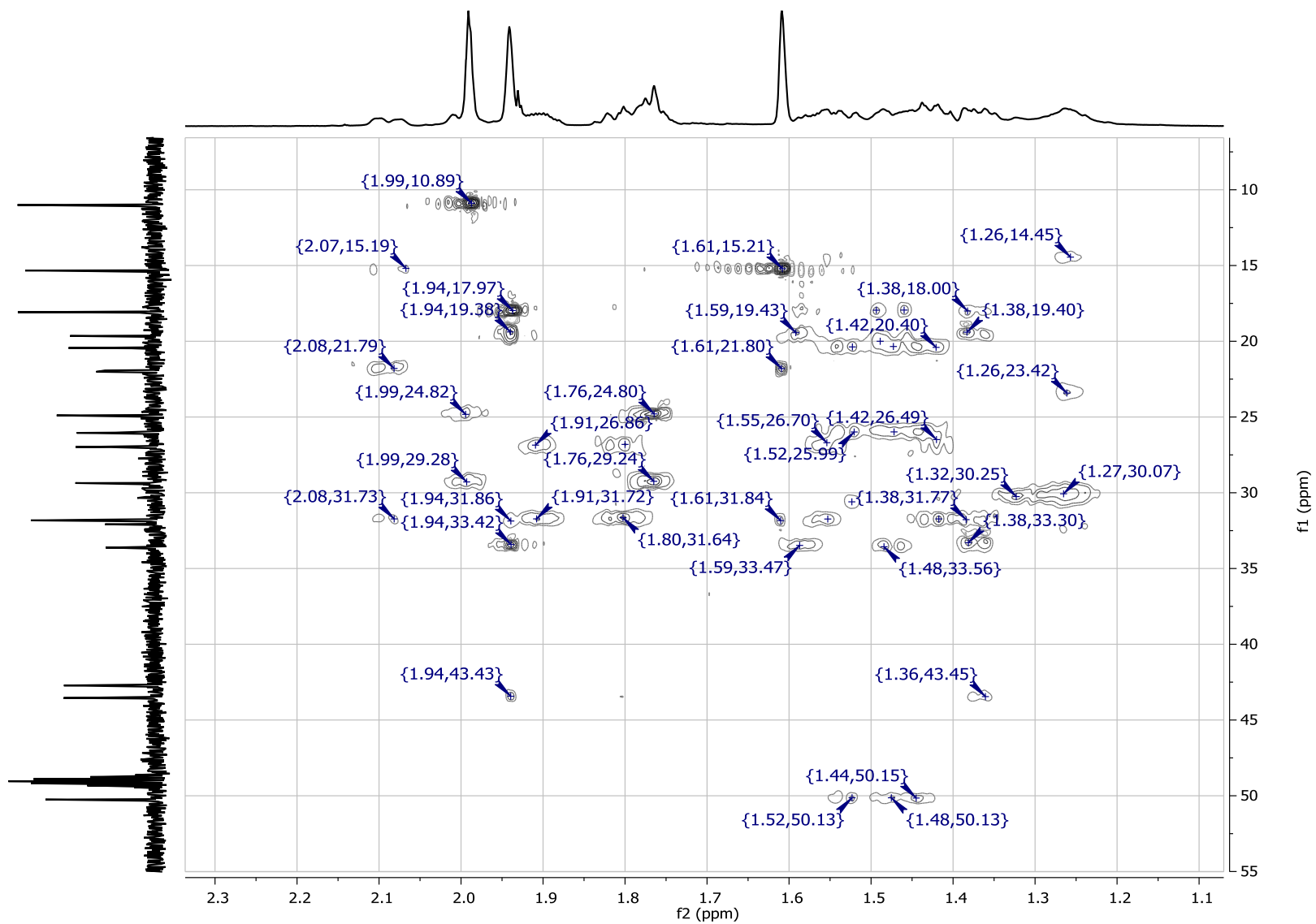


Figure 9.18: Slice 3 of HSQC-TOCSY spectra of 16-desmethyl GYM D (600 MHz Proton frequency, pyridine-d₅).

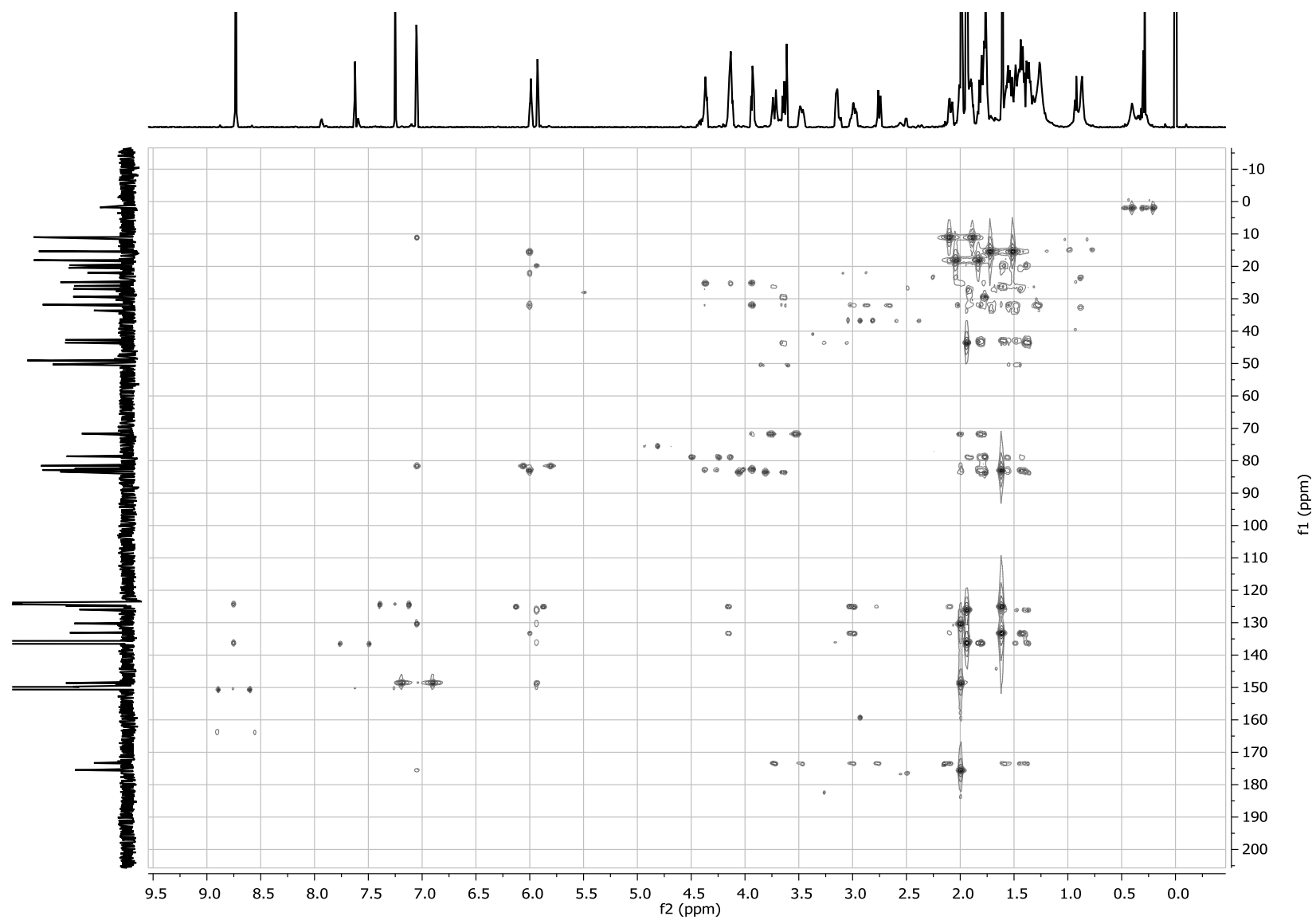
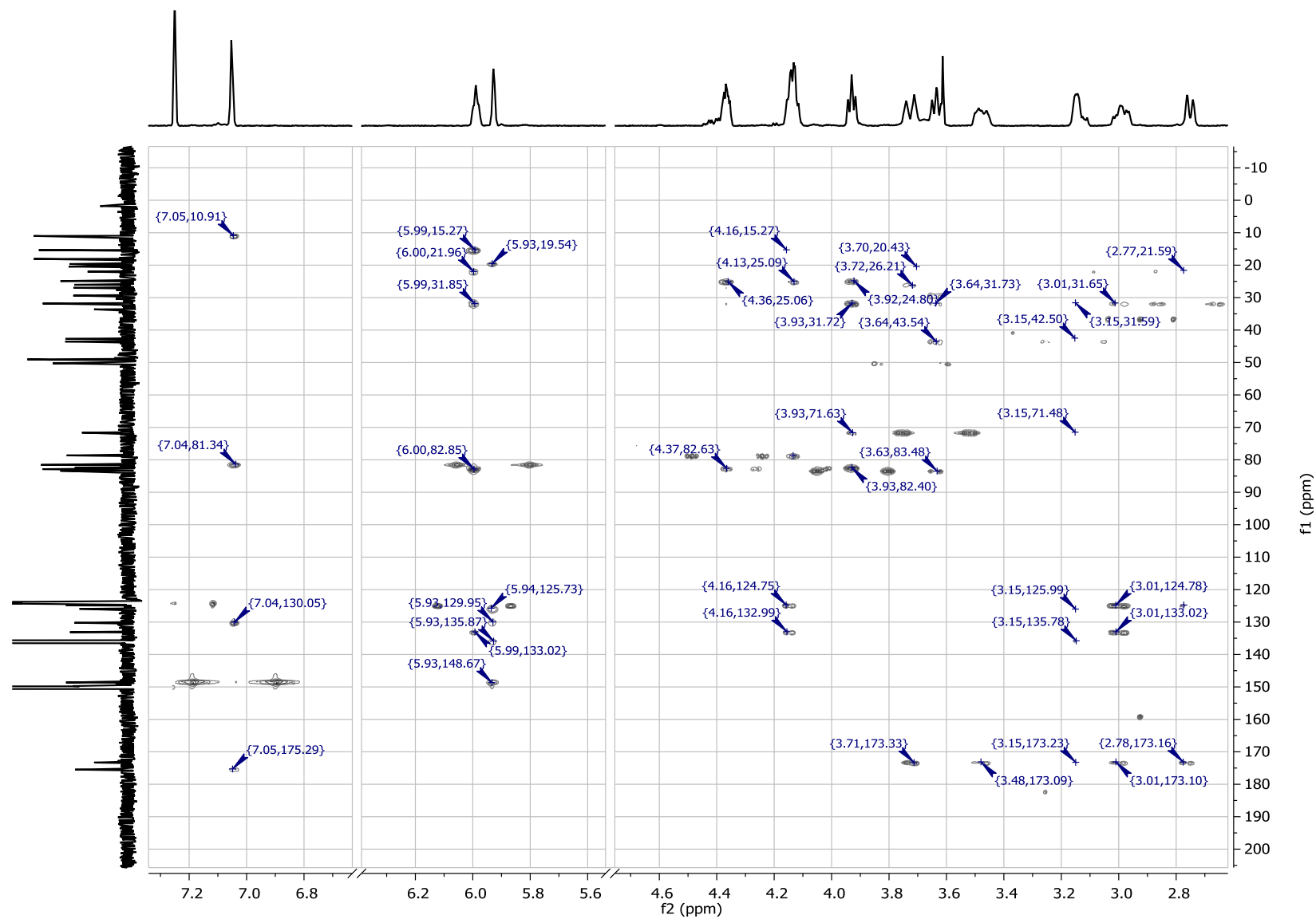


Figure 9.19: 2D IMPACT-HMBC spectra of 16-desmethyl GYM D (600 MHz Proton frequency, pyridine-d₅).

Figure 9.20: Slice 1 of 2D IMPACT-HMBC spectra of 16-desmethyl GYM D (600 MHz Proton frequency, pyridine-d₅).

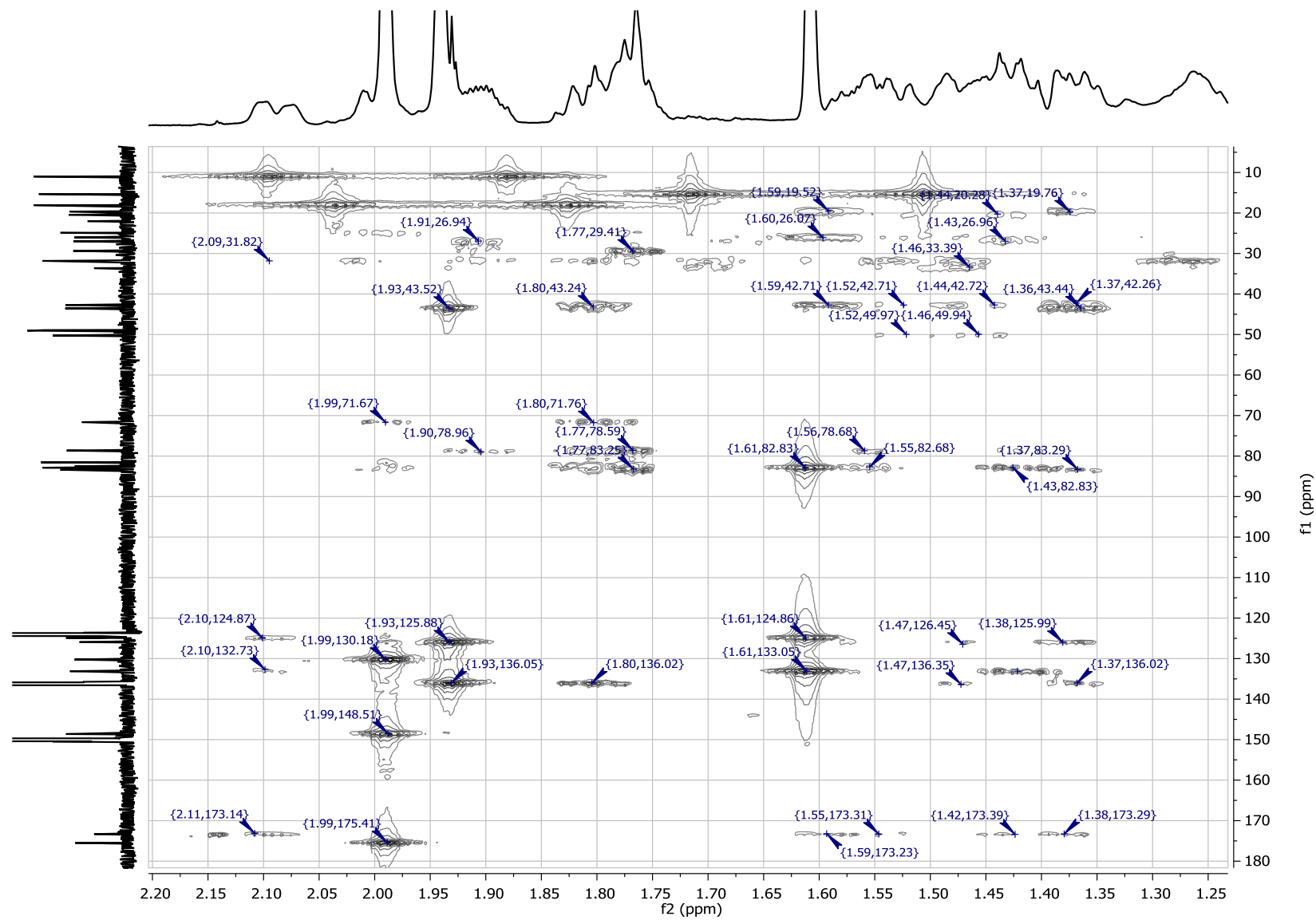


Figure 9.21: Slice 2 of 2D IMPACT-HMBC spectra of 16-desmethyl GYM D (600 MHz Proton frequency, pyridine-d₅).

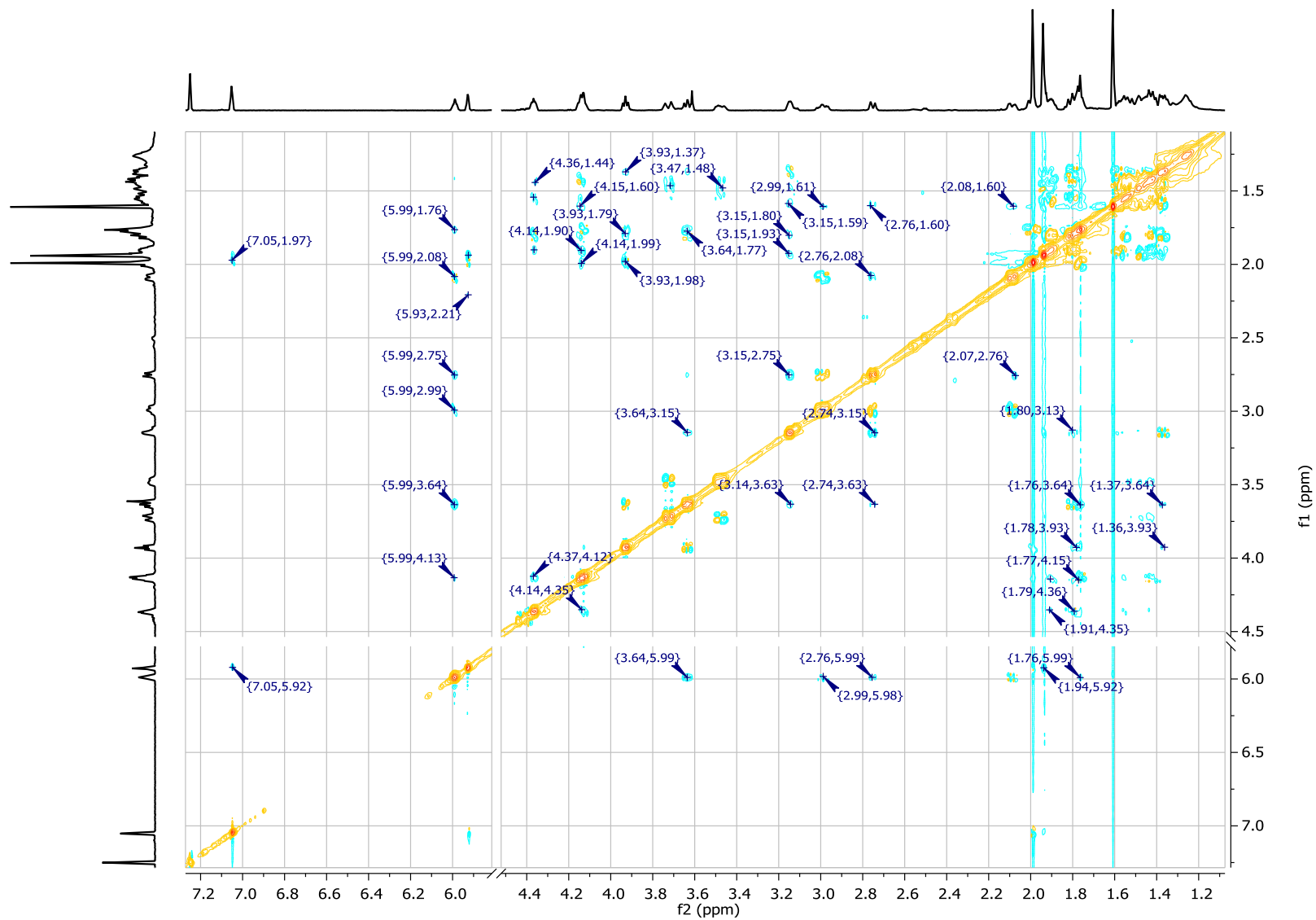


Figure 9.22: ROESY spectra of 16-desmethyl GYM D (600 MHz Proton frequency, pyridine-d₅).

9.1.2 CD-spectra

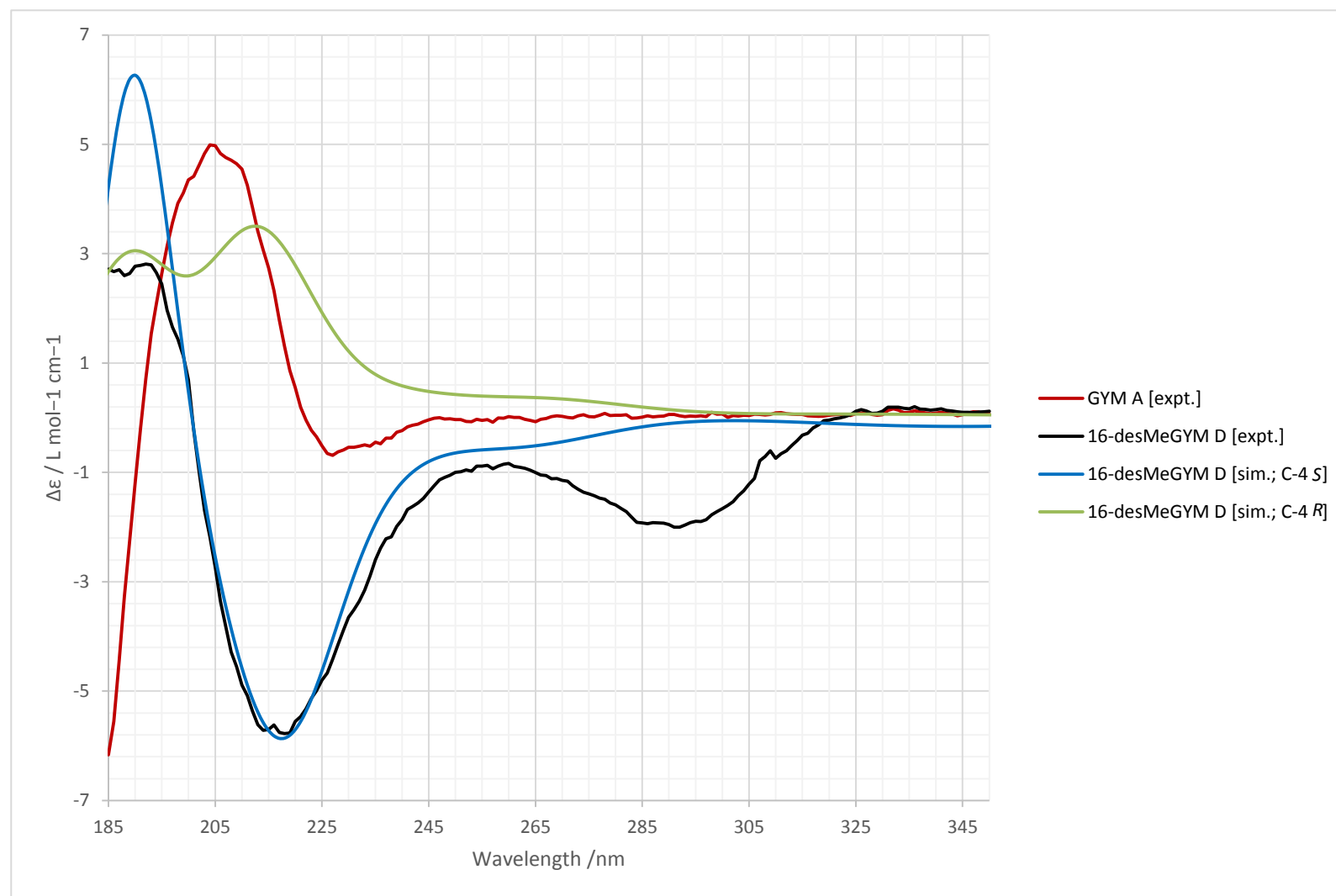
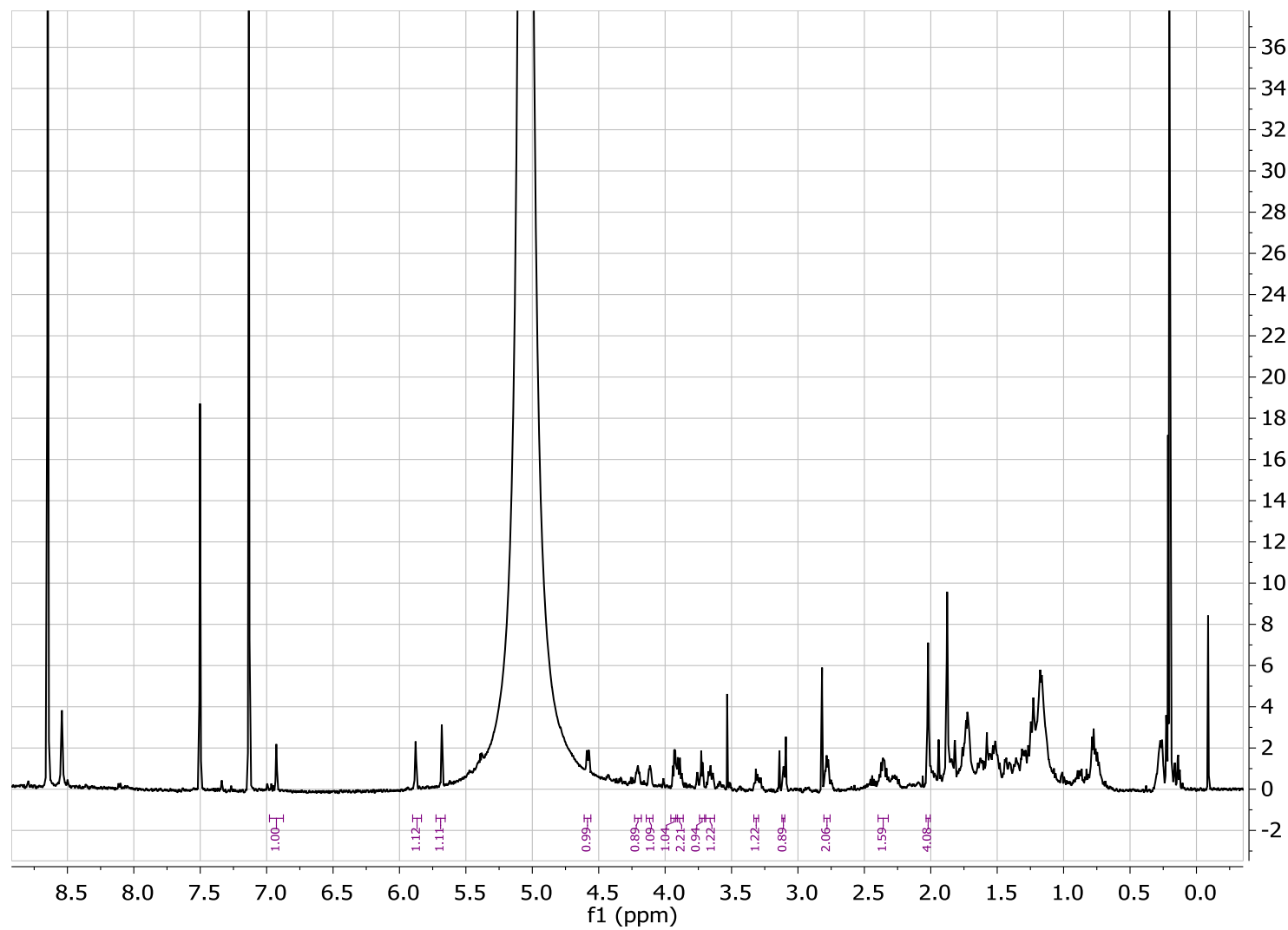


Figure 9.23: Measured CD-spectra [expt.] of 16-desmethyl GYM D (1) and GYM A (4) with simulated spectra of 1 with both configuration at C-4.

9.1.3 NMR-spectra of GYM E

Figure 9.24: 1D Proton spectra of GYM E (600 MHz, pyridine-d₅).

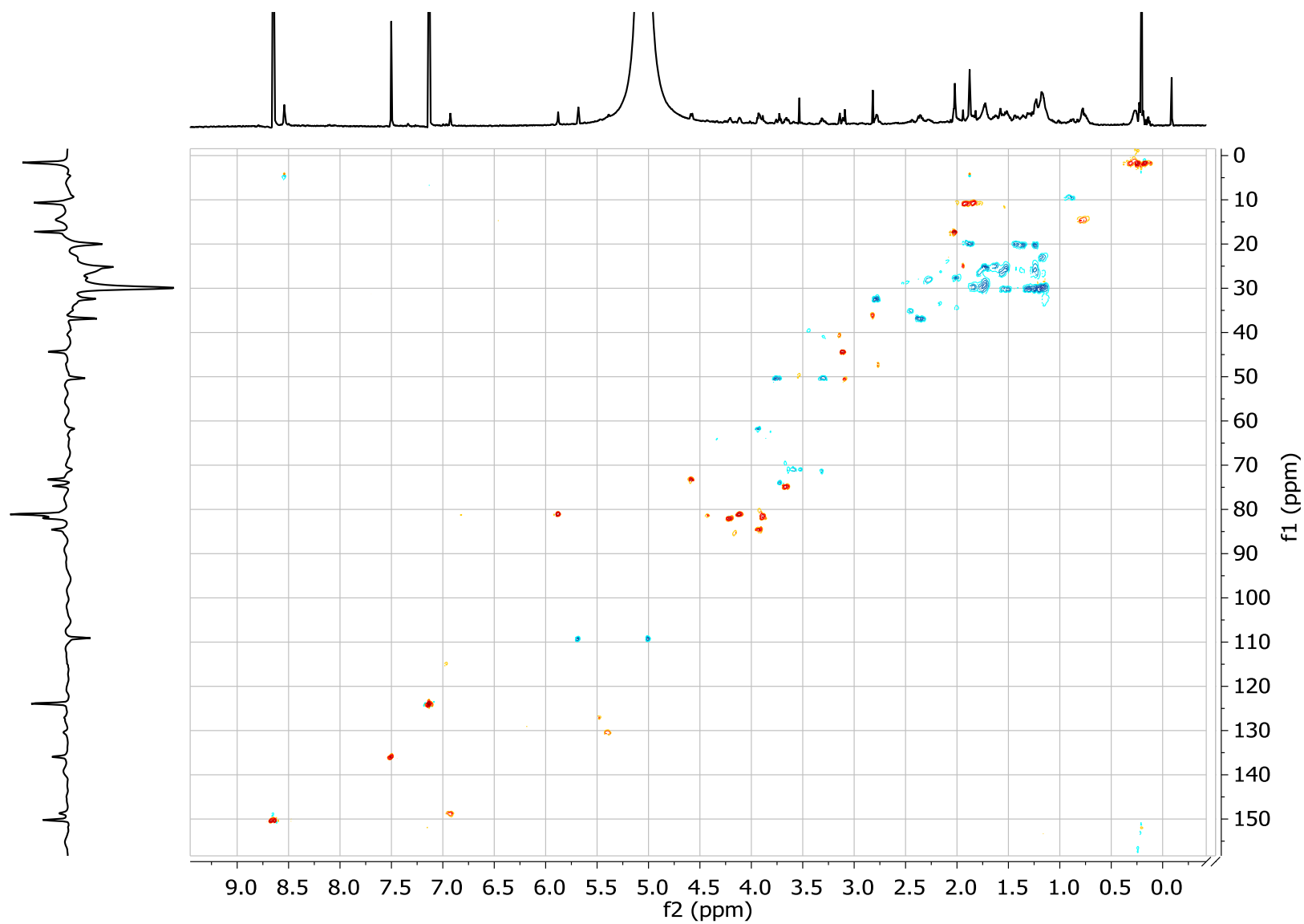


Figure 9.25: Multiplicity-edited 2D HSQC spectra of GYM E (600 MHz Proton frequency, pyridine-d₅).

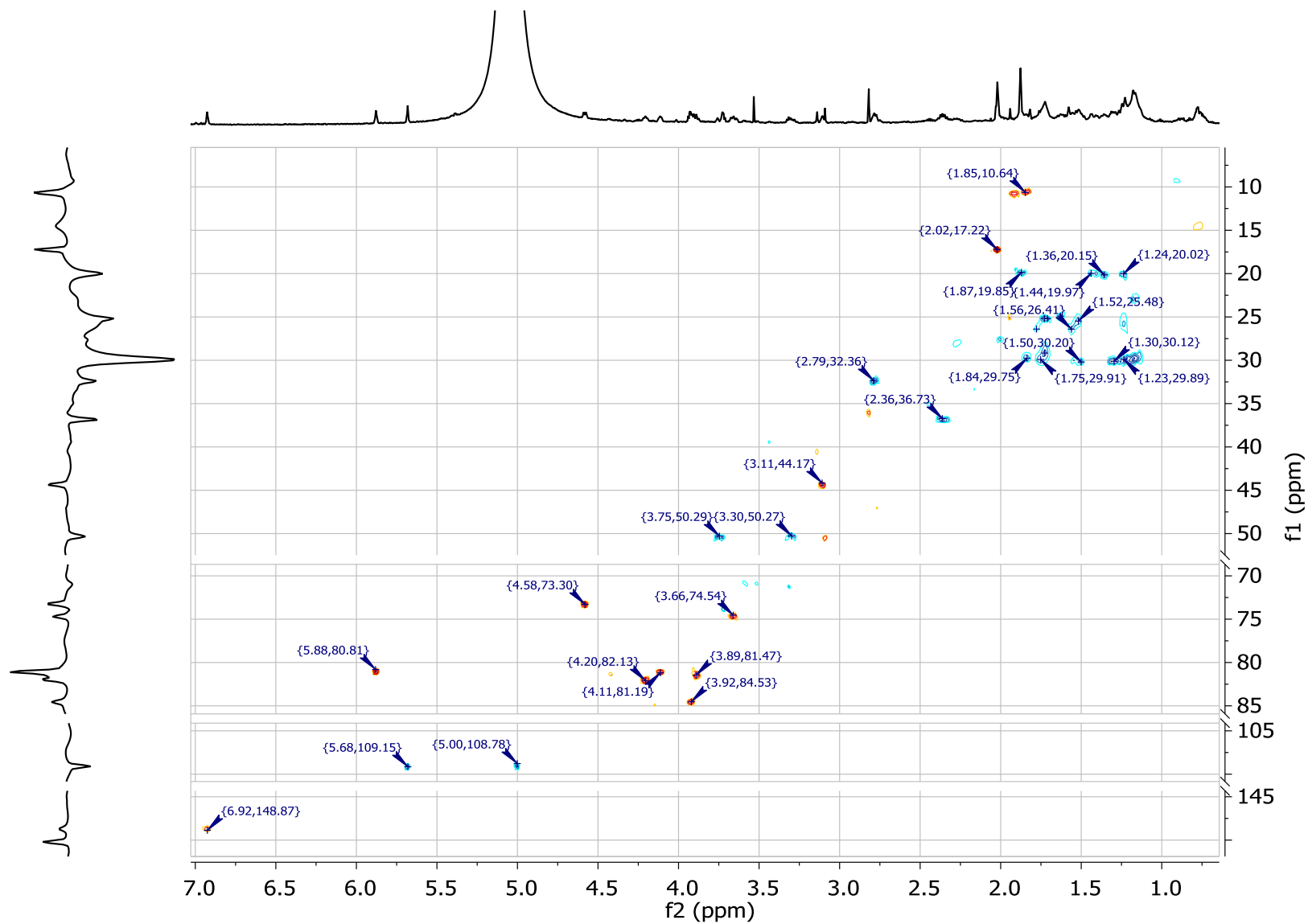


Figure 9.26. Slice 1 of Multiplicity-edited 2D HSQC spectra of GYM E (600 MHz Proton frequency, pyridine- d_5).

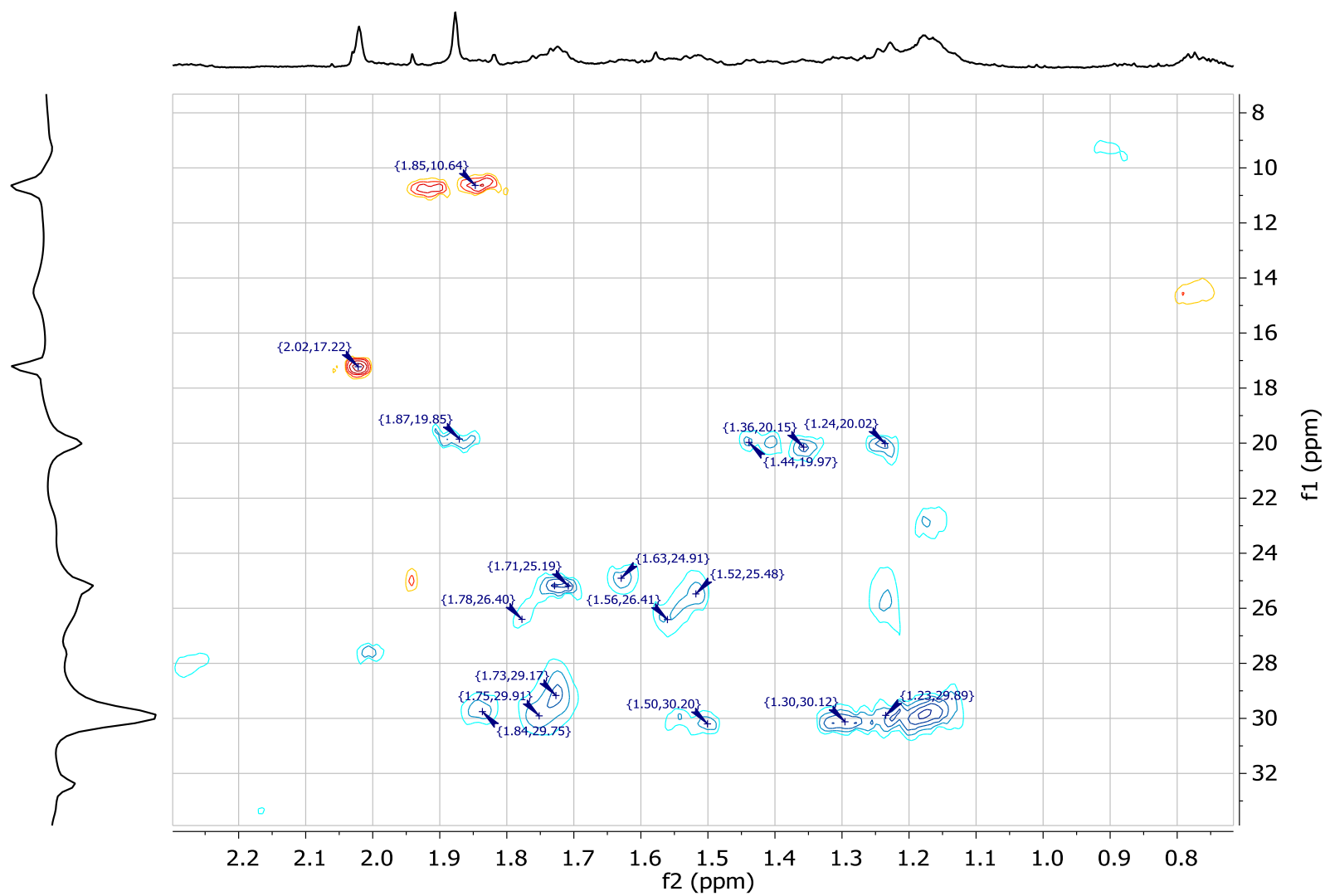


Figure 9.27: Slice 2 of Multiplicity-edited 2D HSQC spectra of GYM E (600 MHz Proton frequency, pyridine-d₅).

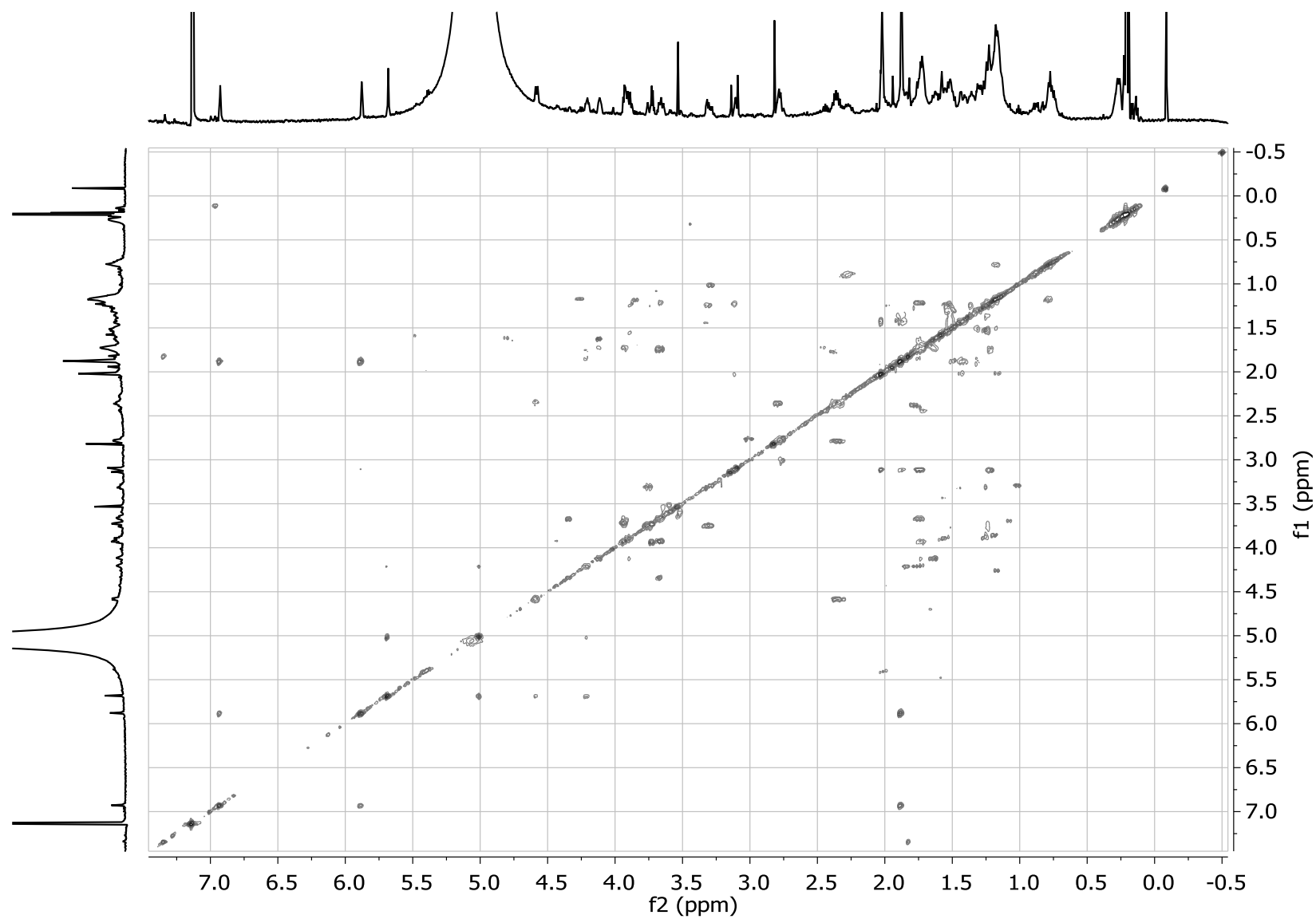


Figure 9.28: 2D COSY spectra of GYM E (600 MHz, pyridine-d₅).

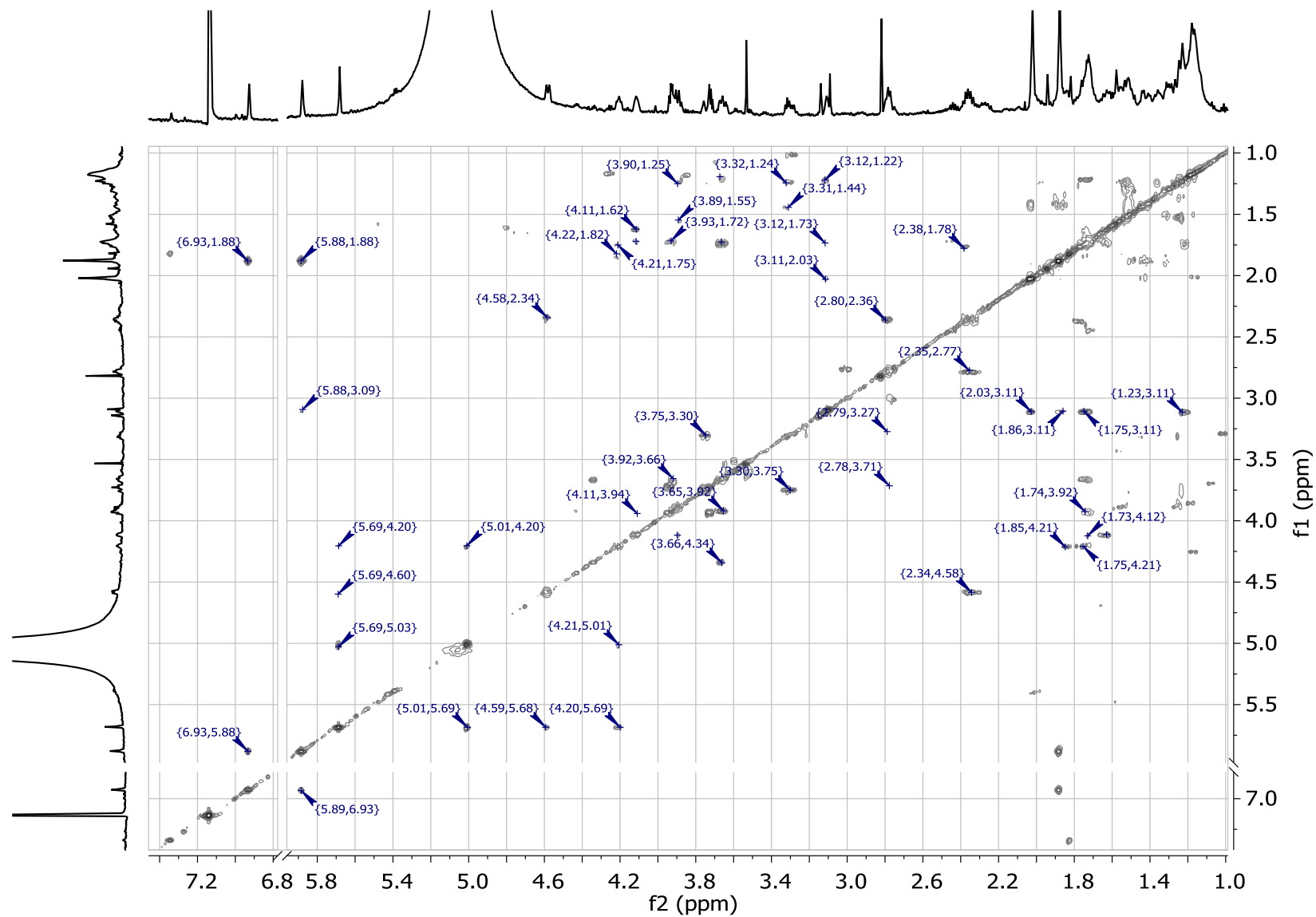


Figure 9.29: Slice of COSY spectra of GYM E (600 MHz Proton frequency, pyridine-d₅).

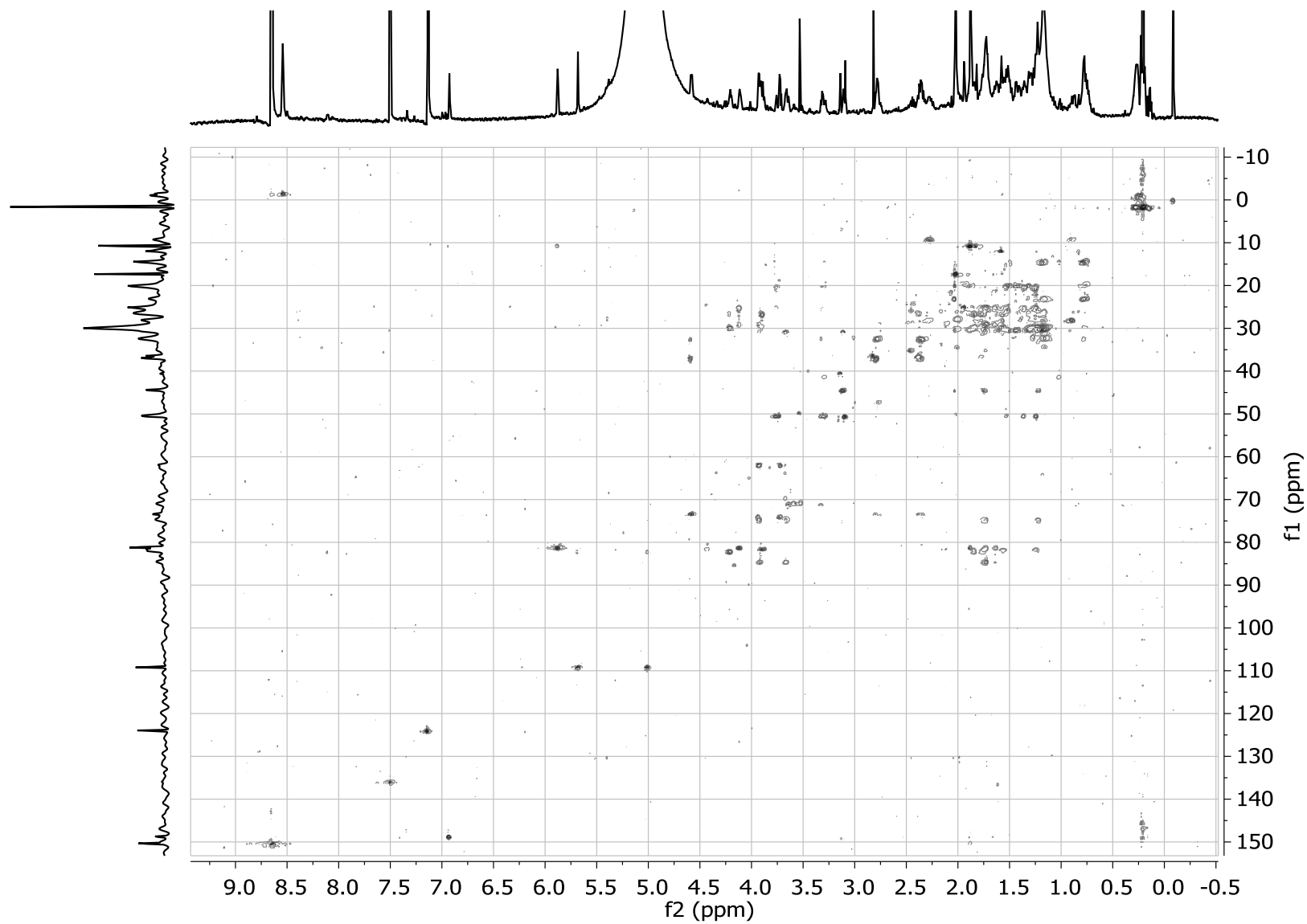


Figure 9.30: 2D HSQC-TOCSY spectra of GYM E (600 MHz Proton frequency, pyridine-d₅).

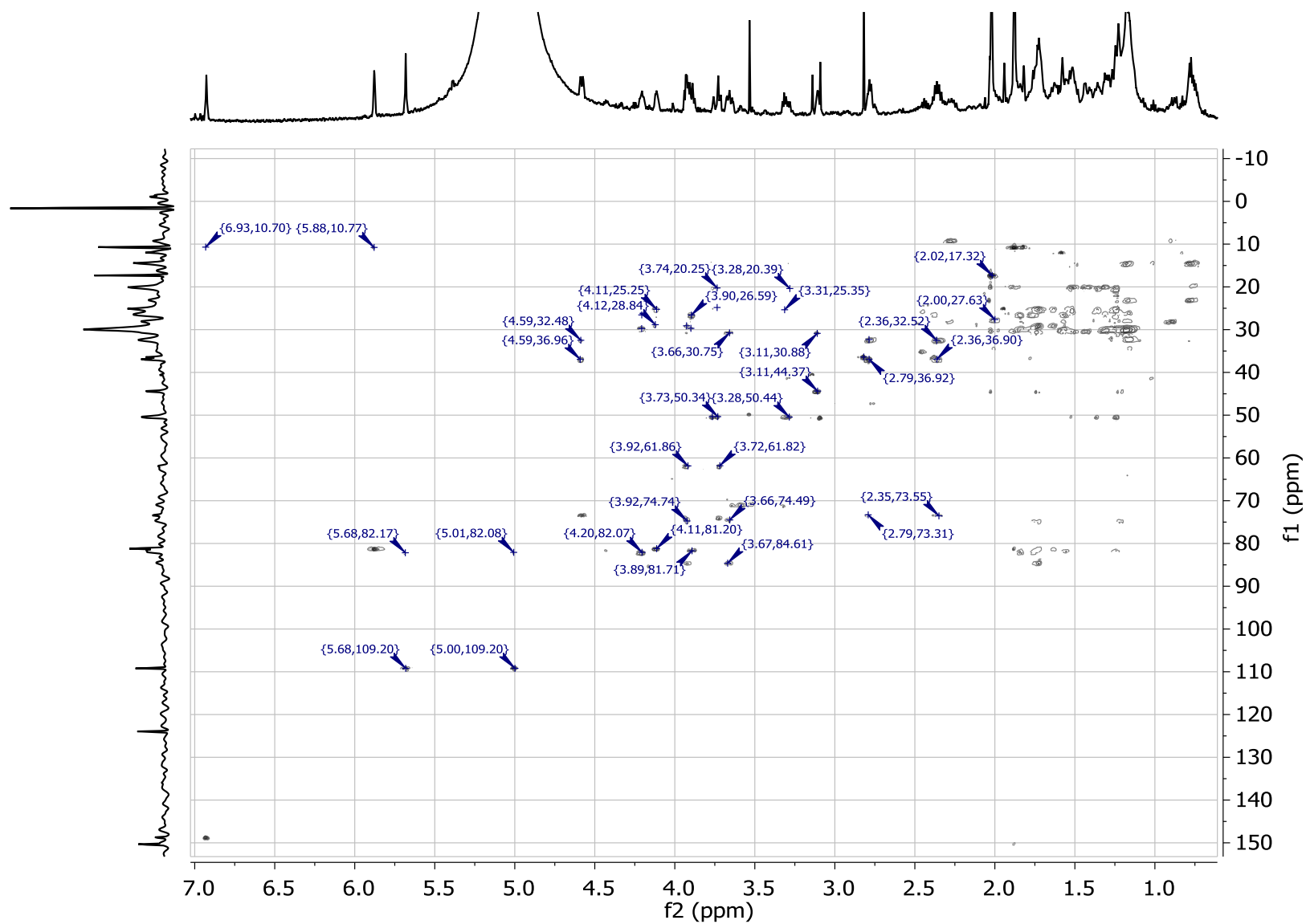
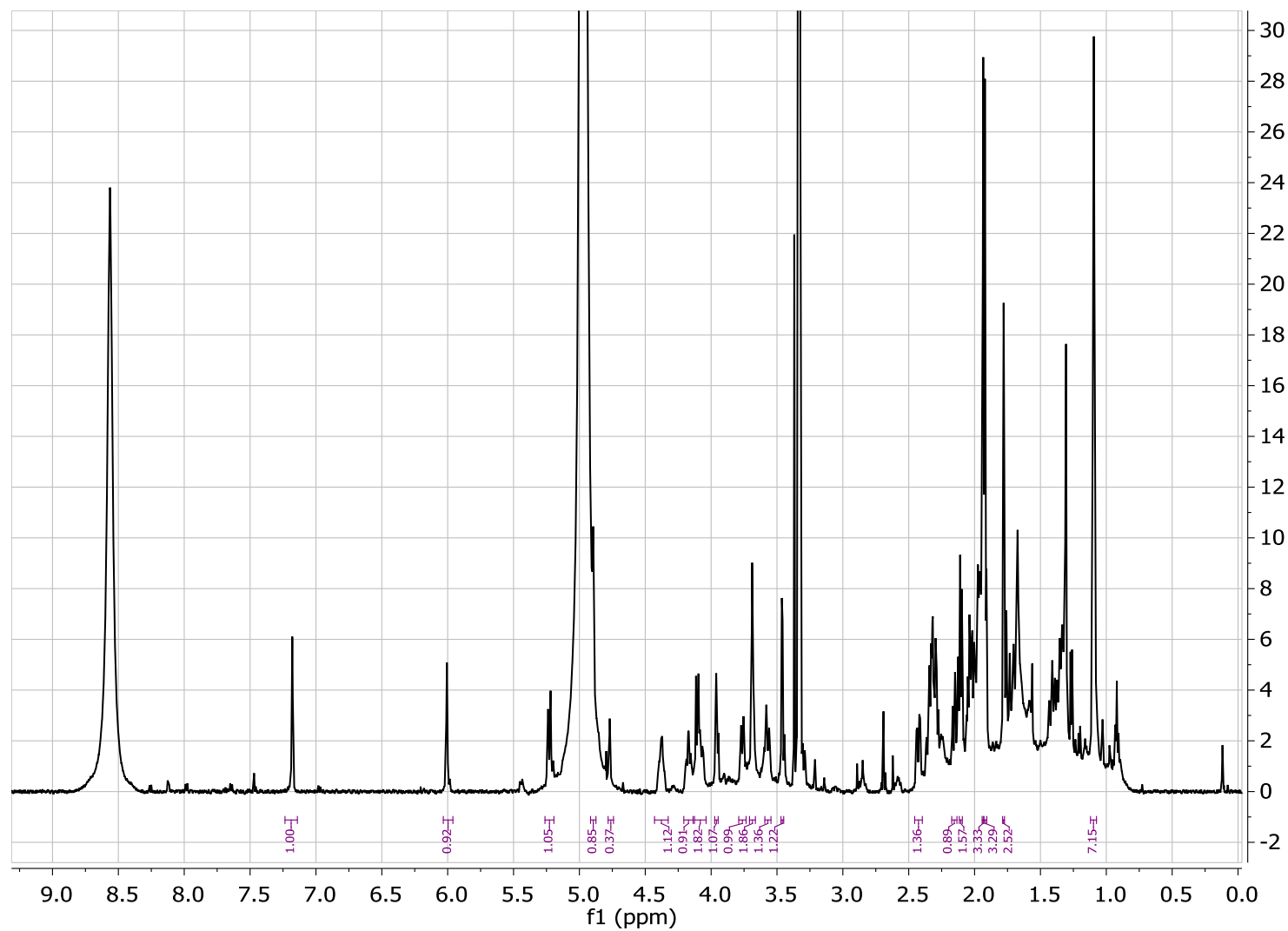


Figure 9.31: Slice of 2D HSQC-TOCSY spectra of GYM E (600 MHz Proton frequency, pyridine-d₅).

9.1.4 NMR-spectra of 20-hydroxy-13,19-didesMethyl SPX C

Figure 9.32: 1D Proton spectra of 20-hydroxy-13,19-didesmethyl SPX C (600 MHz, CD₃OD).

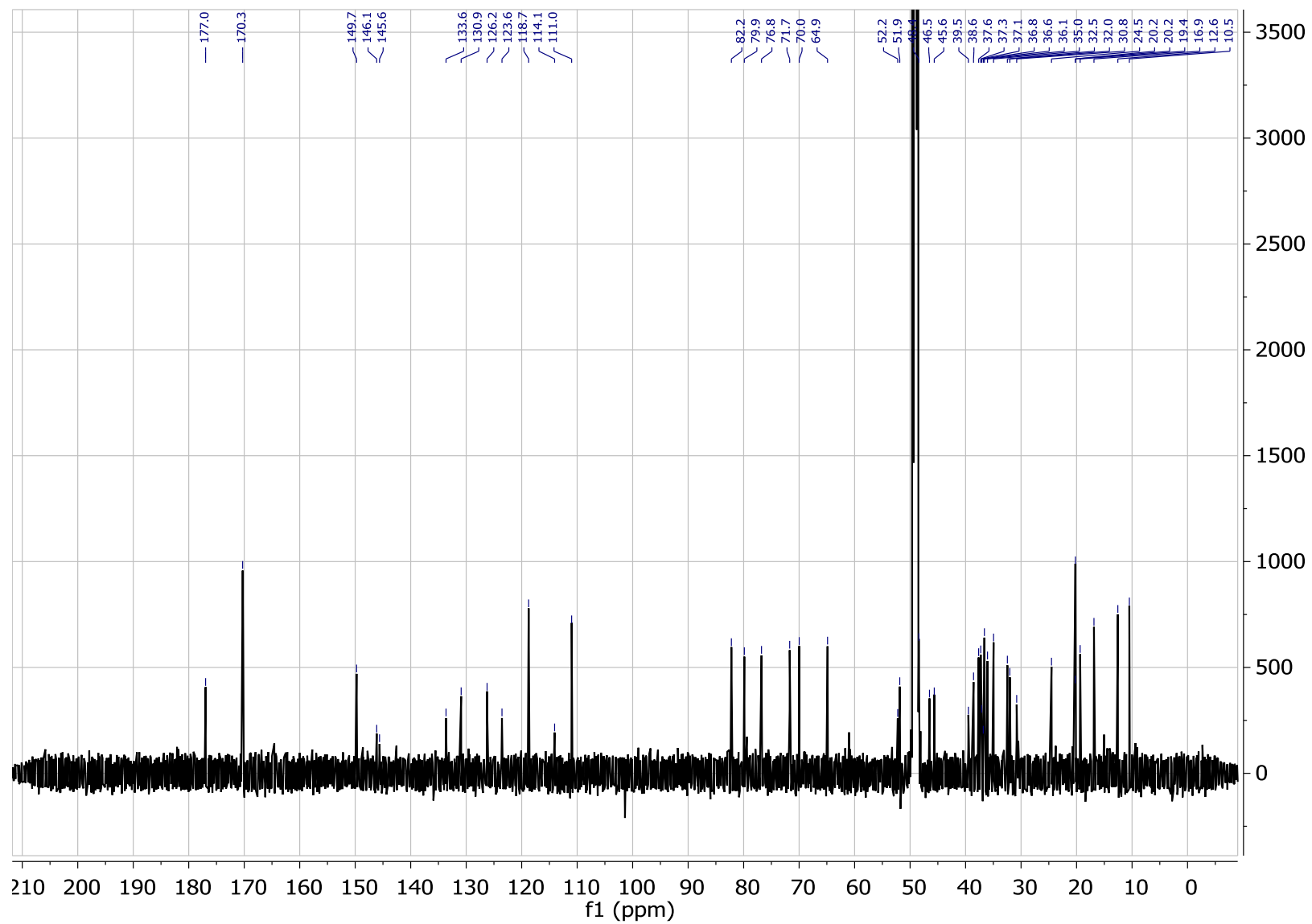


Figure 9.33: 1D ^{13}C -spectra of 20-hydroxy-13,19-didesmethyl SPX C (150 MHz, CD_3OD).

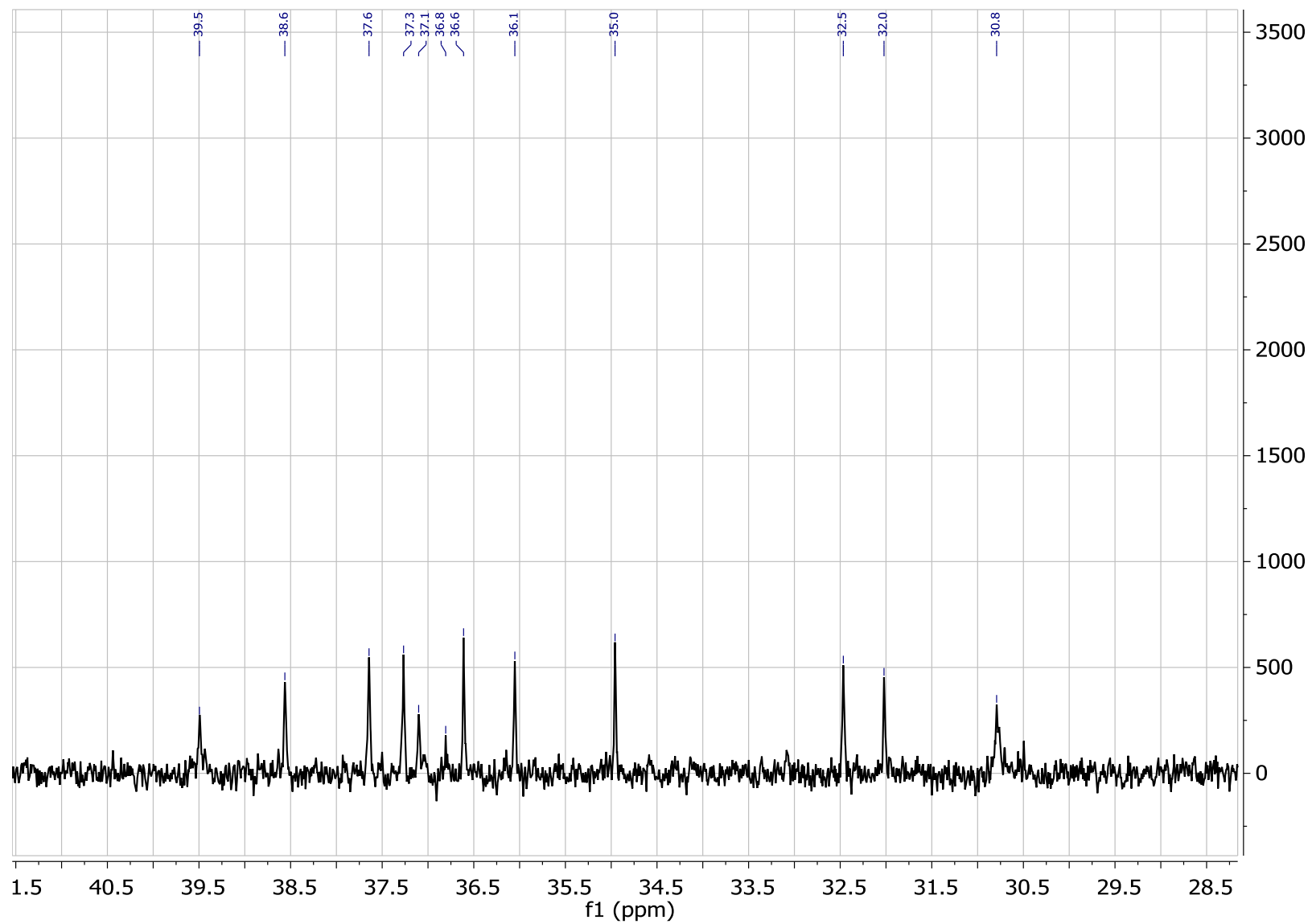


Figure 9.34: Slice of 1D ¹³C-spectra of 20-hydroxy-13,19-didesmethyl SPX C (150 MHz, CD₃OD).

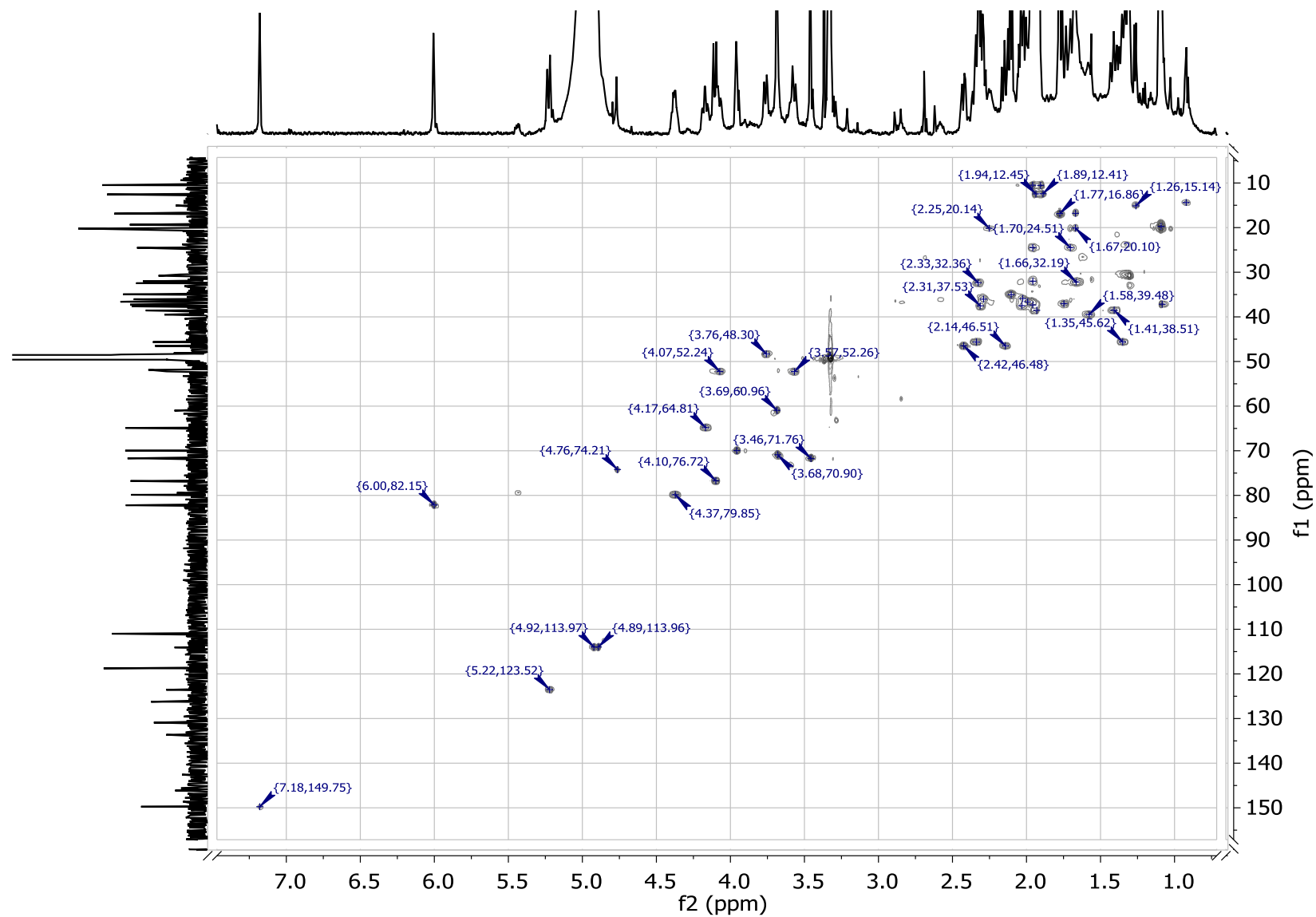


Figure 9.35: 2D HSQC spectra of 20-hydroxy-13,19-didesmethyl SPX C (600 MHz Proton frequency, CD_3OD).

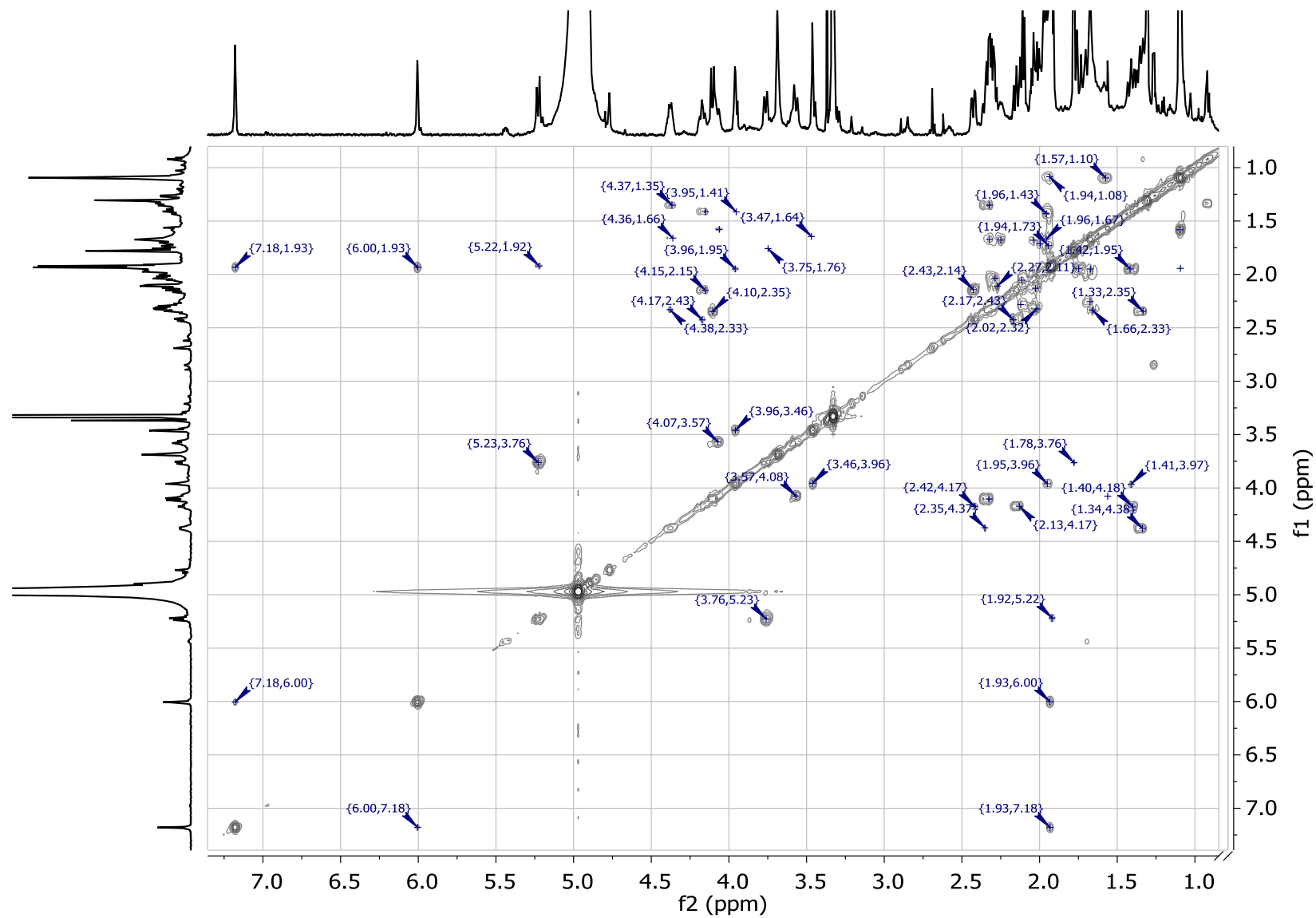


Figure 9.36: COSY spectra of 20-hydroxy-13,19-didesmethyl SPX C (600 MHz Proton frequency, CD₃OD).

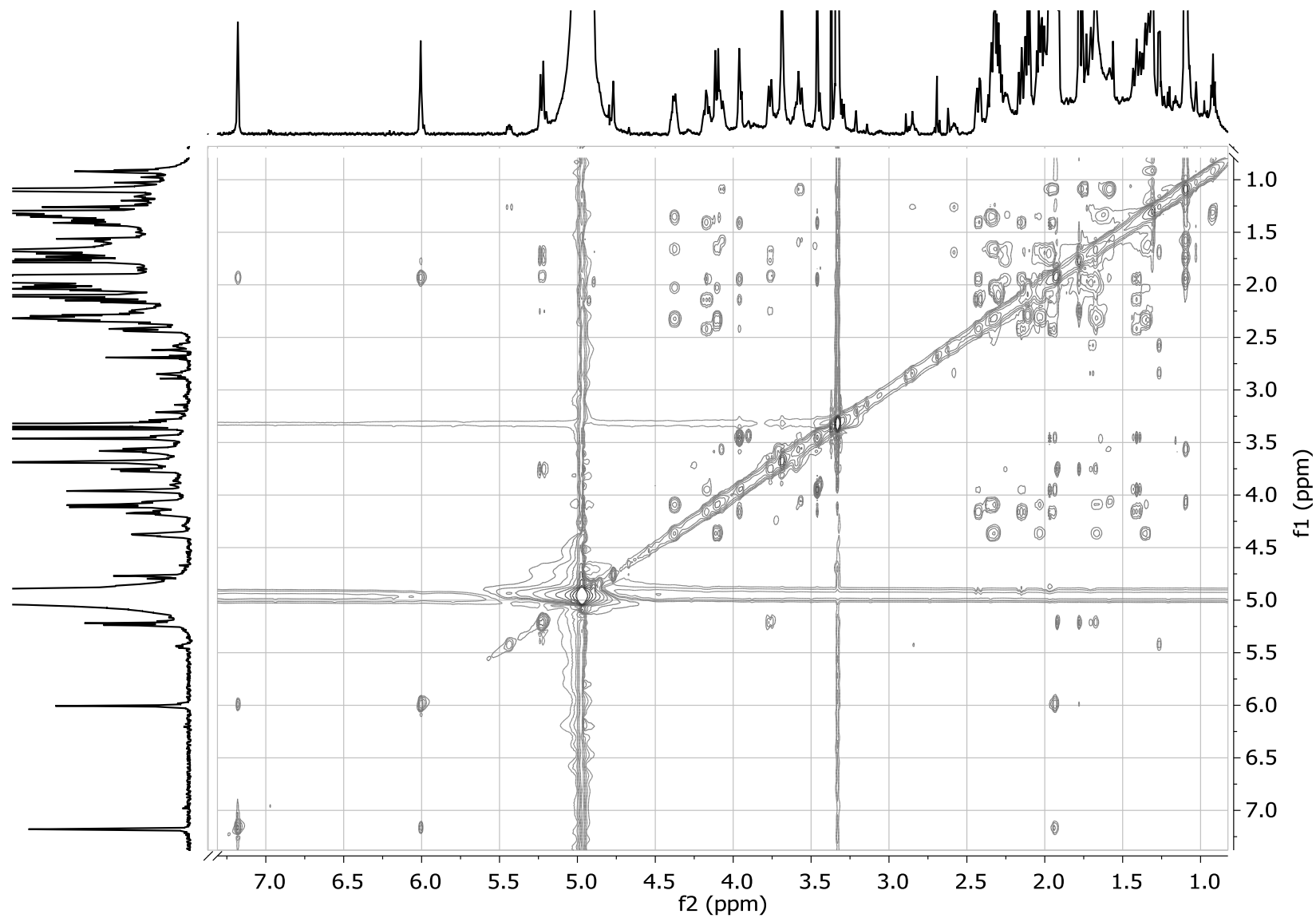


Figure 9.37: 2D TOCSY spectra of 20-hydroxy-13,19-didesmethyl SPX C (600 MHz, CD₃OD).

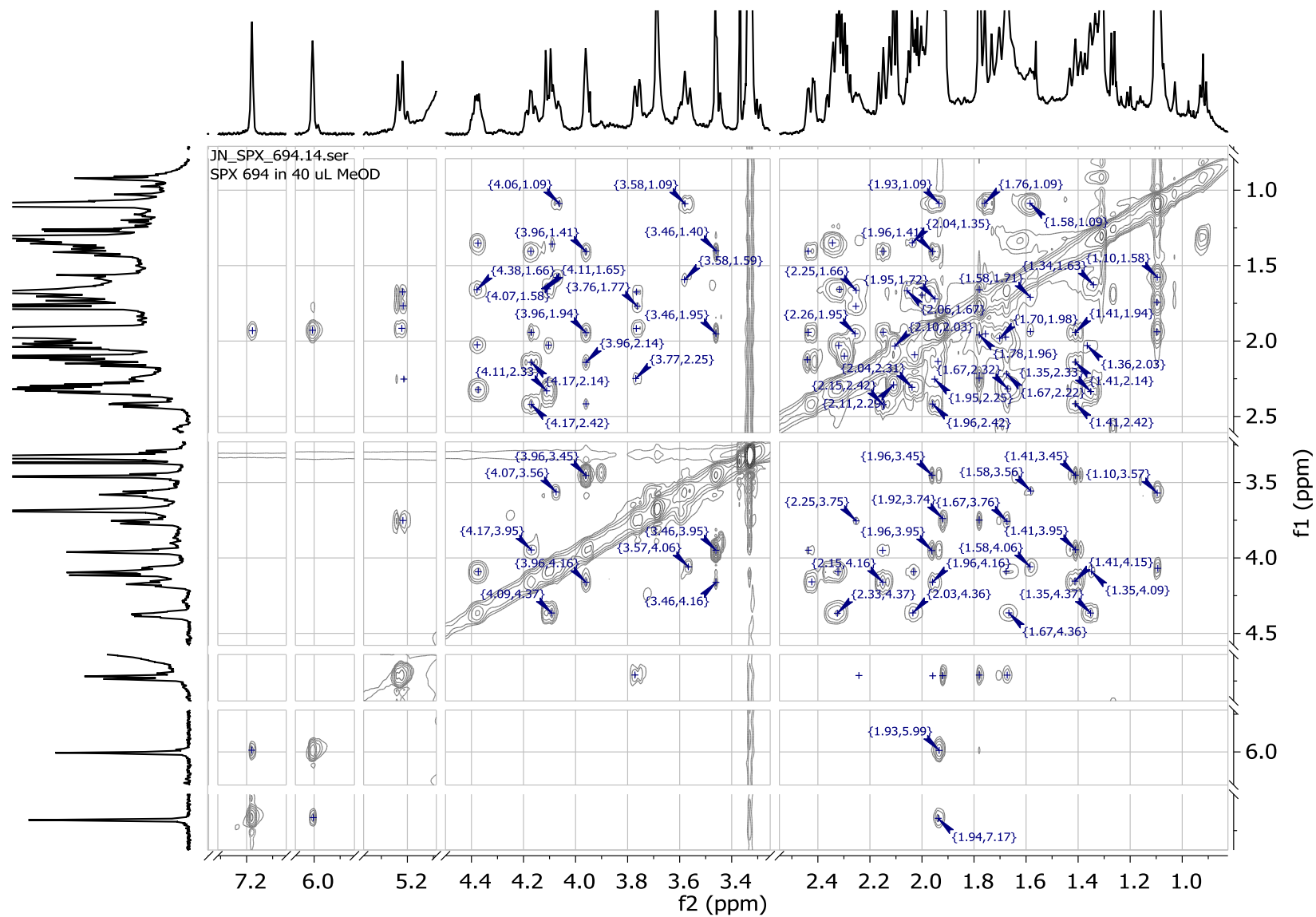


Figure 9.38: Slice of 2D TOCSY spectra of 20-hydroxy-13,19-didesmethyl SPX C (600 MHz, CD₃OD).

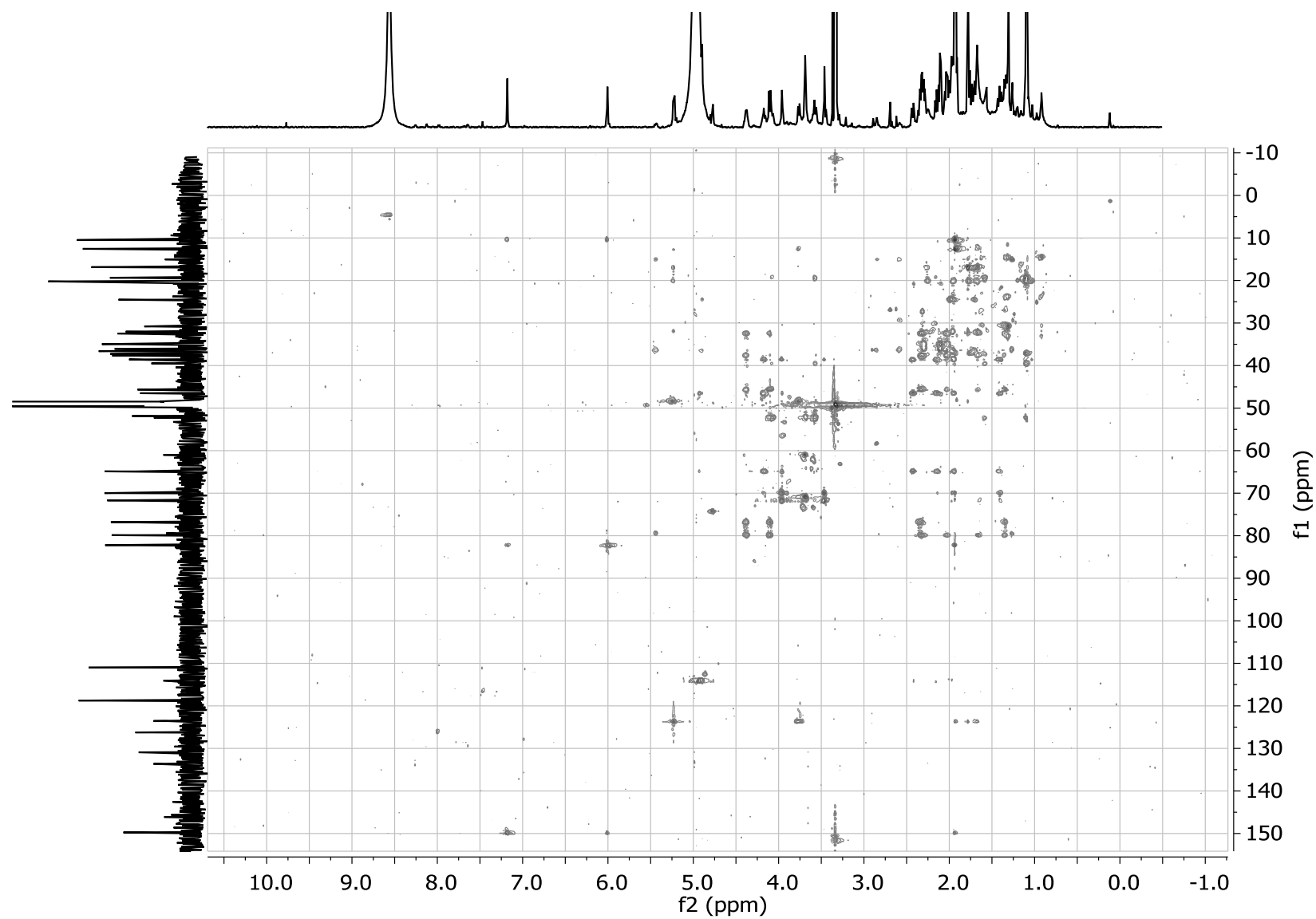


Figure 9.39: HSQC-TOCSY spectra of 20-hydroxy-13,19-didesmethyl SPX C (600 MHz Proton frequency, CD₃OD).

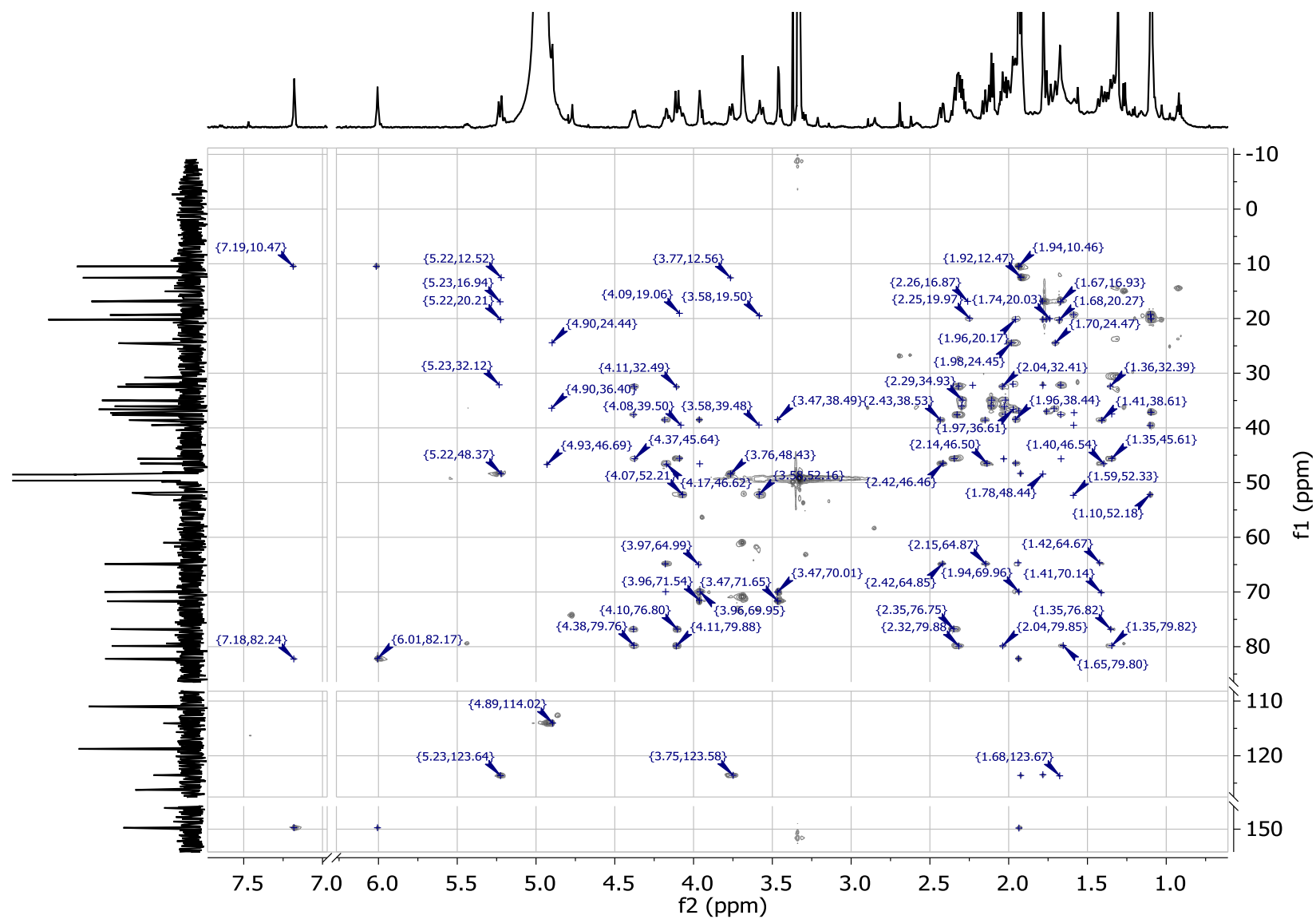


Figure 9.40: Slice of HSQC-TOCOSY spectra of 20-hydroxy-13,19-didesmethyl SPX C (600 MHz Proton frequency, CD₃OD).

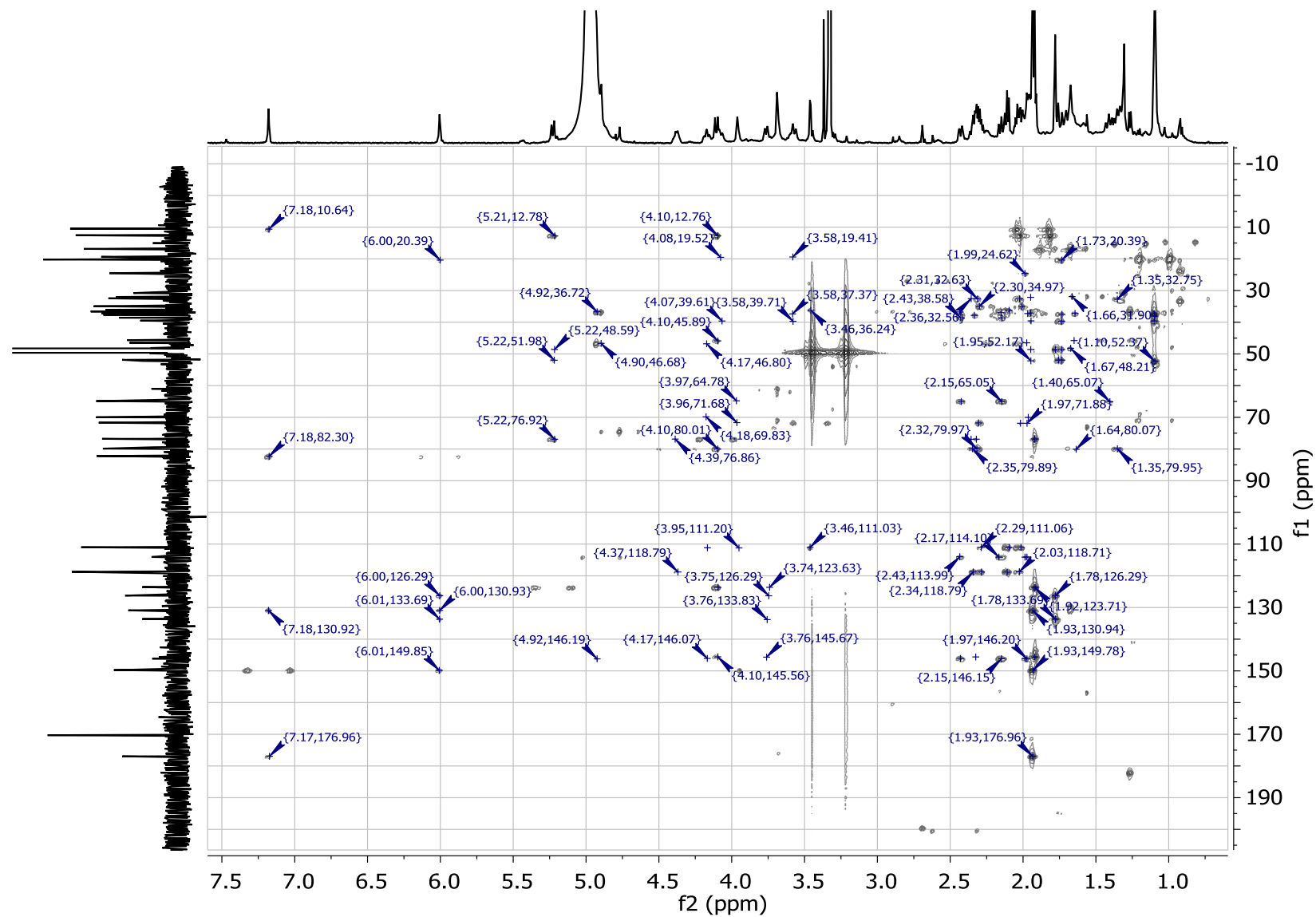
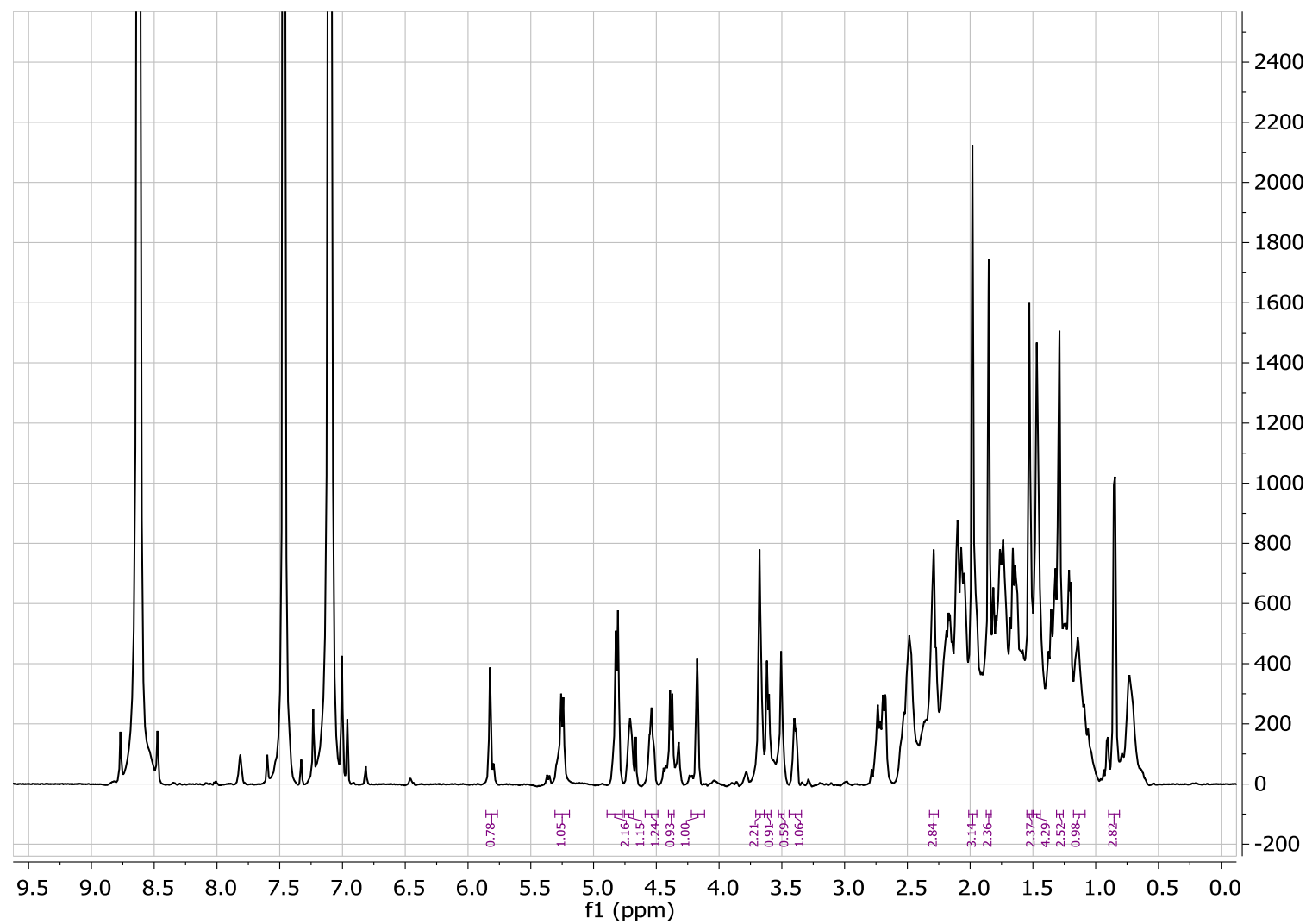


Figure 9.41: HMBC spectra of 20-hydroxy-13,19-didesmethyl SPX C (600 MHz Proton frequency, CD₃OD).

9.1.5 NMR-spectra of 20-hydroxy-13,19-didesmethyl SPX C in pyridine

Figure 9.42: 1D Proton spectra of 20-hydroxy-13,19-didesmethyl SPX C (600 MHz, pyridine-d₅).

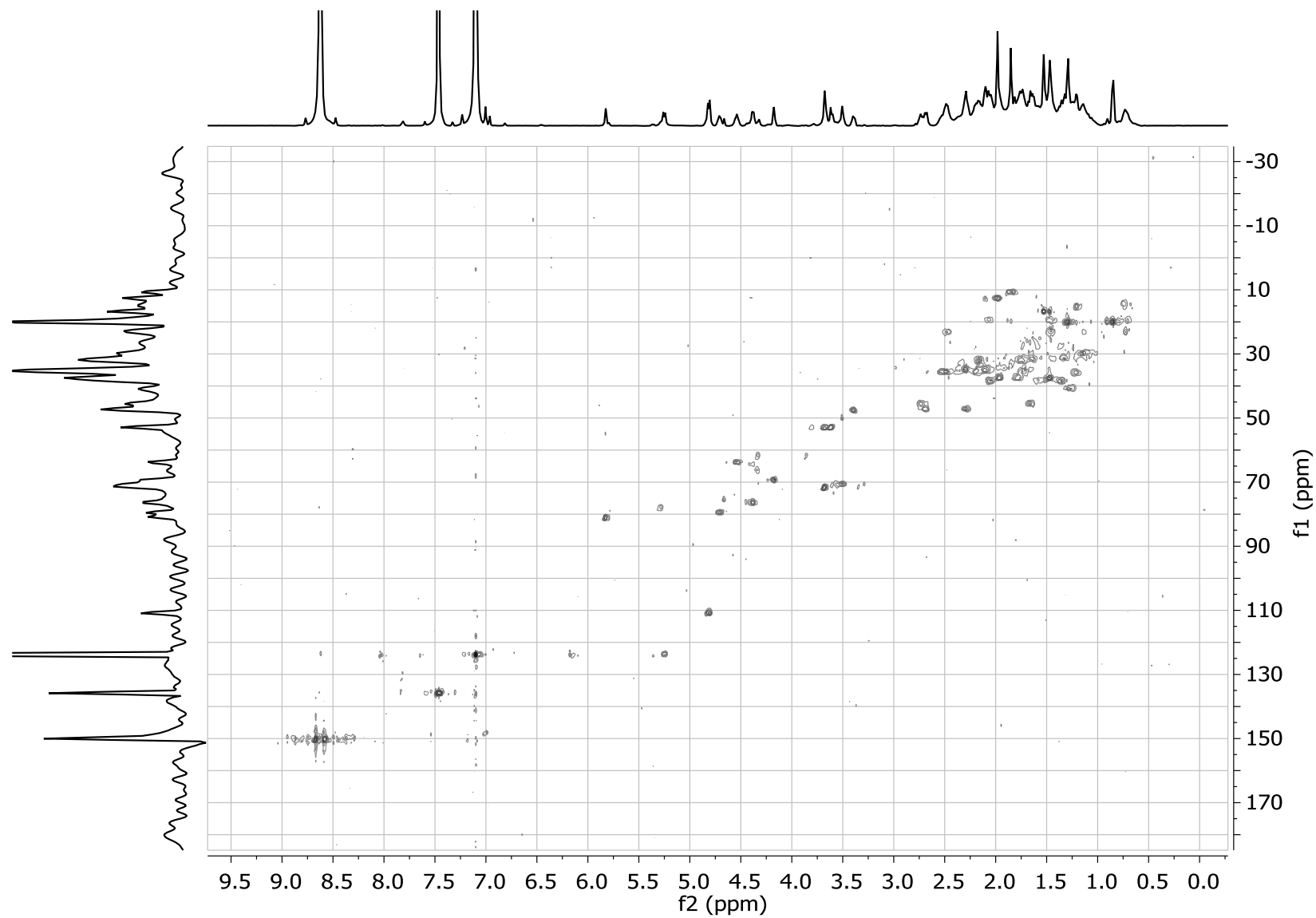


Figure 9.43: 2D HSQC spectra of 20-hydroxy-13,19-didesmethyl SPX C (600 MHz Proton frequency, pyridine-d₅).

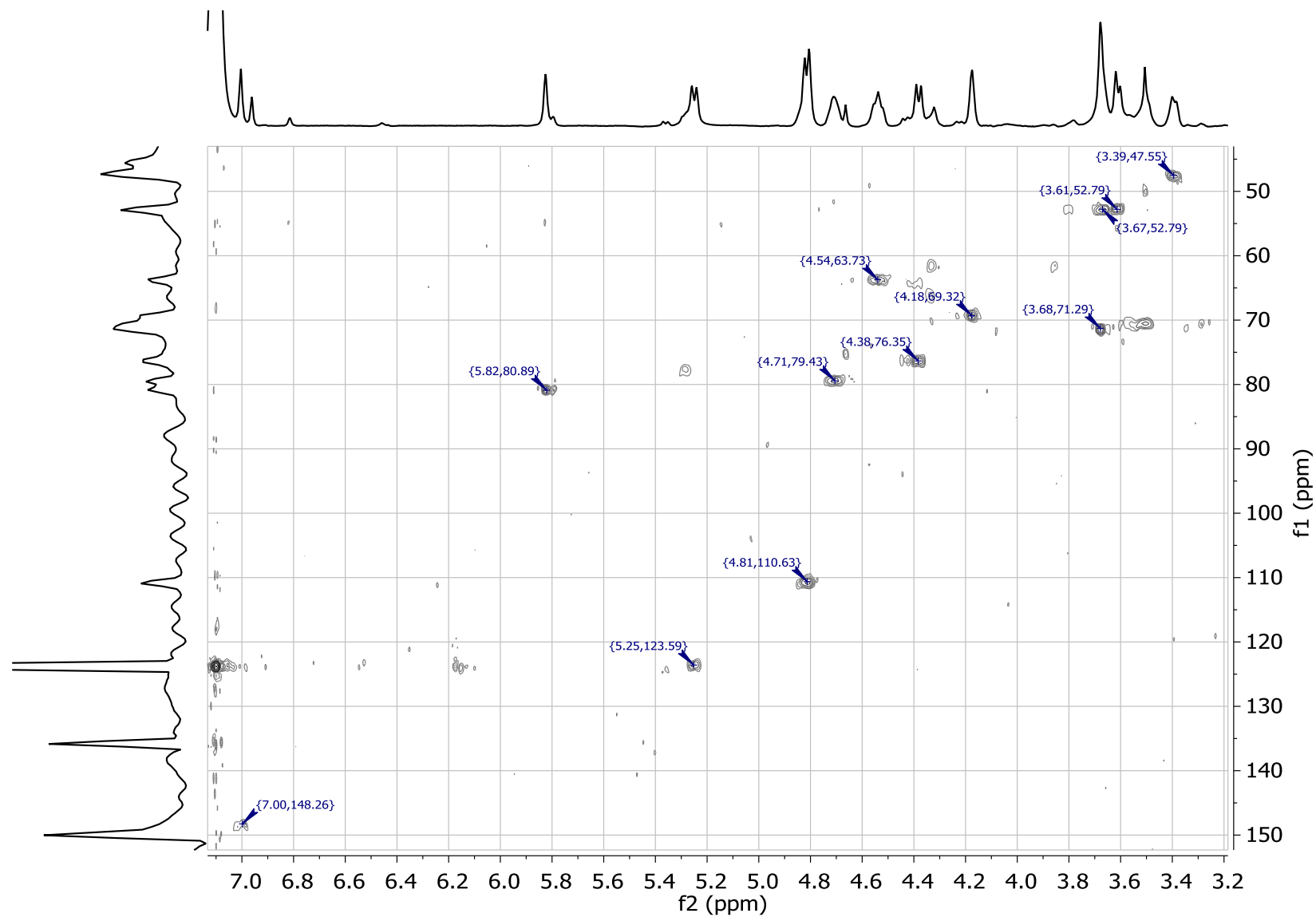


Figure 9.44: Slice 1 of 2D HSQC spectra of 20-hydroxy-13,19-didesmethyl SPX C (600 MHz Proton frequency, pyridine-d₅).

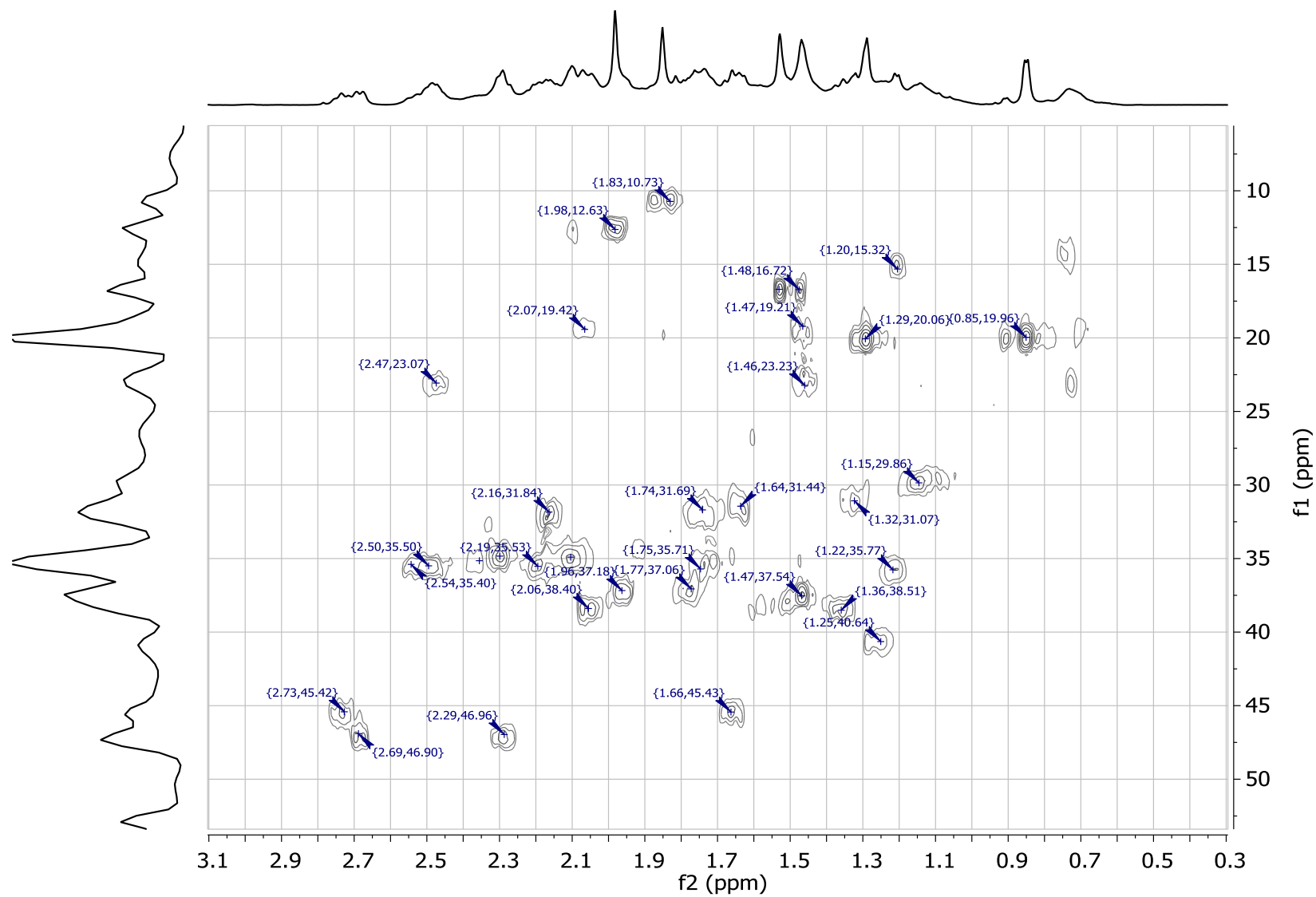


Figure 9.45: Slice 2 of 2D HSQC spectra of 20-hydroxy-13,19-didesmethyl SPX C (600 MHz Proton frequency, pyridine-d₅).

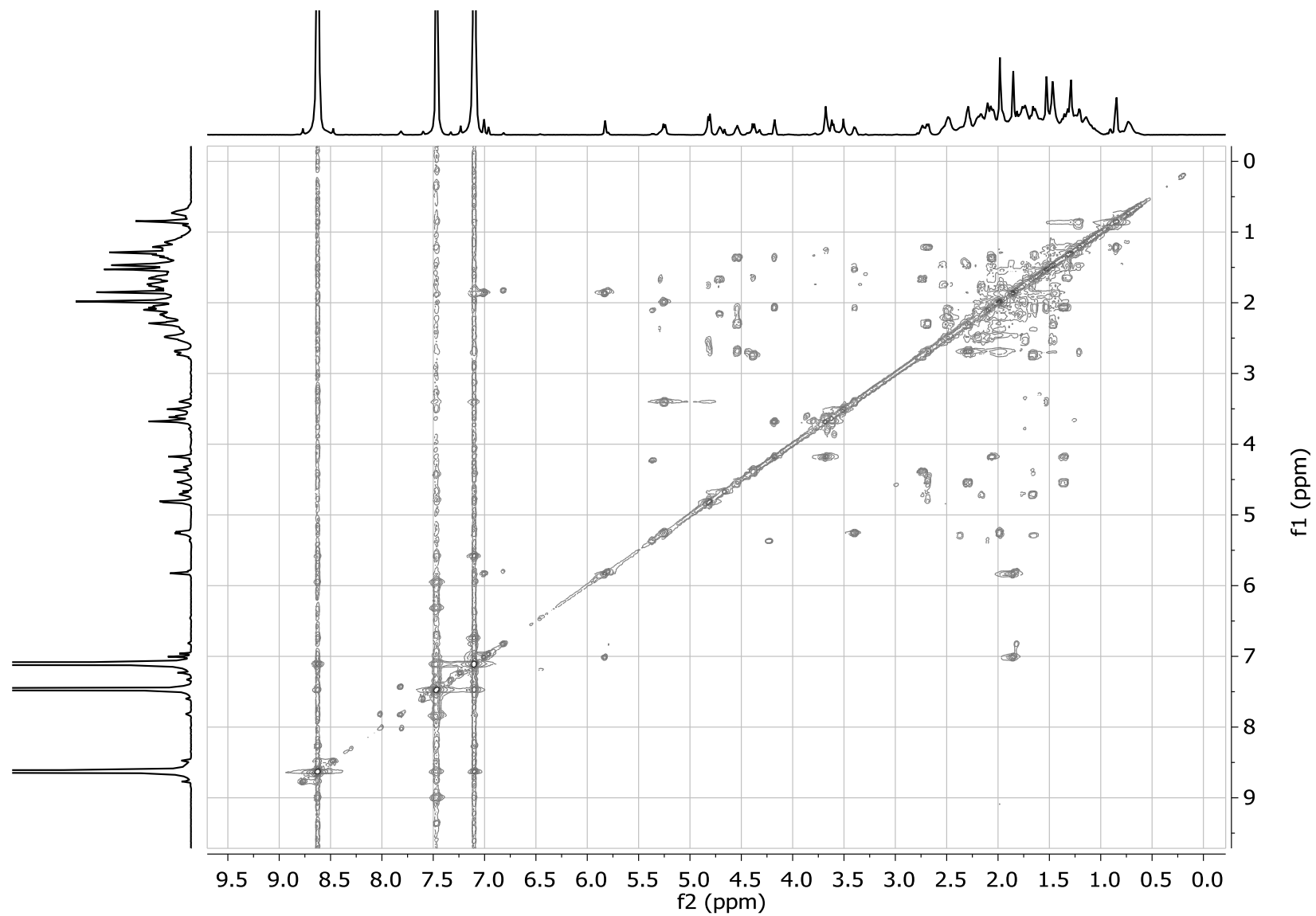


Figure 9.46: 2D COSY spectra of 20-hydroxy-13,19-didesmethyl SPX C (600 MHz, pyridine- d_5).

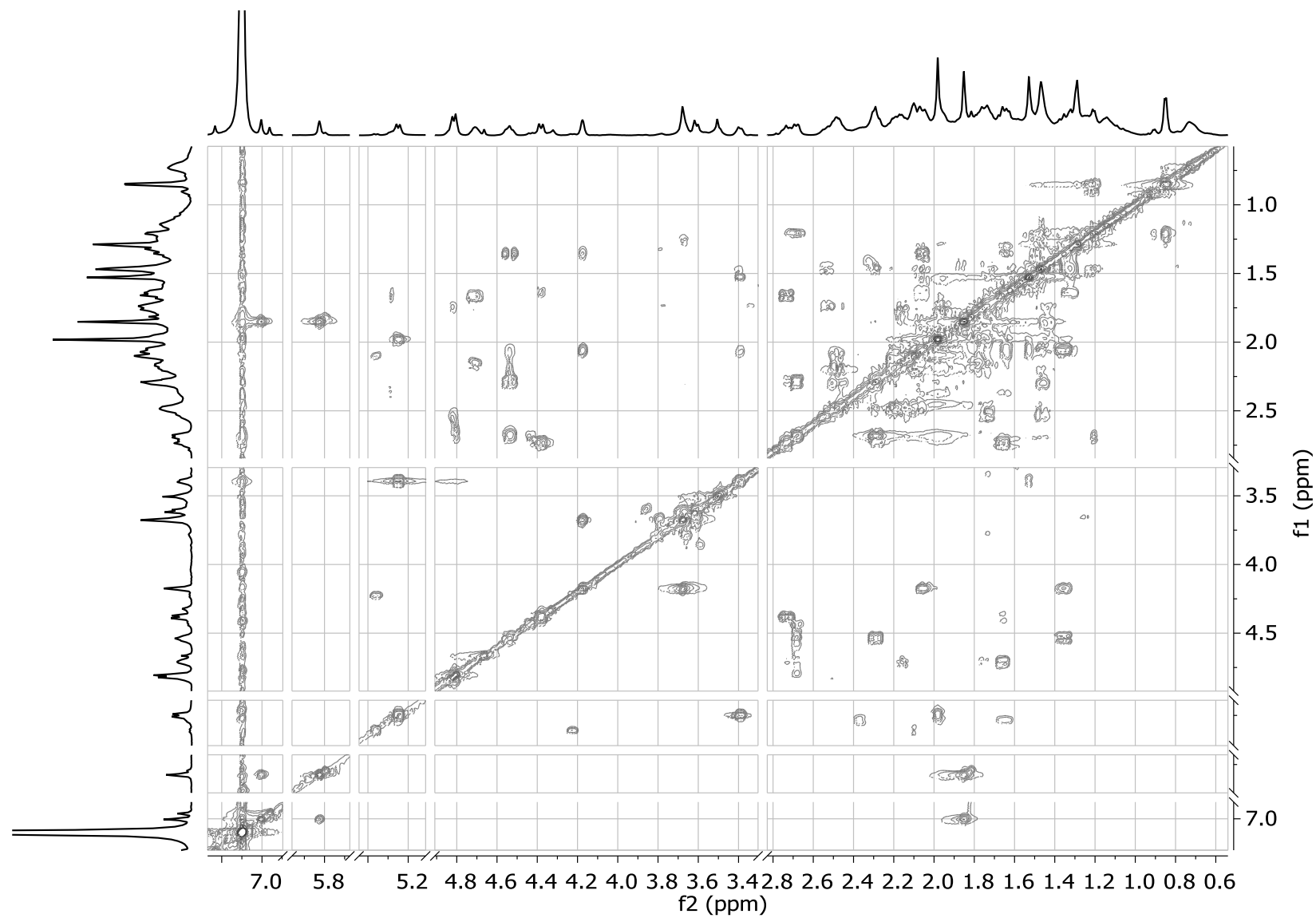


Figure 9.47: Slice of 2D COSY spectra of 20-hydroxy-13,19-didesmethyl SPX C (600 MHz, pyridine-d₅).

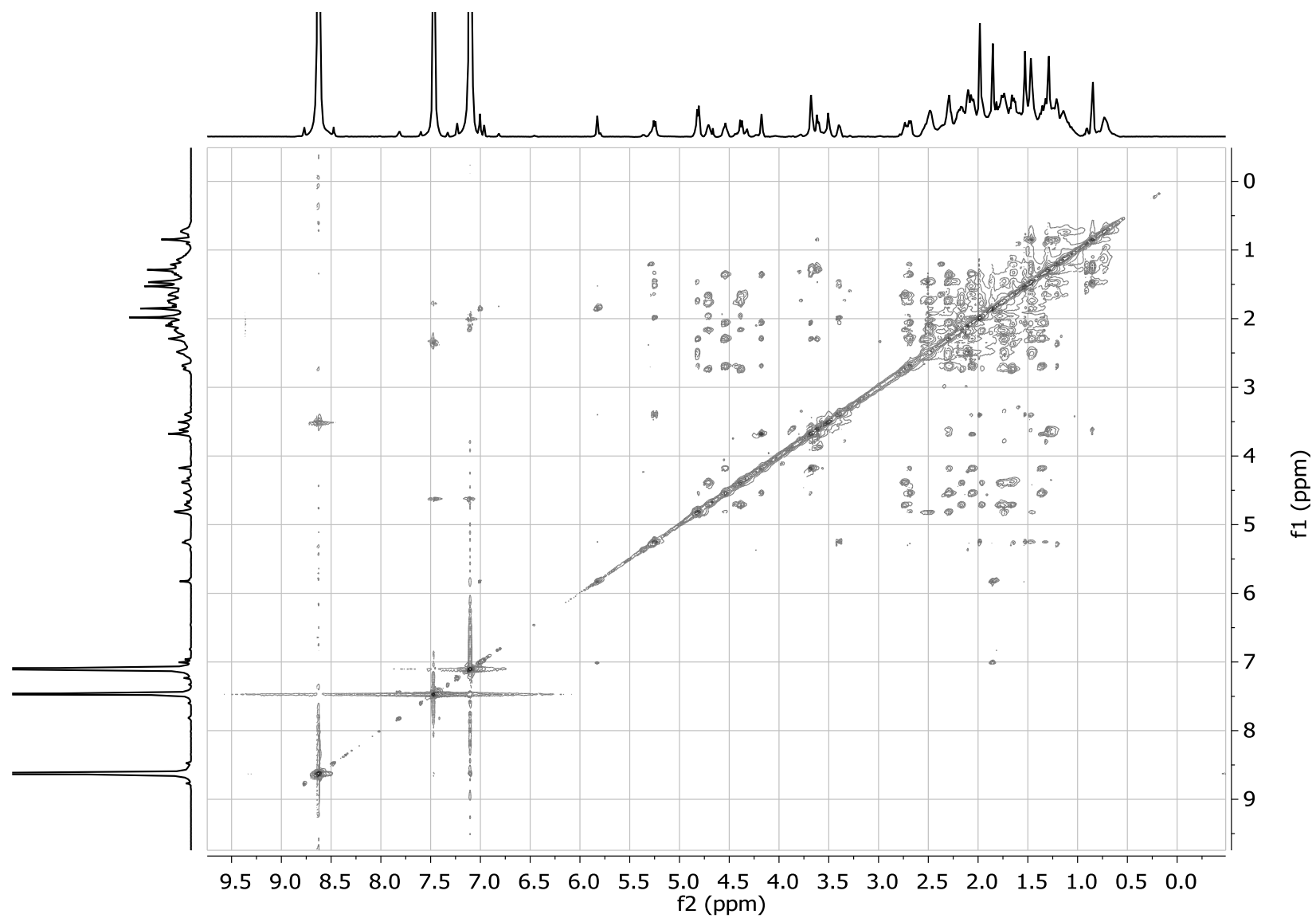


Figure 9.48: 2D TOCSY spectra of 20-hydroxy-13,19-didesmethyl SPX C (600 MHz, pyridine- d_5).

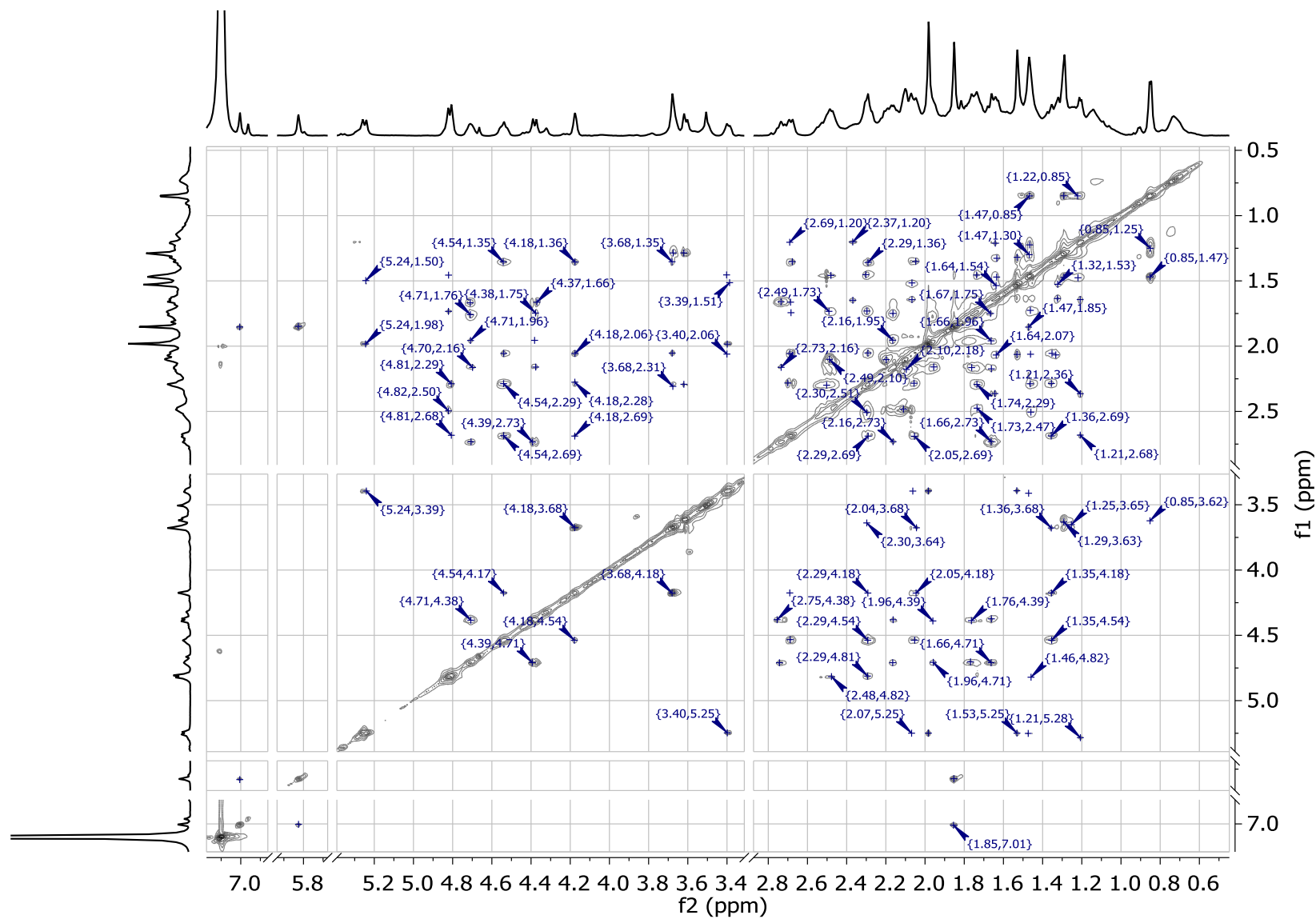


Figure 9.49: Slice of 2D TOCSY spectra of 20-hydroxy-13,19-didesmethyl SPX C (600 MHz, pyridine-d₅).

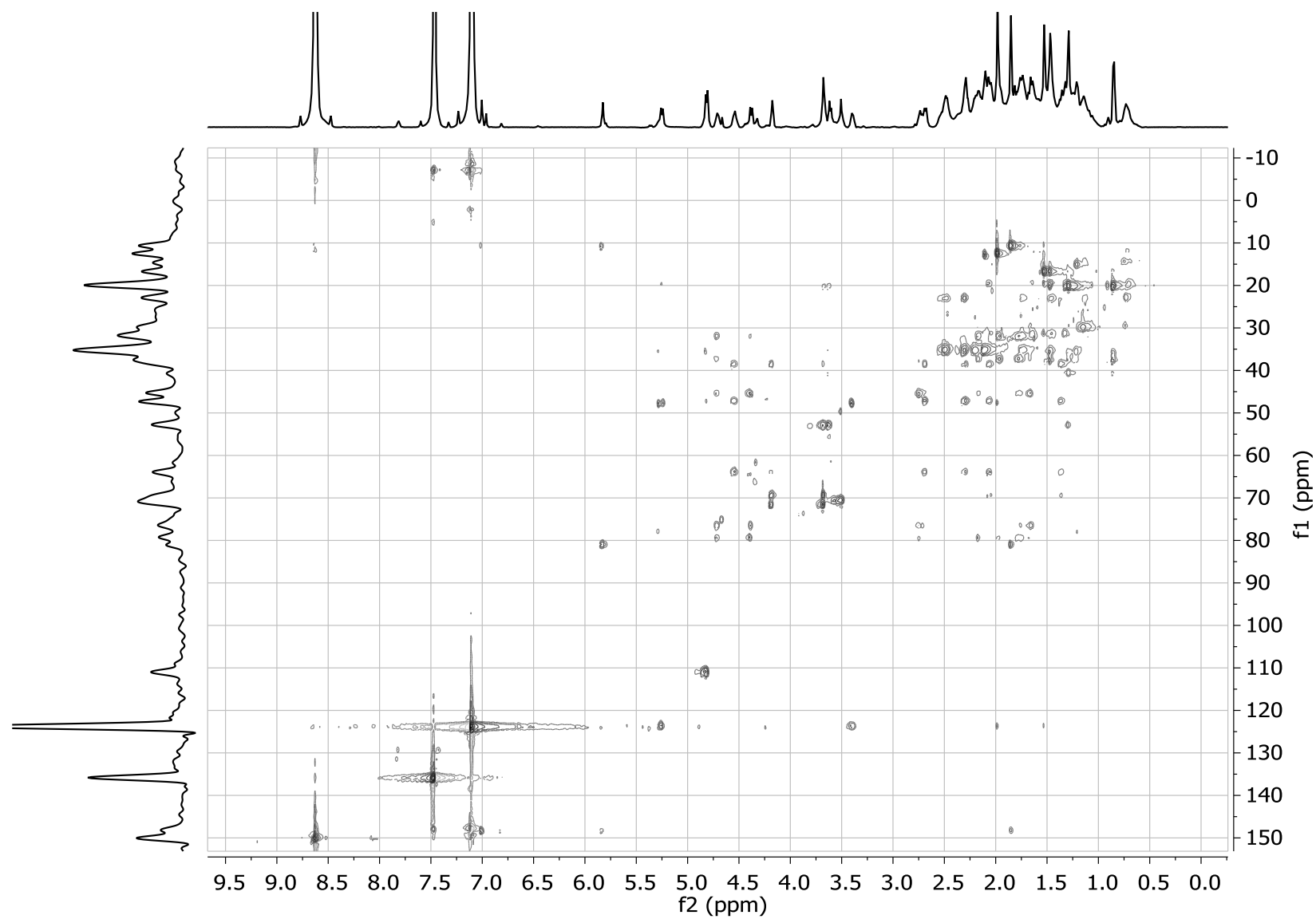


Figure 9.50: 2D HSQC-TOCSY spectra of 20-hydroxy-13,19-didesmethyl SPX C (600 MHz Proton frequency, pyridine-d₅).

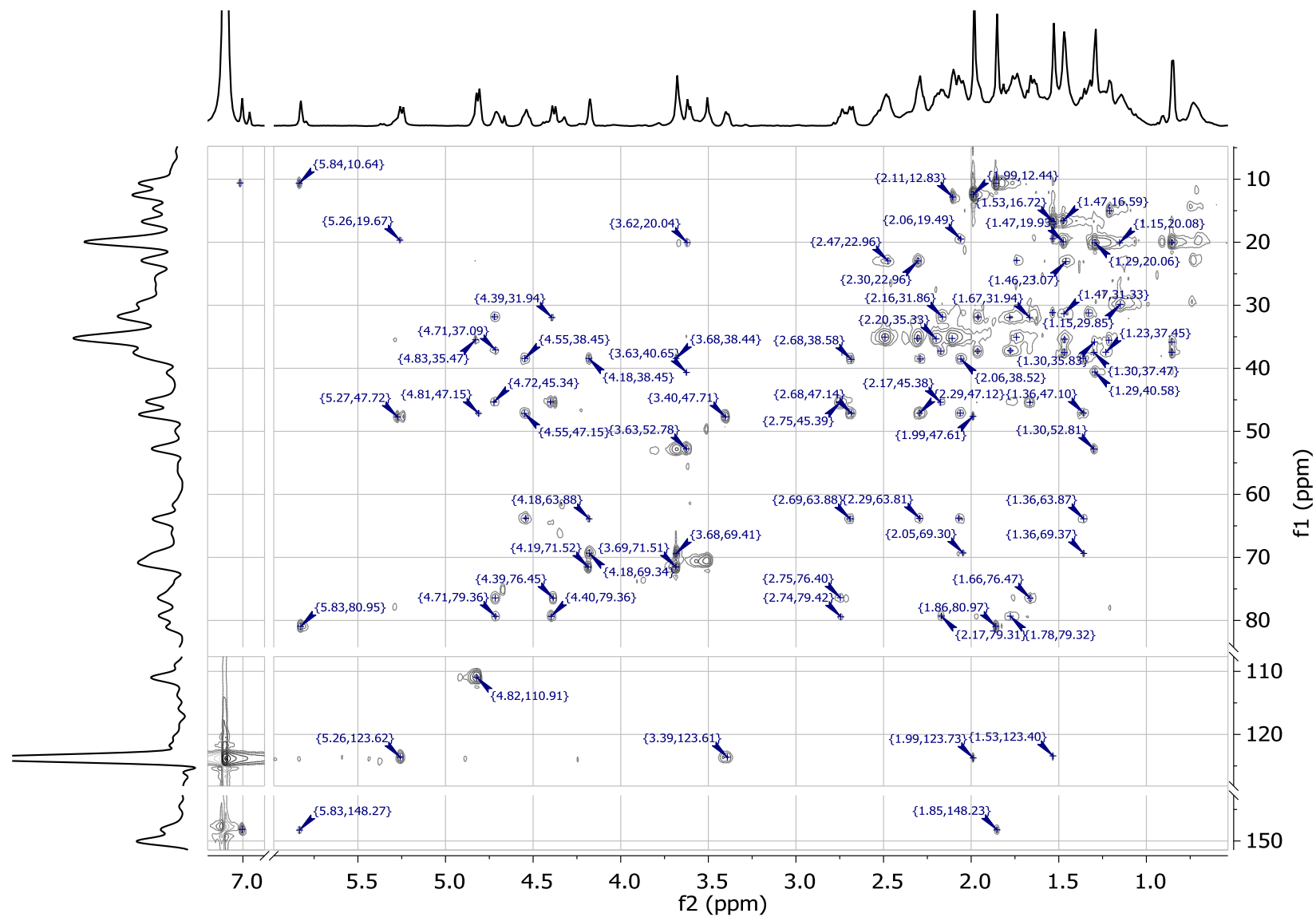


Figure 9.51: Slice of 2D HSQC-TOCOSY spectra of 20-hydroxy-13,19-didesmethyl SPX C (600 MHz Proton frequency, pyridine-d₅).

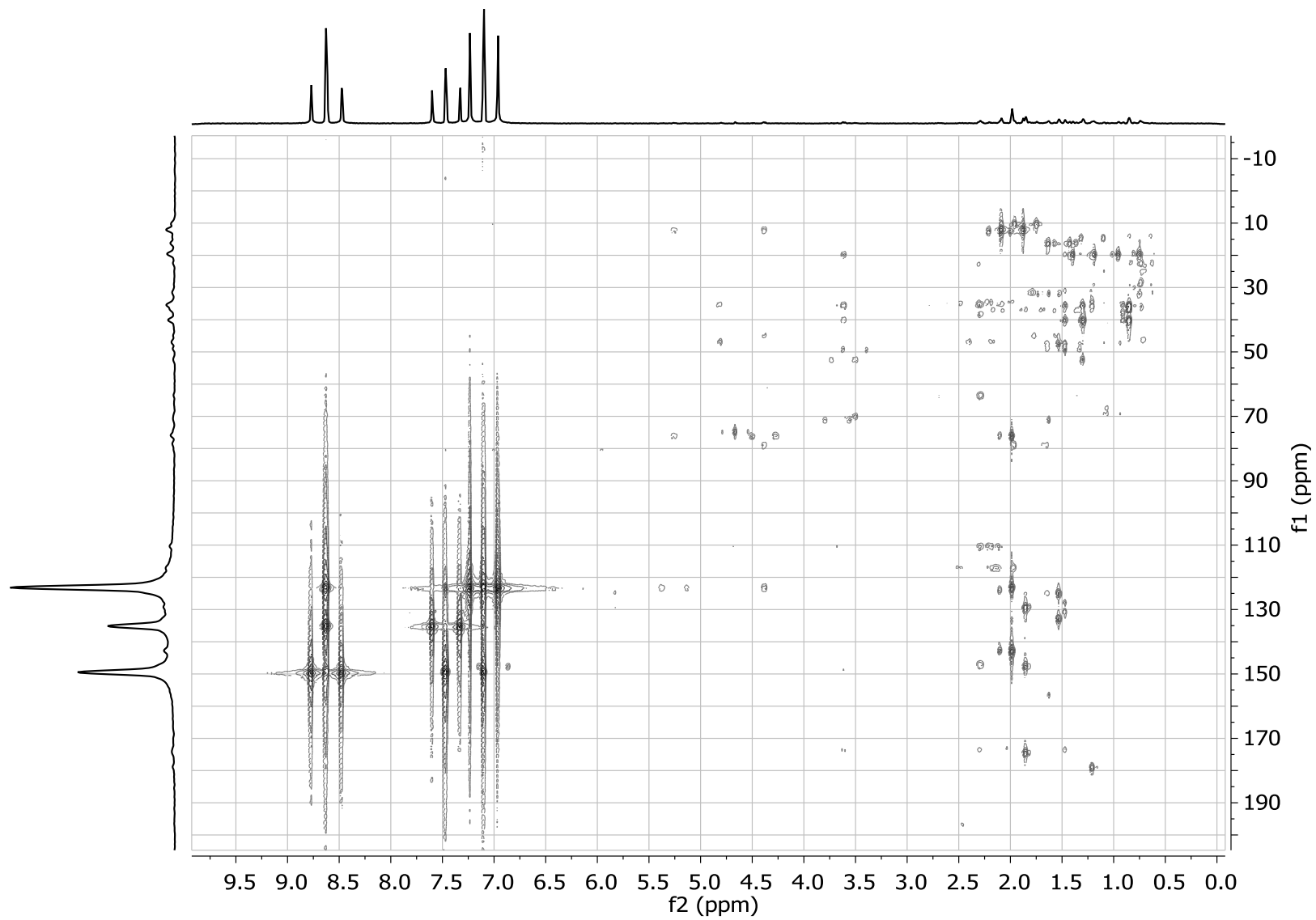


Figure 9.52: 2D HMBC spectra of 20-hydroxy-13,19-didesmethyl SPX C (600 MHz Proton frequency, pyridine-d₅).

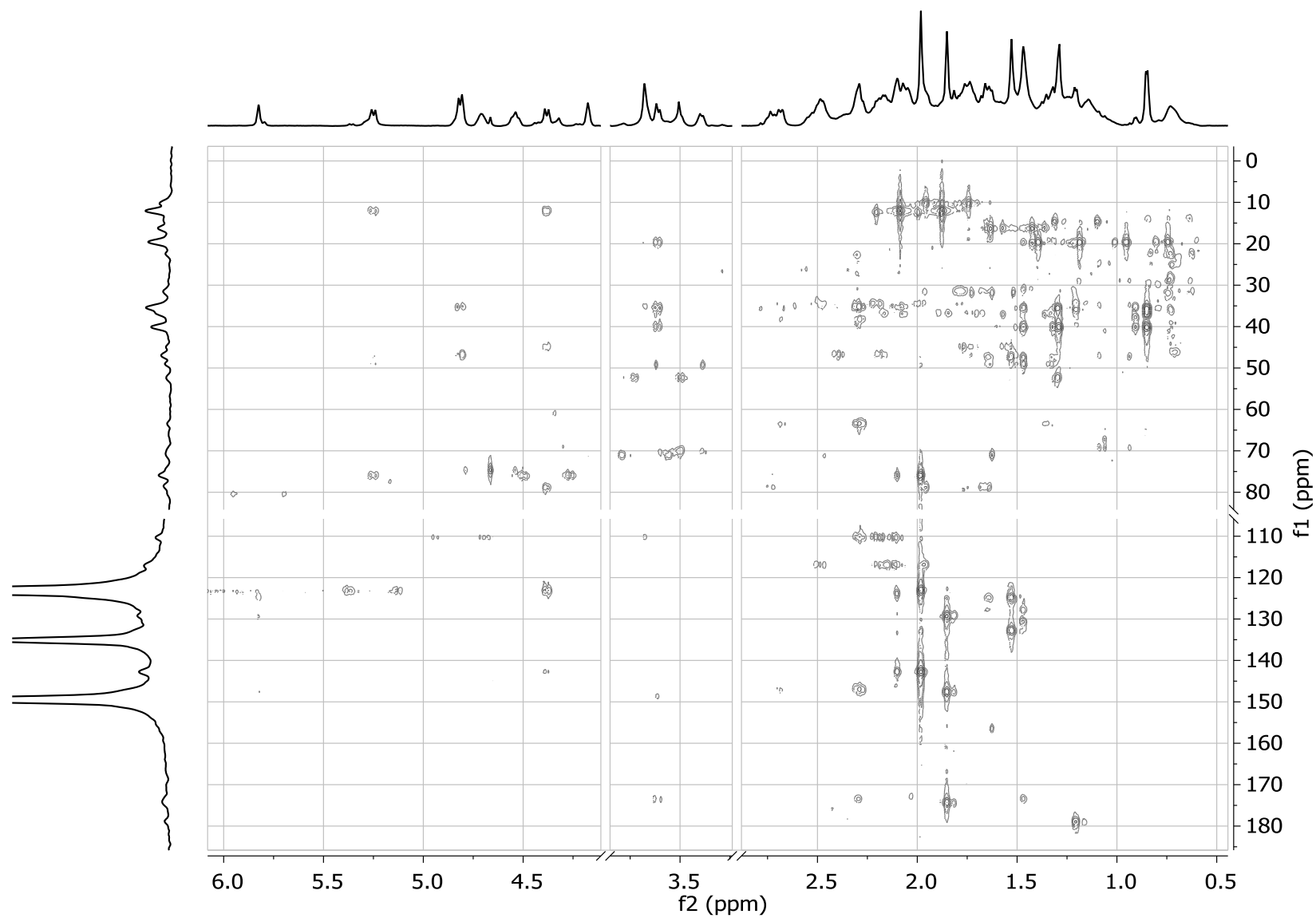
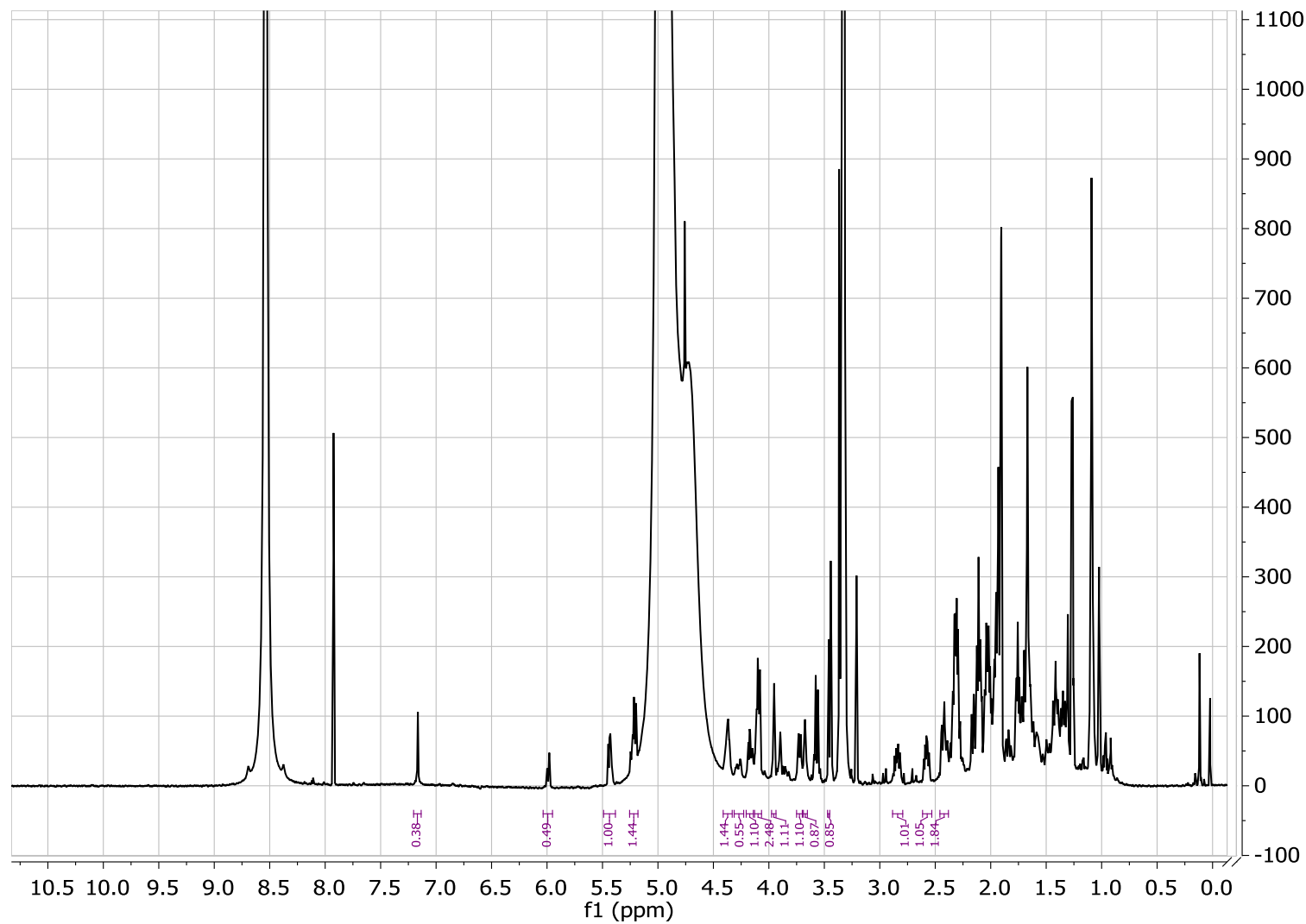


Figure 9.53: Slice of 2D HMBC spectra of 20-hydroxy-13,19-didesmethyl SPX C (600 MHz Proton frequency, pyridine-d₅).

9.1.6 NMR-spectra of 20-Hydroxy-13,19-didesMethyl-SPX D

Figure 9.54: 1D Proton spectra of 20-hydroxy-13,19-didesmethyl SPX D (600 MHz, CD₃OD).

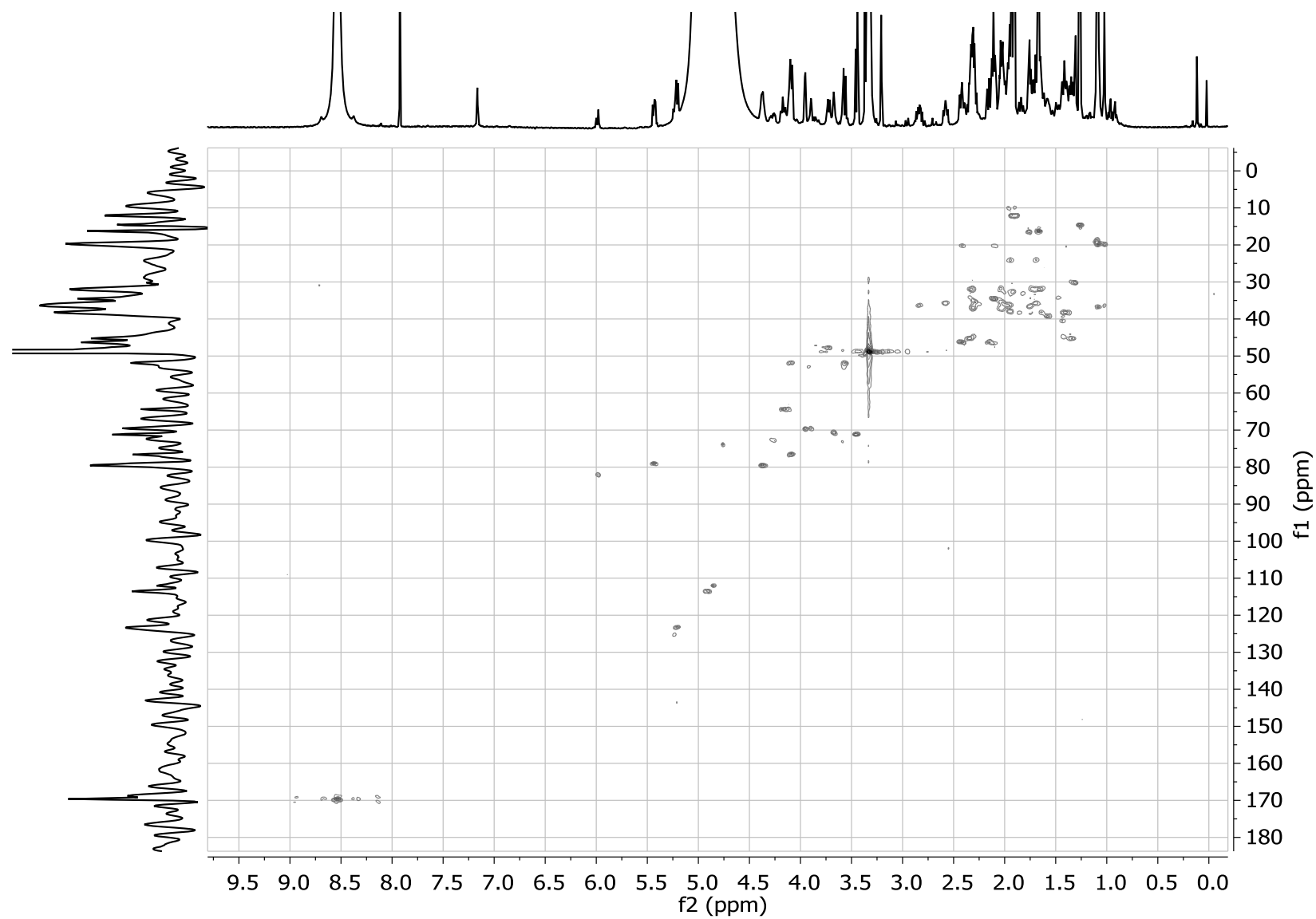


Figure 9.55: 2D HSQC spectra of 20-hydroxy-13,19-didesmethyl SPX D (600 MHz Proton frequency, CD₃OD).

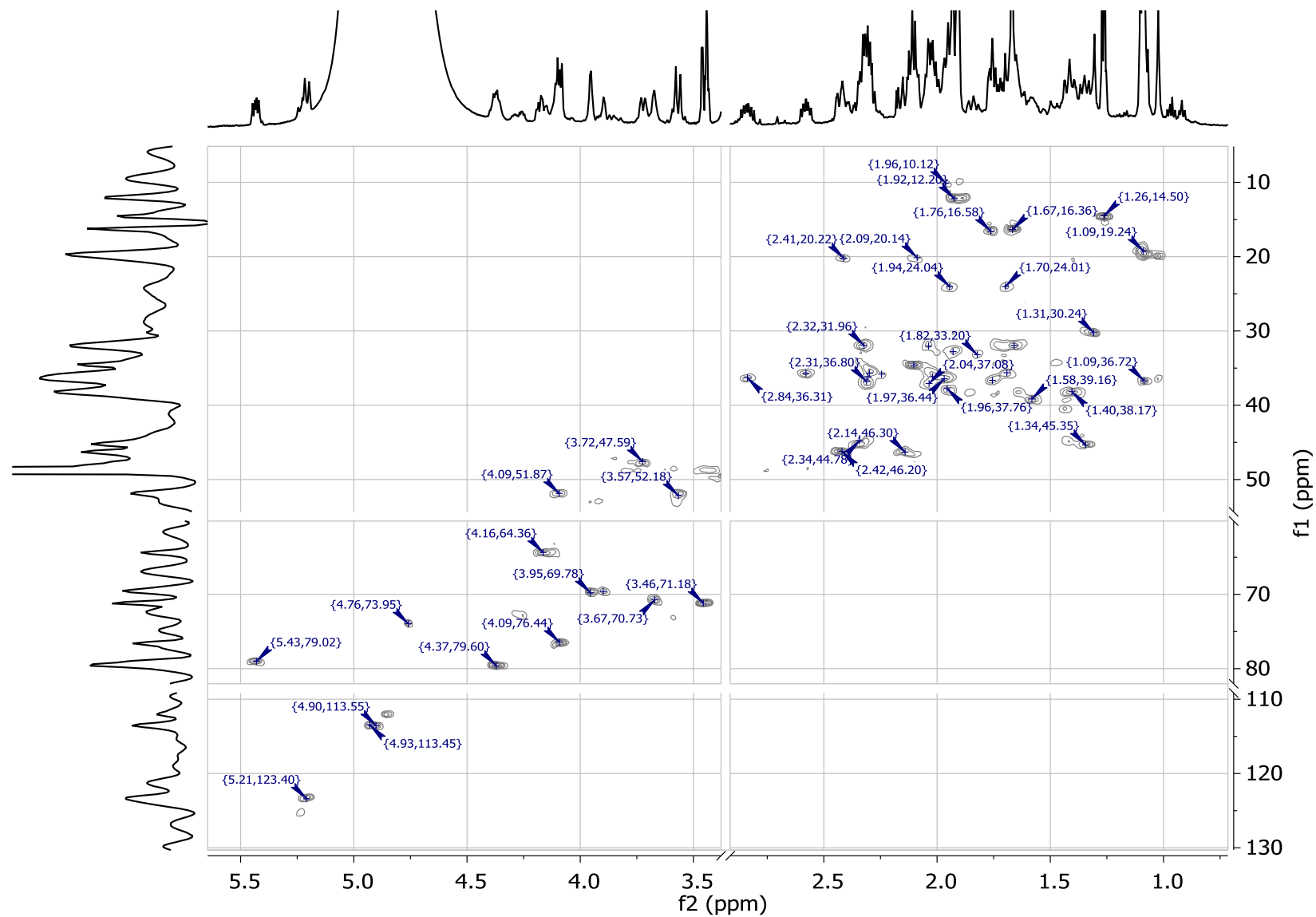


Figure 9.56: Slice of 2D HSQC spectra of 20-hydroxy-13,19-didesmethyl SPX D (600 MHz Proton frequency, CD₃OD).

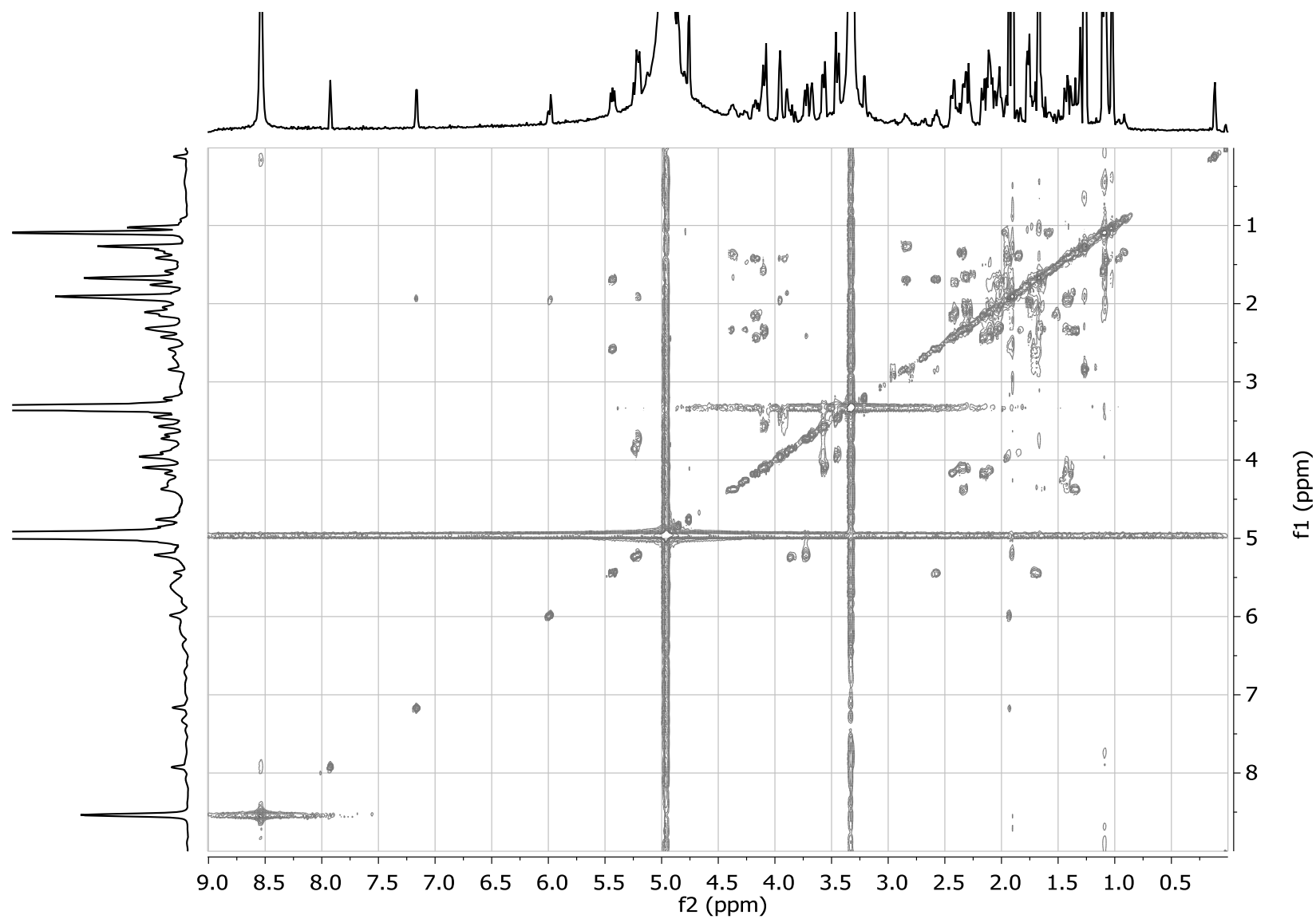


Figure 9.57: 2D COSY spectra of 20-hydroxy-13,19-didesmethyl SPX D (600 MHz, CD₃OD).

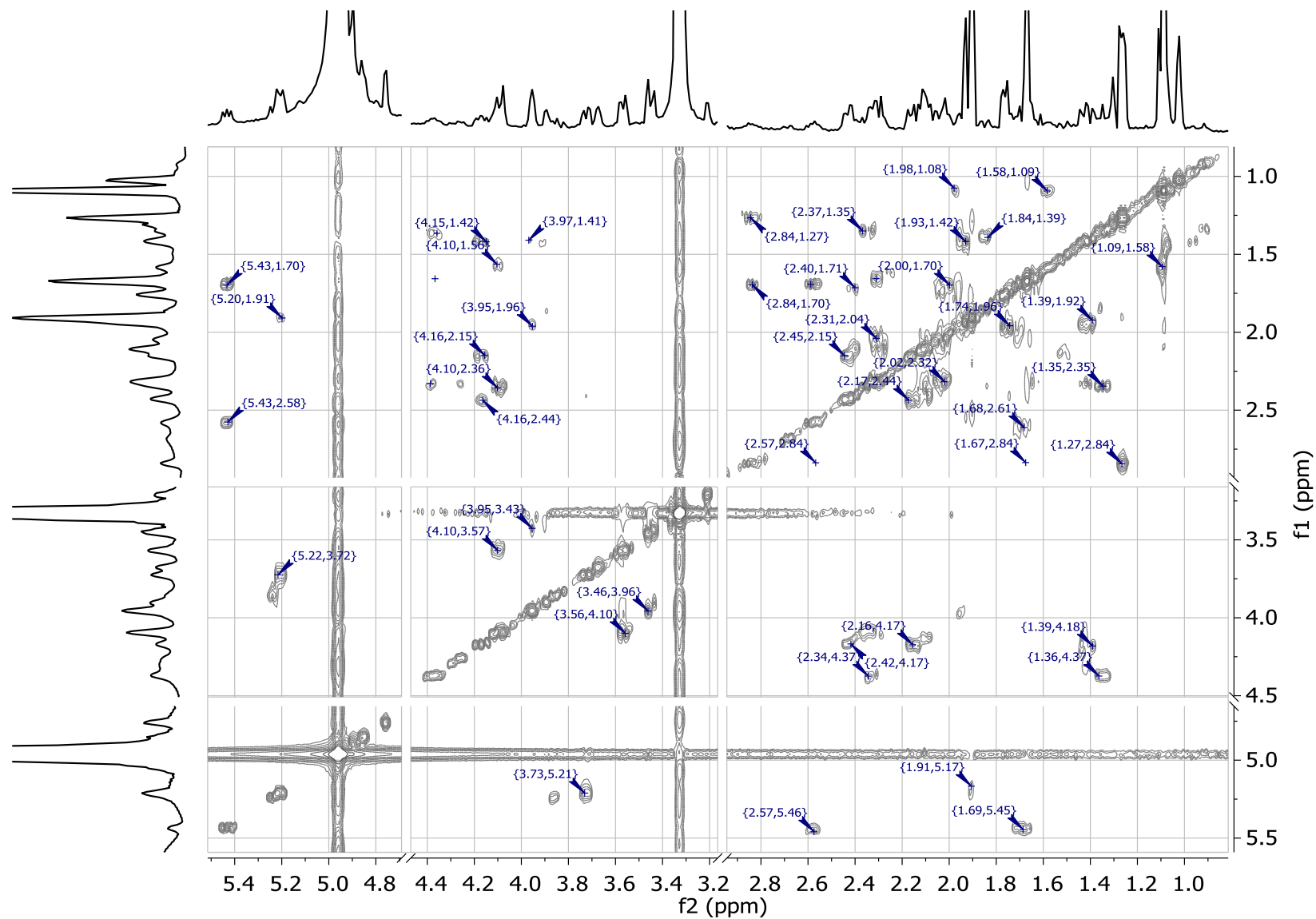


Figure 9.58: Slice of 2D COSY spectra of 20-hydroxy-13,19-didesmethyl SPX D (600 MHz, CD₃OD).

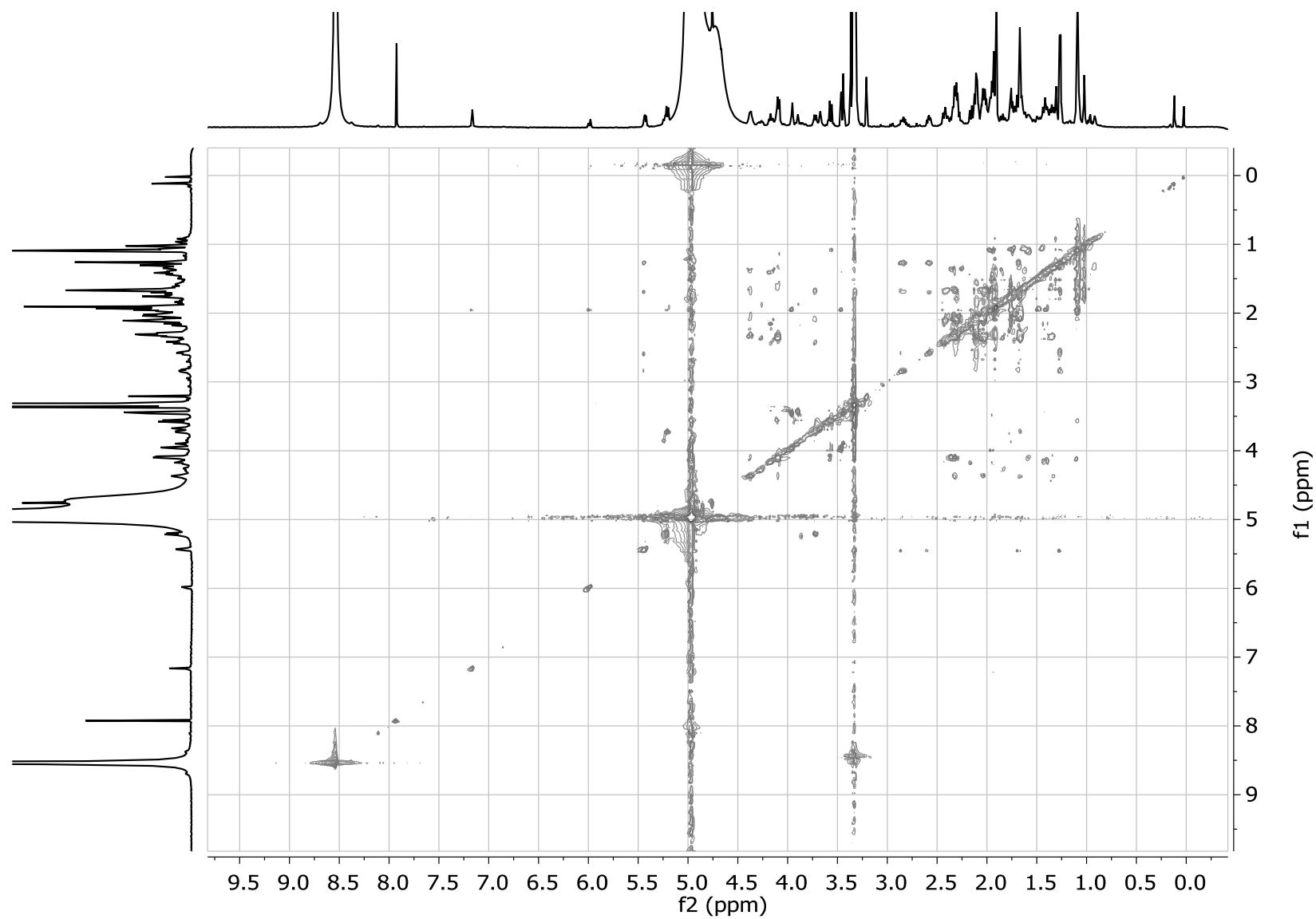


Figure 9.59: 2D TOCSY spectra of 20-hydroxy-13,19-didesmethyl SPX D (600 MHz, CD₃OD).

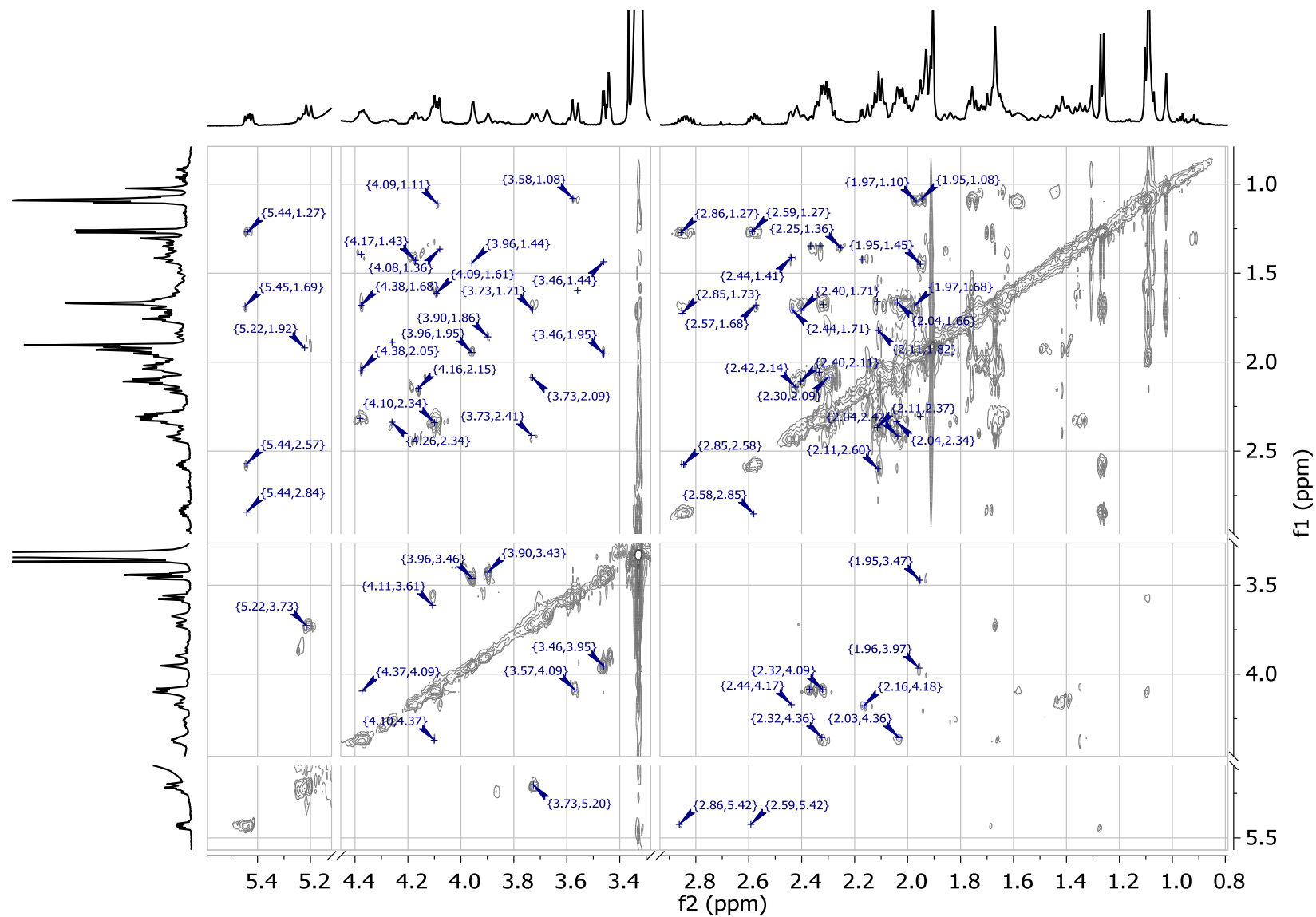


Figure 9.60: Slice of 2D TOCSY spectra of 20-hydroxy-13,19-didesmethyl SPX D (600 MHz, CD_3OD).

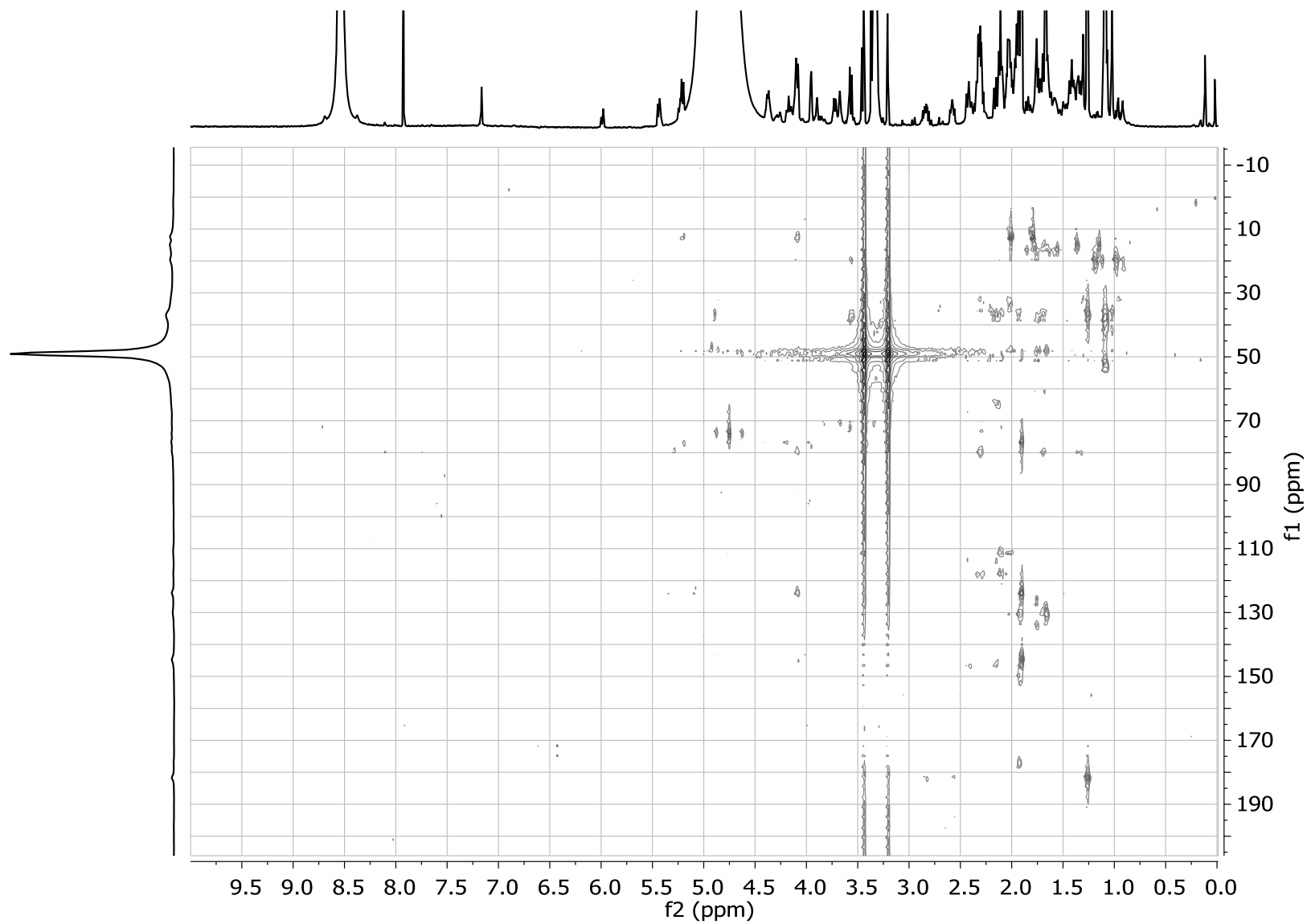


Figure 9.61: 2D HMBC spectra of 20-hydroxy-13,19-didesmethyl SPX D (600 MHz Proton frequency, CD₃OD).

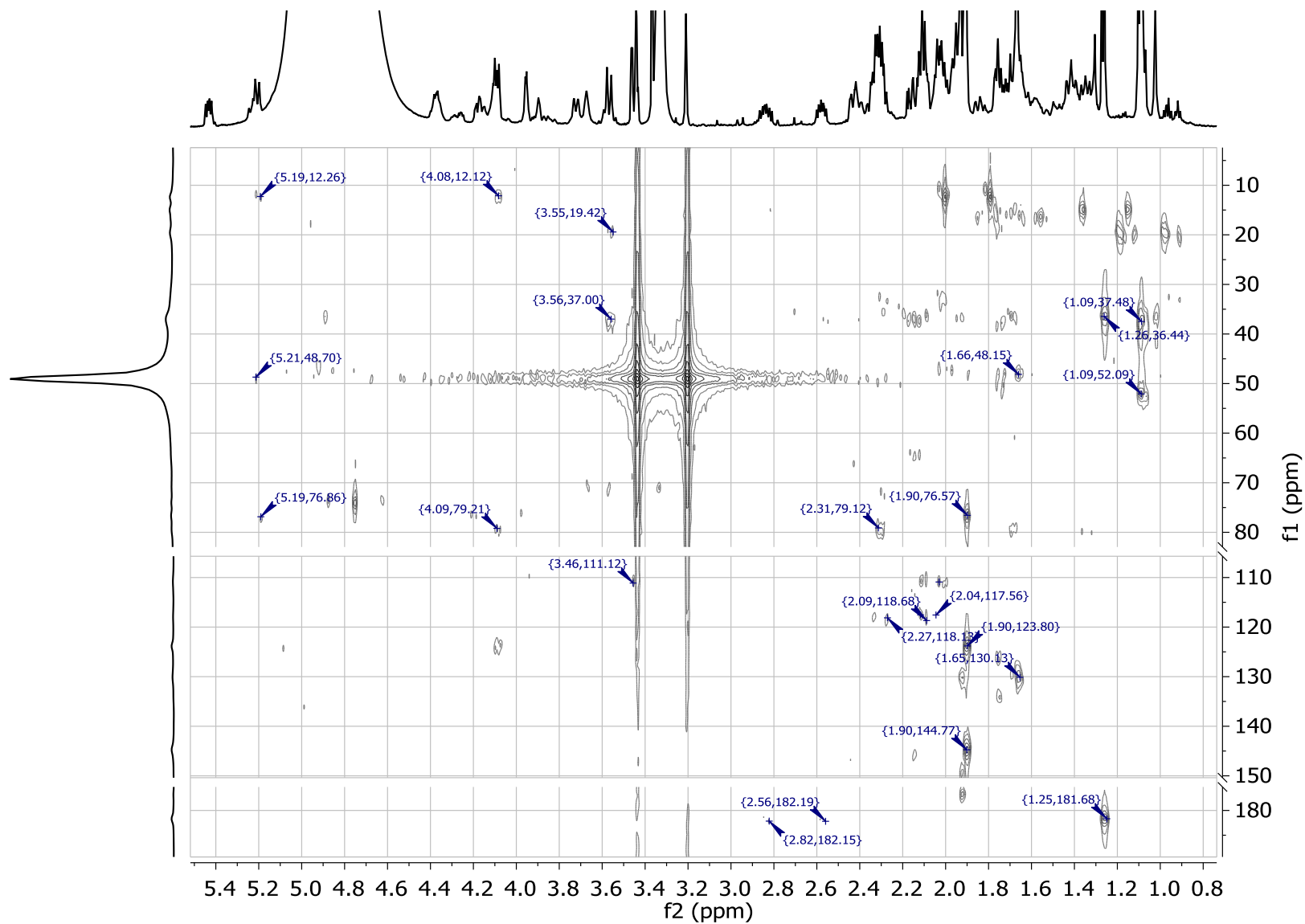


Figure 9.62: Slice of 2D HMBC spectra of 20-hydroxy-13,19-didesmethyl SPX D (600 MHz Proton frequency, CD₃OD).

9.1.7 LC-MS/MS chromatogram of station SL92-2

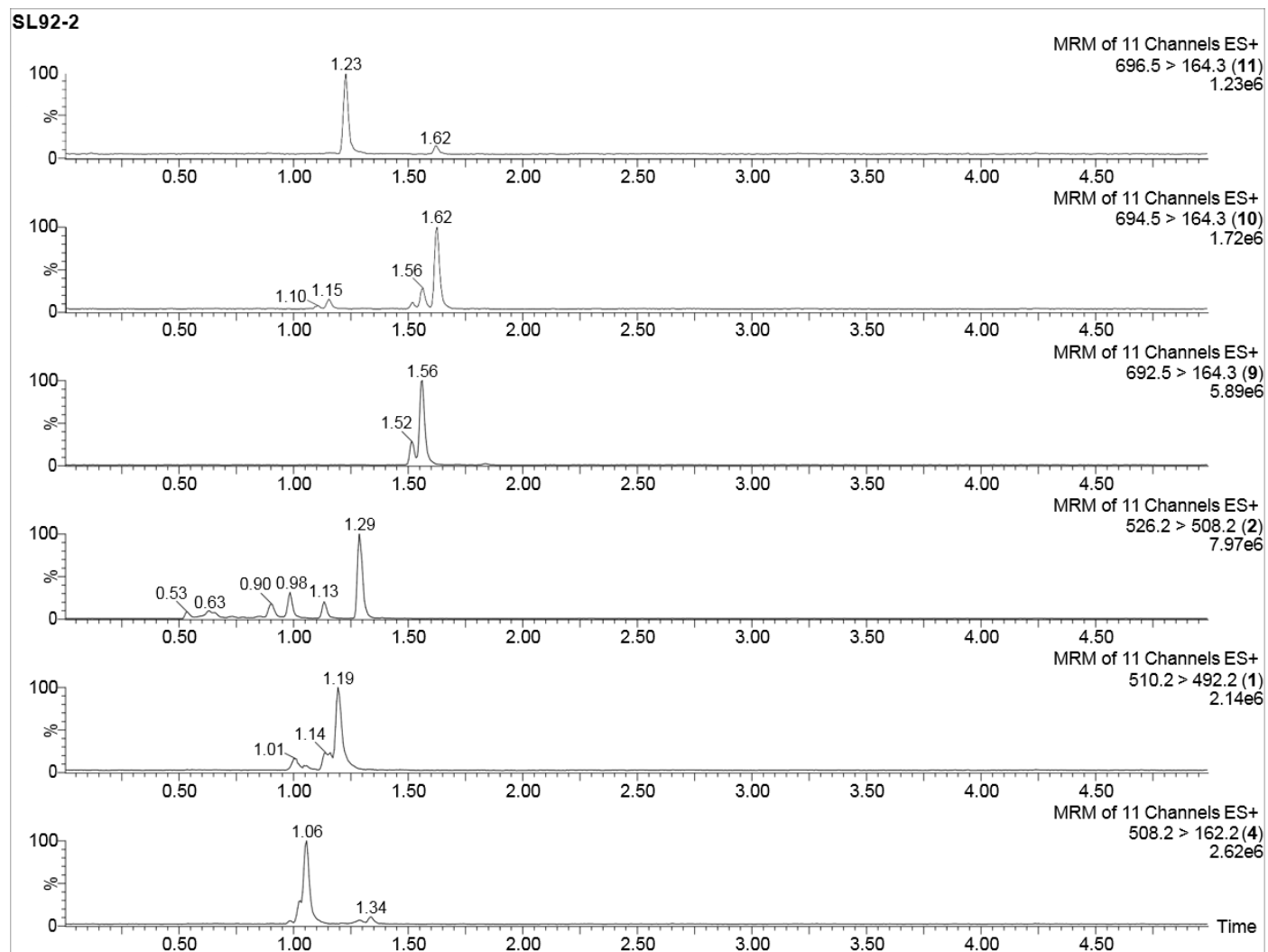


Figure 9.63: LC-MS/MS chromatogram of station SL92-2.

9.2 Identification of novel Azaspiracids from *Azadinium poporum*

9.2.1 NMR-spectra of AZA-40 (6)

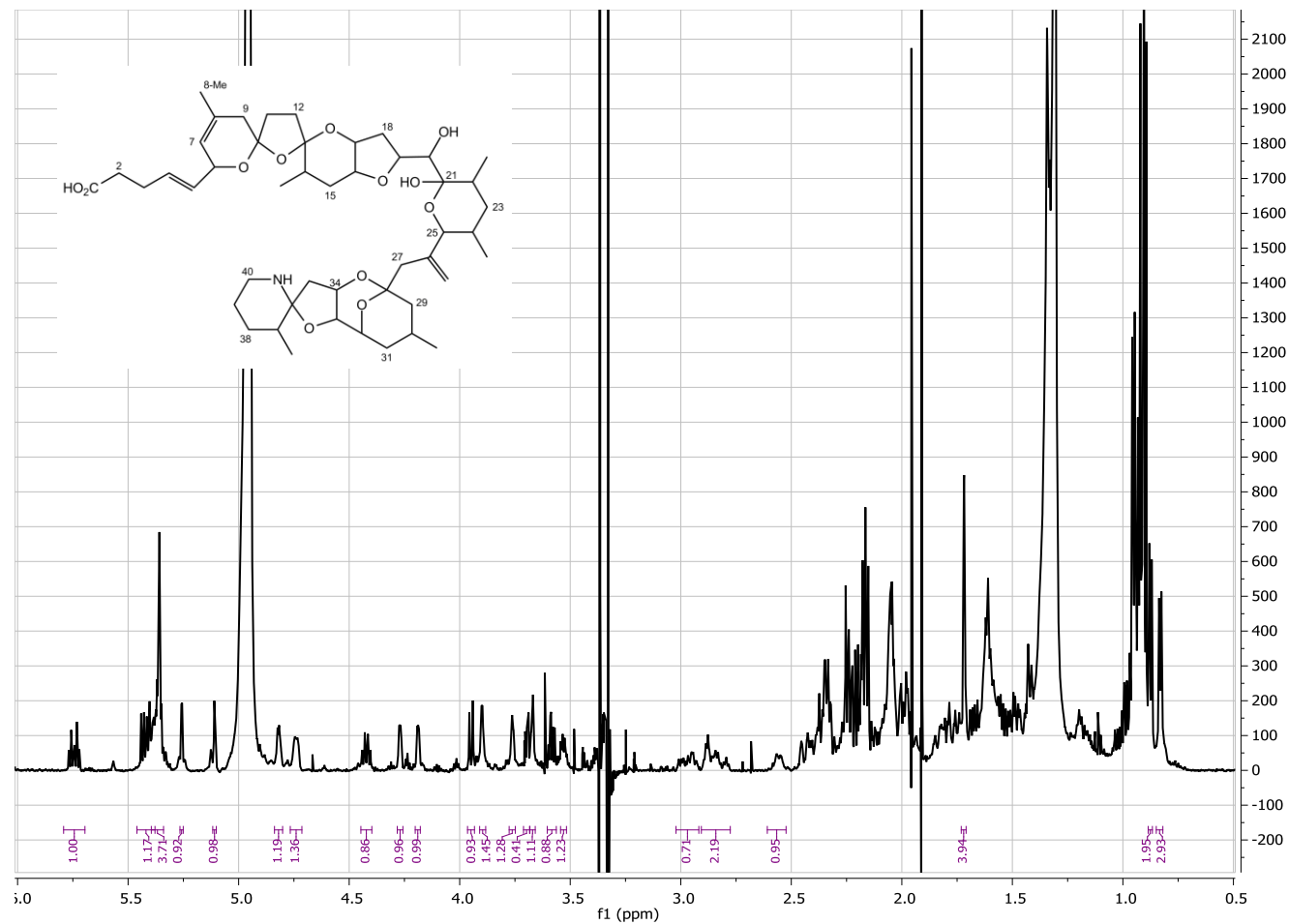


Figure 9.64: Structure and 1D proton spectra of AZA-40 (600 MHz, d₄-methanol).

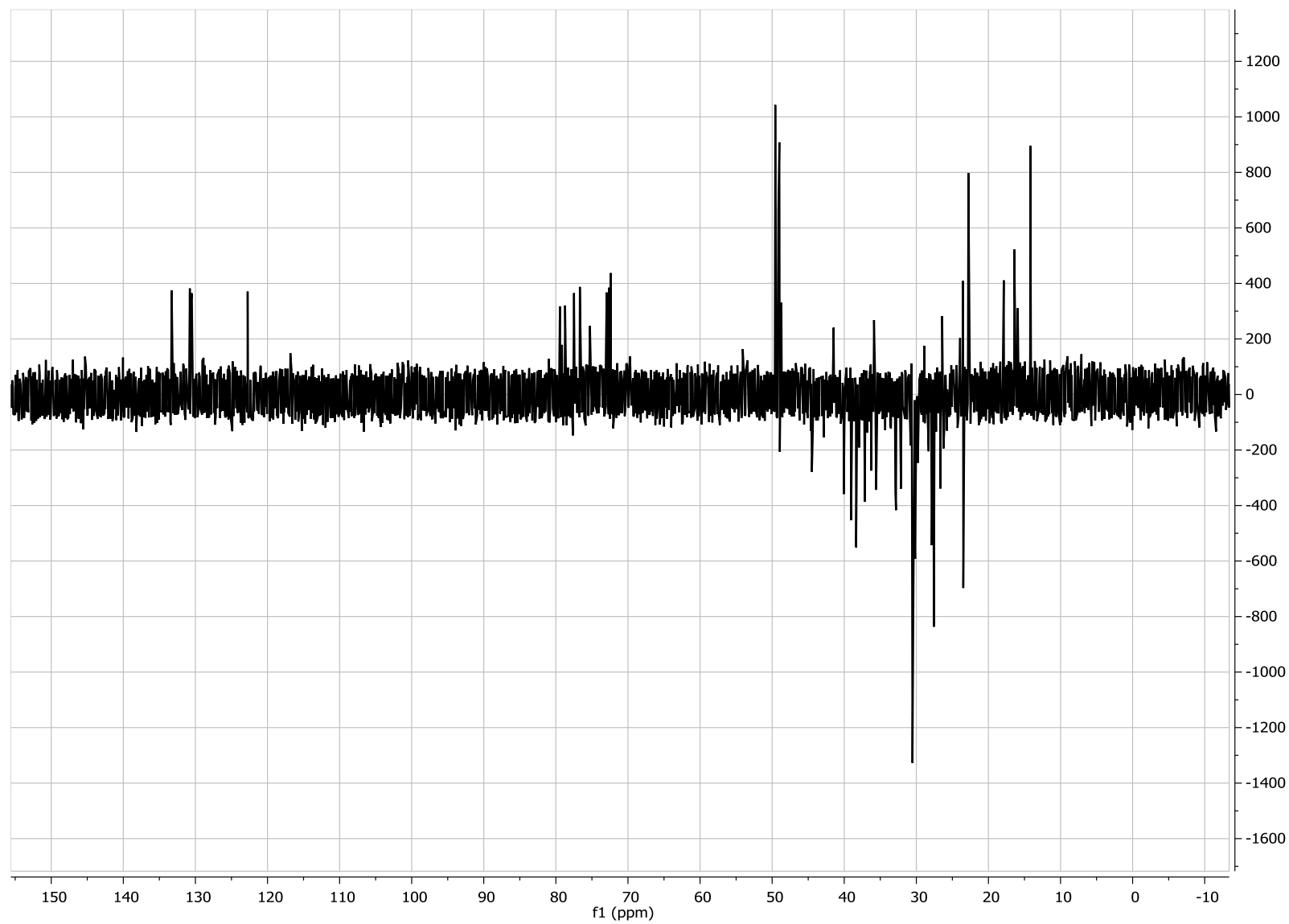


Figure 9.65: 1D DEPT spectra of AZA-40 (600 MHz, d₄-methanol).

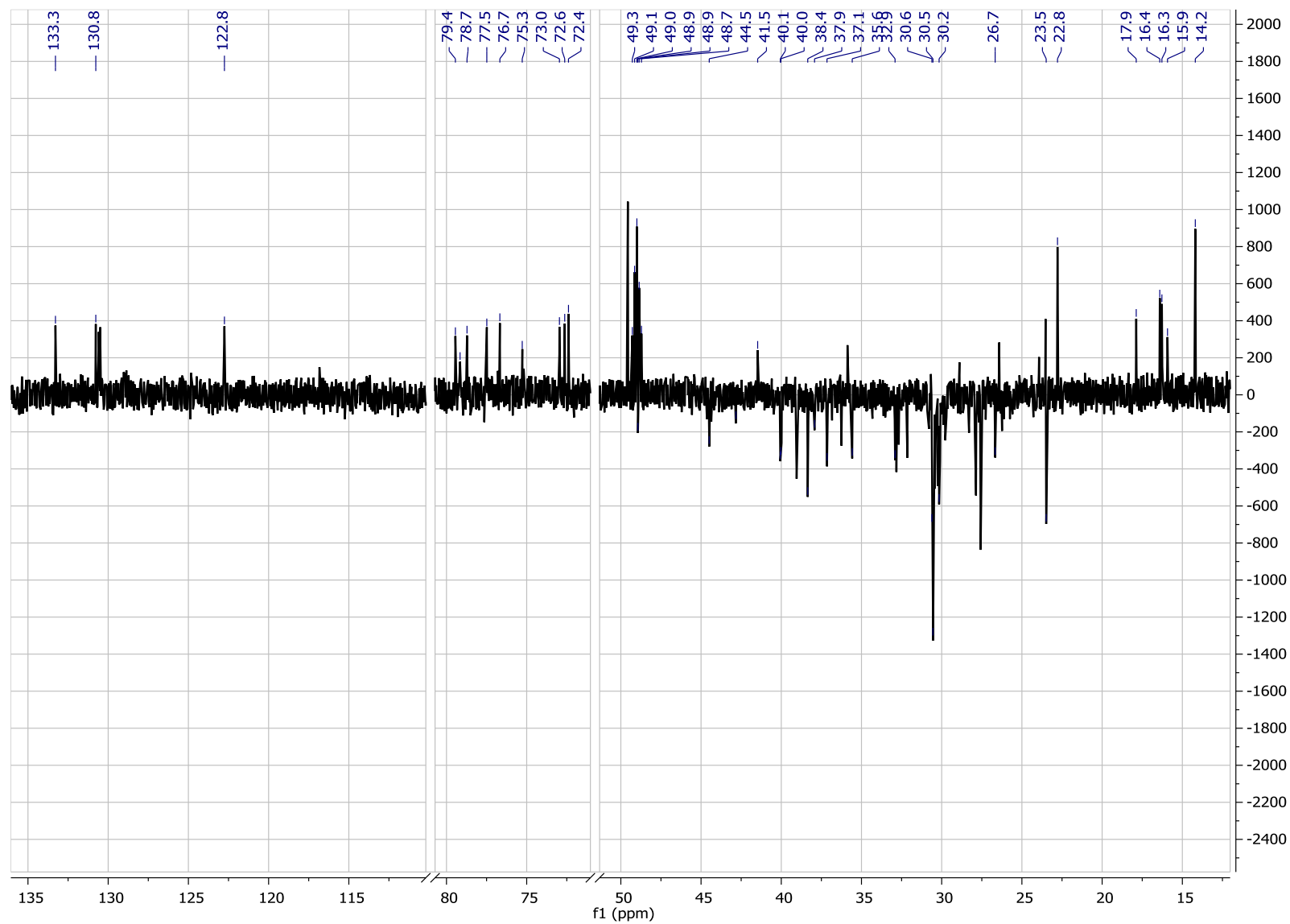


Figure 9.66: Slice of 1D DEPT spectra of of AZA-40 (600 MHz, d₄-methanol).

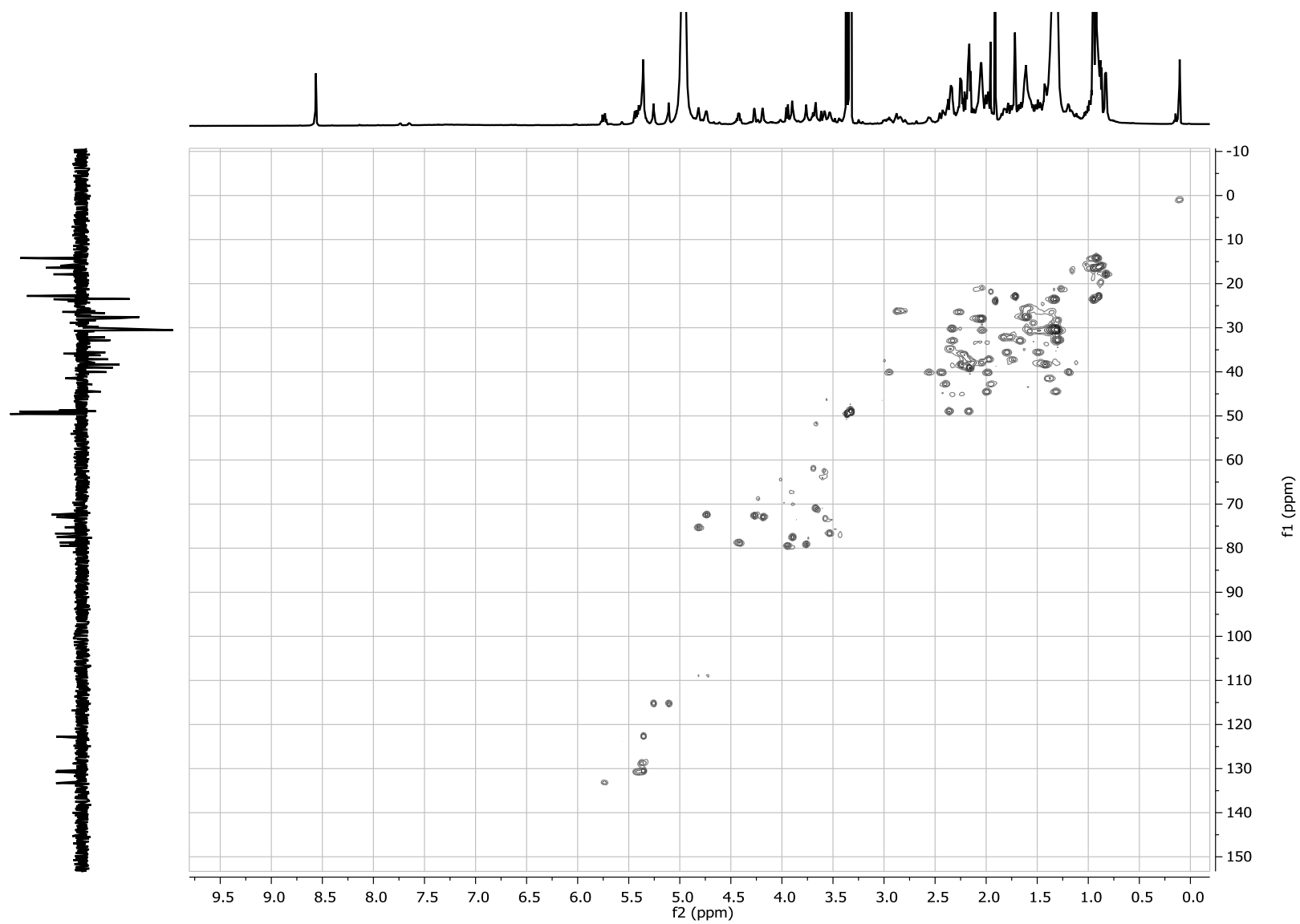


Figure 9.67: 2D HSQC spectra of AZA-40 (600 MHz Proton frequency, d4-methanol).

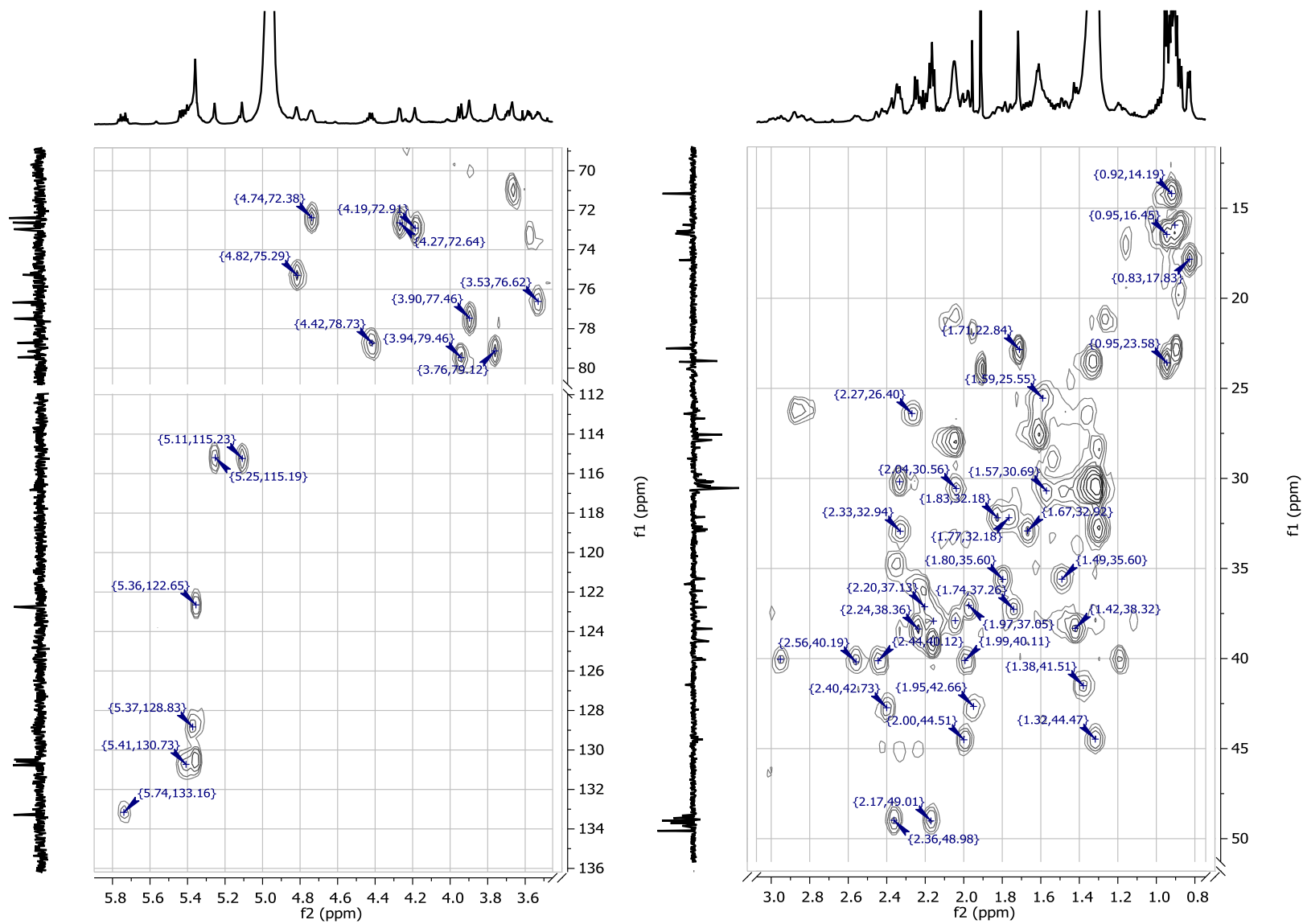


Figure 9.68: Slice of 2D HSQC spectra of AZA-40 (600 MHz Proton frequency, d₄-methanol).

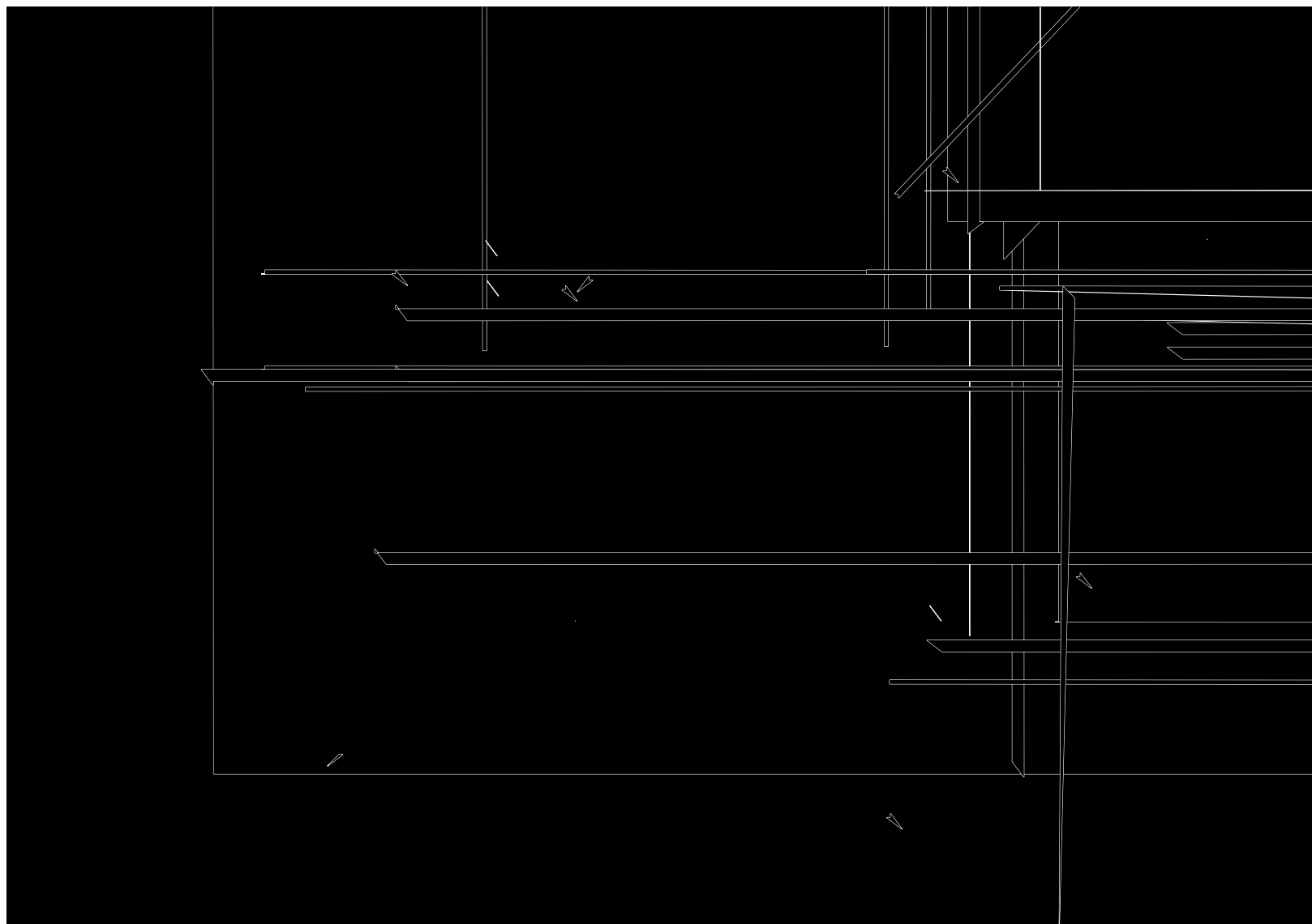
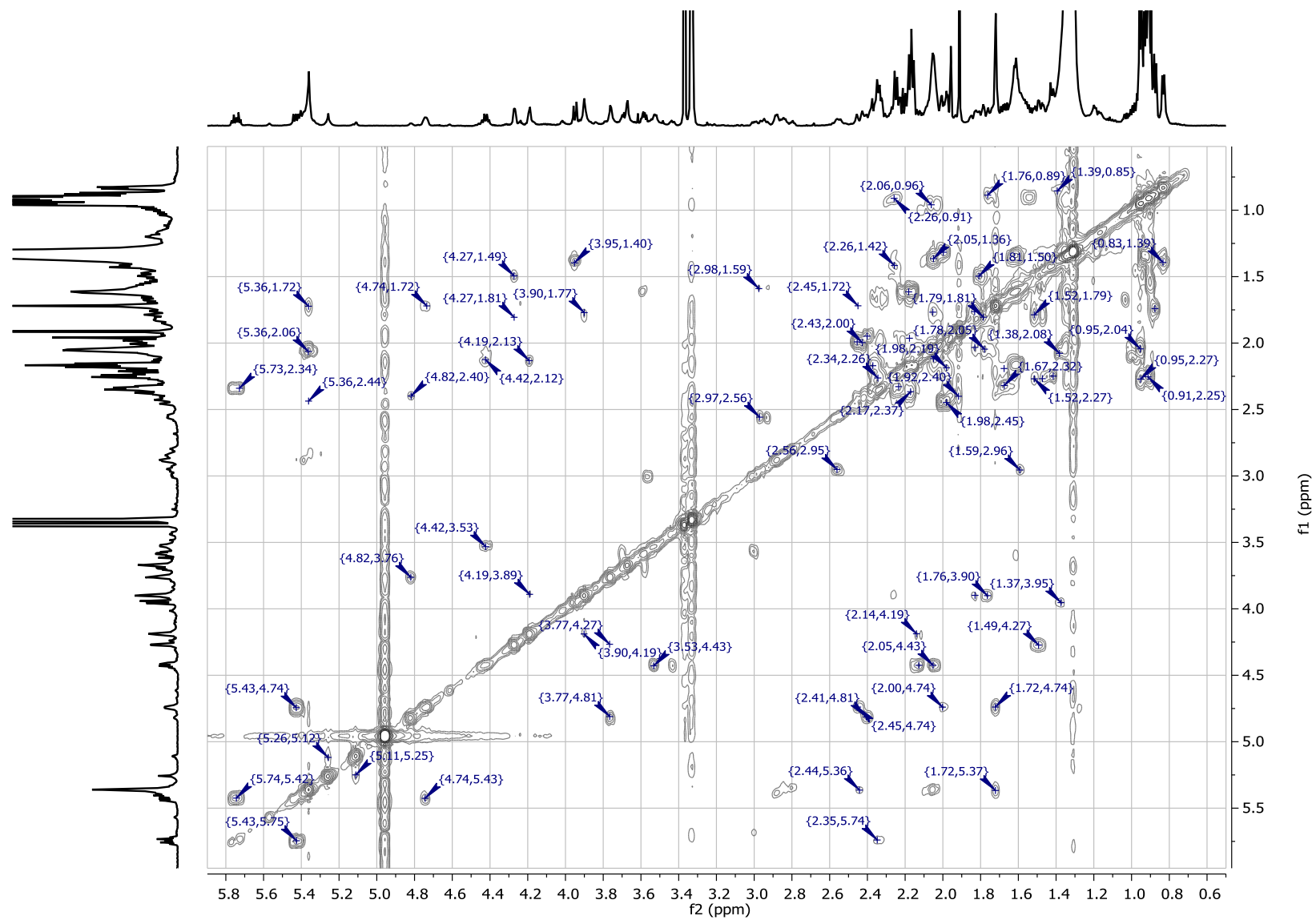


Figure 9.69: multiple quantum filtered 2D-DOSY spectra of AZA-40 (600 MHz Proton frequency, d4-methanol).

Figure 9.70: 2D-DOSY spectra of AZA-40 (600 MHz Proton frequency, d₄-methanol).

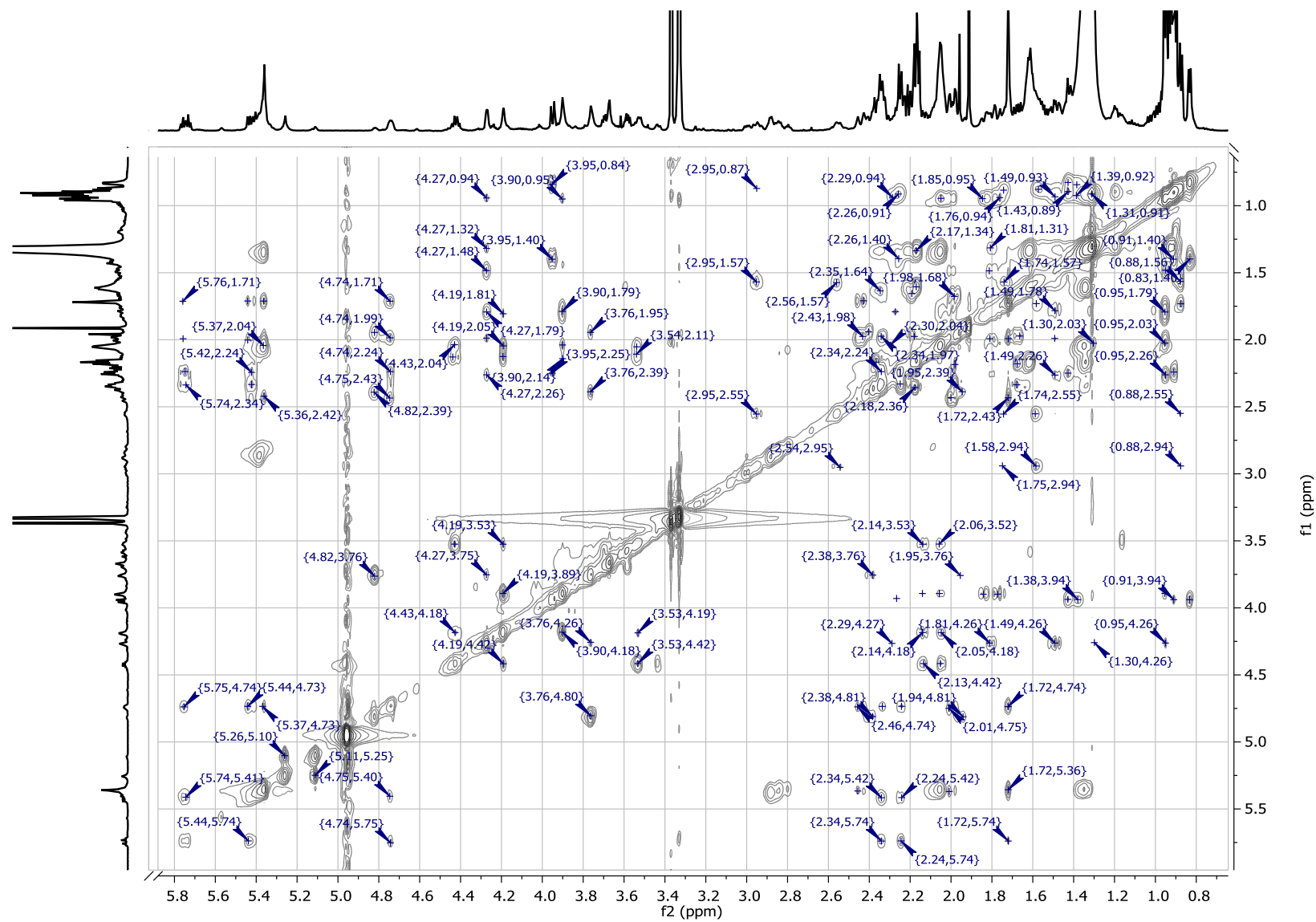
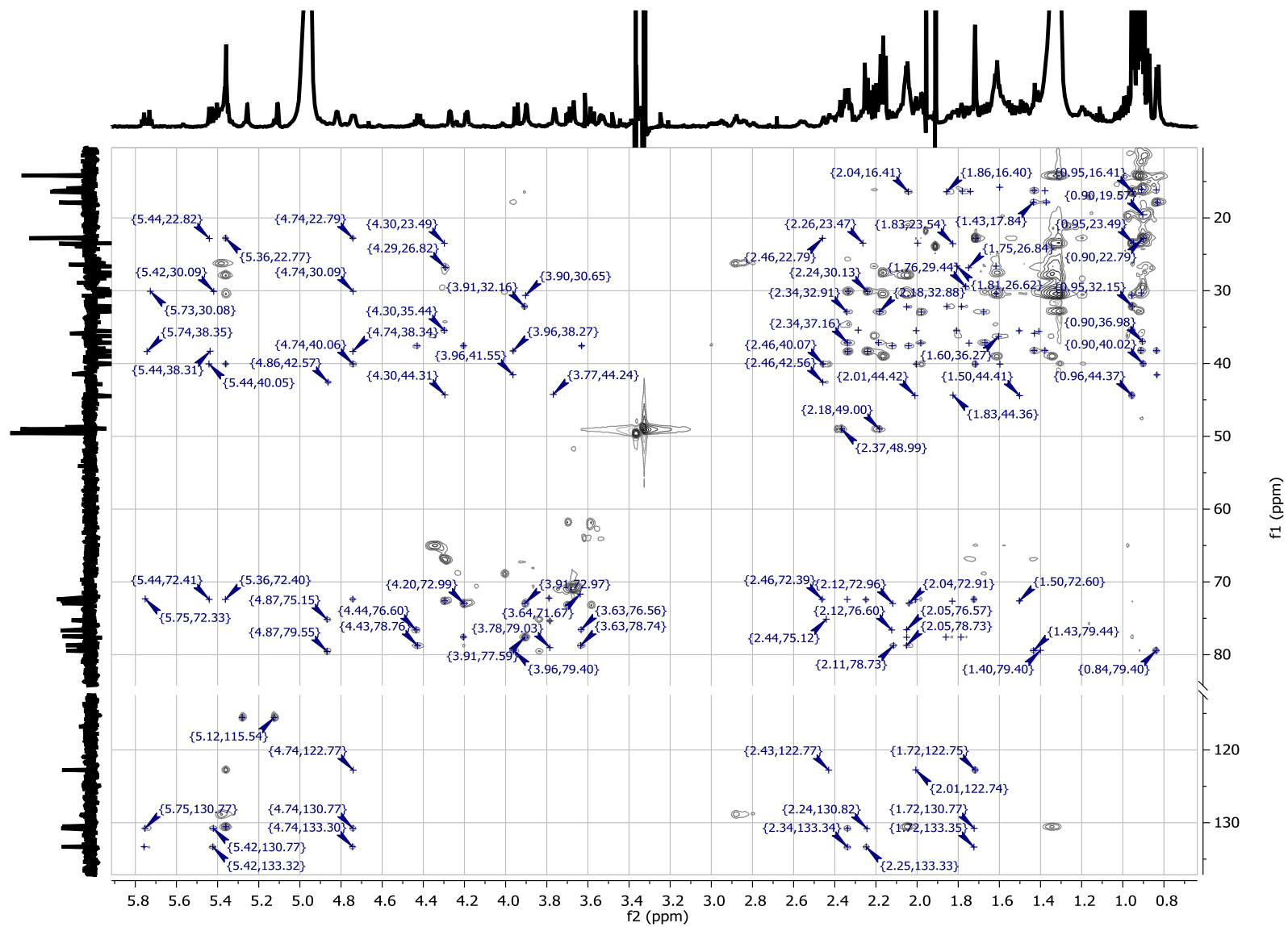


Figure 9.71: 2D-TOCSY spectra of AZA-40 (600 MHz Proton frequency, d₄-methanol).

Figure 9.72: 2D-HSQC-TOCSY spectra of AZA-40 (600 MHz Proton frequency, d₄-methanol).

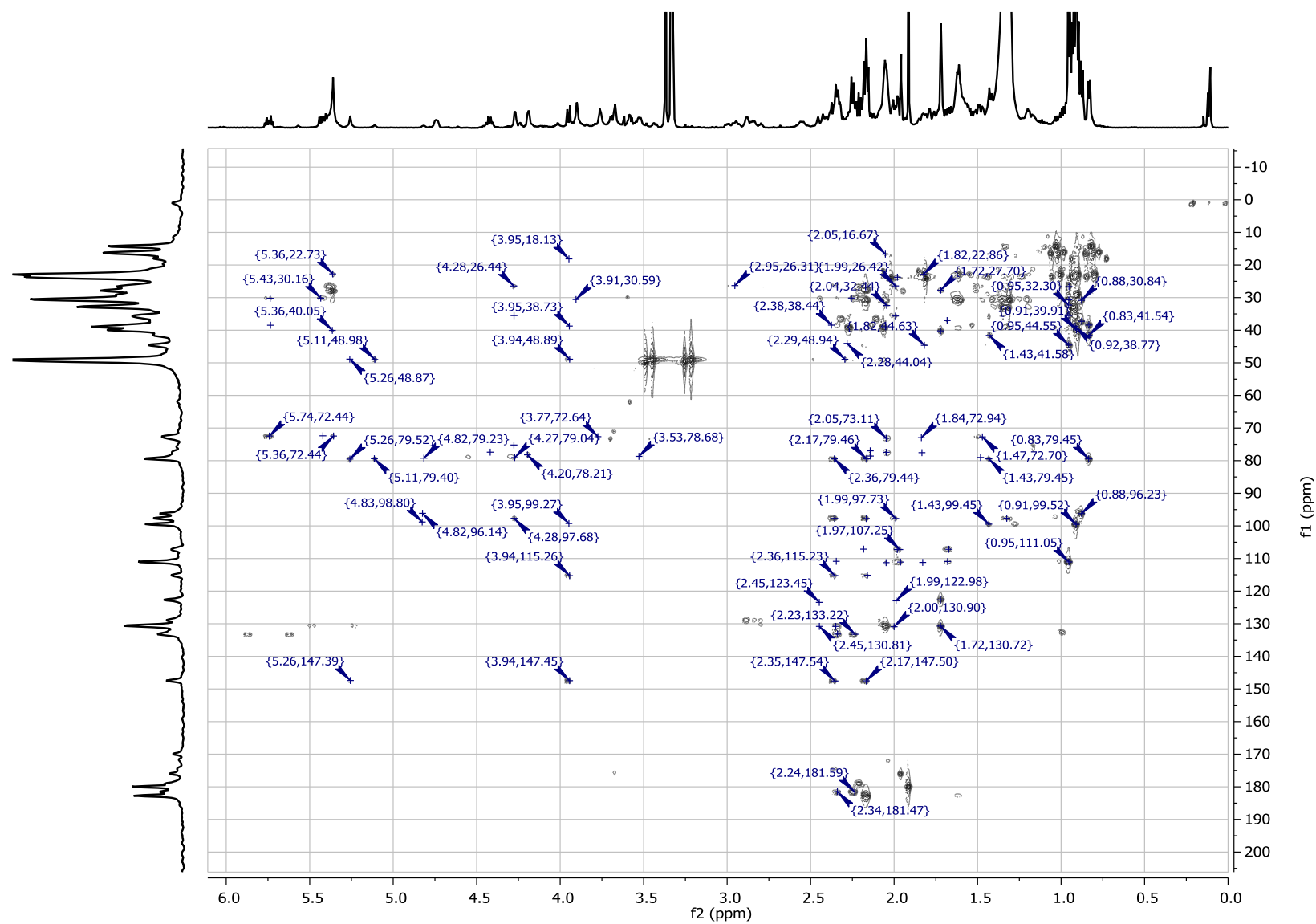


Figure 9.73: 2D-HMBC spectra of AZA-40 (600 MHz Proton frequency, d4-methanol).

9.2.2 NMR-spectra of AZA-59 (10)

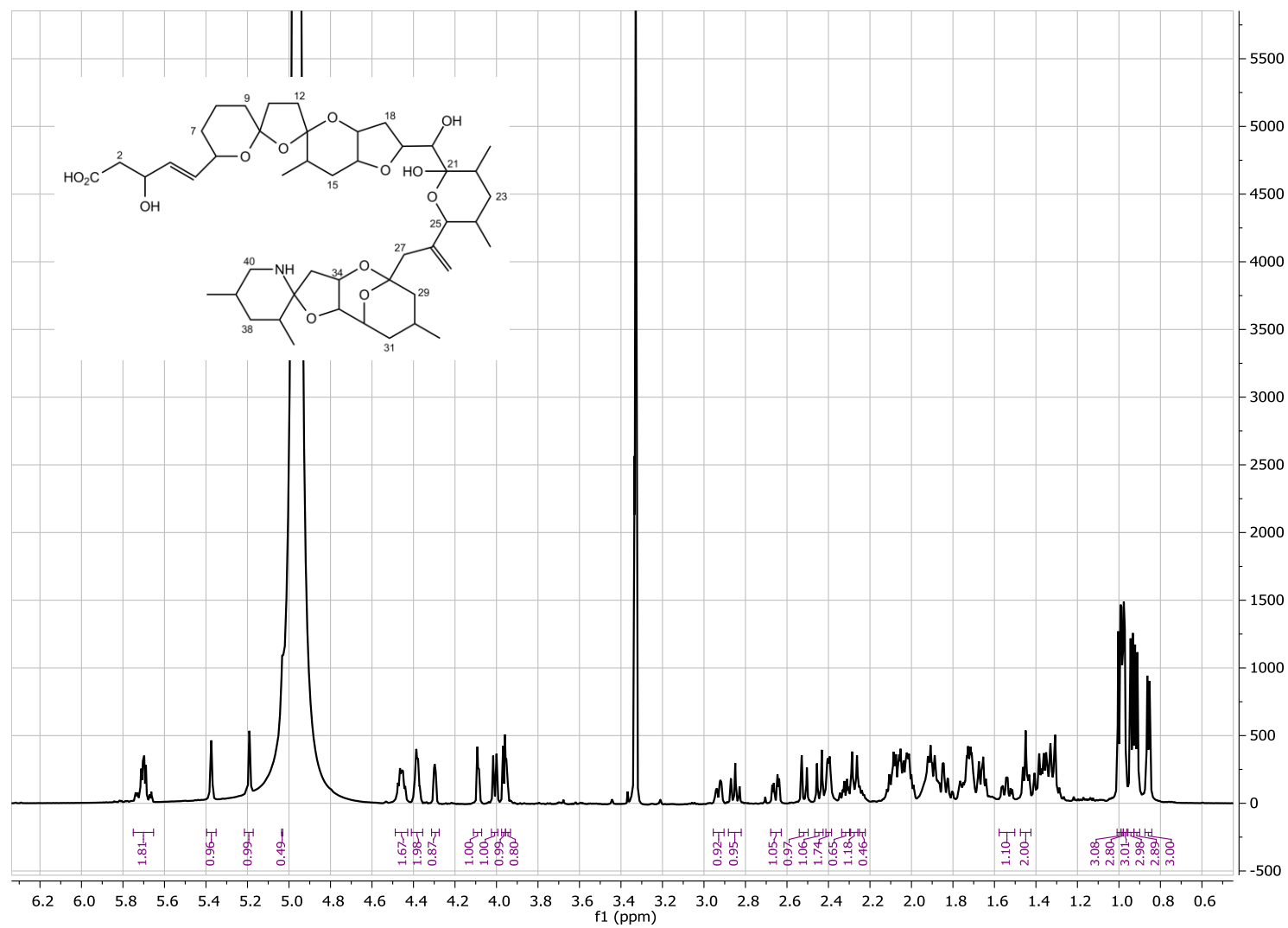


Figure 9.74: Structure and 1D proton spectra of AZA-59 (600 MHz, d4-methanol).

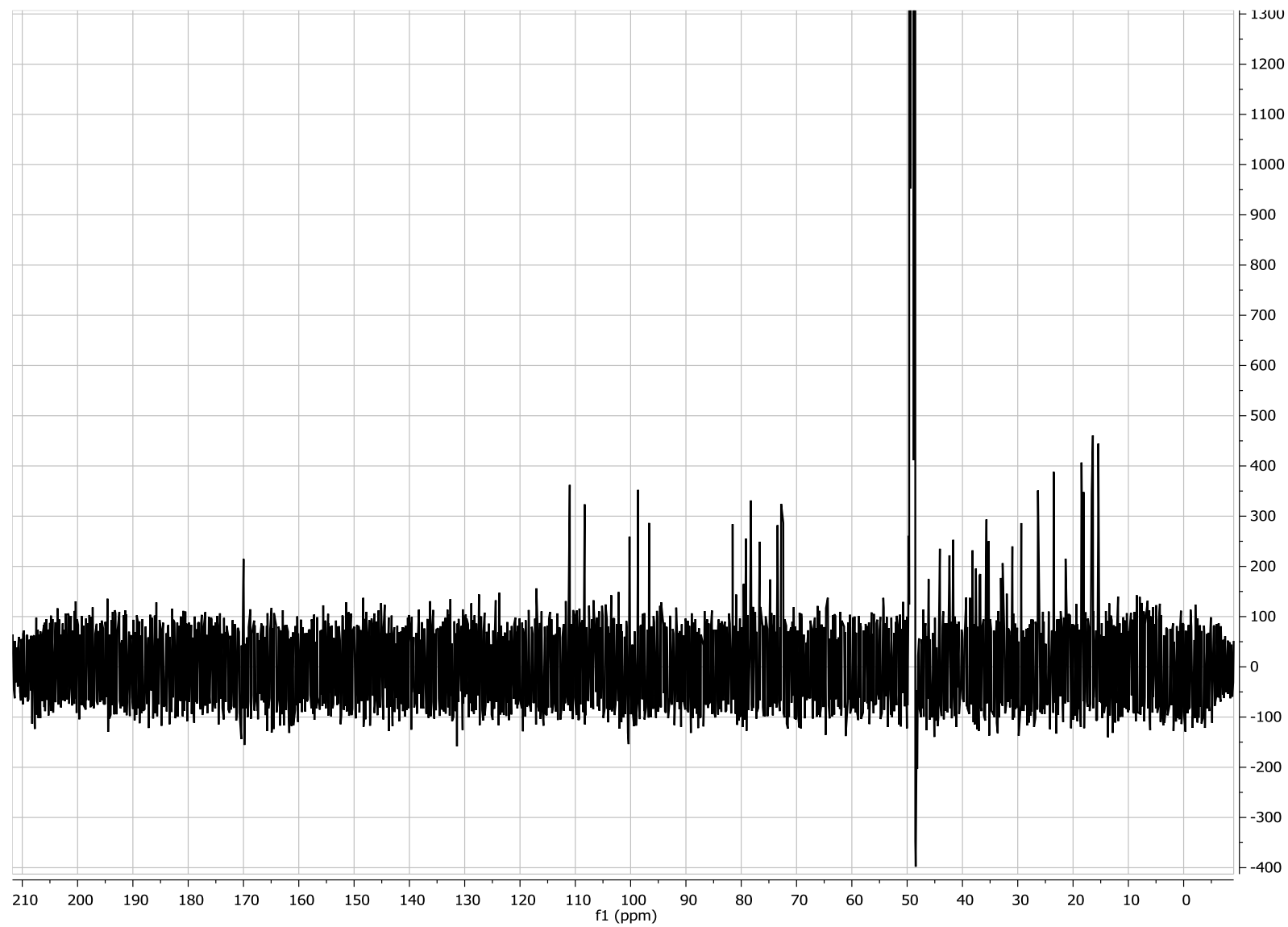


Figure 9.75: 1D carbon spectra of AZA-59 (150 MHz, d₄-methanol).

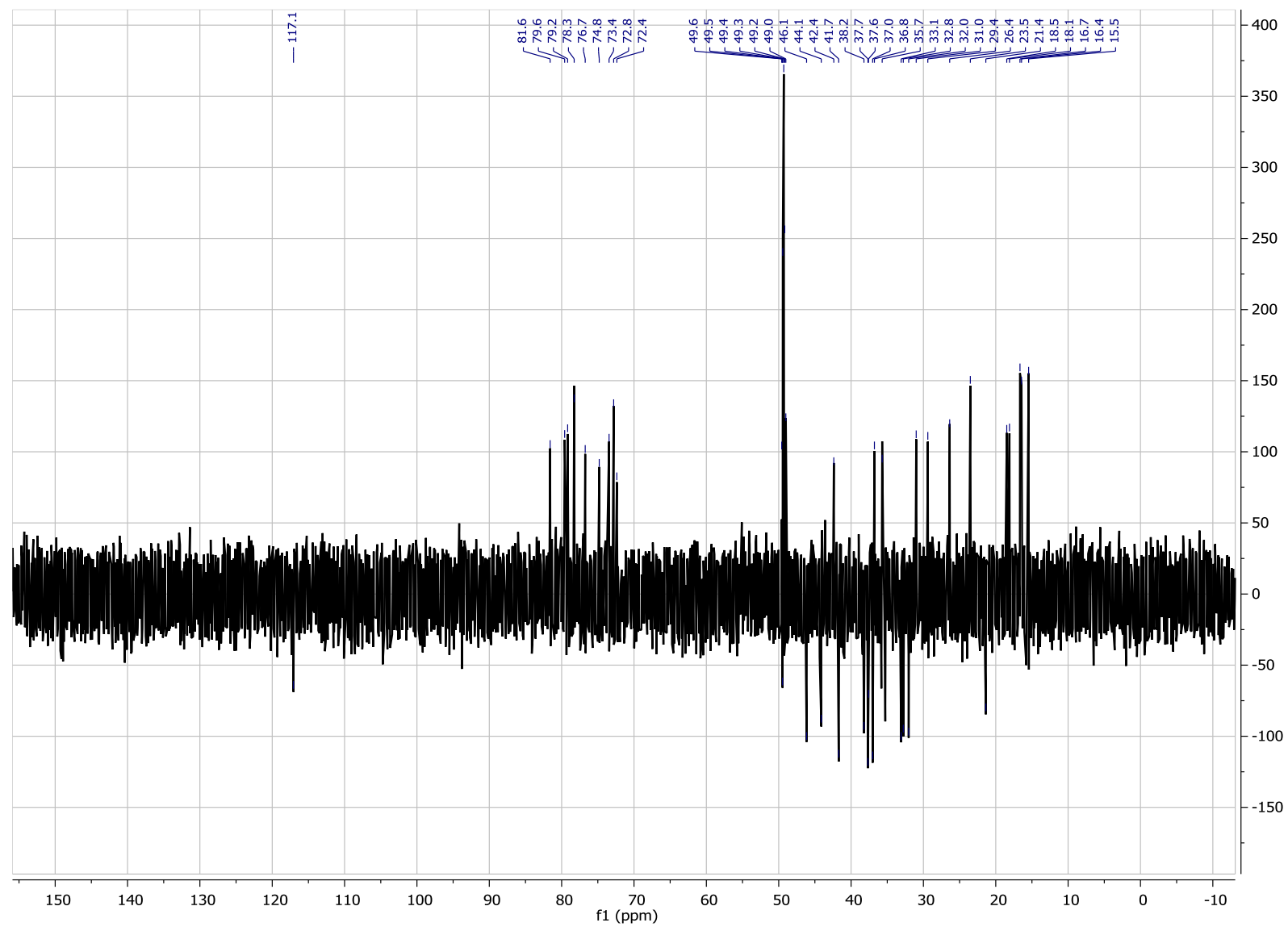


Figure 9.76:1D DEPT spectra of AZA-59 (150 MHz, d₄-methanol).

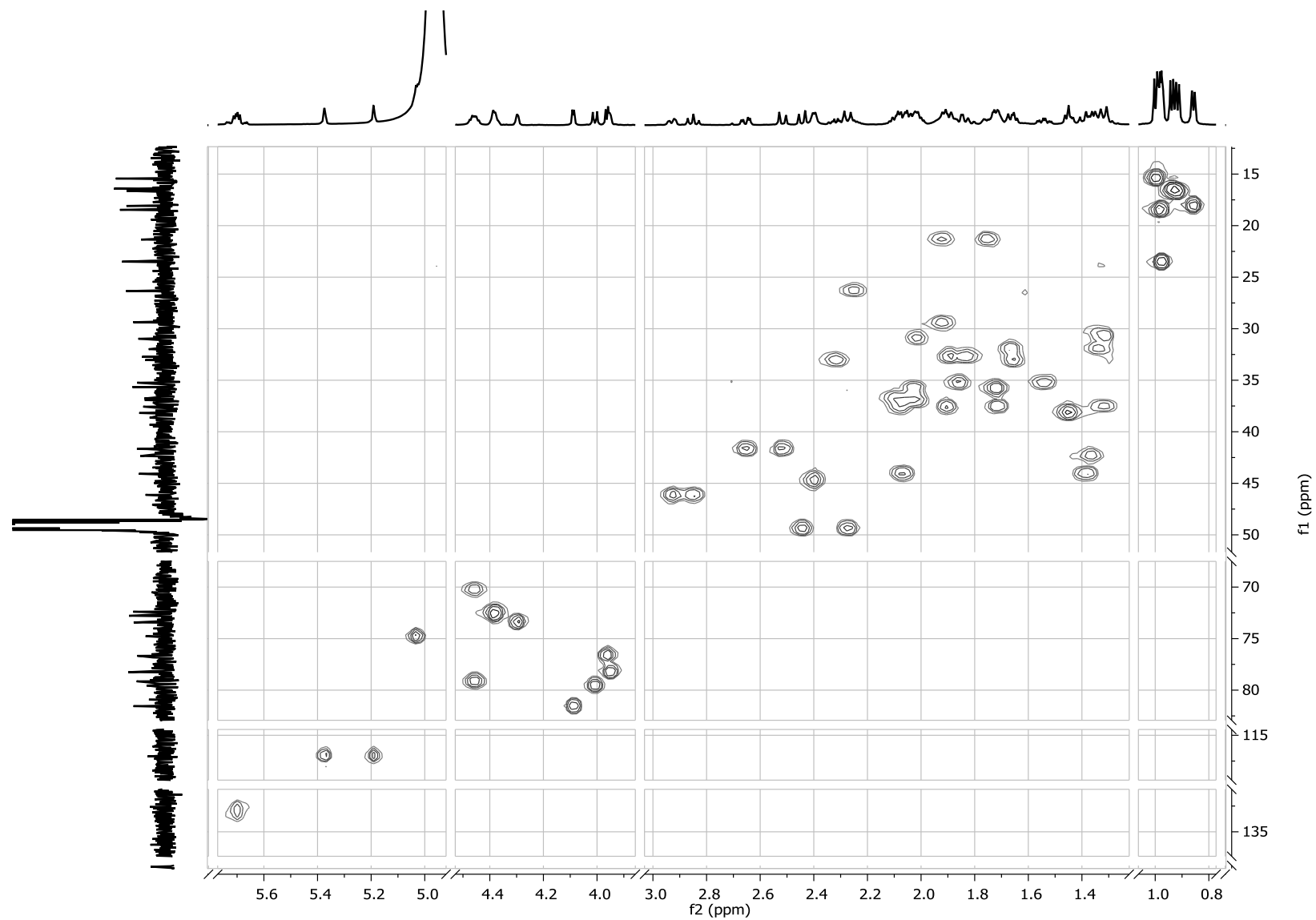


Figure 9.77: 2D HSQC spectra of AZA-59 (600 MHz Proton frequency, d₄-methanol, cf. Figure 9.78 and Figure 9.79 for picked peaks).

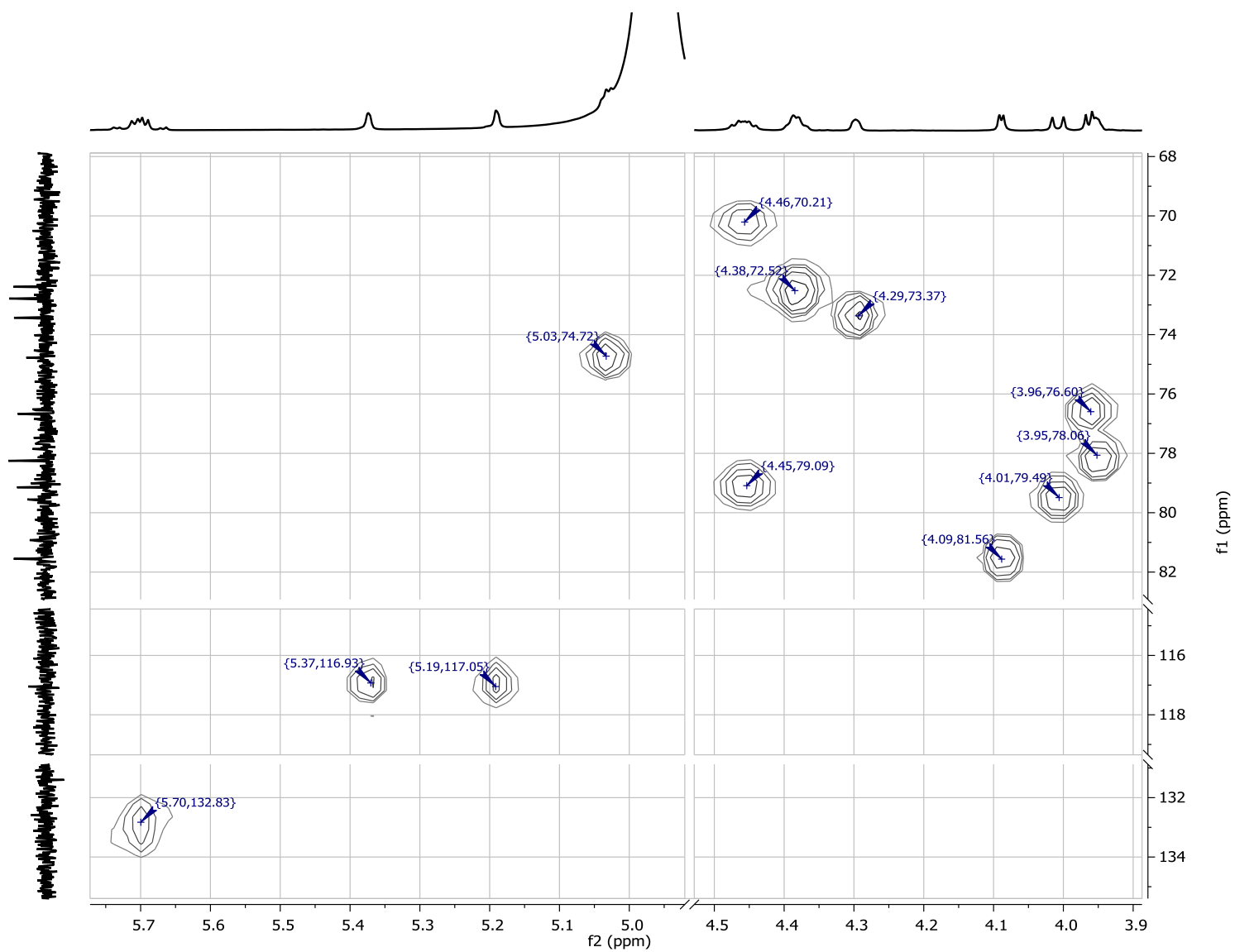


Figure 9.78: Slice of 2D HSQC spectra of AZA-59 (600 MHz Proton frequency, d₄-methanol).

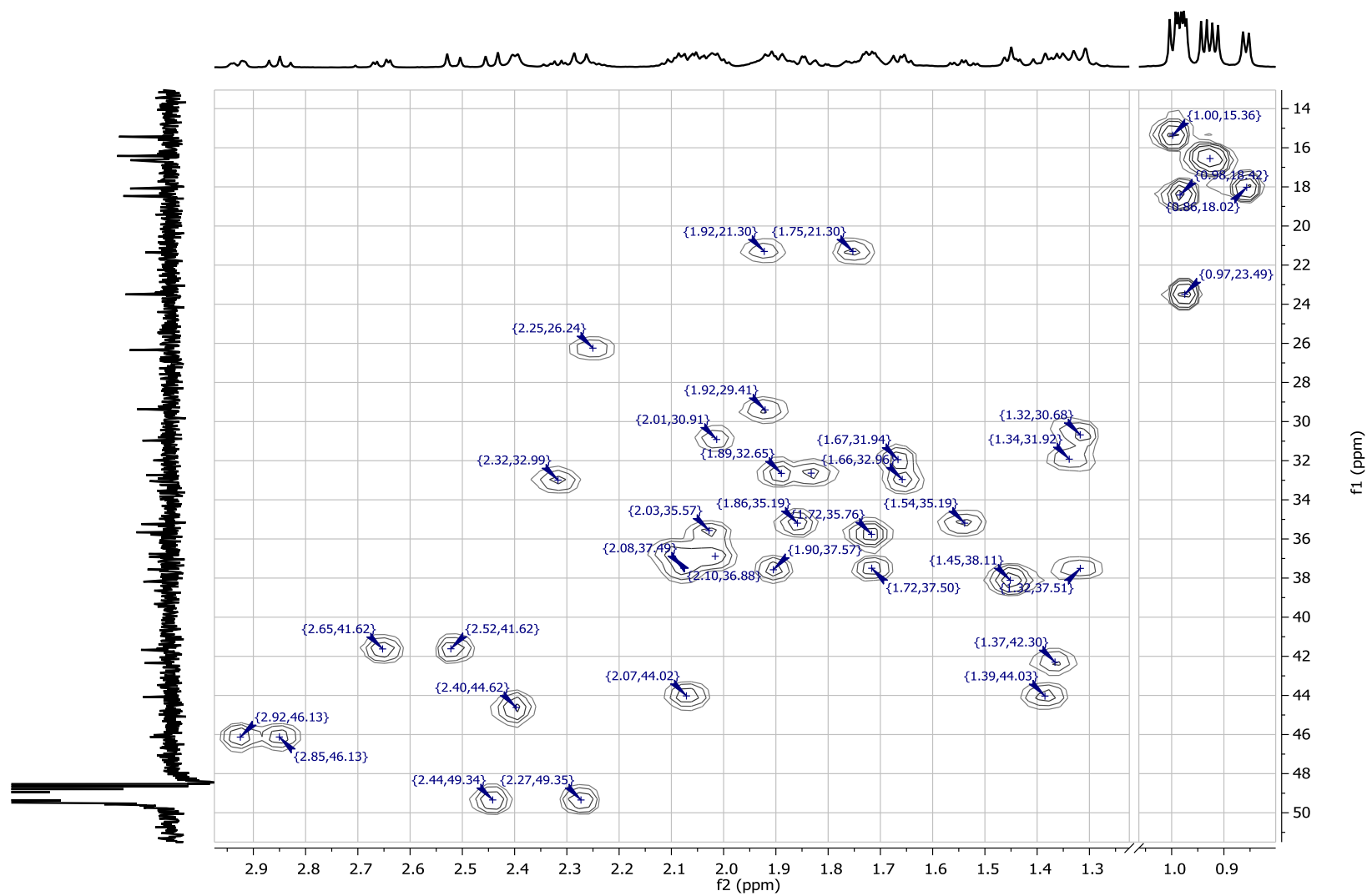


Figure 9.79: Slice of 2D HSQC spectra of AZA-59 (600 MHz Proton frequency, d₄-methanol).

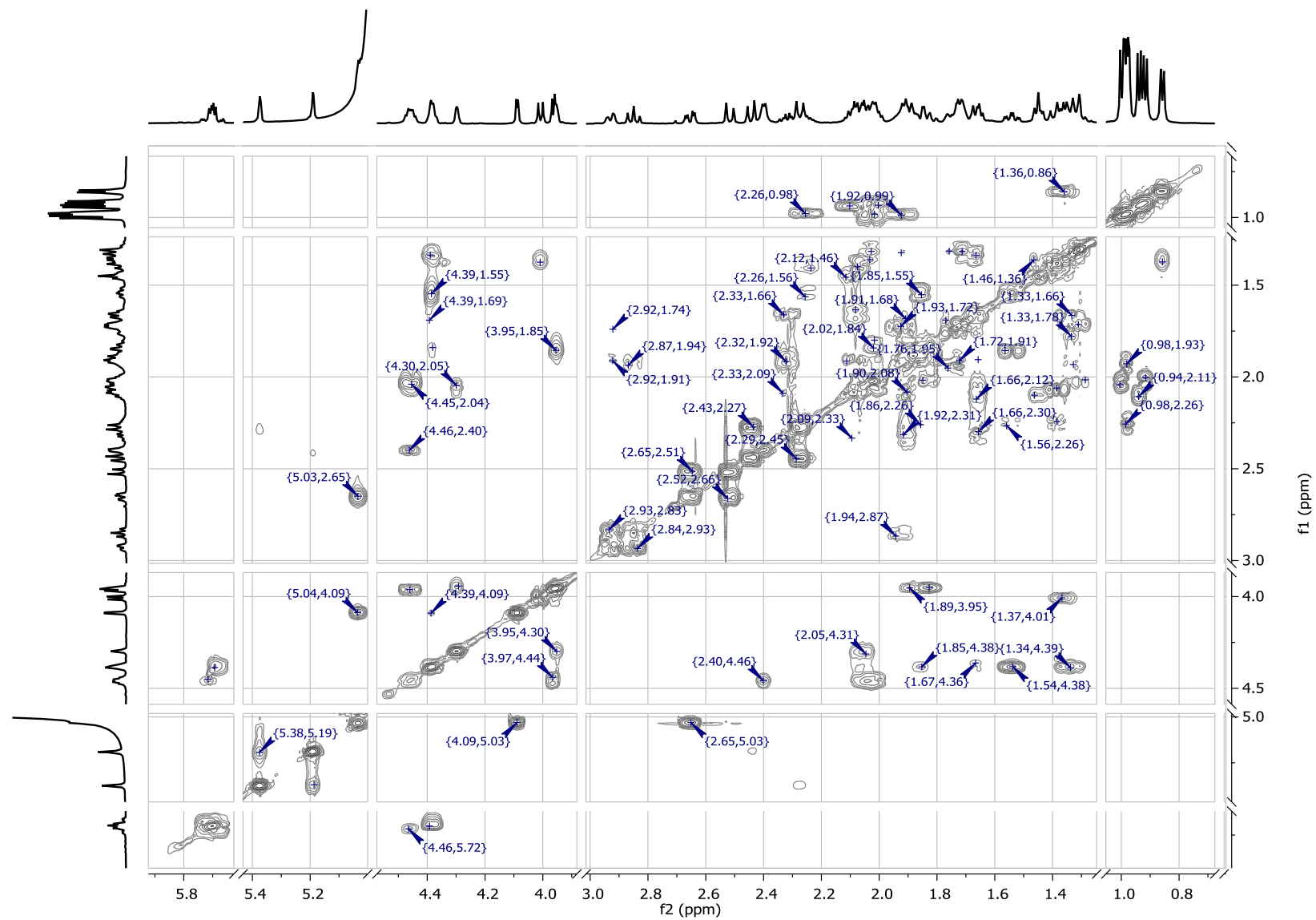


Figure 9.80: 2D COSY spectra of AZA-59 (600 MHz Proton frequency, d4-methanol).

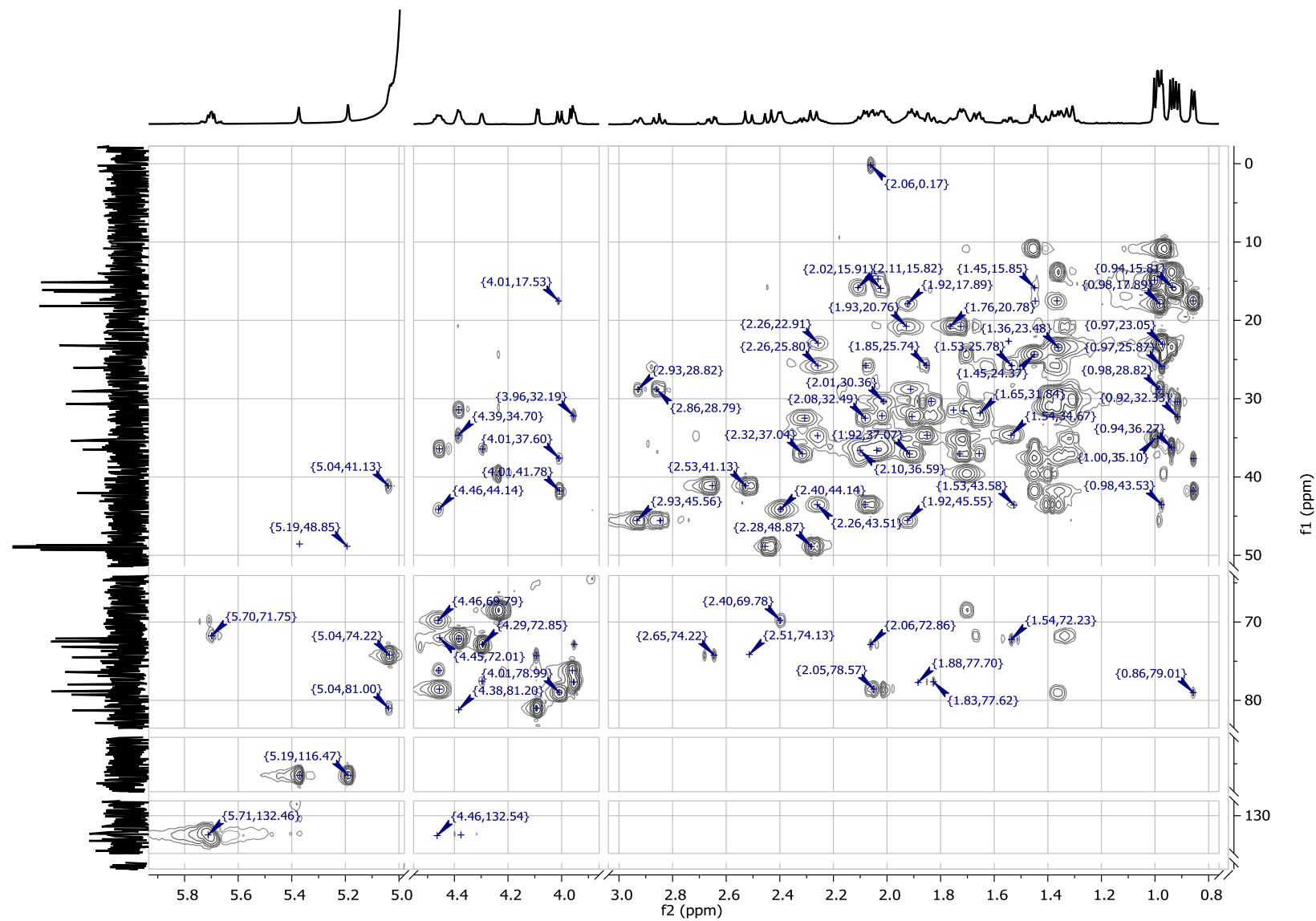


Figure 9.81: 2D HSQC-TOCSY spectra of AZA-59 (600 MHz Proton frequency, d4-methanol, mixing time 10 ms).

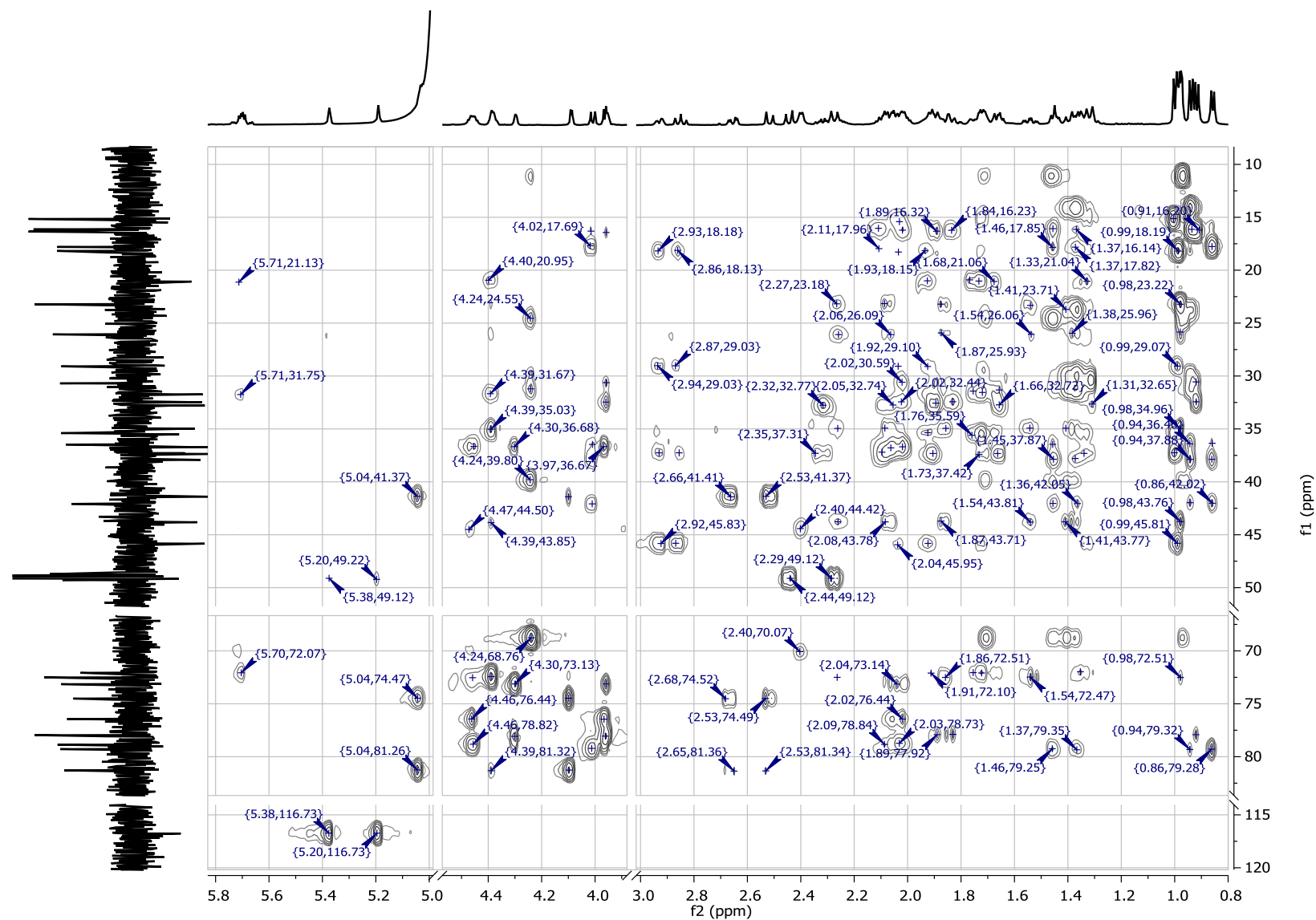


Figure 9.82: 2D HSQC-TOCSY spectra of AZA-59 (600 MHz Proton frequency, d4-methanol, mixing time 60 ms).

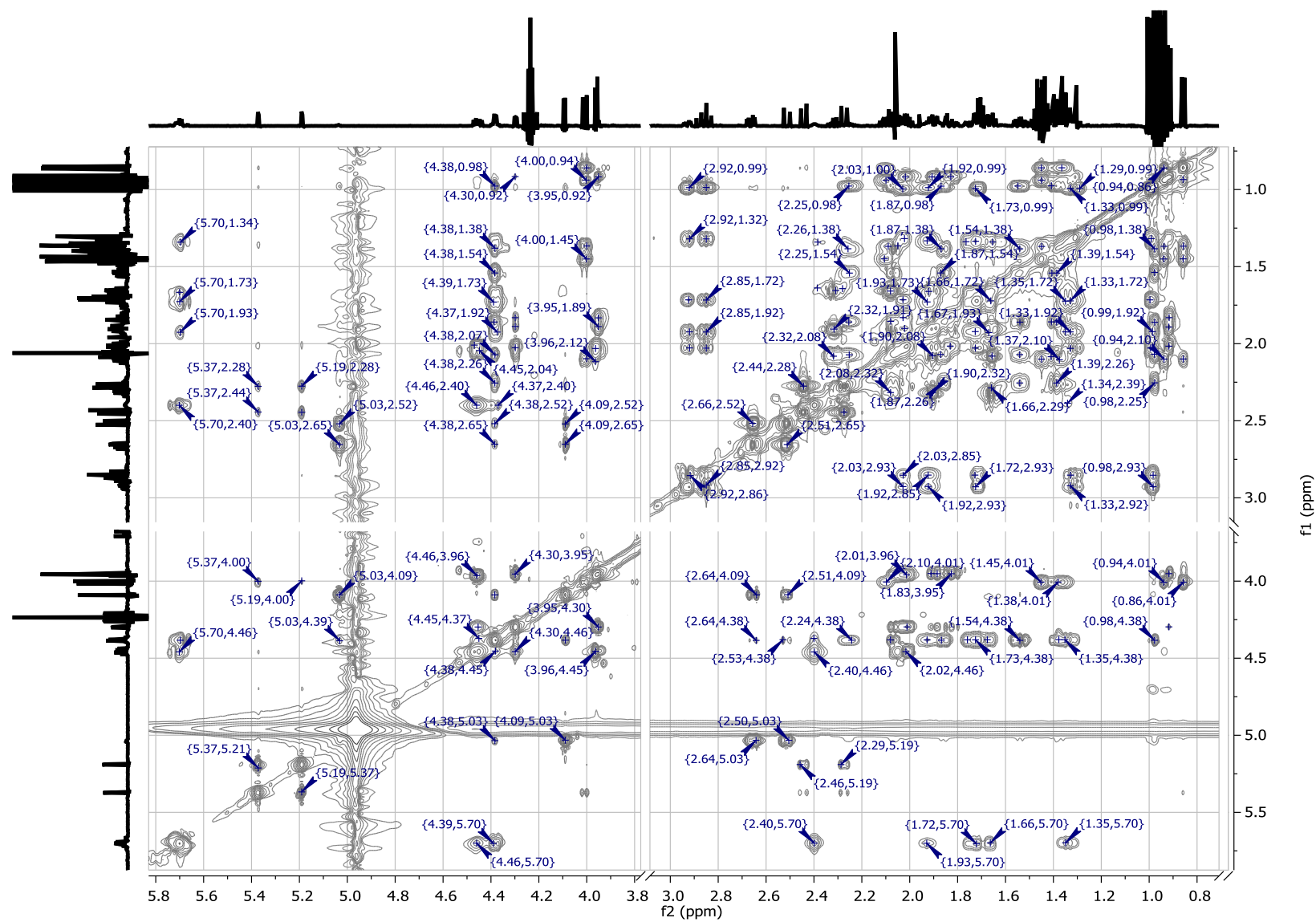


Figure 9.83: 2D HSQC-TOCSY spectra of AZA-59 (600 MHz Proton frequency, d4-methanol, contaminated with a phthalate ester).

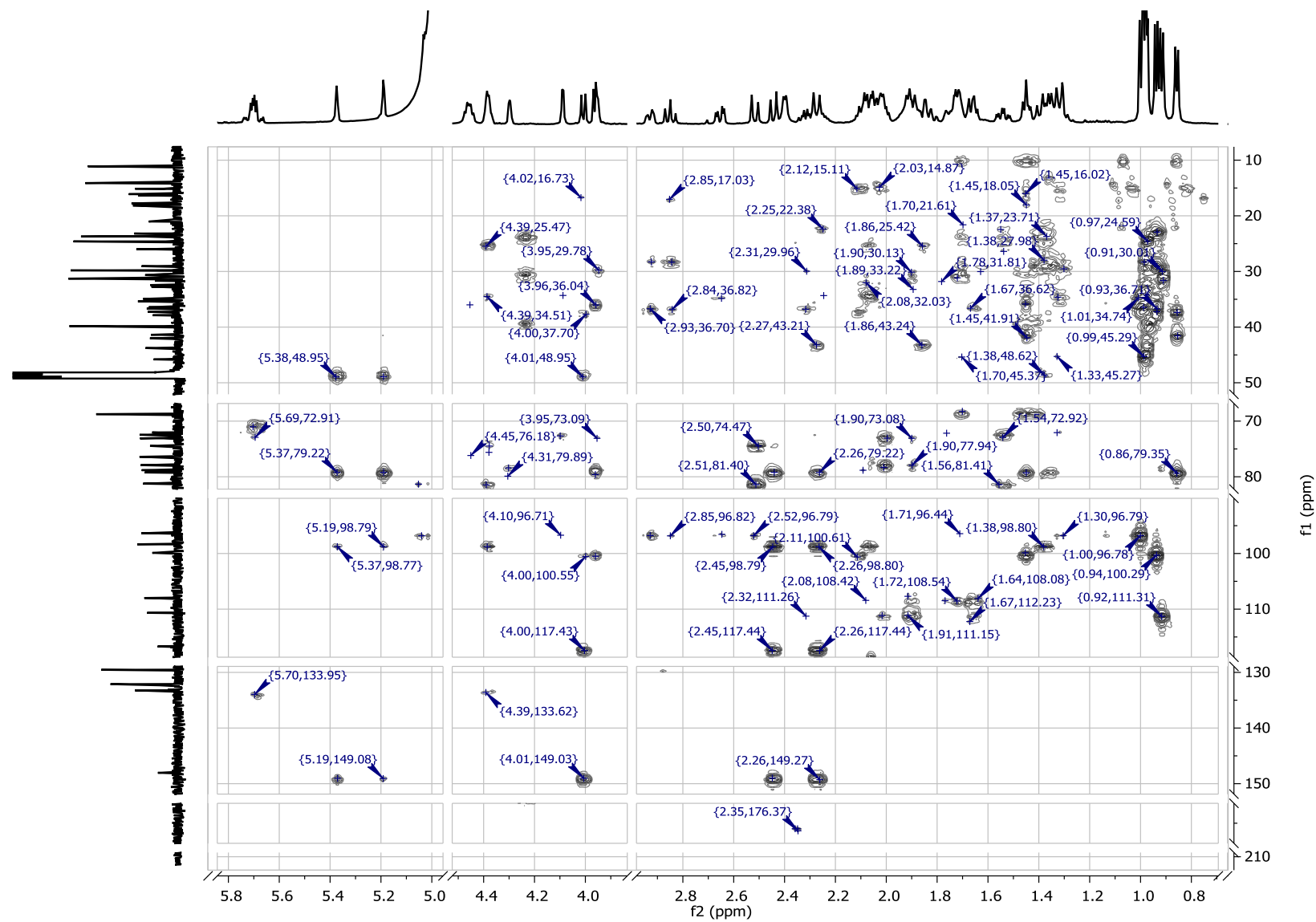


Figure 9.84: 2D HMBC spectra of AZA-59 (600 MHz Proton frequency, d4-methanol).

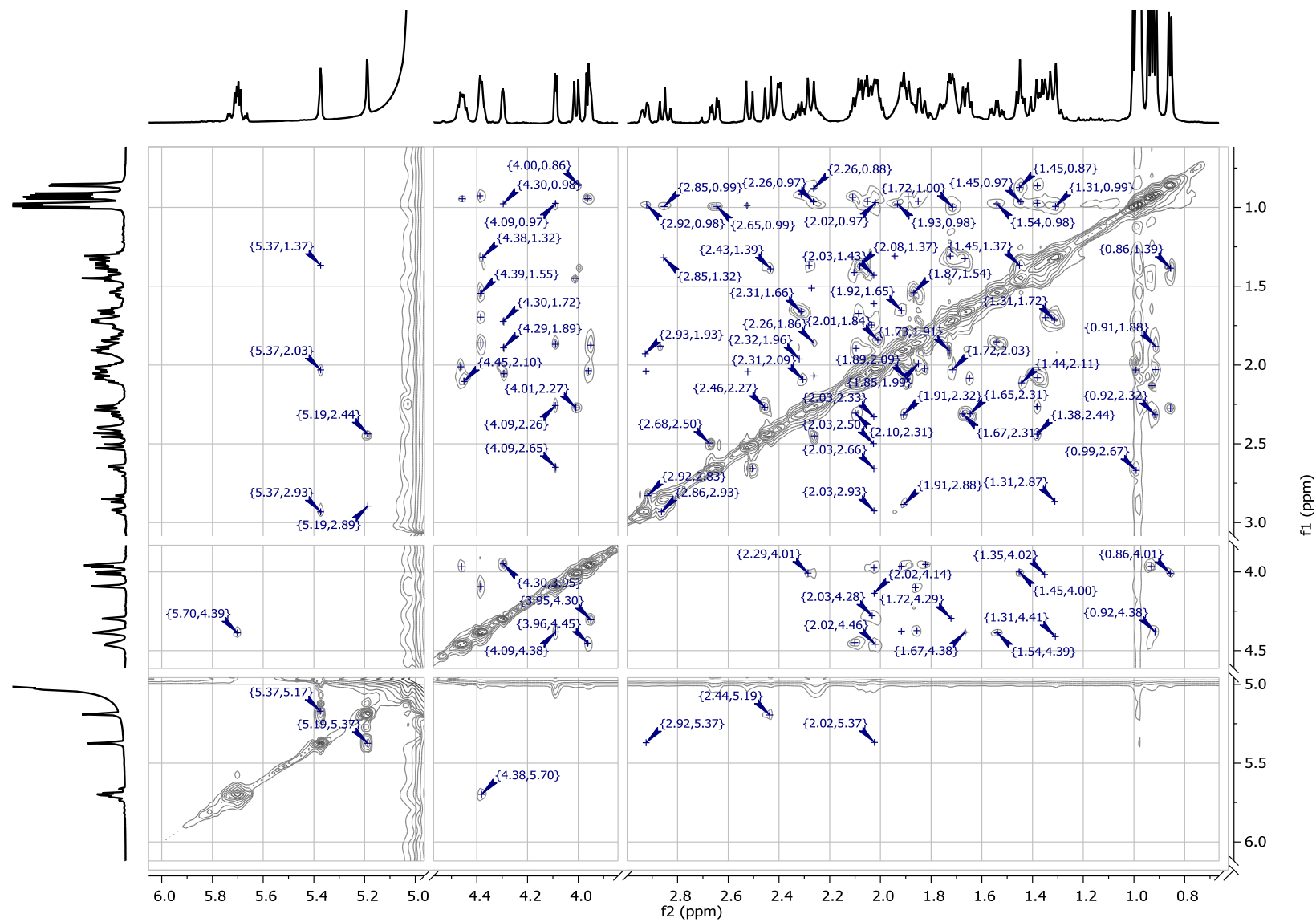


Figure 9.85: 2D ROESY spectra of AZA-59 (600 MHz Proton frequency, d4-methanol).

9.3 Full relative assignment of stereochemistry and conformational analysis of GYM_s and SPX_s by NMR- and molecular modeling-based techniques

9.3.1 16-desmethyl GYM D (11)

Table 9.1: Simulated and measured chemical shifts of 16-desmethyl GYM D.

No.	Nuc.	C-4, C-10, C-17: S C-13, C-14 : R		C-10, C-17: S C-4, C-13, C-14: R		C-4, C-13, C-14: S; C-10, C-17: R		measured
		CPCM	no CPCM	CPCM	no CPCM	CPCM	no CPCM	
1	C	172.3	171.8	171.6	169.2	171.7	169.2	175.5
2	C	129.0	129.6	129.7	133.1	128.9	132.2	130.2
3	C	149.8	147.6	148.2	144.5	149.2	145.0	148.6
4	C	82.5	81.9	80.8	79.2	81.0	80.5	81.6
5	C	123.5	125.9	126.2	129.2	124.2	126.5	125.9
6	C	139.9	138.4	142.6	139.6	141.2	137.9	136
7	C	43.2	43.4	43.0	43.6	44.6	44.5	43.6
8	C	30.2	30.3	25.2	27.0	30.5	31.0	31.8
9	C	72.4	72.7	73.1	74.3	77.1	76.3	71.6
10	C	81.4	82.1	80.8	83.3	84.7	86.4	83.4
11	C	25.7	26.4	26.5	27.0	29.8	29.0	27
12	C	29.7	29.9	29.2	29.1	28.7	29.9	24.9
13	C	79.9	80.5	79.4	80.1	78.5	80.0	78.6
14	C	79.5	79.3	79.2	81.6	83.4	85.1	82.5
15	C	27.7	27.8	27.4	27.2	26.8	27.5	29.4
16	C	32.1	32.4	31.7	29.7	26.9	27.4	32.1
17	C	82.6	82.8	82.0	82.6	81.8	83.0	82.9
18	C	136.4	137.9	136.4	136.6	134.9	135.2	133.1
19	C	123.6	123.9	122.6	125.1	121.0	124.6	124.9
20	C	23.2	24.6	23.0	22.7	22.2	22.8	21.9
21	C	32.7	32.3	32.0	32.6	34.4	34.4	31.8
22	C	173.3	173.3	172.0	171.7	172.1	172.4	173.3
23	C	46.8	45.5	48.4	45.8	47.2	45.8	42.7
24	C	32.4	32.1	36.4	36.1	34.5	31.7	33.6
25	C	20.8	20.4	22.5	20.6	20.3	19.3	19.7
26	C	10.9	10.3	10.5	10.2	9.2	10.3	11
27	C	17.4	18.7	14.3	14.0	15.0	14.6	18.1
29	C	13.9	13.8	13.6	13.4	13.1	13.7	15.3

No.	Nuc.	C-4, C-10, C-17: S C-13, C-14 : R		C-10, C-17: S C-4, C-13, C-14: R		C-4, C-13, C-14: S; C-10, C-17: R		measured
		CPCM	no CPCM	CPCM	no CPCM	CPCM	no CPCM	
30	C	23.1	22.6	29.9	29.1	26.4	22.0	26
31	C	20.5	19.8	19.7	20.6	19.0	19.3	20.5
32	C	51.4	49.6	50.1	49.3	49.6	50.5	50.3
3	H	7.02	7.07	7.02	6.84	7.22	6.87	7.05
4	H	6.13	5.78	6.11	5.95	6.18	5.87	5.93
7	H	3.34	3.41	3.28	3.34	2.96	3.17	3.16
8	H	1.36	1.57	1.40	1.64	1.74	1.54	1.43
8	H	1.88	1.63	2.03	1.79	1.78	1.85	1.9
9	H	4.17	4.20	3.77	3.60	3.43	3.57	3.66
10	H	4.21	4.29	4.32	4.14	3.58	3.62	3.94
11	H	1.85	1.80	1.93	1.83	1.72	1.83	1.56
11	H	1.96	2.03	2.10	1.97	2.05	1.86	1.79
12	H	1.88	1.86	1.87	1.87	2.06	2.09	1.77
12	H	1.95	1.97	2.00	2.19	2.17	2.10	1.77
13	H	3.76	3.87	3.86	3.99	4.11	4.08	4.36
14	H	4.01	4.00	4.01	3.93	3.89	3.81	4.13
15	H	1.71	1.74	1.72	1.75	1.59	1.46	1.76
15	H	1.96	1.97	2.00	1.88	1.86	2.01	1.99
16	H	1.76	1.76	1.77	1.79	2.03	1.93	1.79
16	H	2.18	2.21	2.22	2.23	2.19	2.25	1.79
17	H	4.30	4.30	4.33	4.41	4.38	4.39	4.15
19	H	5.51	5.52	5.54	6.00	5.96	6.26	5.99
20	H	2.01	1.99	2.06	2.07	2.27	2.16	2.1
20	H	2.63	2.81	2.75	2.85	2.40	2.57	3
21	H	2.39	2.22	2.48	2.50	2.50	2.55	2.76
21	H	2.70	2.98	2.81	2.85	2.67	2.57	2.76
24	H	1.75	1.50	1.12	1.07	1.35	1.67	1.37
24	H	1.79	1.75	1.88	1.79	1.80	1.67	1.59
25	H	1.58	1.40	1.75	1.80	1.72	1.42	1.94
25	H	2.04	2.02	2.01	1.95	1.88	2.17	1.49
26	H	1.92	1.92	2.00	1.94	1.94	1.84	1.99
26	H	1.96	1.99	2.00	1.96	2.03	1.95	1.99
26	H	2.12	2.11	2.13	2.00	2.03	1.96	1.99
27	H	1.74	1.78	1.79	1.70	1.93	1.66	1.92

No.	Nuc.	C-4, C-10, C-17: S C-13, C-14 : <i>R</i>		C-10, C-17: S C-4, C-13, C-14: R		C-4, C-13, C-14: S; C-10, C-17: <i>R</i>		measured
		CPCM	no CPCM	CPCM	no CPCM	CPCM	no CPCM	
27	H	1.82	2.01	1.94	2.17	2.00	1.90	1.92
27	H	2.52	2.24	2.49	2.18	2.23	2.62	1.92
29	H	1.40	1.42	1.43	1.40	1.61	1.34	1.61
29	H	1.50	1.45	1.50	1.52	1.67	1.84	1.61
29	H	2.12	2.19	2.20	2.23	2.07	2.10	1.61
30	H	1.47	1.42	1.28	1.32	1.48	1.44	1.44
30	H	1.80	1.72	1.60	1.69	1.57	1.82	1.54
31	H	1.52	1.50	1.50	1.51	1.54	1.52	1.47
31	H	1.68	1.82	1.57	1.55	1.59	1.59	1.47
32	H	3.40	3.57	3.35	3.57	3.56	3.62	3.48
32	H	3.71	3.74	3.63	3.79	3.78	3.98	3.71

9.3.2 GYM E (12)

Table 9.2: Simulated and measured chemical shifts of GYM E.

No.	Nuc.	C-4: S; C-19: R	C-4, C-19: S	C-4: R; C-19: S	measured
1	C	174.2	173.8	174.5	
2	C	136.3	136.0	137.8	
3	C	149.2	149.3	149.3	149.8
4	C	81.4	80.5	80.4	81.0
5	C	132.9	133.9	134.6	
6	C	141.8	142.3	144.6	
7	C	43.8	43.8	43.3	44.5
8	C	30.6	31.3	31.0	30.3
9	C	73.2	74.3	74.4	74.9
10	C	84.4	85.7	85.5	84.5
11	C	26.0	28.5	28.9	29.0
12	C	28.6	27.6	27.5	25.2
13	C	83.5	81.7	81.8	81.1
14	C	81.1	81.7	82.1	81.6
15	C	30.1	29.5	29.7	26.4
16	C	33.0	30.3	30.0	29.7
17	C	85.7	82.9	83.1	82.1
18	C	164.0	161.5	163.2	
19	C	69.7	74.3	74.2	73.4
20	C	27.7	33.0	32.1	36.9
21	C	28.6	28.3	28.6	32.4
22	C	179.4	178.7	179.2	
23	C	46.0	46.3	46.3	
24	C	36.9	35.8	35.4	30.3
25	C	20.5	20.0	20.0	19.9
26	C	10.0	7.9	9.5	10.7
27	C	15.0	14.6	14.3	17.3
29	C	107.4	106.6	106.9	109.2
30	C	29.1	28.9	29.0	25.2
31	C	20.3	19.2	18.8	20.2
32	C	50.1	50.2	49.9	50.3
3	H	6.74	6.88	6.74	6.93
4	H	5.86	5.81	5.85	5.88

No.	Nuc.	C-4: S; C-19: R	C-4, C-19: S	C-4: R; C-19: S	measured
7	H	3.32	3.11	3.23	3.11
8	H	1.47	1.31	1.23	1.22
8	H	1.60	1.97	1.90	1.74
9	H	3.96	3.46	3.47	3.66
10	H	4.32	4.04	4.03	3.92
11	H	1.81	1.82	1.88	1.74
11	H	1.88	2.04	2.09	1.74
12	H	1.71	1.72	1.73	1.52
12	H	1.99	2.13	2.09	1.73
13	H	3.71	3.96	3.96	4.12
14	H	4.15	4.07	4.11	3.89
15	H	1.99	1.77	1.80	1.56
15	H	2.12	2.23	2.29	1.76
16	H	2.03	2.23	2.25	1.84
16	H	2.32	2.25	2.25	1.84
17	H	4.96	4.92	4.94	4.21
19	H	4.62	4.72	4.70	4.58
20	H	1.61	1.85	1.77	2.36
20	H	2.40	2.40	2.41	2.36
21	H	2.20	2.19	2.25	2.79
21	H	2.88	2.34	2.43	2.79
24	H	1.19	1.24	1.08	1.30
24	H	1.78	1.64	1.75	1.51
25	H	1.54	1.57	1.70	1.42
25	H	2.07	1.88	1.86	1.88
26	H	1.85	1.86	1.90	1.85
26	H	1.96	1.91	2.01	1.85
26	H	1.96	2.21	2.03	1.85
27	H	1.70	1.74	1.62	2.03
27	H	2.06	1.83	2.05	2.03
27	H	2.16	2.22	2.19	2.03
29	H	4.96	5.11	5.13	5.00
29	H	5.01	5.34	5.28	5.69
30	H	1.37	1.35	1.24	1.62
30	H	1.94	1.85	1.77	1.72
31	H	1.47	1.55	1.54	1.24

No.	Nuc.	C-4: S; C-19: R	C-4, C-19: S	C-4: R; C-19: S	measured
31	H	1.51	1.67	1.62	1.36
32	H	3.45	3.71	3.69	3.30
32	H	3.84	3.78	3.82	3.75

9.3.3 13-desmethyl SPX C (4)

Table 9.3: Simulated and measured chemical shifts of 13-desmethyl SPX C (measured data taken from Hu *et al.* 2001).

No.	Nuc.	C-4: S		C-4: R	C-4: S cation	C-4: R cation	measured*
		no CPCM	CPCM	CPCM	CPCM	CPCM	
1	C	173.1	176.3	175.5	172.2	171.6	176.8
2	C	135.6	131.7	131.9	129.7	130.3	131
3	C	148.0	153.1	154.1	150.0	150.4	149.5
4	C	81.6	84.1	82.3	82.5	81.0	82
5	C	131.1	126.6	126.3	125.3	124.5	126.4
6	C	139.1	140.8	144.0	136.7	140.2	133.2
7	C	51.4	50.5	50.5	51.1	51.0	48.1
8	C	123.2	125.3	125.6	117.8	117.1	122.5
9	C	148.6	145.6	145.1	146.3	146.0	146
10	C	77.8	79.4	79.1	76.6	76.3	76.8
11	C	40.6	43.7	43.6	40.0	40.1	45.2
12	C	83.7	81.0	80.4	82.9	82.9	79.8
13	C	32.4	31.2	31.0	33.5	33.3	32.8
14	C	38.1	39.3	39.3	37.6	37.6	38.2
15	C	121.6	120.7	120.2	119.2	119.0	118.1
16	C	34.5	34.3	34.2	34.6	34.7	35.2
17	C	31.1	31.8	31.7	32.5	32.8	32.1
18	C	116.5	114.3	113.9	112.3	112.2	112.2
19	C	71.7	72.3	72.0	71.8	71.6	71.1
20	C	36.9	36.6	36.5	36.5	36.5	35.7
21	C	28.7	28.5	28.4	29.0	28.9	29.9
22	C	70.1	69.4	69.2	68.6	68.6	69.1
23	C	47.8	46.9	47.0	47.0	46.6	46.3
24	C	155.2	155.1	154.8	149.8	149.6	145.6
25	C	33.4	35.0	35.2	33.1	32.9	34.6
26	C	20.9	21.3	22.5	20.5	20.5	21.8
27	C	34.4	35.0	35.1	36.4	36.2	36
28	C	179.0	179.5	179.0	204.1	203.7	201.3
29	C	52.7	53.3	52.9	54.8	55.0	52.4
30	C	37.4	37.3	37.0	36.5	36.4	36.7
31	C	36.3	37.0	36.6	37.6	37.7	37.5

No.	Nuc.	C-4: S		C-4: R	C-4: S cation	C-4: R cation	measured*
		no CPCM	CPCM	CPCM	CPCM	CPCM	
32	C	42.5	42.5	42.4	40.2	40.0	38.8
33	C	53.5	53.9	53.6	51.8	51.7	51.8
34	C	32.5	32.4	32.4	34.9	34.9	32.4
35	C	19.7	19.8	21.5	21.3	23.5	20.3
36	C	9.9	9.7	9.9	11.1	11.2	10.5
37	C	15.7	16.5	17.1	17.3	17.9	16.7
38	C	14.4	10.1	9.9	16.2	15.9	12.9
40	C	18.4	18.7	18.7	19.4	19.2	22.7
41	C	107.4	105.3	105.6	105.1	104.9	112.6
42	C	16.8	17.6	17.4	17.6	17.4	18.9
43	C	18.2	18.4	18.2	20.0	20.0	20.1
3	H	6.63	6.96	6.99	6.90	6.95	7.13
4	H	5.75	5.97	5.96	5.92	5.89	5.98
7	H	3.59	3.58	3.59	3.72	3.74	3.78
8	H	5.19	5.20	5.22	4.95	4.99	5.16
10	H	4.26	4.01	4.00	4.22	4.21	4.15
11	H	1.70	1.46	1.41	1.33	1.34	1.37
11	H	1.86	2.31	2.35	2.00	2.00	2.25
12	H	4.24	4.21	4.20	4.23	4.22	4.30
13	H	1.97	1.78	1.76	1.80	1.80	1.70
13	H	2.05	2.20	2.21	2.11	2.11	2.27
14	H	1.78	2.04	2.03	1.83	1.84	1.95
14	H	1.99	2.13	2.12	1.96	1.95	2.29
16	H	1.89	2.14	2.13	2.02	2.02	2.07
16	H	2.56	2.29	2.28	2.29	2.29	2.21
17	H	1.67	1.71	1.72	1.61	1.61	1.79
17	H	2.22	2.20	2.19	2.14	2.17	2.20
20	H	1.52	1.53	1.53	1.45	1.43	1.49
20	H	1.57	1.64	1.63	1.54	1.53	1.81
21	H	1.16	1.25	1.26	1.22	1.22	1.28
21	H	1.57	1.48	1.51	1.36	1.36	1.58
22	H	3.96	3.91	3.89	3.77	3.80	3.97
23	H	1.99	2.08	2.08	2.01	2.01	2.06
23	H	2.44	2.35	2.36	2.27	2.27	2.41
25	H	1.88	1.58	1.66	1.50	1.48	1.83

No.	Nuc.	C-4: S		C-4: R	C-4: S cation	C-4: R cation	measured*
		no CPCM	CPCM	CPCM	CPCM	CPCM	
25	H	1.94	2.00	1.96	2.14	2.16	2.05
26	H	1.13	1.21	1.24	1.79	1.81	1.83
26	H	2.47	2.06	2.00	1.89	1.84	2.01
27	H	2.08	2.09	2.11	2.73	2.76	2.82
27	H	2.25	2.37	2.37	2.79	2.79	3.10
30	H	1.59	1.53	1.46	1.79	1.73	1.79
30	H	1.66	1.66	1.62	1.80	1.75	2.01
31	H	1.26	1.12	1.09	1.15	1.15	1.04
32	H	1.27	1.31	1.30	1.54	1.53	1.67
33	H	3.66	3.41	3.40	3.34	3.30	3.55
33	H	3.75	3.73	3.71	3.95	3.89	4.18
34	H	1.40	1.47	1.51	1.57	1.59	1.67
34	H	1.84	1.75	1.76	1.89	1.87	1.98
35	H	1.46	1.54	1.65	1.69	1.83	1.72
35	H	2.37	2.17	1.97	2.24	2.01	2.27
36	H	1.87	1.87	1.90	1.78	1.82	1.90
36	H	1.87	1.96	1.93	1.84	1.86	1.90
36	H	1.93	1.96	1.97	1.89	1.86	1.90
37	H	1.50	1.63	1.77	1.41	1.38	1.74
37	H	1.70	1.67	1.79	1.65	1.59	1.74
37	H	1.77	1.94	1.86	1.87	2.11	1.74
38	H	1.78	1.85	1.80	1.75	1.68	1.91
38	H	2.00	1.95	1.99	1.94	2.02	1.91
38	H	2.33	1.97	2.01	2.13	2.15	1.91
40	H	0.83	1.06	0.96	0.85	0.91	1.20
40	H	1.04	1.19	1.24	1.14	1.01	1.20
40	H	1.48	1.24	1.28	1.21	1.29	1.20
41	H	4.71	4.67	4.68	4.71	4.72	4.81
41	H	4.81	4.80	4.79	4.81	4.81	4.92
42	H	0.99	0.96	1.01	0.67	0.89	1.05
42	H	1.08	1.04	1.02	1.04	0.92	1.05
42	H	1.19	1.16	1.10	1.15	1.01	1.05
43	H	0.80	0.89	0.82	0.70	0.83	1.11
43	H	0.99	0.93	0.94	1.04	0.98	1.11
43	H	1.13	1.21	1.24	1.33	1.27	1.11

9.3.4 20-Hydroxy-13,19-didesmethyl SPX C (13)

Table 9.4: Simulated and measured chemical shifts of 20-Hydroxy-13,19-didesmethyl SPX C.

No.	Nuc.	C-4, C-20: S	C-4: R, C-20: S	C-4: S, C-20: R	measured
1	C	168.6	167.9	169.1	175.7
2	C	132.6	133.0	133.1	130.0
3	C	143.8	145.5	144.4	148.3
4	C	79.8	78.5	80.3	80.9
5	C	128.5	127.4	129.5	124.9
6	C	134.3	139.4	134.8	133.5
7	C	49.0	51.3	50.7	47.6
8	C	125.7	120.9	123.1	123.6
9	C	143.5	144.3	146.0	143.5
10	C	79.0	76.4	73.3	76.4
11	C	45.3	41.0	42.8	45.4
12	C	79.2	82.4	77.8	79.4
13	C	30.3	32.6	31.9	31.8
14	C	37.0	37.6	38.9	37.2
15	C	118.3	119.7	120.7	117
16	C	35.5	33.7	33.3	34.8
17	C	36.6	33.4	32.8	35.5
18	C	113.4	112.8	111.9	110.3
19	C	72.0	69.5	69.4	71.3
20	C	70.8	70.7	71.1	69.3
21	C	37.2	36.8	37.2	38.4
22	C	64.4	63.7	63.0	63.7
23	C	49.2	47.8	48.4	46.9
24	C	150.0	150.7	150.6	147.5
25	C	36.6	33.6	35.2	35.6
26	C	24.3	21.8	21.9	23.0
27	C	36.1	34.4	35.2	34.9
28	C	172.9	173.6	173.4	174.4
29	C	51.9	51.8	52.3	52.7
30	C	36.6	37.5	37.3	37.5
31	C	35.8	35.9	36.1	35.8

No.	Nuc.	C-4, C-20: S	C-4: R, C-20: S	C-4: S, C-20: R	measured
32	C	41.9	42.7	42.5	40.6
33	C	52.4	53.0	53.2	52.8
34	C	31.9	32.5	32.5	31.4
35	C	19.2	21.3	20.0	19.2
36	C	10.1	11.1	10.7	10.7
37	C	15.8	17.2	16.6	16.7
38	C	9.2	15.3	16.5	12.6
41	C	107.6	105.3	106.7	110.6
42	C	17.3	18.3	18.3	20.1
43	C	18.1	19.1	18.8	20.0
3	H	6.76	6.71	6.66	7.00
4	H	5.87	5.89	5.78	5.82
7	H	3.66	3.80	3.74	3.39
8	H	5.49	5.33	5.40	5.25
10	H	4.07	4.37	4.27	4.38
11	H	1.69	1.83	1.85	1.66
11	H	2.47	2.02	1.86	2.73
12	H	4.58	4.40	4.61	4.71
13	H	1.83	2.04	1.96	2.16
13	H	2.36	2.26	2.10	2.16
14	H	2.21	1.99	2.06	1.77
14	H	2.22	2.31	2.41	1.96
16	H	2.05	2.08	1.97	2.10
16	H	2.39	2.61	2.68	2.30
17	H	2.37	1.91	1.85	2.19
17	H	2.37	2.63	2.64	2.50
19	H	3.41	3.34	3.32	3.68
20	H	3.89	3.88	3.87	4.18
21	H	1.45	1.45	1.45	1.36
21	H	2.27	2.13	2.16	2.06
22	H	4.19	4.22	4.14	4.54
23	H	2.30	2.17	2.27	2.29
23	H	2.65	2.68	2.61	2.69
25	H	1.80	2.09	1.52	1.75
25	H	2.39	2.18	2.37	2.55
26	H	1.50	1.35	1.42	1.46

No.	Nuc.	C-4, C-20: S	C-4: R, C-20: S	C-4: S, C-20: R	measured
26	H	2.29	2.71	2.62	2.47
27	H	2.25	2.32	2.36	2.10
27	H	2.42	2.45	2.38	2.30
30	H	1.76	1.64	1.77	1.47
30	H	1.82	1.71	1.86	1.47
31	H	1.34	1.41	1.40	1.22
32	H	1.46	1.40	1.48	1.25
33	H	3.86	3.81	3.81	3.61
33	H	3.89	3.84	3.85	3.67
34	H	1.57	1.71	1.60	1.32
34	H	1.98	2.00	2.05	1.64
35	H	1.64	2.07	1.68	1.47
35	H	2.52	2.08	2.55	2.07
36	H	2.06	2.06	2.07	1.85
36	H	2.09	2.07	2.11	1.85
36	H	2.14	2.11	2.13	1.85
37	H	1.83	1.62	1.64	1.53
37	H	1.92	1.74	1.86	1.53
37	H	1.93	2.40	2.05	1.53
38	H	2.01	1.69	2.15	1.98
38	H	2.03	2.35	2.23	1.98
38	H	2.21	2.69	2.57	1.98
41	H	4.97	4.88	4.89	4.81
41	H	5.06	4.94	4.96	4.83
42	H	1.23	1.27	1.31	1.29
42	H	1.32	1.35	1.37	1.29
42	H	1.34	1.38	1.39	1.29
43	H	1.08	0.94	0.99	0.85
43	H	1.22	1.17	1.29	0.85
43	H	1.24	1.29	1.32	0.85